Well-controlled and well-described SAMs-based platforms for the study of material-bacteria interactions occuring at the molecular scale

Judith Böhmler

Thèse présentée pour obtenir le grade de

Docteur de l'Université Haute-Alsace

Discipline : Chimie-Matériaux

Par

Judith Böhmler

Well-controlled and well-described SAMs-based platforms for the study of material-bacteria interactions occurring at the molecular scale

Soutenance publiquement le 11 Septembre 2012

Membre du Jury

Directrice de Thèse	Dr. Karine Anselme
Co-directrice de Thèse	Dr. Lydie Ploux
Co-directeur de Thèse / Invité	Dr. Arnaud Ponche
Rapporteur Externe	Prof. Jean-Claude Block
Rapporteur Externe	Prof. Paul Rouxhet
Examinateur	Prof. Thierry Jouenne
Examinateur	Prof. Vincent Ball
Invité	Prof. Yannis Missirlis

Abstract

The aim of this work is to investigate the effect of the accessibility of functional groups of solid surfaces on bacterial adhesion. For this purpose, well-controlled and well-described smooth self-assembled monolayers on surfaces with various surface chemical densities were developed and used as substrate for bacterial adhesion experiments. These experiments were performed under liquid and static conditions and bacterial behavior was analyzed by confocal microscopy. In addition, bacteria's metabolism was investigated aiming at visualizing possible changes induced by the surface.
In a first time, a study was conducted to determine the approach of characterization and analysis of the surfaces, which is necessary to describe composition, structure and organization of the molecular layer. Commonly used model surfaces based on 3-aminopropyltriethoxysilane (APTES) and N(6-aminohexyl)aminopropyltriethoxy-silane (AHAPS) self-assembled monolayers (SAMs) were used to test relevance and efficiency of the approach. A multimodal combination of techniques, was chosen. The obtained characterization results were carefully analyzed and surface descriptions were proposed on this basis. In a first stage, elementary composition obtained by XPS survey spectra, wettability evaluated by static water contact angle, and topography evaluated by the mean roughness were taken into account for describing the surface, however failing at highlighting defects in structure and organization of the molecular layer. In a second stage, the potential improvements to the surface description resulting from knowing the chemical functional groups determining by using XPS high-resolution spectra of carbon (C1s) and nitrogen (N1s), the surface homogeneity evaluated by the advancing and receding water-contact angles, the thickness obtained by XPS (in vacuum) and by ellipsometry (in air and in liquid), the surface morphology evaluated by AFM images, and the surface charge measured by zeta potential measurements were evaluated. The ability of each technique or their combination to point out defects in the layer was considered in particular. On the contrary to the first stage, the second one allowed to describe layer structure and molecular organization with precision, demonstrating the necessity of a thorough surface analysis for the development of well-controlled and well-described model surfaces. As an example, this thorough analysis approach allowed to reveal that, under the used conditions, the overlayer properties of the surfaces could not be well-controlled.

In a second time, well-controlled chemically mixed model surfaces suitable for further bacterial adhesion studies, were realized and comprehensively characterized for achieving their well-description. Based on bromosilanes that were already shown to allow chemically

mixed SAMs, we investigated the effect of various parameters, crucial for the adsorption of the silane on the substrate aiming at achieving surfaces with monolayer structure and well molecular assembling. Thorough characterization as previously defined was applied at each step of this development. The final protocol allowed to prepare controlled SAMs-modified surfaces under "normal" laboratory conditions, i.e. usable in every laboratory. The use of two different silanes with different terminal functional groups, allows to achieve mixed NH_2/CH_3 monolayers (MMLs). Because of the similar chain lengths of the used silanes, surfaces do not reveal any nanotopography. Furthermore, they contain different densities of amine backfilled with methyl functionalities, which are controlled by the silane ratio in the initial solution. These surfaces also reveal varying wettability character.
Such mixed monolayers are ideal to further create surfaces with different densities of grafted biomolecules, for biointerface studies. Therefore, a preliminary study was conducted to assess the feasibility of a further grafting of biomolecules. The objective was to reach grafting yields, which would assume to conserve well-control of the surface chemical density. For that purpose, homogeneous amine terminated surfaces were used for further investigating the amino acid glycine and different strategies were considered. Comparing the use of three homobifunctional linker molecules of different size, reactive groups and stiffness to graft glycine to amine groups a thoroughly analysis by XPS showed that the obtained reaction yield was quasi similar and beyond 50 %. In a second approach, glycine was activated and directly grafted on the amine terminated surfaces. However, our results demonstrated that the reaction was not enough controlled and that some reagents in the solution were reacting with the amine modified surface.
In the third and last part of this work, the thoroughly characterized MMLs (NH_2/CH_3) were used for bacteria adhesion studies, conducted with two bacteria strains: *E. coli* and *S. epidermidis*. Both bacteria strains adhered less on surfaces with a high amount of amine when cultivated in saline solution. Furthermore, no linear correlation between the amount of amine and the number of adherent bacteria was found. It could be demonstrated that the bacteria adhesion behavior is divided in two groups. The first group is represented by surfaces with a high amount of methyl functionalities resulting in an elevated number of adherent bacteria, while the second group is represented by surfaces with a high amount of amine functionalities resulting in lower number of adherent bacteria. The difference between the two groups and the corresponding number of adherent bacteria was changed by changing the culture media. To limit the potential effect of an ion double layer that exists between the surface and bacterial cells, the experiments were also performed under low shear hydro-dynamic conditions. Bacterial adhesion significantly differs between static and dynamic experiments but non-linear relationship between the amount of amine on the substrate and the bacteria adhesion was found as well.
In general, these results demonstrate for the first time that chemical heterogeneities of the surface play an important yet neglected role in bacterial adhesion. This was confirmed by comparing bacterial adhesion on homogeneous NH_2 surfaces revealing well-controlled (i.e. bromosilane-based) and uncontrolled (i.e. APTES- and AHAPS-based) layer structure

and molecule organization. Aside from differences in the coverage of the adhered bacteria number compared to well-controlled surfaces, the reproducibility of experiments was significantly reduced on uncontrolled surfaces. Finally, preliminary investigations of the metabolism of bacteria adhered to NH_2CH_3 MML were conducted. Sessile and planktonic *S. epidermidis* cells were investigated for the production of the polysaccharide intercellular adhesin (PIA). Under moderate shear rate, surfaces with high amount of methyl groups were selective for PIA-less bacteria cells. Surfaces with high amount of amine and all surfaces under high shear rate expressed a similar high level of PIA as planktonic bacteria. This result was attributed to physical-chemical character of PIA that is more favorable to bacterial adhesion to NH_2-rich surfaces than to CH_3-rich ones.

A specific protocol adapted for proteomic analysis of adhered bacteria was also developed, which should allow, in the future, investigation of the composition of the adhered bacteria membrane for better understanding bacteria/material interactions at the molecular scale.

Résumé française

Un biofilm est un assemblage de bactéries intégrées dans une matrice de substances extracellulaires produites par les bactéries elles-mêmes. Les biofilms peuvent présenter des avantages dans certaines applications, comme par exemple pour la purification de l'eau ou dans le domaine de la santé, (parle alors de (biofilms positifs), ou des désavantages (biofilms négatifs) quand ils sont la source d'encrassement biologique de surfaces (*biofouling*) ou d'infections récurrentes. L'étape cruciale pour la formation d'un biofilm est l'adhésion de bactéries sur une surface. L'adhésion des bactéries est dépendante de plusieurs facteurs environnementaux comme la température du milieu de culture ou la souche de bactéries. Un autre facteur crucial est le matériau support et ses propriétés mécaniques, topographiques et chimiques. Dans la littérature, il existe plusieurs études qui démontrent un effet de la chimie de surface sur l'adhésion des bactéries. Cependant, dans ces études, les surfaces sont rarement suffisamment bien décrites ou caractérisées. Nous nous sommes donc intéressés dans ce travail à l'effet d'un matériau présentant des hétérogénéités chimiques à l'échelle moléculaire sur l'adhésion de bactéries. Pour mieux comprendre ce processus, il était nécessaire de disposer d'un outil efficace pour étudier le rôle de la chimie du matériau sur l'adhésion de bactéries. Dans ce but, des surfaces modèles bien contrôlées et bien caractérisées ont été développées comme outil pour cette étude.

Le travail pratique a été séparé en trois parties dans ce manuscrit. La première partie (2éme chapitre) décrit la démarche suivie pour valider la méthodologie de caractérisation d'une couche mince organique déposée sur un wafer de silicium. Dans la deuxième partie (3éme chapitre) des surfaces modèles avec un contrôle de la chimie à l'échelle moléculaire ont été réalisées, optimisées et caractérisées. Ces surfaces " à chimie contrôlée" ont ensuite été utilisées dans la troisième partie (4éme chapitre) comme des outils pour étudier l'impact de l'hétérogénéité chimique à l'échelle moléculaire sur l'adhésion de bactéries.

Le deuxième chapitre comporte un article publié en 2011 dans le " *Journal of Physical Chemistry C* ". Dans cet article, l'importance d'une caractérisation détaillée des surfaces modèles et l'avantage d'une analyse à chaque étape de leur fabrication sont démontrés. Deux silanes communément utilisés (APTES et AHAPS) ont permis de fonctionnaliser un wafer de silicium par une amine. Le glutaraldéhyde (GAD) a ensuite été utilisé pour obtenir des surfaces fonctionnalisées par la glutamine. Ainsi, quatre surfaces différentes (surface-APTES, surface-AHAPS, surface-AHAPS-GAD et surface AHAPS-GAD-glutamine) ont été obtenues, caractérisées et analysées. La caractérisation des échantillons a été effectuée par une combinaison de techniques différentes qui permettent d'obtenir des informations sur la structure, l'organisation, l'homogénéité de la surface ainsi que le rendement de la réaction. En suivant cette

procédure, des descriptions précises des surfaces ont été proposées tout en prenant les résultats expérimentaux en considération.

La technique de caractérisation la plus efficace pour décrire la couche moléculaire à la surface a été la spectroscopie de photoélectrons X (XPS). Elle donne des informations sur la composition atomique et l'environnement chimique des atomes de la surface. De plus, des mesures de mouillage et d'épaisseurs ont été nécessaires pour la compréhension de la structure de la couche greffée sur la surface.

En comparant une méthode de caractérisation courante et une méthode de caractérisation plus approfondie, nous avons montré qu'il était possible de faire ressortir des défauts de structure dans la couche moléculaire greffée grâce à l'utilisation de techniques différentes. Nous avons pu valider que l'AHAPS s'organise effectivement à la surface comme une monocouche bien organisée. Néanmoins, dans nos manipulations, grâce à notre approche d'analyse et à une caractérisation approfondie nous avons pu montrer que les molécules d'AHAPS ont une orientation " tête en bas ". Ceci permet d'expliquer le faible rendement de greffage du glutaraldéhyde observé sur ces surfaces. Nous avons pu montrer que le faible rendement de la réaction de greffage du glutaraldéhyde pouvait être causé par la faible quantité de groupements amines libres, d'une faible densité de glutaraldéhyde présent à la surface, de la formation de ponts glutaraldéhyde entre deux groupements amine et de liaisons réversibles entre les groupements aldéhydes et amines.

Enfin nous concluons qu'une caractérisation approfondie de la surface est cruciale, en particulier si les surfaces sont destinées à des études de bio-interfaces comme des études d'adhésion bactérienne.
En effet, affirmer grâce à une caractérisation par des techniques d'analyse communes que l'APTES est formée de multicouches, comme déjà montré dans la littérature, est simple. Par contre, seule une caractérisation approfondie, permet de décrire les interactions moléculaires spécifiques à l'intérieur de la couche greffée. De plus, l'approche commune ne suffit pas pour montrer les défauts dans la structure de la couche AHAPS.

Après la mise au point de la méthodologie de caractérisation, des surfaces modèles avec un contrôle de la densité de surface de groupements NH_2 ont été développées. Le chapitre 3 est séparé en deux parties différentes : la première partie décrit le développement et l'élaboration de surfaces modèles avec des densités variables de groupement NH_2 et la deuxième partie décrit le greffage d'un acide aminé sur les surfaces 100 % NH_2. Les résultats et la discussion des deux parties sont présentés sous la forme de deux articles (2a et 2b) en cours de publication.

Dans l'article 2a nous démontrons l'optimisation d'un substrat adapté à des études de bio-interfaces. Le substrat doit être bien contrôlé et bien caractérisé. En parti-

culier des surfaces fonctionnalisées par de l'amine ont été réalisées dans ces études, dans la mesure où des silanes avec une terminaison amine sont souvent utilisées pour le greffage de biomolécules. Cependant, ces silanes forment de manière non contrôlée des mono- ou multi-couches, en raison d'interactions entre l'amine et le substrat. De ce fait, des silanes fonctionnalisés par un brome ont été préférés afin d'obtenir des monocouches auto assemblées (Self-assembled monolayers, SAM) bien organisées sur des substrats de silicium. La fonctionnalisation du brome permet une conversion chimique en une amine par la suite. Ainsi, des surfaces bien contrôlées, bien caractérisées et fonctionnalisées par une amine, idéales pour des études de bio-interfaces,ont pu être obtenues.

Dans un premier temps le protocole d'auto-assemblage d'un silane fonctionnalisé par le brome a été optimisé. Au cours de cette procédure, des paramètres différents comme la température, le solvant et le temps de la réaction ont été étudiés. Ainsi les paramètres finaux nécessaires pour obtenir des surfaces SAMs bien contrôlées ont été déterminés. Ensuite, les surfaces fonctionnalisées par le brome ont été converties en surfaces fonctionnalisées par des amines. On peut noter que ces conditions de préparation peuvent être mises en place aisément au sein d'un laboratoire de biomatériaux. Suite à l'optimisation des surfaces bromes, des surfaces avec des monocouches mixtes ont été obtenues grâce à l'utilisation d'un deuxième silane dont la terminaison chimique est un groupement CH_3. Les surfaces sont donc fonctionnalisées par les amines f en concentrations variables dans un continuum de groupements CH_3. Grâce à ces surfaces, des questions intéressantes peuvent être étudiées comme l'influence de la densité de fonctions sur un système biologique directement sur la surface ou après greffage d'une biomolécule sur la surface à densité variable.

Enfin, des études d'adhésion de bactéries ont été effectuées sur trois surfaces fonctionnalisées par des amines. Dans ce but des surfaces fonctionnalisées par amine (APTES et AHAPS) et des surfaces fonctionnalisées par le brome transformées ensuite en amine ont été utilisés. Les surfaces sont différentes dans l'organisation de leur couche de SAMs, comme cela a été montré dans le premier article. L'APTES forme des multicouches alors que l'AHAPS forme une monocouche organisée, mais dont quelques-unes des molécules ont une orientation " tête en bas ". Au contraire, les silanes bromés forment une couche de SAMs lisse et bien contrôlée. Par conséquent, l'impact de l'organisation de la couche de surface sur l'adhésion de bactéries a pu être étudié. Les résultats montrent que la reproductibilité des expériences de l'adhésion de bactéries augmente avec l'organisation du substrat (APTES $<$ AHAPS $<$ 100 % NH_2).Ceci démontre l'importance de l'organisation de substrat à l'échelle moléculaire sur l'adhésion des bactéries. Dans l'article 2b est démontré le potentiel de l'analyse XPS du pic C1s haute résolution pour suivre l'efficacité du greffage

d'un acide aminé. Pour cette démonstration l'acide aminé glycine a été greffé sur des surfaces 100 % NH_2 plus ou moins organisées. Les surfaces sont donc entièrement couvertes par des groupements d'amine en contact direct entre eux. Cette haute densité d'amine peut donc provoquer des contraintes stériques limitant le greffage de la glycine. Par conséquent, chaque étape du greffage de glycine a été analysée par XPS et le rendement de réaction a été calculé par différentes approches.

Le contrôle du greffage de biomolécules fait l'objet de beaucoup d'intérêt dans le domaine, à croissance extrêmement rapide, des sondes biologique mais aussi des études fondamentales sur les biointerfaces. Dans ce cadre, le rendement des réactions de greffage ou la quantité de biomolécules greffées est un paramètre crucial pour l'interprétation du résultat des analyses. Dans l'article 2b, trois molécules d'accroche souvent utilisées dans la littérature et portant deux groupements terminaux identiques ont été utilisées pour réaliser le greffage de la glycine. Les trois molécules d'accroche présentent une rigidité différente et réagissent différemment avec la surface et la glycine. Tout d'abord, la molécule d'accroche glutaraldéhyde (GAD) a été étudiée. Le groupement fonctionnel de GAD réagit avec un groupement amine de la surface ainsi qu'avec un groupement amine de la glycine. Un rendement élevé de greffage de la glycine à la surface a été calculé grâce à l'analyse des spectres de haute résolution C1s en XPS. Cependant, il a été démontré que la GAD polymérisait sur la surface et que quelques molécules de GAD se trouvaient sous la forme de ponts entre deux groupements amine de surface. Par conséquent, le greffage ultérieur de glycine est limité par le degré de polymérisation de la GAD dans la mesure où le greffage dépend de l'accessibilité des groupements aldéhydes libres. Comme prévu, une quantité réduite de glycine a été greffée sur les surfaces activées par la GAD.

Pour cette raison, deux autres molécules d'accroche ont été testées pour le greffage de glycine sur des surfaces fonctionnalisées par des amines, et les surface analysées par XPS. Tout d'abord, le di-(N-succidinimidyl)oxalate (DSO), qui contient deux groupement ester-NHS a été utilisé. Ces groupements ester-NHS activent des molécules sur lesquels ils sont accrochés puis sont supprimés pendant la réaction avec un groupement amine. Le greffage de DSO sur un substrat fonctionnalisé par une amine et le greffage de glycine sur des surfaces activées par la DSO peut être suivi par le changement du composant carbone COO dans le spectre de haute résolution en XPS. Ensuite, le phényle-1 ,4-diisothiocyanate (PDITC) a été utilisé. Le PDITC contient un cycle aromatique qui lui permet s'organiser grâce à l'interaction d'électrons π-π. Néanmoins le spectre C1 de haute résolution peut toujours être utilisé pour calculer le rendement de la réaction.

En définitive, le rendement du greffage de la glycine sur la surface activée par des molécules d'accroche est de 30 % pour la GAD et 50 % pour le DSO et le PDITC.

Pour les trois options de greffage de la glycine, le rendement de la réaction a été estimé par des analyses XPS. Le greffage de glycine dépend fortement de la nature de la molécule d'accroche. Le GAD fournit plusieurs aldéhydes réactives. Cependant, ces aldéhydes ne sont pas tous accessibles pour le greffage ultérieur de la glycine, en raison de la polymérisation de la GAD sur la surface. Le greffage de la glycine via le DSO et le PDITC permettent d'obtenir rendement plus élevé. Par contre, il semble qu'il y ait des effets stériques, même avec cet acide aminé qui est le plus petit acide aminé, qui limitent la réaction.

Les surfaces modèles bien définies et bien caractérisées avec des densités différentes de NH_2 complétées par des CH3 ont donc été utilisées pour étudier l'adhésion de bactéries en conditions statique et dynamique. Avant les études d'adhésion de bactéries, les surfaces ont été caractérisées par XPS, mesures d'angles de contact, ellipsométrie, microscopie à force atomique et potentiel zêta. La caractérisation indique que les surfaces modèles possèdent une structure de monocouche moléculaire bien organisée comme attendu pour des SAMs. Cette étude et les résultats de l'adhésion bactérienne sur des surfaces avec différentes densités de NH_2 et dans différentes conditions de culture sont présentées dans l'article 3 intitulé "*The role of chemical heterogeneities of surfaces in the adhesion of bacteria*".

Pour les études d'adhésion bactérienne, deux souches de bactéries différentes ont été utilisées : la souche gram-négative et auto-fluorescente *Escherichia coli* (*E. coli*) SCC1 et la souche gram-positive *Staphylococcus epidermidis* (*S. epidermidis*) ATCC35984. Les essais ont été réalisés pendant 2 h en solution saline pour les deux souches de bactéries mais à 30 °C pour *E. coli* et 37 °C pour *S. epidermidis*. Des expériences supplémentaires avec *E. coli* ont été réalisées en condition statique dans le milieu sélectif M63G-B1. Les bactéries ont été cultivées initialement soit dans le milieu LB pour *E. coli* soit dans le milieu BHI pour *S. epidermidis*. Après une centrifugation, le culot de bactéries a été remis en suspension soit dans la solution saline soit dans le milieu M63G-B1. La solution de bactéries a été diluée jusqu'à atteindre une concentration donnant 0.01 d'adsorption à 600 nm (Abs_{600nm}) pour les études en condition statique et 0.1 pour les études en conditions dynamiques. Les expériences ont été réalisées sous un microscope confocal à balayage laser (CLSM, Zeiss, LSM700).

Après deux heures d'expérience en condition statique à la température idéale pour chaque souche de bactérie, les surfaces ont été rincées soigneusement avec une solution saline afin d'enlever les bactéries non-adhérentes. Au cours de ce processus, les bactéries non fluorescentes ont été marquées par le Syto9®.
Les expériences de culture en condition statique ont été réalisées trois fois, et dix régions différentes sur les surfaces ont été photographiées en mode fluorescent grâce au microscope confocal. Le nombre de bactéries sur la surface a été compté et le

moyenne de bactéries adhérentes sur les surfaces avec des densités différentes de NH_2 a été comparée à la moyenne du nombre de bactéries adhérentes sur la surface de référence. Les résultats ont été analysés statistiquement.

Les expériences en conditions dynamiques ont été réalisées dans une cellule à flux avec un seul échantillon par essai. Pour chaque substrat avec une certaine densité de NH_2, les essais ont été réalisés deux fois. Pour l'analyse de l'adhésion des bactéries des images ont été réalisées en mode fluorescent et en mode réflexion avec le microscope confocal. Ensuite, le nombre de bactéries adhérentes, le taux d'adhésion des bactéries et la dynamique des bactéries sur les surfaces ont été évalués.

Les expériences d'adhésion bactérienne en statique, réalisées en solution saline indiquent la même tendance de comportement pour les bactéries *E. coli* SCC1 et *S. epidermidis* ATCC35984. Les bactéries adhèrent en nombre plus élevé sur les surfaces avec une concentration élevée de CH_3. La comparaison des bactéries adhérentes sur les surfaces avec des concentrations différentes de NH_2 montre la formation de " plateaux ". Dans ces plateaux l'adhésion des bactéries n'est pas significativement différente. Entre les plateaux, des phases de transitions apparaissent dans lesquelles l'adhésion des bactéries change fortement avec la concentration de NH_2. Cette évolution de l'adhésion des bactéries sur des surfaces de monocouches mixtes, présente une similitude avec les courbes de dosage acide-base. Le nombre de bactéries adhérentes sur les surfaces avec une concentration élevée de CH_3 reste stable malgré l'augmentation de la concentration de NH_2 sur la surface jusqu'à un certain seuil de concentration. A partir de ce seuil (premier seuil), le nombre de bactéries adhérentes sur la surface diminue très rapidement jusqu'à une deuxième concentration en groupements NH_2 sur la surface (deuxième seuil). Par contre, si la concentration en groupements NH_2 sur la surface augmente encore, le nombre de bactéries reste stable. Une explication de ce comportement d'adhésion pourrait être liée à la composition de l'enveloppe des bactéries. Malgré la charge globale négative de l'enveloppe des bactéries, il existe des groupements fonctionnels divers dans l'enveloppe qui sont chargés positivement. Sur le substrat, la concentration en groupements chargés positivement, comme les NH_3^+, augmente avec la concentration en amine. Une grande concentration en groupements CH_3 et/ou une faible concentration en groupements NH_3^+ semble être favorable pour l'adhésion des bactéries, puisque un nombre de bactéries plus important adhère sur ces surfaces. Cependant, l'interaction entre l'enveloppe des bactéries et le substrat diminue avec l'augmentation de NH_3^+ et/ou la diminution de CH_3. Après cette transition, l'interaction entre la bactérie et le substrat se stabilise à nouveau, comme le montre le nombre stable de bactéries attachées malgré l'augmentation de NH_3^+. La distribution discrète de la charge positive sur l'enveloppe de la bactérie pourrait donc être un paramètre crucial, résultant dans des interactions non favorables ou des interactions répulsives entre la bactérie et

la surface. En outre, la composition de l'enveloppe de chaque souche de bactéries est différente et donc ce fait pourrait expliquer les légères différences de résultat d'adhésion obtenues pour *E. coli* et *S. epidermidis*.

Pour *E. coli* la même expérience a été réalisée en milieu sélectif M63G-B1. De manière surprenante, la tendance de l'adhésion des bactéries est inversée par rapport à la tendance obtenue en solution saline. Il y a plus de bactéries adhérentes sur les surfaces avec une concentration élevée de NH_3^+.
Le nombre de bactéries adhérentes sur les surfaces avec une concentration élevée de NH_3^+ est comparable pour les deux milieux : solution saline et M63G-B1. Par contre, le nombre de bactéries adhérentes sur des surfaces avec une concentration élevée de CH_3 est différent. Les milieux utilisés pour ces expériences semblent donc changer l'interaction entre les bactéries et les surfaces quelque soit le ratio NH_2/CH_3. Cet effet paraît être plus fort pour les interactions avec les surfaces présentant une concentration élevée de groupement CH_3. L'hypothèse proposée pour expliquer ces résultats est basée sur la formation de doubles couches d'ions venant du milieu sur l'enveloppe des bactéries et les surfaces modèles. Ces doubles couches d'ions forment des obstacles à l'adhésion des bactéries sur les surfaces. Cette double couche d'ions est dépendante de la composition ionique des milieux utilisés pour les expériences. Les ions sont plus grands dans le milieu M63G-B1 qu'en solution saline et peuvent donc former des doubles couches plus épaisses. Ceci peut donc diminuer les interactions entre les bactéries et les surfaces.

Néanmoins, les interactions hydrophobes (prédominantes sur les surfaces riches en CH_3) et les interactions répulsives électrostatiques entre les charges positives de l'enveloppe des bactéries et la charge positive de surface pourraient être plus sensibles aux augmentations de distance entre la bactérie et la surface des matériaux. Les interactions attractives électrostatiques entre les bactéries et la surface des matériaux sont causées par la charge globalement négative de l'enveloppe des bactéries, même si des charges positives sont présentes. Par conséquent, de telles interactions pourraient être prédominantes en milieu M63G-B1 et conduire à une augmentation du nombre de bactéries adhérentes sur les surfaces avec l'augmentation de la concentration en NH_2.

Pour diminuer l'effet stérique de la double couche d'ions et pour mieux étudier l'adhésion bactérienne, des expériences en dynamique (ou en temps réel) ont été réalisées. Les taux d'adhésion bactérienne en condition dynamique sur des surfaces de différentes concentrations de NH_2 ont été comparés.

Comme pour les résultats des expériences en statique, les taux d'adhésion bactérienne présentent des zones de transition brusques qui dépendent de la concentration de NH2 sur la surface. Par contre, les zones de transition obtenues dans les expéri-

ences en statique et dynamique sont nettement différentes. De plus, l'analyse des taux d'attachement et de détachement révèlent des zones de courbe, qui correspond à la concentration de NH_2 sur la surface avec une adhésion plus ou moins stable des bactéries.

Avec cette étude nous avons pu confirmer que le milieu utilisé pour les expériences peut affecter l'adhésion bactérienne. De plus, nous avons démontré pour la première fois, que des changements subtils de la composition chimique d'une surface peuvent influencer l'adhésion et la prolifération de bactéries. Les expériences en temps réel confirment que l'hétérogénéité chimique de surface joue un rôle important pour les interactions entre des bactéries et des surfaces dans un environnement complexe. Par contre, les phénomènes impliqués restent à analyser de manière plus approfondie. Néanmoins, les expériences permettent de démontrer que la stabilité des bactéries est plus élevée sur les surfaces riches en NH2 que sur les surfaces riches en CH_3.

Contents

General introduction

A material e.g. a medical implant that is exposed to common biological liquid environment has high risks to be contaminated by microbes [1,2]. This contamination typically results in a biofilm (figure 0.1) that can cause serious health problems due the resistance that it offers to bacteria against antibiotics and other environmental stresses and its role as a reservoir, for the regular release of planktonic bacteria [1]. The initial bacterial adhesion (step 2 in figure 0.1) is considered to be a crucial step in the process of biofilm formation. Bacteria interact physically and chemically with the surface, which is controlled by the properties and reactive domains of the bacteria surface [3–5], the material surface [6], as well as environmental conditions such as pH, concentration of ions, temperature, shear stress etc. [7–9]. If bacterial adhesion could be controlled, biofilm formation could be avoided, and free-living bacteria could be easily cleared by antibiotics. Hence, the interaction and the understanding of the initial adhesion step of bacteria is the focus of many investigations [10–21].

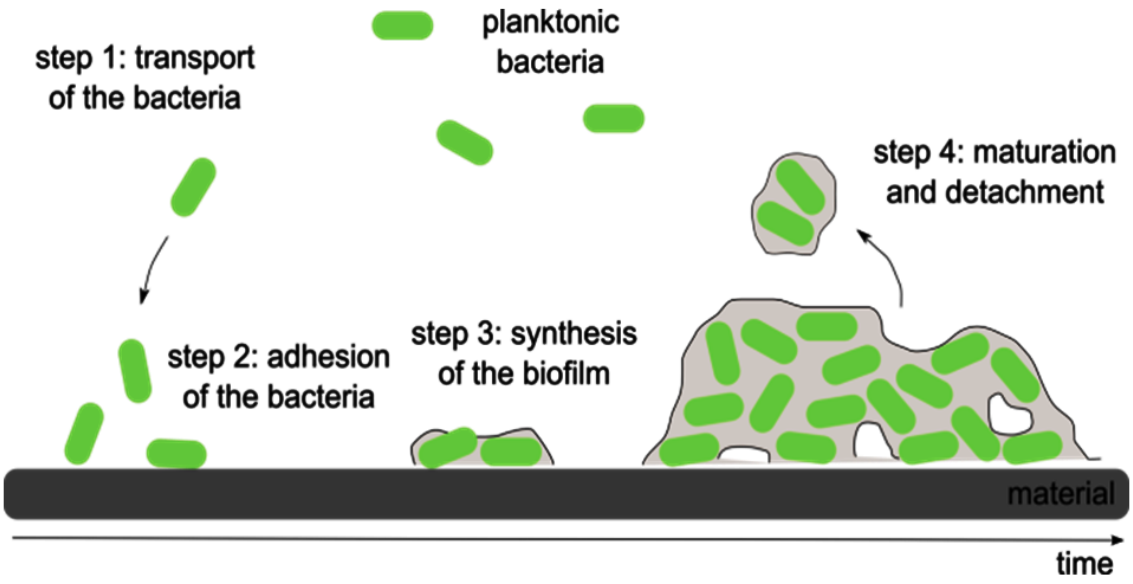

Figure 0.1: The biofilm formation is generally described by 4 more or less overlapping steps. Step 1: Planktonic bacteria are passively or actively transported near the surface. Step 2: Bacteria adhere at the surface. Step 3: Bacteria form a biofilm and produce exopolysaccharides. Step 4: Bacteria can detach from the mature biofilm. Illustration from Ploux et al [3].

Material surface properties play a crucial role in the first bacterial adhesion step. Despite number of publications, the understanding of the interactions between bacterium and material surface caused by physical-chemical properties remains largely partial. In particular, some aspects of the material surface properties have been totally neglected. This is the case of the potential impact on the bacterial behavior of chemical heterogeneities of a surface and, more generally, the accessibility of individual chemical functionalities.

For studying such aspects, well-characterized and defined substrates might be the key point of significant, relevant and reproducible results. The specific physical-chemical surfaces properties must be reproducible and have constant properties, only affected by the environmental conditions. These surfaces must be easy to fabricate and have to be stable under long-term physiological conditions, different shear rates, temperature and pH. Above all, the definition, control and description of their properties like the chemical functionalities exposed to the bacterial surface, charge, hydrophilic and hydrophobic character must be comprehensive. For example, if surfaces with immobilized biomolecules are considered, such a description is crucial for understanding the bacterial response to differently exposed biomolecules. However, model surfaces adapted for investigating the impact of chemical heterogeneities of surface on bacterial behavior are rare and incomprehensively described.

In other respects, the study of bacteria adhering onto and developing on such surfaces, needs specific and careful methodology to have access to the expected, subtle differences in bacterial behavior. Experiments in dynamic conditions, which allows to apply specific stress at the bacteria/surface interface, and genomic and proteomic analysis approaches, which allow to assess the bacterial metabolism, are still rare. Yet, they should favor a comprehensive understanding of the impact of specific surface features on bacterial behavior and should allow to determine whether bacteria are able to sense these features.

Scope of the thesis

In this frame, the first main objective of the thesis was to develop adequate model surfaces for studying the effect of chemical heterogeneities of a material surface on bacterial adhesion and biofilm development. For that purpose, it was necessary to also establish a methodology to characterize and thoroughly analyze these surfaces. The second, main object was to investigate the adhesion and the proliferation of bacteria on these surfaces in terms of quantity, kinetics and metabolism.

For preparing the adequate model-surfaces, presenting mixed controlled chemistry at molecular scale, silicon wafers modified with self-assembled monolayers were chosen. They can be fabricated in almost every laboratory, result in stable surfaces and provide the opportunity to introduce various functional groups in different densities. A huge variety of possible functional groups can be used to change the surface character and to investigate the impact of different physical-chemical surface properties on bacterial adhesion. However, their layer structure and molecular organization are often far from the expected properties, especially due to unintentional almost inevitable chemical side reactions.

In the present work, we therefore choose to develop SAMs surfaces based on bromine terminated silane and to associate their development with a thorough characterization methodology, mainly based on X-ray photoelectron spectroscopy (XPS), to reach well-known and well-described model surfaces (in collaboration with Prof. Vincent Ball). Aiming at preparing further studies about the impact on bacterial adhesion of the accessibility of immobilized biomolecules, we also preliminary investigated the possibility to use the chemically mixed model surfaces for the grafting of an amino acid on amine terminated surfaces (in collaboration with Dr. Delphine Josien). Finally, the impact of the well-characterized model surfaces on bacterial adhesion and proliferation of *Escherichia coli* SCC1 and *Staphylococcus epidermidis* was investigated under static and dynamic conditions. In addition, the production of PIA by planktonic and sessile *S.epidermidis* was investigated by real time polymerase chain reaction (in collaboration with Prof. Iris Spiliopoulou and Prof. Yannis Missirlis). Furthermore, preliminary works led to a protocol to analyze the protein production of adherent bacteria (in collaboration with Prof. Thierry Jouenne). The organization of the main part of this work is pictured in figure 0.2.

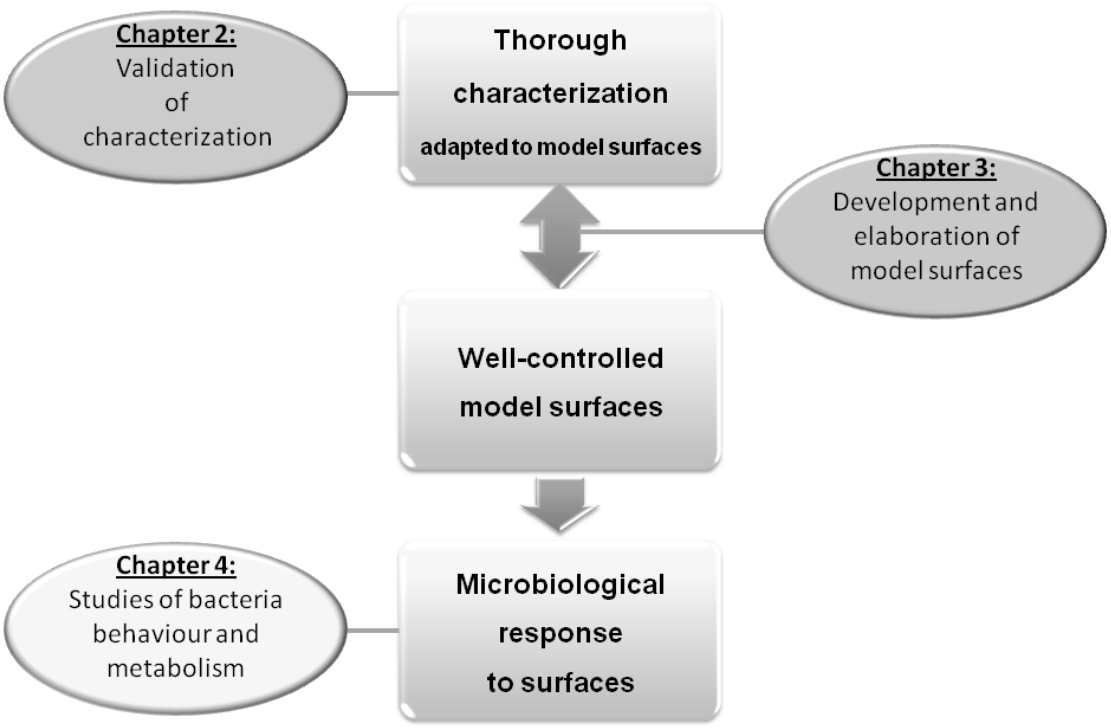

Figure 0.2: The work of the thesis is described in three different chapters. In chapter 2, the characterization of model surfaces was validated. In chapter 3, model surfaces were developed and elaborated. Finally, the bacterial response of those model surfaces was investigated in chapter 4.

Organization of the manuscript

The manuscript of this work is organized in 4 chapters. After the general introduction, the context of the work is given in chapter 1. The description of the practical work starts from chapter 2. The chapters 2, 3 and 4 consist in a short introduction, the STATE OF THE ART, RESULTS AND DISCUSSION, SUPPLEMENTARY INFORMATION and finally a CONCLUSION. The manuscript closes with the GENERAL CONCLUSION and the OUTLOOK of the work.
The sections RESULTS AND DISCUSSION are written in form of scientific articles that are either published, submitted or in preparation except for the second part of the fourth chapter that is written in a classical form. Hence, aside from potential SUPPORTING INFORMATION section belonging to the article, a SUPPLEMENTARY INFORMATION section contains additional results and non included informations related to the subject of the article.

Chapter 1

Context

Nowadays, solid and soft implants, including their coating, attempt to provide better integration and to avoid infections. Yet, in most of the studies regarding implants and their coating, the adhesion response either of (macro)molecules/particles or cells is of the major interest, since the knowledge about the adhesion mechanism of molecules or cells is important to improve the human life quality. Besides, behavior of bacteria on these materials is often of secondary interest while crucial for the success of the implant. Properties of the biomaterial surface have likely a strong influence on bacterial adhesion. However, direct study of bacterial adhesion on biomaterial surfaces with specific properties is needed. Therefore, model surfaces mimicking some subtle surface characteristics are required. Furthermore, thorough knowledge through comprehensive characterization is needed to bring in relation specific bacterial behavior and specific properties of the surface. This chapter begins with a short introduction on biomaterials, especially about what kind of materials are used, followed by a paragraph on biomaterial-related infections, bacterial adhesion and surface properties influencing bacterial adhesion. Subsequently an overview on model surfaces, and their characterization is given.

1.1 Biomaterials

In general, the term "biomaterial" deals with a material that is in contact with a biological system. In 1987 Biomaterials were defined by the European Society for Biomaterials as '*a non viable material, used in a medical device, intended to interact with a biological system*' [22]. In the course of time, the definition was adapted and modified. In 1999, the ESB Consensus Conference II redefined biomaterial as '*a material intended to interface with biological systems to evaluate, treat, augment or replace any tissue, organ or function of the body*' [23]. In 2009, David Williams published a leading opinion article in the journal Biomaterials [24], in which he gave a precise definition of the term. Williams discussed at first the meaning of the prefix "bio" as life or living, i.e. considering if materials are made for biological application or made from biological tissue, '*taking out of life or putting into life*' [24].

Biomaterials are generally used as orthopedic implants (artificial hips, knees, intervertebral discs, bone grafts etc), cardiovascular implants (heart valves, pacemakers, stents etc), dental implants (fillings, enamels, prosthetics etc), soft tissues (intra-ocular lens, breast implants, wound healing etc) and in the surgical field (scalpels, surgical tools). In the classical view, biomaterials can be classified in: polymers, ceramics, metals and their composites [25]. Figure 1.1 illustrates a human body with the potential locations of implants.

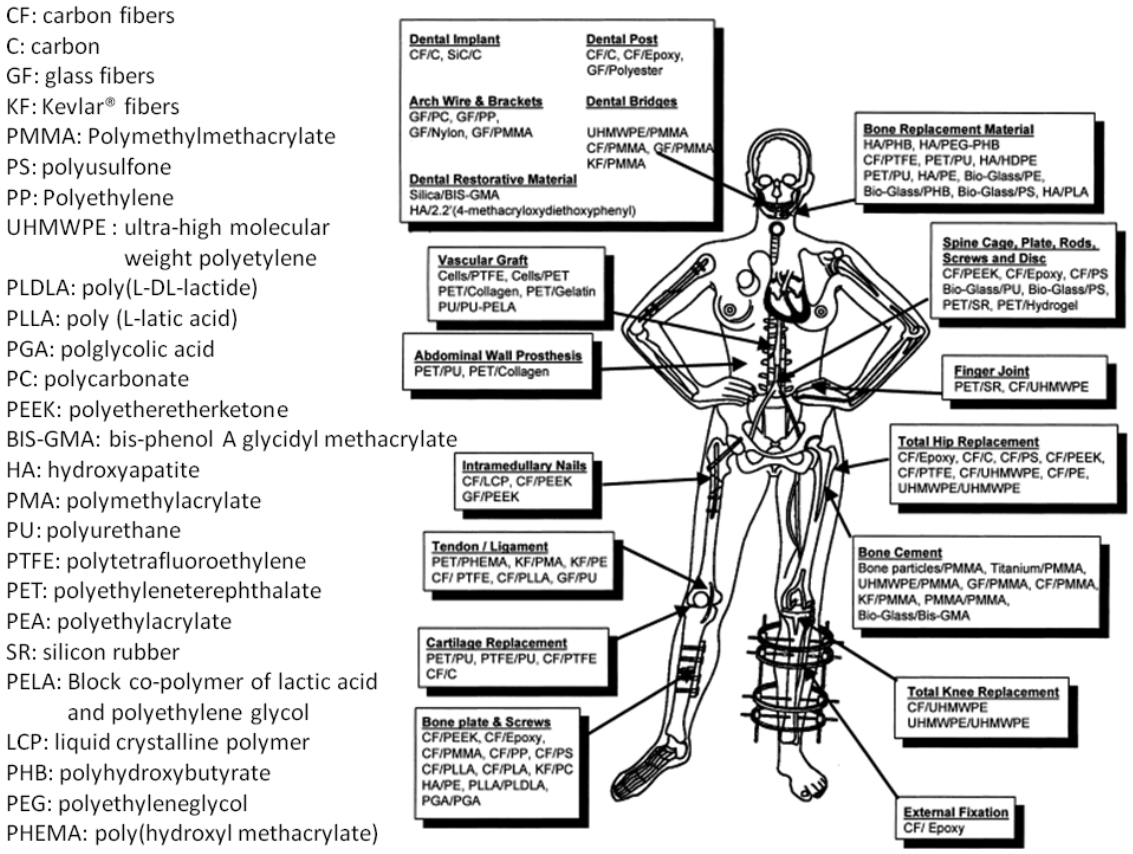

Figure 1.1: Typically, biomaterials like polymers, ceramics and metals are used as implants in the whole human body. Illustrated by Ramakrishna *et al* [26].

The type of biomaterial changes with its application, depending on the requirements of the implant and the material properties. Polymers, ceramics and metallic implants are here briefly addressed.

Polymers which are commonly used as biomaterials are polyurethane (PUE), polyethylene (PE), poly(methyl methacrylate) (PMMA), poly(ethylene terephthalate) (PET, Dacron®), poly(tetrafluoroethylene) (PTFE, Teflon®), hydrogels and biodegradable polymers like PGA, PLA etc. They are often used for the immobilization of biomolecules [27]. An advantage of polymers is that specific chemical properties of the material surface can be easily achieved by different compositions. Furthermore, polymers are easily to fabricate and formed in the required shapes and structures. However, additives that are often used

as stabilizer, degrade fast (chemically and biochemically) leading to life-time limitations of polymer-based biomaterials. Another disadvantage is due to the difficulty to sterilize polymers that may be changed through heating, UV as well as electron beam or gamma irradiation. In addition polymers may be too flexible for the mechanical demand of some implants [26, 27].

Bioceramics mostly consist diamond like carbon, alumina, zirconia, hydroxyapatites and bioglasses and are considered as biocompatible [27]. The advantage of bioceramics is that they have similar properties to bones, a high compressive strength (when they are dense) and their bioactivity can be varied depending on the material. Furthermore, bioceramics can be easily sterilized. One disadvantage of bioceramics is that they are difficult to fabricate [28]. Furthermore, they have a low fracture strength, a low reliability and lack of high density [26, 27].

Metallic biomaterials are typically stainless steel, Ti and Ti alloys, NiTi, Pt-Ir, tantalum, Co-Cr and gold [25, 27], they have a high mechanical strength and are very stiff. They have good fatigue and wear resistance and their fabrication is well-known. Nevertheless, many metals have a low biocompatibility, tend to corrosion and have a too high stiffness compared to the human tissues. Furthermore, some metal ions may be released and cause allergic tissue reactions [26, 27].

Other "materials" could be considered as biomaterials like tissues or organs according to the definition of Williams [24]. Their mechanical, topographical and chemical properties vary in a large range. In all cases, however, biomolecules constitute their surface.

Finally there are a huge variety of biomaterials in respect of the needs of their application. They are usually described with their global properties, like stiffness, strength, or physical-chemical properties. However, their description at the molecular scale is usually missing, although it is probably an important factor to understand biomaterial behavior, like success (i.e. integration) and failure (i.e. infection and removal) of implants.
Moreover, whatever their initial composition, biomaterials are covered with a layer of host proteins, shortly after their implantation and prior to any accumulation of inflammatory cells [29–32]. The chemical complexity of the biomaterial surface is therefore still increased.

In other respects, the surface of biomaterials can have been modified to achieve better integration of the implant [27]. In the last twenty years many surface modification techniques have been developed mostly to improve the ability of the biomaterial to alter the extent of protein adsorption [29] or to improve the colonization by eukaryotic cells [33]. This can be changed by the modification of the surface properties like surface wettability, hydrophobicity and surface charge [29, 34–36] or by the addition of specific functional groups like methyl (CH_3), carboxy (COOH), amine (NH_2) and hydroxyl (OH) [27, 37–39]. All these surface functionalizations induce chemical modifications that obviously still increase the molecular complexity of the surface.

1.2 Biomaterial-related infections

Gristina predicted in 1987 that "*ultimately, almost every human in technologically advanced societies will host biomaterials*" [28]. Hence, today, the number of patients that have a surgery to insert an implant increases over the time and with an aging population [40]. In 2030, for example the number of hip and knee replacements will increase by 174 % and 673 %, respectively [41]. Unfortunately, infections caused by implants parallely increases, consequently leading to pain for the patient. This also results in increasing costs of treatments, removal of numbers of implant and, in the worst case may lead to the death of the patient [28,42].

Biomaterial-related infections may occur when a non-living substrate is introduced in the human body. Such foreign materials have potential, favorable sites for bacterial adhesion. Then, bacteria can adhere and colonize the substrate, resulting in host response and infection [28]. In general, the infection of biomaterials can occur by following two different processes [40]. One is the direct inoculation, which happens during the time of implantation or through the manipulation of the implant giving a nosocomial infection. It is thought to be the predominant origin of infection. The second process is the so-named haematogenous seeding [40]. In this process, bacteria from a different infection site, e.g. the skin, are transported by the blood stream to the implant, and finally attach on the implant. It is an important cause of infection and may lead to in-situ deep infections [43].

Bacteria develop on implant surfaces as biofilms that, far from a simple accumulation of sessile bacteria, are bacterial communities embedded in exopolysaccharides that they produce [1]. Bacteria in a biofilm are notoriously resistant to antibiotics and host defense. They can persist on the substrate until its removal [28,40]. Indeed, although host defense is able to clear bacteria by antibiotics and phagocytes (see figure 1.2 A), it cannot fight against bacteria included in biofilms (see figure 1.2 B). The phagocytes are attracted by the biofilm and release phagocytic enzymes (see figure 1.2 C) but phagocytic enzymes damage the host tissues, while planktonic bacteria cells are released from the biofilm and may cause another infection in the neighboring tissue (see figure 1.2 D) [1].

Biomaterial-related infections involves the inoculation of pathogens, like *Staphylococcus aureus* or the transformation of nonpathogens, like *Staphylococcus epidermidis* to a virulent organism that produces a biofilm matrix [28]. Approximately 50 % of all the prosthetic joint infections are caused by gram-positive *Staphylococcus* species, followed by infections caused by gram-negative bacteria like *P.aeruginosa* and *E.coli* in 12.7 % of the cases [40]. The coagulase-negative *S.epidermidis* is the leading cause of infections related to medical devices [44,45].

Of course, the risk of infection depends on procedure of surgery, sterilization and patient-related factors. Factors like age, gender, body mass index, diseases or life style factors like smoking or alcohol habits may significantly increase the risk of infection [40,44]. However,

the type of prosthesis that is used also appears to influence the risk of infection [46]. Aside from the location of implantation, and the life-time of the implant in the body, properties of the biomaterial and its surface are crucial in this process.

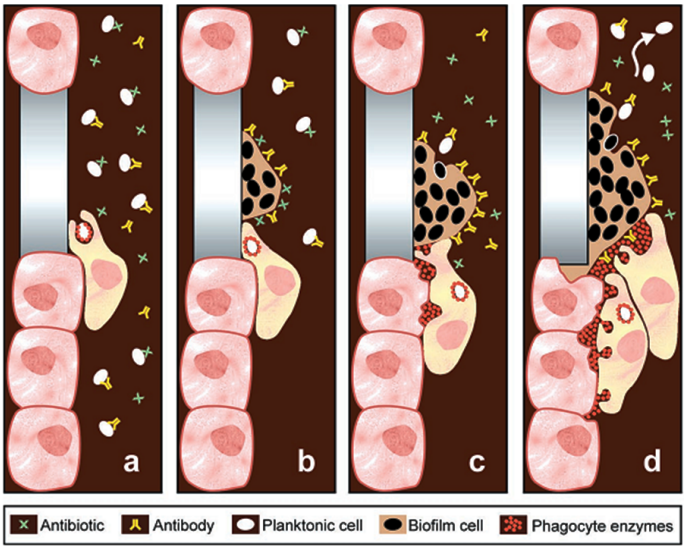

Figure 1.2: An implant in the human body can lead to infection of the surgery site by bacterial biofilm. (A) shows planktonic bacteria arriving near the implant. Bacteria are cleared by antibiotics, antibodies and phagocytes. (B) Bacteria adhere on preferentially inert surfaces and form a biofilm, being consequently protected from antibiotics, antibodies and phagocytes. (C) Phagocytes are near the biofilm and release phagocytic enzymes. (D) While the biofilm releases planktonic bacteria cells, the phagocyte enzymes damage the host tissue. Illustrated by Costerton *et al* [1].

1.2.1 Physical-chemical surface properties influencing bacterial adhesion

The physical-chemical properties of material surface play a crucial role in bacterial adhesion. Aside from impact of the roughness, the influence of chemistry was investigated in the last two decades. Thereby, the impact of three chemical main groups were investigated: The negative and positive charge introduced by chemistry, the hydrophobic and hydrophilic character, and various functional groups.

It was demonstrated that the surface charge of the substrate has an impact on bacterial adhesion and on bacterial growth [11, 47]. Typically, Gottenbos *et al.* showed that gram-positive and gram-negative bacteria adhere faster on positively charged surfaces than on negatively ones [47]. However, the proliferation behavior of bacteria is quite the opposite: Gram-positive and gram-negative bacteria grew less or did not even grow on the positively charged surfaces. Gottenbos *et al.* explained the favorable bacterial adhesion on positively charged surfaces by the absence of repulsive forces between negatively charged bacteria and positively charged substrate surfaces. However, the interaction between the positively

charged surfaces may affect the elongation process of bacteria cells, which is required for cell division. Depending on the nature of bacterial cell membrane, i.e. gram-positive or gram-negative, cell division may be possible or inhibited by the interaction with the substrate [11, 47].

Aside from surface charge, wettability character and corresponding surface energy are considered to be an important factor for bacterial adhesion. However, results of different studies often seem to be contradictory [3, 12, 14]. As an example, hydrophilic and hydrophobic hydrogels were used by Bruisnsma *et al.* to investigate bacterial adhesion [12]. The used gram-negative *Pseudomonas aeruginosa* bacteria strains were shown to adhere less on hydrophobic than on hydrophilic hydrogels. Furthermore they obtained a higher number of attached *Pseudomonas aeruginosa* than of attached *Staphylococcus aureus*, and the *Pseudomonas aeruginosa* were stronger attached to the surface than *Staphylococcus aureus* [12]. An example of contradictory study was reported by Cerca *et al.* [14]. They performed bacterial adhesion studies with eleven *Staphylococcus epidermidis* strains on glass substrate and acrylic substrates. The glass substrate was considered as hydrophilic with a water contact angle of 23 ° and the acrylic substrate was considered hydrophobic with a water contact angle of 85 °. They found that the acrylic surface favored the adhesion of eight strains out of eleven initial strains and furthermore, the amount of biofilm on acrylic substrate was higher than on glass substrate. These results are therefore apparently opposite of those of Bruinsma *et al.*. However, materials and methodology used in most of the literature are, like in these two examples, very different. For resolving such apparent contradiction and determining the effect of more subtle surface properties, model surfaces, such as created by self-assembled monolayers and more sophisticated biological investigations appear to be essential.

The impact of functional groups like CH_3 [13,16,17,20,21,48], NH_2 [16,20,48], OH [13,20, 21,48] and COOH [21,48] on bacterial adhesion have been showed. However, the surfaces have always been simply described by their wettability character [10,13,16,49] or, in some cases, their zeta potential [20,48]. Some authors reported similar colonization on CH_3 and OH [21] or CH_3 and NH_2 [16] terminated surfaces.

In addition, mixed monolayers (MMLs) can be obtained by a mixture of two or more silanes to achieve surfaces with various densities of one functionality backfilled with a second (OH and CH_3). Wiencek *et al.* [10,49] studied the adhesion of *Pseudomonas* strain under hydrodynamic conditions. They showed that bacteria adhered less on surfaces with a high amount of OH, than on surfaces with a high amount of CH_3. Further, they showed that the desorption rate of bacteria was lower from surfaces with a high amount of CH_3. Despite a comprehensive approach of the bacterial behavior on these model surfaces, the incomplete description of substrates, mainly based on wettability measurements, prevents to address the topic of the relationship between bacterial behavior and the chemical surface composition at the molecular scale.

The effect of shear rate on bacterial/material interface has also been studied. At a low shear rate 50 s^{-1}, Tegoulia *et al.* showed similar bacterial adhesion on CH_3, COOH and OH terminated surfaces. However, by increasing of the shear rate (250 s^{-1}), more bacteria were adherent on CH_3 surfaces than on COOH and on OH. Katsikogianni *et al.* found the same tendency of bacterial adhesion for *S.epidermidis* strain; (CH_3 > (NH_2) > COOH > OH) [48], which however, was maintained whatever the shear rate (from 50 s^{-1} to 2000 s^{-1}).

Finally, even if the literature already demonstrated that the physical-chemical properties like the wettability or surface charge play a crucial role for bacterial adhesion (see figure 1.3) and also allowed to extract some general tendencies, the results of performed experiments remain contradictory. They depend strongly on the (model-) surfaces, experimental set-up and bacteria strains. Above all, the global surface description using wettability or charged character at a macroscale may screen subtle effects that the functional groups present at the surface may induce to bacterial adhesion and development.

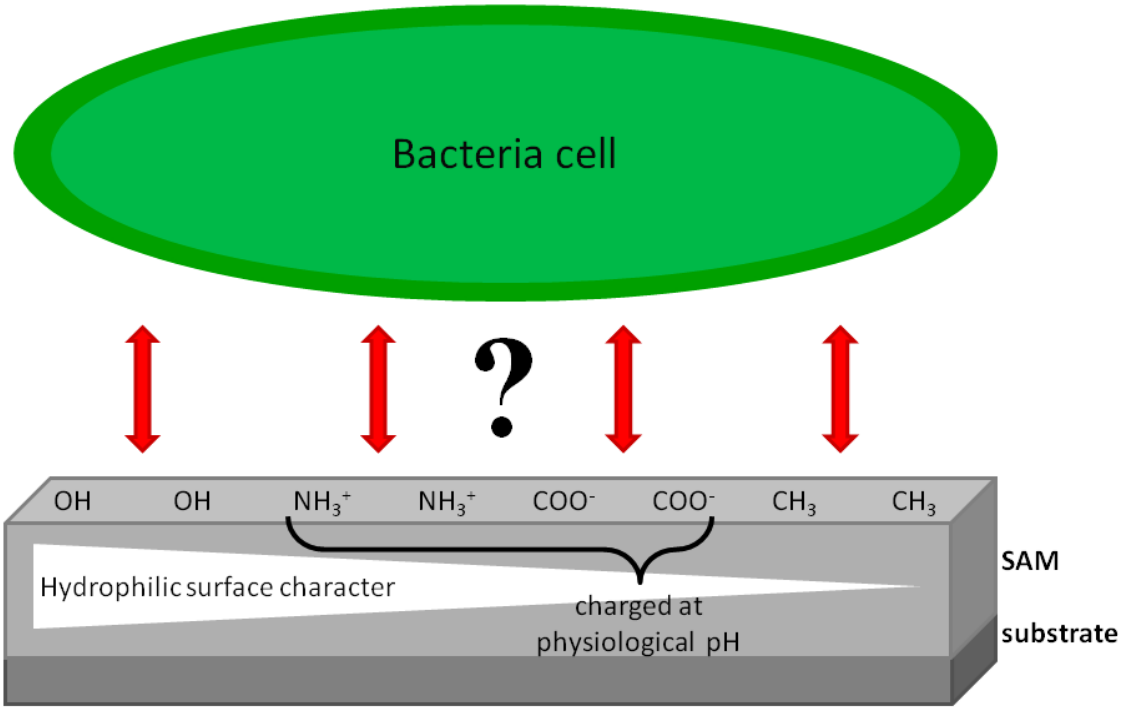

Figure 1.3: Bacterial adhesion is often studied on self-assembled monolayers, however the impact of the functional groups remains unclear.

1.2.2 Understanding bacteria sensing of the surface and its biological response

Aside from the role of the material surface on bacterial adhesion, the question of whether bacteria are able to sense the surface and its properties has not been elucidated yet.

Specific interaction between surfaces properties and bacteria cells was also shown in an experiment performed on *Escherichia coli* [50]. Within the first hour of cell adhesion on hydrophobic surfaces, bacteria were activating the Cpx-signaling pathway, which is suspected to play a crucial role in the control of initial cell-surface interaction. However, the expression of the Cpx-pathway in adherent cell on hydrophilic surfaces showed no differences compared to the gene expression of planktonic cells. Hence, certain physical-chemical properties of the surfaces may activate specific processes in the bacteria metabolism during the initial bacterial adhesion [50,51]. Specific changes in the expression of curli in *E.coli* cells, caused by the interaction between a material surface and bacteria cells, have been reported by Cottenye *et al.* [52]. In this study, the used bacteria strain produced GFP parallel to the curli synthesis. Cottenye *et al.* hypothesized that the curli over-expression was induced by interactions between bacteria and the negatively charged oligonucleotides functionalizing the substrate.

Although literature addressing this topic is rare, it was already demonstrated that the gene expression changes between initial adhesion, biofilm formation/maturation and final detachment [50,53]. For example, it was shown that *Pseudomonas putida* expresses genes for flagella in planktonic cells, but after adhesion to surface, the expression was down-regulated until a mature biofilm was reached [53].
In mature biofilms, Prigent-Combaret *et al.* showed in 1999 that 38 % of the genes are differently expressed in sessile and planktonic *E.coli* K12 mutants, including genes, which are responsible for e.g. flagella, exopolysaccharide or cell-to-cell signaling [54]. This was also shown for *Pseudomonas aeruginosa* with more than 50 % of differences in gene expression between sessile and planktonic bacteria [55]. However, whether bacteria change their gene expression just when interacting with a surface, which may result in changes of the membrane protein that have an influence on bacterial attachment, remains difficult to prove experimentally.

Finally, surface sensing and especially sensing of material surface properties by bacteria is still a mystery.

1.3 Model-surfaces and surface description for studies at biointerfaces

Several methods have been proposed to develop homogeneous and well-defined surfaces. The required surface modification can be achieved by plasma mediated techniques, modifications by chemical grafting, and self-assembled monolayer techniques [29]. Through plasma modifications, various functionalities can be obtained and the process of plasma modification is compatible with most of the materials used in medicine [27, 29, 39] like polymers [56], ceramics [57] and metals [58]. Modifications by chemical grafting allows to chemically immobilize compounds, e.g. protein or monomer, onto the surface of bioma-

terials through covalent grafting, thus altering the surface chemistry [29]. Nevertheless, both methods do not allow to control conformation and organization of the molecules. Furthermore, surface topography in particular at the molecular- and nanoscale, cannot be rigorously controlled.

On the contrary, self-assembled monolayers (SAMs) offer the possibility to control the density and the conformation of single or multiple functional groups on the surface. Furthermore, they provide flat and chemically well defined surfaces. They are therefore, very good candidates to prepare very well-defined and well-organized platforms for studies at the bacteria/material biointerface [59,60].
Nevertheless, their careful and detailed development and elaboration must then be supported by a comprehensive description through a thorough characterization of their properties.

1.3.1 Self-Assembled-Monolayers

In 1946, Bigelow *et al.* discovered a reversible adsorption of molecules in hexadecane on platinum or glass substrates. They argued that long-chain molecules adsorbed on surfaces are densely packed, and giving less roughness than the underlaying substrate [61]. They further concluded that non-Langmuir-Blodgett[1] orientated monolayers can be prepared in different solvents with different polar molecules. The same research group conducted several experiments and pointed out that the control of relative humidity and temperature are crucial for the experiment. Various molecules with different chain-lengths were used and also the effect of solvent was investigated [61].

Despite this early article, the researchers payed attention to self-assembled-monolayers only in the 80ths. Then SAMs became of high interest. At the beginning, glass slides were used as substrates [63]. In 1983, Nuzzo and Allara prepared the first thiolate-based SAMs on a gold substrate [64], and this work promoted the investigations of SAMs on gold substrates until today [65]. Pomerantz and Sagiv performed many basic studies in which SAMs, deposited on different substrates, mainly on silicon wafers, were thoroughly characterized [66–68] and compared to Langmuir-Blodgett films [67,68]. SAMs were then used for many applications including the modification of surface properties like hydrophobicity, hydrophibility or biocompatibility [69].

SAMs are formed in a spontaneous, simple process, where the molecules are adsorbed onto a solid surface (see Figure 1.4). Therefore, the molecules are dispersed in a liquid support (active solution) [70]. The molecules are assembling themselves on the surface resulting in a well defined two-dimensional system. Commonly used self assembling molecules are silanes, diphosphates and thiolates. Thiolates form SAMs on gold, while silanes and diphosphates

[1] Langmuir-Blodgett films are one or more monolayers of organic molecules formed by immersing or emersing of a substrate, the molecules being physisorbed [62].

are forming SAMs on hydroxylated metals [65] such as silicon wafer.

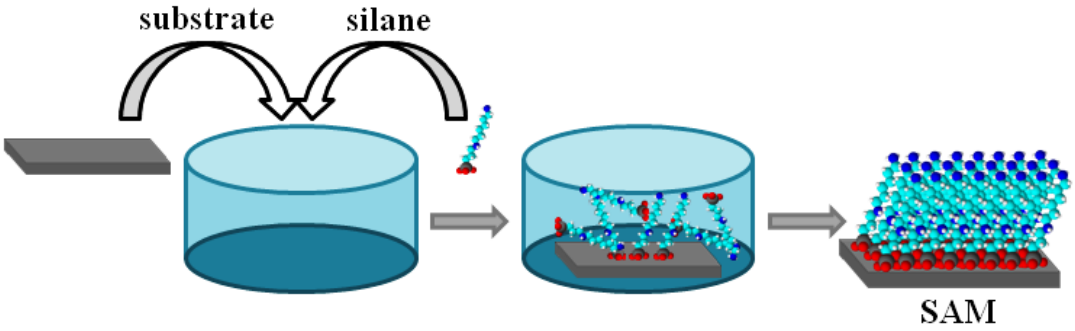

Figure 1.4: The figure shows the preparation of self-assembled-monolayer on a surface. In the first step, the substrate and the self-assembling molecules are put together in a vessel. The molecules are adsorbed on the surface and finally self-assembled-monolayers are obtained on a solid substrate.

Controlled surfaces on silicon wafers are generally difficult to obtain by introducing organosilanes (especially aminosilanes) in liquid phase [71]. The grafting mechanism of trichlorosilanes was first published in 1991 by Silberzan *et al* [62], a schematic of this mechanism is shown (in figure 1.5). It can be described in four separate steps [72, 73]:

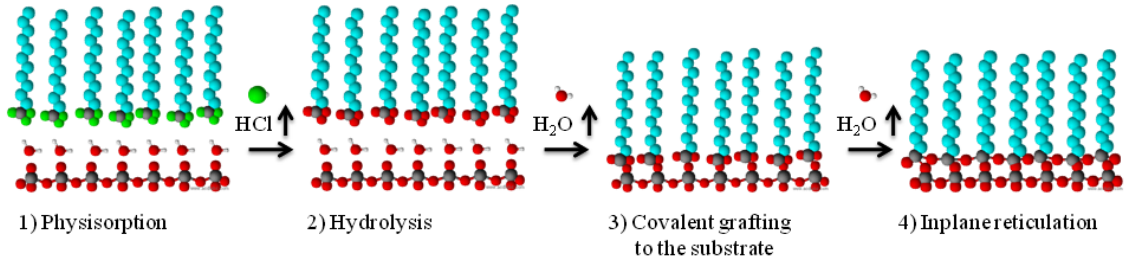

Figure 1.5: Schematic of the grafting mechanism of trichlorosilanes. The first step of the silanization is the physisorption of the silane, the approach and the alignment of the silane. In the second step, the chlorosilane hydrolyzes. The hydrolyzed silanes are then able to react with the silanol groups of the surface, after release of water. To stabilize the silane, an annealing step is required to remove residual water traces.

(1) the physisorption of the silane on the substrate, followed by (2) the hydrolysis of side chains. In these first two steps, an aqueous phase is intercalated between the substrate and the silane. Finally, the silane is grafted covalently (3) onto the substrate and (4) an in-plane reticulation takes place [73] between the neighboring Si-OH-groups, by a removal of a water molecule. The aqueous phase is important for the physisorption, and the exchange of the chloryl- by hydroxyl-groups. Nevertheless, it is not required to add additional water: some publications show that after complete dehydration of the system, the grafting is not optimal and that a small quantity of water is necessary to achieve good grafting as well as good compaction [74]. Dehydration of the layer by a final annealing step favors retic-

ulation between adjacent silanol groups and appears to be crucial for the stabilization of the monolayer. Hence, by increasing the stability a long term stable [75] 2D polysiloxane networks [71] can be obtained. This stable substrate is important for application in liquid ambiance. Silanes can carry reactive groups, like amine groups, which are necessary for further immobilization of the biomolecules of interest [59].

In the following, the characteristic and the principle of the self-assembled monolayers is described.
Self assembling molecules can be separated in three different parts: the head group, the chain, and the surface group. The head groups, mostly illustrated as SiX_3 where X=Cl,OCH_3 or OC_2H_5, reacts (exothermic) with surface groups of the substrate. The Van der Waals forces increase with the lengths of the chain, mostly an alkyl chain -(CH_2)-, which leads to a highly organized structure. The surface group is the terminal group and determines the functionalization of the surface.

Aside from the homogeneous SAMs, so-named mixed monolayers can be also obtained by the use of two or more surfactants with two or more functional groups [63]. Mixed monolayers are of particular interest to modulate surface properties like wettability character or charge at the molecular scale.

Hence, SAMs and mixed monolayer provide a high potential for biointerface studies. In example, they offer the possibility to graft other (bio)molecules to further modify the surface chemistry.

1.3.2 Characterization of surfaces for biointerface studies

As we already evoked, interactions between a biological system and a material depend strongly on the physical-chemical properties of the material. We believe that these properties are able to play a role, not only at "macro-" but also "nano-" and molecular scale. Hence, for an accurate interpretation of the experimental data, the surface has to be thoroughly characterized and analyzed [76]. However, in literature addressing interactions between SAMs and bacteria, the surfaces are rarely completely characterized [19, 77].

The substrates are mostly analyzed by contact angle measurements [10, 12, 13, 16, 33, 47, 52, 78–80], but surface energy [20] is rarely calculated. XPS (X-ray photoelectron spectroscopy) measurements [10, 13, 18, 20, 52, 81–85] are frequently used, yet mainly only to determine the elementary composition. In addition, thickness is determined by ellipsometry [13, 86], roughness by AFM (atomic force microscopy) [12, 16, 20, 33, 80, 87–89] and surface potential (charge) is expressed by zeta potential measurements [12,20,47,78,83,90]. Amorphous silica substrates were also characterized by TOF-SIMS (time of flight-secondary ion mass spectroscopy), along with zeta potential [91] while, very recently, Huang *et al.* fabricated a LR-SPR (long range-surface plasma resonance) chip on which the thickness of the coating was determined by ellipsometry [52,86,87,89,92].

Despite this variety of techniques, techniques are rarely used together for a careful and thorough characterization of the structure and the molecular organization. In addition, several researcher assume the ideal structure of SAMs substrates that is used for biointerface studies. However, as shown partial in literature [93–95] and in the following chapter, SAMs deposited on surfaces may be organized in multilayers etc. Hence, an accurate characterization, by an appropriate combination and careful analysis of data, should allow to comprehensively describe the surface [76].

Finally, despite the use of sometimes sophisticated methods, the surfaces used for bacterial adhesion studies are seldom fully understood. Not rarely, surface properties are finally "confirmed" by bacterial adhesion behavior [19, 77].

1.4 Conclusion

In this frame, the goal of the present work is to establish a material that can be used for bacterial adhesion investigations focusing on subtle properties of the surfaces as those really present on biomaterial surfaces. It should be therefore a well defined material, where the chemistry can be specifically changed as requested, without modification of the surface topography. This last property should be kept as smooth as possible. Silicon wafers are therefore the substrate of choice, thanks to its negligible surface roughness, when cut from a single crystal. The well-studied system of self-assembled monolayers (SAMs) was chosen to modify the surface of this metal. SAMs allow to control density and organization of the molecules, as well as structure of layer. Finally, these model surfaces will be used to study whether the chemical properties of the surface at the nano-/molecular scale are able to impact bacterial behavior and biofilm formation.

Chapter 2

Characterization of model surfaces based SAMs

2.1 Introduction

The characterization of the surface is crucial to understand the physico-chemical features of the substrate and subsequently for understanding the mechanisms of bacterial adhesion or molecule/particle adsorption. The importance of a well-known surface is usually accepted by all authors. Nevertheless, there are many examples in literature, where apparently well-known systems are used without the necessary characterization. Hence, the fabricated surface may have quite different properties to the assumed ones.

Silicon wafers are often used as substrates, with the purpose of diverse applications or studies. The use of SAMs on silicon substrates is common and allows the functionalization of the surfaces as required. Hence, one is prone to assume that by the use of SAMs, the "ideal" surface is obtained. However, results coming from single technique are mainly not sufficient to describe the nature of the surface and many other physical-chemical features are not considered. It is well known, in literature, that APTES leads to multilayer [76]. The short silane 3-aminopropyltriethoxy-silane (APTES) deposited on a silicon wafer is one example of such misleading characterization. Nevertheless, APTES functionalized surfaces are commonly used as substrates for biointerface studies. The characterization of such surfaces shows the presence of nitrogen, which together with a hydrophilic contact angle, may convince of the presence of an APTES monolayer. Yet this amount detected by XPS is often too high for a monolayer, finally indicating the multilayer structure. APTES for example is widely discussed to form multilayers [93–95], as mentioned above.

Results obtained on a wrong assumption may lead to a wrong interpretation of the experiment and consequently to a wrong conclusion. Therefore, it is important to carefully characterize the whole system as well as each step of reaction on the surface to be sure of the surface properties used for further biointerface studies.

Two silanes, APTES and N(6-aminohexyl)aminopropyltriethoxy-silane (AHAPS), that are often used in literature, were chosen to study the efficiency of the characterization of model surfaces grafted on silicon wafers. In a second step a biomolecule was grafted on AHAPS functionalized surfaces by the commonly used linker glutaraldehyde. The chosen silanes are not ideal candidates to obtain SAMs, prepared in liquid conditions. However, they are relevant tools to study the ability of a surface characterization approach to highlight potential defects in layer structure and molecular organization. The surfaces were investigated by combination of different characterization techniques and the results carefully analyzed.

The characteristics of the layers made of the two used silanes are discussed and it is figured out, which combination of characterization techniques is necessary to sufficiently describe the surface in a more realistic model. Due to the knowledge of the surface and its structure, bacterial adhesion experiments should be better interpreted, founded on the realistic properties of the surface.

In this second chapter, four model surfaces were fabricated under simple conditions, thus they can be prepared in every laboratory. Alkoxysilanes were used to functionalize the silicon substrate. These silanes are commonly used to modify inorganic and organic surfaces since they bind covalently to the surfaces [96]. Model surfaces used in this work were obtained by two one-step (APTES and AHAPS), one two-steps (AHAPS-GAD) and one three-steps (AHAPS-GAD-glutamine) procedures. The surfaces were analyzed systematically using different characterization techniques (XPS, contact angle measurements, ellipsometry, zeta potential and AFM) and the experimental data were combined together. By combining the results, the description of the APTES surface which was already illustrated in literature could be confirmed. New descriptions were developed for the other three surfaces (AHAPS, AHAPS-GAD, AHAPS-GAD-glutamine).

The chapter is based on the article *Necessity of a Thorough Characterization of Functionalized Silicon Wafers before Biointerface Studies* that has been published in the *Journal of Physical Chemistry C* in 2011 (volume 115, pages 11102-11111, doi:10.1021/jp201377n). A supplementary information section addresses related topics that are not evoked in the publication.

2.2 State of the art

As mentioned above model surfaces are developed to describe the physical-chemical features of the surfaces. Here, the model surfaces are SAMs deposited on silicon wafer. In general, different features of such monolayers can be analyzed by diverse techniques. Thereby, the quality of the SAMs can be determined through five characteristics of the deposited layer: (i) chemical composition, (ii) thickness, (iii) molecular orientation and ordering, (iv) uniformity and coverage and (v) the thermal and chemical stability [70].

The most commonly used technique to characterize the chemical composition (i) of surfaces is X-ray photoelectron spectroscopy (XPS). XPS analyses can give information about the oxidation of elements and about the chemical environments (chemical bonds) [97]. Two different modes are commonly used to analyze the surface: the chemical composition by monitoring a survey spectrum and the chemical environment by recording a high resolution spectrum, a spectrum over a certain interval of the kinetic energy. Thereby, the high resolution spectra provides detailed information about the structure [76]. The chemical deposition can also be analyzed by other techniques as Auger electron spectroscopy (AES) and secondary ion mass spectroscopy (SIMS) [70].
An advantage of XPS is that through changing the take off angle the depth of the probe changes, too. Over 90 % of the probed signal arises from a depth into the solid within 3λ, while the probe depth is defined by equation 2.1

$$d \; = \; 3\lambda \; \sin\alpha, \tag{2.1}$$

where λ is the inelastic mean free path of the emitted electrons, and $\sin\alpha$ is determined by the take off angle of the emitted electrons to the surface [97].
The thickness (ii) is frequently characterized by optical ellipsometry. The experimental obtained thickness can be compared with a calculated fully extended length of the molecule by adding bond lengths [70, 98]. For methyl terminated silanes the following equation 2.2 is used:

$$l\,[\mathring{A}] \; = \; 1.26 \; \cdot \; (n-1) \cdot \phi \; + \; 1.33 \; + \; 1.521 \; + \; 1.93, \tag{2.2}$$

where l is the length of the extended silane, 1.26 is the length of $(n-1)$ CH_2 units in the main chain, ϕ is the tilt angle of the monolayer and 1.33, 1.521 and 1.93 are the bond lengths of Si-O, C-Si and terminating CH_3 groups, respectively [70,98]. Methyl terminated n-alkylsilanes are assumed to deposit with a tilt angle of $< 30°$ [70]. Beside ellipsometry other techniques that are used to measure the thickness of SAMs are plasmon surface polarization [99] and X-ray techniques [98, 100].
Informations about the molecular orientation and ordering (iii) is provided by Fourier-transform infrared spectroscopy (FTIR). The FTIR measurements are usually done in two different spectroscopy modes: attenuated total reflection (ATR) and reflection-adsorption (RA) mode. This technique allows to calculate the tilt angle of the deposited monolayer, which can be used for the calculation of the theoretical thickness. Further, information about the molecular order in the monolayer can be obtained by analysis of the peak position of symmetric and assymetric stretching modes of CH_2 groups [101, 102]. However, the characterization by IR measurements of SAMs on silicon wafer need special attention [103]. Due to the fact, that the Brewster angle of the air/silicon interface is close to the grazing angle, most of the light passes through the sample and can not be detected. Therefore, Liu *et al.* modified the set up of multiple internal reflection (MIR) technique and combined it with grazing angle mirror-backed reflection (GMBR) method [104], to increase the sensibility of the technique. These modification allows quantitative analyses of SAMs on silicon wafer [103].

X-ray [105], electron and neutron diffraction [106, 107], high resolution electron loss spectroscopy [108], Raman spectroscopy [102, 109], near-edge X-ray absorption fine structure spectroscopy (NEXAFS) [110, 111] are used as well to obtain information about the orientation and the ordering of SAMs.
The uniformity and coverage (iv) and thus the quality of the layer can be assessed by its wetting character [98, 102] or by the imaging of the topography [110, 112, 113]. The wettability character of a surface is determined by simple contact angle measurements. The shape of the liquid depends on the free energies of the liquid and the solid. The contact angle is determined by the properties of the functional groups, the alkyl chain may influence the angle through ordering, packing and the tilt. The topography can be visually analyzed by atomic force microscopy (AFM), scanning electron microscopy (SEM). Several research groups investigated e.g. the growth, aggregation and covering of a monolayer on surfaces by AFM [110, 112, 113]. Aswal *et al* depicted the process of the monolayer growth as a function of time (see figure 2.1) [70].

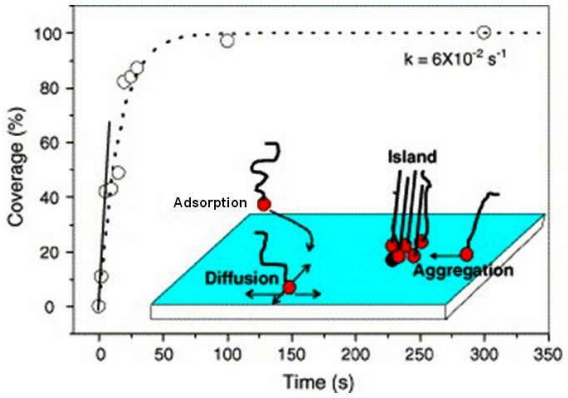

Figure 2.1: At first, small islands are formed through well packed surfactants (i.e. silanes). These islands serve as centers for aggregation, for molecules diffusing on the surface and adsorbing from solution. In the final stages, the areas between domains are filled in by surfactants [113].

Further, SAMs modified electrodes can be electrochemically characterized by e.g. cyclic voltammetry (CV) and electrochemical impedance spectroscopy (EIS), which give information about the surface coverage and the defects in the structure. Such defects are commonly pinholes in the monolayer [114–116]. The principle of these techniques is based on the capacity of densely packed SAMs, which provide an effective blocking of the chemical reactivity at the coated electrodes. Hence, with the decrease of the blocking ability, the defects in the layer increases [114, 115]. The uniformity of the coverage can be analyzed by low angle reflection, which indicates if the surface is uniformed covered or if there are regions without surface coverage and regions with multilayer coverages [98].
Finally, the thermal and chemical stability (v) is usually evaluated by the following, the thickness or the contact angle. Thereby, the SAMs are immersed e.g. in acid or base solu-

tion over time, while either the contact angle or the thickness is monitored. As reviewed by Aswal *et al.*, the thermal stability was found to be independent of the chain length and the SAMs begin to decompose at a temperature higher than 350 °C, through the cleavage of the C-C bonds [70]. SAMs seem to be stable when washed in 1 % detergent solvent, hot water or organic solvents. However, SAMs are fast degraded, when exposed to aqueous base (0.1 N NaOH). Through the hydrolysis of the Si-O bonds, the monolayer can be removed within one hour [98].
In general, there are diverse possibilities and techniques to characterize SAMs. Beside this variety, especially for biointerface studies, the SAM substrate is often only poorly described. In some cases, the substrates used for bacterial adhesion studies are only analyzed thanks to the bacterial response [19, 77]. Hence, the results of these studies are based on the assumption of an ideal monolayer deposited on the surface. Nevertheless, for biointerface studies, a thorough characterization of the substrate is crucial to be able to consider all physico-chemical features and to correlate them to bacterial response.

In this work, the following techniques were used to obtain enough results for a adequate description of the analyzed model surfaces: X-ray photoelectron spectroscopy, water contact angle measurements, ellipsometry, atomic force spectroscopy and zeta potential.

2.3 Material and Methods

2.3.1 Substrate

Silicon wafers can be used as basis for biosensors, because of their semi-conductive properties. Further, well and highly organized surface functionalization can be obtained by using SAMs.
One side polished N/phosphorus doped silicon wafers with a crystallographic orientation of [100] $\pm$ 0.5 $^\circ$ (resistance of 3.5-5.5 Ω/cm, thickness of 380 $\pm$ 25 μm and a diameter of 76.2 $\pm$ 0.6 mm) furnished by MCR in Germany were used as substrates. The wafers were cut into 1x1 cm^2 pieces. They were cleaned by 10 min ultrasonical rinsing in $CHCl_3$ and afterwards activated by piranha treatment: the wafers were immersed for 30 min and at 50 °C in a solution of 1:3 H_2O_2 25 % vol to H_2SO_4 99 %, followed by a thorough rinsing with MilliQ water to remove all piranha solution from the surface. The immersion in $CHCl_3$ provides the removal of organic contaminations due to the atmosphere. The second cleaning step, removes an existing oxide layer. This layer contains a lot of traps, hence it is recommended to remove the existing one and form a new thin oxide layer with a high density of silanol groups [70]. Activated wafers were immediately used for surface modifications.

2.3.2 Surfaces

In this chapter model surfaces used for the characterization of monolayers on silicon wafer are: (i) APTES (3-aminopropyltriethoxy-silane) and (ii) AHAPS (N(6-aminohexyl) aminopropyltriethoxy-silane), AHAPS-GAD (N(6-aminohexyl)aminopropyltriethoxy-silane-GAD) and AHAPS-GAD-glutamine (see Figure 2.2).

The preparation of the surfaces, their properties and conditions are described in detail in article 1 (see chapter 2.4).
The APTES surfaces were prepared in solution, which should lead to a multilayer. The activated wafers were immersed overnight in a solution of 1 mM silane in acetone. Afterwards, the samples were rinsed with acetone and rinsed shortly in acetone by ultrasonication.
For the second group of surfaces, the activated wafers were first immersed overnight at room temperature in ethanol containing 1 mM of N(6-aminohexyl)aminopropyltriethoxy-silane (AHAPS). Subsequently rinsing with ethanol and a short ultrasonical rinsing in ethanol removed residual ungrafted molecules. AHAPS functionalized surfaces were immediately used for further reactions.
In this chapter, GAD is used as a linker between AHAPS functionalized surfaces and glutamine. AHAPS samples were immersed for 2 h in a solution of 10 vol-% GAD in MilliQ water at pH 5-6. Afterwards, the surfaces were rinsed with MilliQ water to remove ungrafted aldehyde molecules.

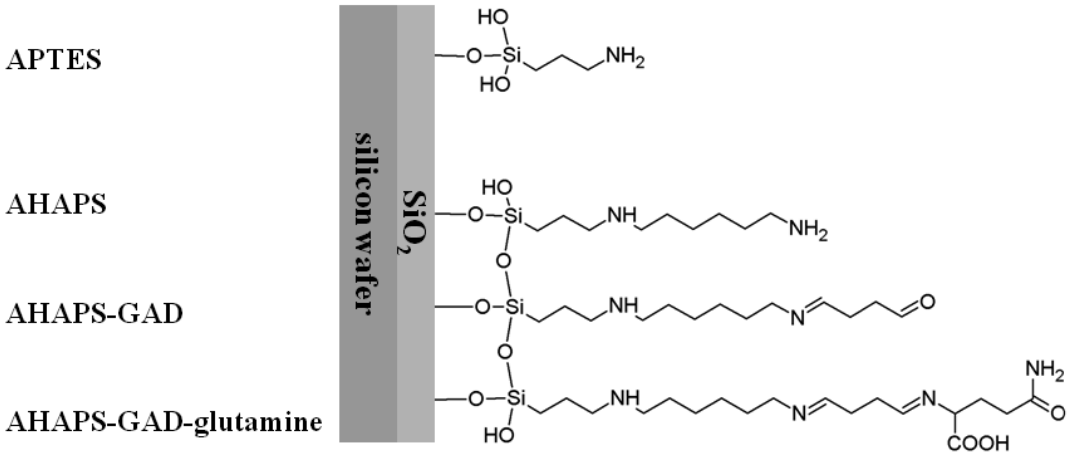

Figure 2.2: Schematic of SAM model surfaces on silicon wafer, including two single SAM model surfaces with APTES and AHAPS, the two step model surface AHAPS-GAD and eventually the three step model surface AHAPS-GAD-glutamine, where glutamine represents a biomolecule that is grafted onto a functionalized surface.

The essential amino acid glutamine was used as model biomolecule. Glutamine was grafted onto GAD activated surfaces. The GAD-activated surfaces were immersed overnight in a solution of 1 mM glutamine in MilliQ water and a pH between 5-6 to favor the formation of Shiff bases. Afterwards, the samples were rinsed thoroughly with MilliQ water (see article 1 on page 35).

2.3.3 Surface analysis and treatment of results

The atomic ratio and the chemical environment were analyzed by XPS. Also based on XPS measurements, the thickness of a homogeneous covered surface in vacuum was calculated based on the intensity of the substrate signal. This value of the grafted layer thickness, gives a complementary information to the thickness values determined by ellipsometry in air and in liquid. These two techniques give information on the silane films into three states of dehydration: (1) fully dehydrated (XPS, ultra high vacuum condition), (2) fully hydrated (ellipsometry in liquid), and (3) in partially dehydrated state(ellipsometry in air). The water contact angle indicated whether the surface had a hydrophilic or hydrophobic character. The hysteresis, i.e. the difference between the advancing and receding contact angle, indicated whether the surface was homogeneous (small hysteresis) or heterogeneous (large hysteresis). AFM images displayed the surface topography, also revealing homogeneous or heterogeneous character of the surfaces. In addition to these common characterization techniques, the pH titration was performed to determine the iso electric point (IEP) of the surface, which provides indications about the charge of functional groups on the top of the layer, as well as the zeta potential of the surface at a physiological pH (pH = 7).
Technical conditions and the use of the different techniques are described in article 1 (see

chapter 2.4). Supplementary information about the principle of each technique and the analysis of the data that they provide are presented below.

2.3.3.1 X-Ray photoelectron spectroscopy

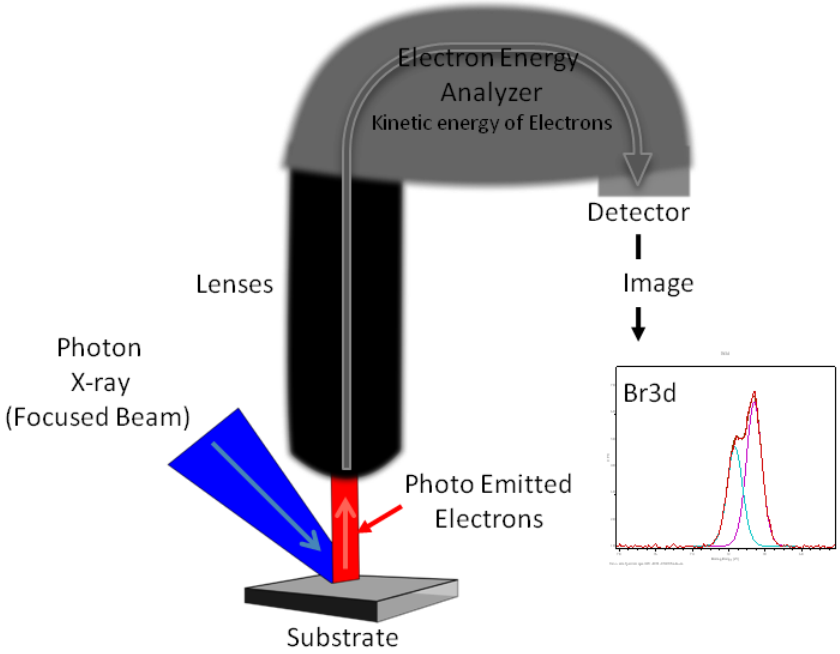

Figure 2.3: XPS analysis: The sample is irradiated by X-rays resulting in electron emission from the surface of the sample into an ultra high vacuum. Electrons are focused/collected by lenses, passing an electron energy analyzer and are detected by an electron detector. An imaging software plots the counted number of electrons versus the binding energy and allows for subsequent analysis of the raw data.

2.3.3.1.1 The principle of XPS measurements

XPS is a quantitative spectroscopy, which is well qualified for the analysis of element composition and chemical environment of, in general, solid samples. The principle of XPS is depicted in figure 2.3. A beam of X-rays irradiates the sample and induces photoelectron emission. The photoelectrons escape from the surface i.e. from a depth of approximately 9 nm from the surface into ultra high vacuum. The emitted electrons pass several lenses before their kinetic energy $E_{kinetic}$ is analyzed by an electron energy. Finally, the electrons are detected and their number is counted in time units. A raw data spectrum is obtained in which the number of detected electrons is plotted versus their corresponding kinetic energy. According to Ernest Rutherford (1914), the kinetic energy is correlated to the binding energy $E_{binding}$, the energy of the X-ray source E_{photon} and the work function ϕ

of the spectrometer, as defined by equation 2.3.

$$E_{binding} = E_{photon} - (E_{kinetic} + \phi)\,, \tag{2.3}$$

where $E_{binding}$ is the binding energy of the ejected energy, E_{photon} is the photon energy, $E_{kinetic}$ is the kinetic energy of the photoelectrons and ϕ is the work function of the spectrometer. The work function depends on the spectrometer. Specific peaks are obtained for each element due to the characteristic of the electron configuration for each element. Except for elements with an atomic number (Z) ≤ 3 like hydrogen, helium and lithium, the probability of detection is very low, due to their small size of the atom. Atomic percentages can be determined by analyzing and normalizing the area of an XPS peak. XPS photopeaks are normalized by the relative sensitivity factor (RSF, Scofield cross-section factors) that is also characteristic or an element or an electron configuration.

In this work, the chemical composition of the surfaces was determined with a Gammadata Scienta XPS spectrometer, equipped with a monochromated Al K_α X-ray source (1486.6 eV) under ultra high vacuum and a take off angle of 90 °. Survey and high resolution spectra were recorded at a pass energy of 500 eV and 100 eV, respectively. For high resolution experiments, the energetic resolution was estimated to 0.45 eV. All spectra were analyzed and peak-fitted using CasaXPS 2.3.12 software (Casa Software Ltd, Teignmouth, UK, www.casaxps.com). All components were referenced according to the CH_x component at 285.0 eV and the full width half maximum (fwhm) of the fitted peaks was constrained to be constant for all components in the same spectrum. The relative binding energy of all components was fixed and maintained constant for all peak-fitting procedures (see Table 2.1). The evaluation of the organic layer thickness was done according to equation (2.4) [97], which is based on the Lambert-Beer's law, assuming that this layer is homogeneous. The corrected intensity of a surface was calculated according to the conventional integration of the XPS signal given in equation 2.5.

$$I_B = I_B^\infty e^{-\frac{d}{(\lambda(E_B)cos\theta)}}, \tag{2.4}$$

where d is the thickness of the organic layer A on the substrate B, $\lambda(EB)$ is the inelastic mean free path of electron of the substrate B traveling across the overlayer A, as described elsewhere [117, 118], I_B^∞ is the corrected intensity of the signal from the reference surface without chemical modification (assuming that the thickness of the substrate is larger than 9 nm). I_B is the corrected intensity of the signal from the modified surface.

$$I_B = \frac{Area}{RSF \cdot T \cdot \lambda}, \tag{2.5}$$

where *Area* is the raw area under the peak but above the background, determined from the spectrum, *RSF* is the relative sensitivity factor, T is the value of the transmission function at a given kinetic energy and λ is the inelastic mean free path.

2.3.3.1.2 Treatment of XPS survey and high resolution spectra

In this section, the treatment of XPS survey (see figure 2.4) and C1s high resolution (see figure 2.5) spectra of APTES surface is presented. The spectra were treated by use of the CasaXPS software, as described below.

The survey spectrum shows the signals of elements between 0 and 1500 eV, at the corresponding kinetic energies of the electrons. Experimental data are illustrated in spectra using the binding energy instead of the kinetic energy. In figure 2.4 a typical survey spectrum of an APTES surface is shown. The position of the signals were adjusted according to CHx at 285 eV. There are several strong signals, of Si, C, N and O, present in the survey spectrum. The signals of Si2p ($\sim$ 98 eV) and Si2s ($\sim$ 150 eV) are located at lower binding energies. Some smaller signals between the both strong Si peaks are called plasmon loss peaks. The plasmon loss peaks are caused by free electrons, which are located in the bulk of the silicon wafer and which were also excited by the X-rays. Their characteristic frequencies are shifted to higher binding energies than the primary photoelectric peaks. The distance ($\Delta E_{binding}$) between the silicon peaks is constant with a shifting to higher binding energies. Thereby, the intensity of the peaks decrease [119] with the increase of the binding energy. The C1s signal is assigned to a binding energy of 285 eV and N1s at $\sim$ 401 eV. The signals of O1s and of OKLL are assigned at $\sim$ 531 eV and 980 eV respectively. The OKLL peak is caused by an electron that fills a vacant hole, created by the X-ray, while a second electron is ejected at the same time. "KLL" means that the vacant hole is located in the K shell of O1s. One electron from the molecular orbitals relaxes and losses energy to fill the vacant hole while its energy loss is transmitted to another L originated electron, which is emitted.

Areas of the characteristic Si2p, C1s, N1s, O1s signals in the spectrum of the APTES surface were considered. In case of the two silicon signals, only the signal of Si2p was used because of its stronger signal intensity. The signals were fitted by the software using "Shirely" as background type. The line shape model GL(m=30) was used, and was described by the product of Gaussian-Lorentzian, where m=0 is a pure Gaussian and m=100 is a pure Lorentzian shape [119]. The atomic content of the surface (within a thickness of $\sim$ 9 nm) was obtained by taking the ratio of the corrected areas that were calculated by the raw area divided by the RSF (Scofield cross-section factors), the MFP (mean free path) of the photoelectrons and the value of the transmission function of the spectrometer at the at the given energy. RSF values that depends on the element and its transition are listed in table 2.1.

A high resolution spectra is a partial spectra of the survey spectra and is more detailed. Figure 2.5 illustrates a XPS high resolution spectra of C1s, from data of an analyzed APTES surface. At first a region is defined to fit the background line (type Shirley). For the deconvolution procedure, the full width at half maximum (fwhm) are maintained constant with reference to the fwhm of the CH_x component at a binding energy of 285 eV.

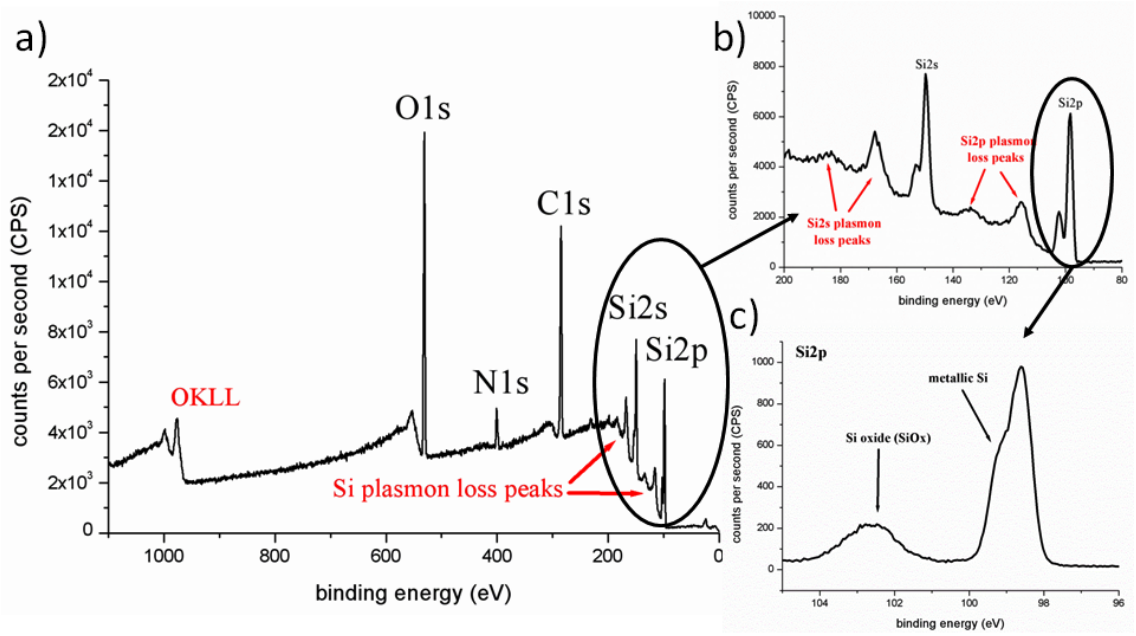

Figure 2.4: A typical survey spectrum of an APTES sample is illustrated (a). (b) shows the profile of the Si2p signal with its two peaks, corresponding to the metallic and oxidized components. In (c) the Si2s and Si2p signals with their plasmon loss peaks are clearly visible.

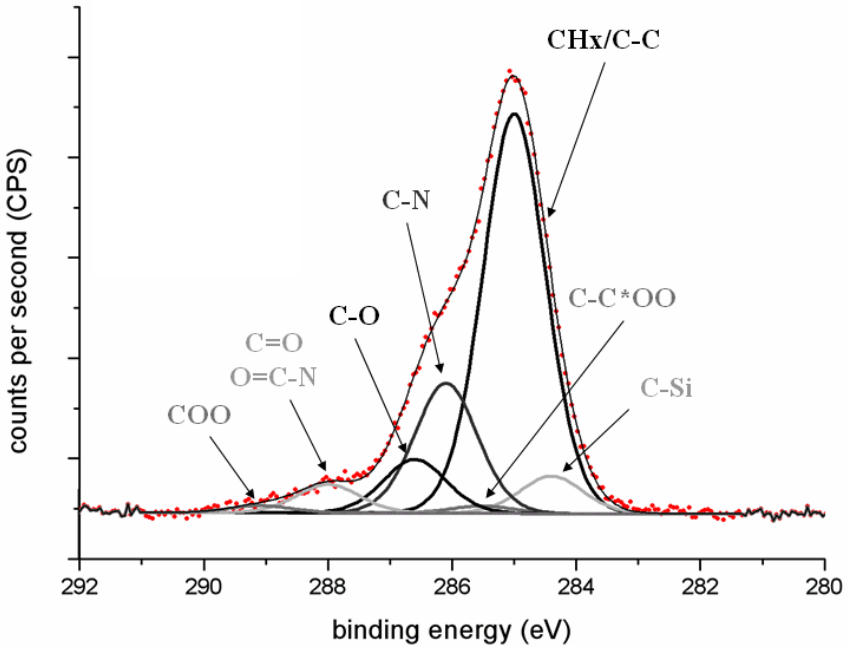

Figure 2.5: The C1s high resolution spectra is deconvoluted in several components. The fwhm of the different components is fixed and referred to the fwhm of the CH_x component.

Finally, the parameters used for the treatment of the XPS C1s and N1s high resolution spectra are listed in table 2.1.

Depending on the carbon bond and its more or less electron negative partner, the carbon groups were assigned to the corresponding positions (see table 2.1 in supporting information). Consequently, the fwhm and position constraints are forced, as well as the area constraint, which is set equally for the components C-C*OO and COO.
All parameters and constraints that were used to analyze XPS data are shown in table 2.1.

Table 2.1: Parameters used to analyse data of XPS high resolution spectra.

	C-Si	CH_x/ C-C	C-COO	C-N	C-O	O=N-C/ C=O	O-C=O
position eV	284.4	285.0	285.5	286.1	286.6	288.0	289.1
FWHM constr.	A · 1	A	A · 1	A · 1	A · 1	A · 1	A · 1
Area constr.	–	–	B	–	–	–	B · 1
RSF	1	1	1	1	1	1	1

	N=C	C_2N-H/ C-NH_2	N-C=O	NH_2- H-bonds	C-NH_3^+
position eV	398.4	399.6	400.1	400.7	401.8
FWHM constr.	A · 1	A	A · 1	A · 1	A · 1
RSF	1.8	1.8	1.8	1.8	1.8

2.3.3.1.3 Simulation of the "Ideal" Spectrum

A comparison was realized to highlight differences between the "real" and the "ideal" chemical environments of the functional groups, thus indicating significant differences between the real and the expected structures of the grafted layers.
The ideal spectrum is calculated on the basis of the ideal structure. An example is depicted in figure 2.6 for the C1s high resolution spectrum of the AHAPS-GAD-glutamine surface. The simulated spectrum and experimental spectrum of the AHAPS-GAD-glutamine surface are superposed. There are clear differences between the theoretical curve (filled out) and the real spectrum, which is decomposed in six components.

Each chemical environment, that is the summary of position and theoretical atomic percentage, it is represented by a Gaussian-Lorentzian peak shape model located at the binding energy given by the literature. The expression of the component is given by equation (2.6).

$$GL(x, E, w, r) = exp\frac{-4\ ln\ 2\left[1 - (\frac{r}{100})(\frac{x-E}{w})^2\right]}{1 + 4(\frac{r}{100})(\frac{x-E}{w})^2}, \tag{2.6}$$

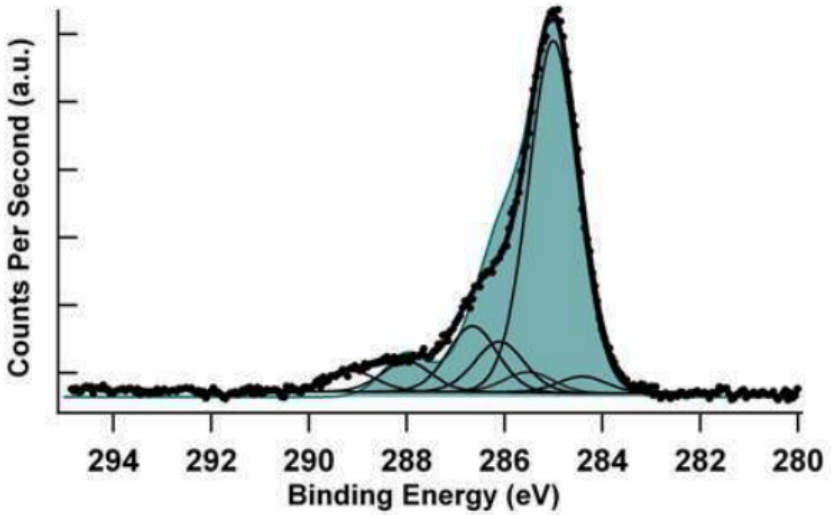

Figure 2.6: C1s peak fitting in the case of experimental AHAPS-GAD substrates (line curve) and the theoretical signal (full curve) as a representation of an « ideal » synthetic envelope in the case of a 100 % yield of glutaraldehyde molecule grafting (7 at % C-Si, 57 at % CHx, 22 at % C- N, 7 at % C-O and 7 at % C=O).

where E is the binding energy (position) of the considered chemical environment, w is the full width at half-maximum of the component (this value is matched with the experimental one), and r is the percentage ratio of Gaussian/Lorentzian character (0.3 for our system).

2.3.3.2 Water Contact Angle Measurements

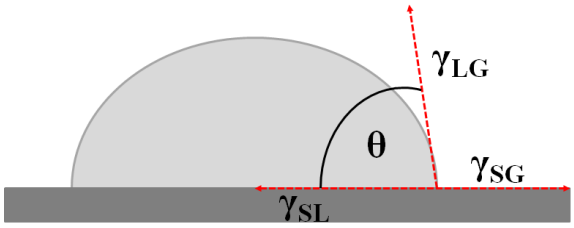

Figure 2.7: The droplet is formed on three different interfaces between the droplet, substrate and air resulting in an equilibrium of their interfacial energies; γ_{LG} liquid/vapor, γ_{SL} solid/liquid and γ_{SG} solid/air. The angle θ was determined after the drop reached the equilibrium state.

For evaluating the hydrophilic/hydrophobic character of the surfaces, water contact angles were measured. Static, advancing and receding contact angles were determined. The difference between advancing and receding angles provides the hysteresis, which is a quantitative indication of the surface homogeneity. Small values indicate a homogeneous surface, while large values imply a heterogeneous surface.
The contact angles were determined by the sessile drop method at room temperature using a Krüss contact angle goniometer. A droplet of 2 μL distilled MilliQ (pH 5.8) was

deposited on the surface. Contact angles were obtained using a camera coupled to an image analyzer. The static contact angle was determined after a delay of 1 min to ensure the equilibration of the droplet. The Young equation (2.7) describes the shape of the droplet on flat surfaces (see figure 2.7) [120].

$$0 = \gamma_{SG} - \gamma_{SL} - \gamma cos\theta, \tag{2.7}$$

where γ_{LG} represents the interfacial energy between liquid and gas phase , γ_{SL} the interfacial energy between solid and liquid phase, γ_{SG} the interfacial energy between solid and gas phase and θ the angle of drop on the surfaces indicated in figure 2.7.
Measurements of static, advancing and receding contact angle (see figure 2.8) were done after each grafting step. Reported values are averages of measurements performed at three different regions on four different samples.

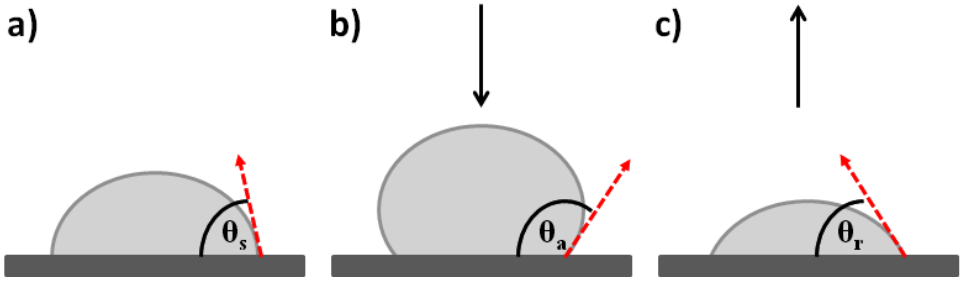

Figure 2.8: Three different contact angles are obtained. (a) Static contact angle: a droplet was deposited on the surface and θ was determined. (b) advancing contact angle: more liquid was slowly added by a syringe to a droplet already placed on the surface. The volume of the droplet increases and thus the contact angle θ changes. The receding angle (c) is obtained by withdrawing liquid from the droplet through a syringe. The volume of the droplet decrease and the contact angle changes, too.

2.3.3.3 Ellipsometry

Ellipsometry is a technique for the determination of the thickness of a film. The technique is non-destructive and contactless. During the measurement, a laser beam that has been polarized is reflected by the surface. The reflective process is accompanied by a change of the polarization of the laser beam and depends on the refraction index and the thickness of the layer on the surface. Before detection, the reflected light passes an analyzer. A schematic of the ellipsometry technique is shown in figure 2.9. The ellipsometer measures the change of the polarization state of light by the determination of the amplitude ratio Ψ and the phase difference Δ caused by the reflection on the surface. Finally, a layer model is used to calculate the thickness of the top layer on the surface based on Ψ and Δ [121]. The layer models are developed according to the layer structure, e.g. pure silicon wafer has a three layer model including Si, SiO_2 and the ambiance. The layer thickness can be determined in air or in liquid.

The ellipsometer used in this work was equipped with a phase modulation multiskop from Physik Instrument (M-O33K001) a HeNe laser working at 532 nm (beam diameter of 0.6 nm, intensity of 20 mW). The incident angle Φ was 70° and the configuration of Null-ellipsometry [121] measurements was used. The thickness of the chemical layers was evaluated at room temperature both in air (denoted as "ellipsometry in air" in the following) and in MilliQ water (denoted as "ellipsometry in liquid" in the following), via the use of a specific cell with quartz windows filled with the solution. The polarizer and the analyzer were positioned in such a fashion that the signal of the laser tended towards zero. Values of Δ and Ψ were measured at three different regions of the sample.

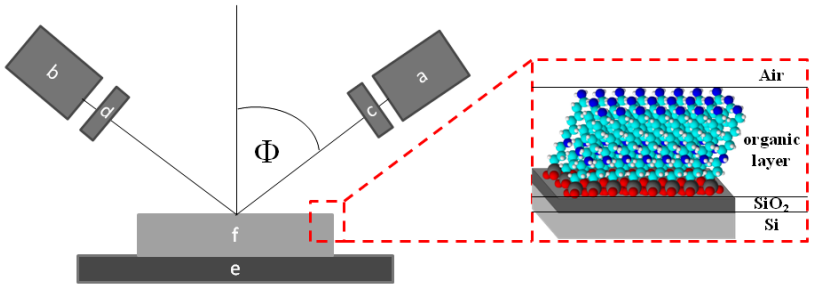

Figure 2.9: The thickness of a thin layer can be measured by ellipsometry. A laser beam (a: light source) is polarized by a polarizer (c) and impact the surface at the angle of incidence (Φ). The laser beam is reflected at the surface (f) on the sample holder (e), and thereby changing its polarization, and passes the analyzer (d) before it reaches the detector (b). In the dotted box a 4 layer model (Si/SiO_2/organic layer/air) is shown.

The thickness of the oxide layer was first determined on pure silicon wafers (reference surface). The model used for that purpose was composed of a layer of pure silicon with an overlayer of silicon dioxide. In order to determine the thickness of the organic layer, a third layer was added to the model while keeping parameters from silicon and silicon dioxide layers constant. Refractive indexes used for the calculation are presented in table 2.2.

Table 2.2: Refractive index values used for modeling the experimental results obtained by ellipsometry [76].

	air	water	SiO_2	organic layer	Si
refractive index	1	1.33	1.46	1.465	4.15

2.3.3.4 Zeta-Potential

Electric surface properties can be indicated by zeta-potential (ZP) measurements at the electric double layer at the surface. A scheme of an electric double layer is shown in figure 2.10. The ζ-potential is the potential of a material in ionic solution and is obtained

at the interface between the Stern-layer and a diffuse layer (Gouy-Chapman layer) [122]. The Stern-layer is the layer of ions (counter ions) that are attracted by the surface charges i.e. either anions or cations. In the Stern layer the concentration of counter ions is quite high, but the density of ions is reduced with the distance to the surface (diffuse layer). The boundary between the Stern-layer and the diffuse layer is also called shear plane. In the experiment, an ionic liquid is forced through a gap of two identical functionalized wafers, with their functionalized surfaces facing each other. Ions in solution form an electric double layer on the surfaces. The charge of the double layer is displaced because of the forced flow. Finally, the zeta potential (the displaced charge) values are measured between two electrodes located on the opposite sides of the flow cell.

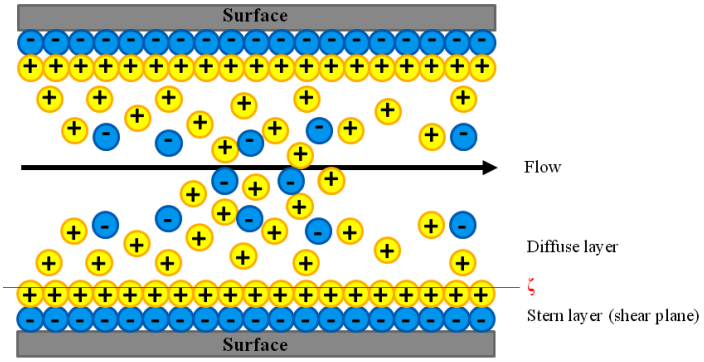

Figure 2.10: The ζ-potential is measured at the interface of the Stern-layer and the diffuse layer. The charges represented by the corresponding ions are temporarily bounded to the surface, but displaced by the applied flow.

If the surface is positively charged, it attracts anions from solution and the zeta potential shows higher values than that of a negatively charged surface, which attracts cations [122]. In this work, ζ-potential measurements were performed with a ZetaCAD (RS232C) Keithley 2000 in 5 mM NaCl, at different pH values ranging from pH 3 up to pH 10. An analyzing flow cell was specifically designed for samples based on silicon wafers, providing optimal measurement conditions. The flow cell is adapted to the thickness of the silicon wafer and allows two wafers to face each other, providing a small gap for the liquid. Two annuli were added on the both long side of the flow cell, allowing to plug electrodes (Ag/AgCl) to the system and also a pump system that provides the flow.
Five independent measurements were realized on one sample of each of the five surface types. Two particular values were extracted for each surface sample type: the zeta potential (ZP) value at physiological pH (∼ pH 7) and the isoelectric point (IEP) value that was determined from the ZP vs. pH curves (see curves in the supporting information, figure 2). In agreement with the Grahame equation (2.8) [123], low ZP

values (i.e., less than 25 mV) were assumed to be proportional to the surface charge density.

$$\zeta = \frac{\Delta E \eta \lambda}{\Delta P \epsilon \epsilon_o}, \tag{2.8}$$

where, ζ is the zeta potential, ΔE are the streaming potential values, measured between two electrodes, while ΔP is the difference of the pressure used in the experiment; η is the viscosity and λ the conductivity of the solution, and $\epsilon\epsilon_o$ the dielectric permittivity of water.

2.3.3.5 Atomic Force Microscopy (AFM)

Atomic force microscopy (AFM) was used to get informations about the topography and the different functionalizations on the surface. A cantilever is scanned over a chosen surface (see figure 2.11) in tapping mode. The tapping mode is a non destructive method for the imaging of delicate samples such as biological tissue and etched silicon electronic products. In the tapping mode, the cantilever is bounced at its resonant frequency with sufficient force to break the surface tension layer. The surface tension layer, which is caused by the presence of water vapor at the surface, is about 10-200 nm above the surface of the sample. Surface tension is an attractive force that can pull down a tip toward the sample surface and is strong enough to indent some material. Topography and different functional groups on the surface are displayed in height and phase contrast images by change of the amplitude and the attraction force of the cantilever [124].
A NanoScopeIII/Dimension 3000 (Digital Instruments) equipped with a phosphorus doped Si cantilever (k = 20-80 N/m) purchased from Veeco was used in tapping mode under ambient conditions, with a scan rate of 1 Hz and an image size of 2 μm^2. Surface morphology was revealed by height and phase contrast images. AFM images were further analyzed using the NanoScope 6.13R1 software (Digital Instruments) to obtain the mean roughness values (parameter R_a, the arithmetic average of the absolute height values). In the absence of differences between height and phase contrast images, only height images were considered for discussion.

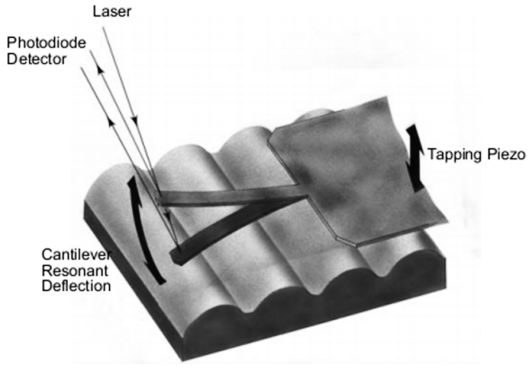

Figure 2.11: The AFM was used in tapping mode, in this mode the cantilever is not steadily in contact with the surface sample, but is oscillating [124,125].

2.4 Results and Discussion

THE JOURNAL OF PHYSICAL CHEMISTRY C

ARTICLE

pubs.acs.org/JPCC

Necessity of a Thorough Characterization of Functionalized Silicon Wafers before Biointerface Studies

Judith Böhmler,[†] Lydie Ploux,*[,†] Vincent Ball,[‡] Karine Anselme,[†] and Arnaud Ponche[†]

[†]Institut de Science des Matériaux de Mulhouse (CNRS LRC7228), Mulhouse, France

[‡]Laboratoire de Biomatériaux et Ingénierie Tissulaire (INSERM U977), Strasbourg, France

Supporting Information

ABSTRACT: Functionalized self-assembled monolayer (SAM) surfaces are frequently used for biological applications. Description of such surfaces is crucial to well-understand surface reactions and to achieve further controlled grafting. However, the difference between "ideal" (i.e., expected) and "real" molecular layers is often disregarded. This paper shows a systematic demonstration that thorough characterization and analysis of such layers are necessary for reaching the description of the "real" surface. Several model surfaces, with SAMs as the basis, were prepared and analyzed. Two steps of the characterization were distinguished. The first step involves commonly used measurements (X-ray photoelectron spectroscopy (XPS), survey spectra, static water-contact angle, atomic force microscopy (AFM) images) that were shown to lead to partial surface description. In the second step, additional measurements (XPS high-resolution spectra, water-contact angle hysteresis, AFM images, zeta potential) were allowed to highlight the modifications related to each grafting step and the morphological and conformational specificities (in particular defects) of the final surfaces.

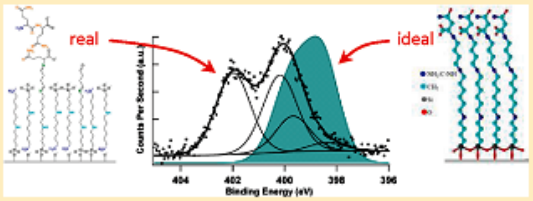

INTRODUCTION

Advances in new technologies have led to promising approaches in the field of rapid detection methods of biological objects (cells, bacteria, and biomolecules). In particular, the field of biosensor research is rapidly expanded with an immense potential market spanning a broad spectrum of applications in biomedical diagnosis,[1,2] environmental monitoring,[1−3] veterinary,[1,3] or food quality control.[1,3−6] Biosensors have been developed to detect a large variety of biomolecular complexes, like oligonucleotides and enzymes,[2,3,7] and biomolecular interactions, like antibody−antigen interactions[2,3,6−8] and antagonist− or agonist−receptor interactions.[4,7] In general, biosensors are defined as analytical devices incorporating a biological, a biologically derived, or a biomimetic material intimately associated with or integrated within a transducing microsystem.[9] The transduction unit converts the molecular recognition in a quantifiable signal, which has been accomplished with a large number of techniques: electrochemical,[3,7,8,10] fluorescent,[2,7,8] magnetic,[3,9] thermometric,[3,9,10] and piezoelectric[3,6,10] transduction, field-effect transistors,[6,7,9,10] or optical absorption.[3,6,9] Nevertheless, the selectivity of the sensor mainly depends on the quality of the selective layer that composes the recognition element.[11,12] Selectivity is then dependent on the morphology of the grafted layer and on the accessibility of the reactive groups. Therefore, obtaining information about this accessibility is crucial for the application of biosensors.

When substrates of biosensors are made of silicon wafers, both handling and characterization are difficult. In general, for elaborating biosensors, chemical modifications through covalent bonds are preferred to other approaches that involve physical interactions like electrostatic ones since covalent attachments of molecular chains onto the material surface are more stable, avoiding therefore the desorption of the immobilized molecules. Usually, monolayers are first grafted on the surface,[13] carrying reactive groups that are necessary for the further immobilization of the biomolecules of interest.[14] Mainly, amino-functionalized monolayers are used. Moreover, such functionalized surfaces are obtained by using self-assembled monolayers (SAMs) and are therefore expected to be well-controlled and well-organized.[15] The structure should be at, or close to, thermodynamic equilibrium, tending therefore to self-healing defects and to a closely packed well-ordered and stable configuration on the surface.[14]

The most frequently used organo-silane for elaborating SAMs in the biomaterial field is the 3-aminopropyltriethoxysilane (APTES).[17] However, many experiments suggested that the process of the monolayer formation is complex and highly sensitive to the reaction conditions. Polymerization of APTES can occur, leading to the formation of multiple APTES layers[16−18] whose structures and reactivity are quite different from those of the expected APTES monolayer.[16] Another frequently used amino-silane is the N-(6-aminohexyl)-aminopropyltrimethoxysilane (AHAPS) which should form monolayers more likely than APTES, due to its longer alkyl chain. The long chain increases the

Received: February 11, 2011
Revised: April 15, 2011
Published: May 18, 2011

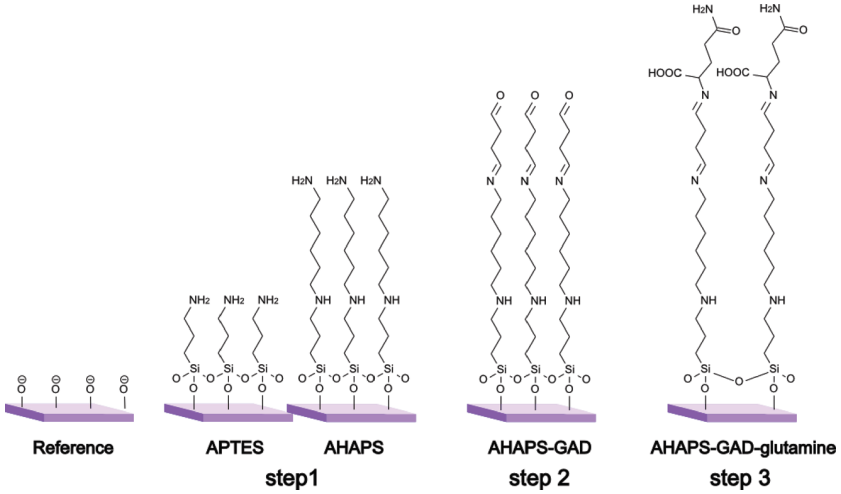

Figure 1. Schematic description of the different surfaces that are considered in this study. Cleaned wafers are used as a reference. Step 1: APTES or AHAPS surfaces are obtained by functionalizing cleaned wafers with APTES or AHAPS, respectively. Step 2: AHAPS-GAD surfaces are obtained by activating AHAPS surfaces through GAD grafting on amine groups. Step 3: AHAPS-GAD-glutamine surfaces are obtained by grafting glutamine on AHAPS-GAD surfaces.

van der Waals forces between adjacent molecules, thus stabilizing the monolayer.[19] Nevertheless, with AHAPS monolayers also, layer structure and reactivity of the functional groups could be different from those initially expected since "nucleophilic attacks" of the amino groups on the electrophilic trimethoxysilane[20] could occur and potentially result in polymerization.

The potential defects of such chemically modified surfaces are known by the specialists, but highlighting their presence remains not obvious. In particular, defects may go unnoticed, due to the lack of convergent characterization results. A typical example is given by the characterization of APTES layers by only considering the XPS survey spectrum, on which the nitrogen peak is pointed out as an indicator of a successful grafting of the layer. When indicated, the nitrogen percentage of APTES surfaces depends strongly on the synthesis procedure[21,22] and the experimental conditions and ranges from 1.3[23] to 8.1[24] atomic %. These high values are the sign of probable multilayer structures on the surfaces, but only more thorough investigations are able to confirm this hypothesis. To our knowledge, however, a systematic demonstration that thorough analysis of such a layer is necessary for knowing defects likely to affect further grafting or/and further studies of the interface between the surface and its environment (in particular, complex biological environments) was never published. The present paper aims at providing a simple but systematic study supporting this idea. Of course, our intention is not to maintain that everybody else does poor characterization but rather to provide a proof of the importance of thorough surface analyses.

In this article, we investigate the importance of the choice of the characterization techniques for highlighting potential defects in such a grafted complex layer. For that purpose, an extensive analysis of chemically modified silicon surfaces is presented. It was provided by using a multimodal approach, combining X-ray photoelectron spectroscopy (XPS), water-contact angle (CA) measurement, atomic force microscopy (AFM), ellipsometry, and zeta potential (ZP) measurement. The analysis was realized in two stages. In the first stage, elementary composition obtained by XPS survey spectra, wettability evaluated by the static water-contact angle, and topography evaluated by the mean roughness (Ra) were taken into account for describing the surface. These characteristics were chosen since their combination is frequently considered for describing surfaces. The related surface description was then compared to the ideal/theoretical one. The second time, the potential improvements to the surface description resulting from knowing the chemical functional groups determined by using XPS high-resolution spectra of carbon (C1s) and nitrogen (N1s), the surface homogeneity evaluated by the advancing and receding water-contact angles, the thickness obtained by XPS (in vacuum) and by ellipsometry (in air and in liquid), the surface morphology evaluated by AFM images, and the surface charge measured by zeta potential measurements were evaluated. In particular, the ability of each technique or their combination to point out defects in the layer was considered. Significant differences between the surface descriptions obtained after the first and the second step, respectively, were observed, demonstrating therefore the necessity of a thorough surface analysis. The importance of taking into account the intermediate steps of grafting for correctly describing the properties and the structure of the final surface is also demonstrated.

Two different types of chemically modified surfaces were considered for testing the influence of the characterization precision on the surface description quality. The first one consists of a silicon wafer grafted in one step with APTES or AHAPS (Figure 1). The second one consists of a silicon wafer that was grafted following a multistep procedure consisting of grafting successively an initiator layer made of AHAPS, a layer of glutaraldehyde as a linker, and finally a layer of glutamine as a model biomolecule (Figure 1). Finally, the consequence of potential incomplete or erroneous surface descriptions for the further surface grafting steps is also discussed in this article.

EXPERIMENTAL METHODS

Substrate and Chemical Modifications. Silicon wafers (100), one side polished, purchased from MCR (Germany) were used as substrate for chemical modifications and cut into pieces of 1 × 1 cm^2. Substrate pieces were ultrasonically (frequency 45 kHz) cleaned for 10 min in chloroform (Sigma-Aldrich) to

remove organic contamination, followed by 30 min of cleaning in piranha solution (3:1 mixture of sulfuric acid and hydrogen peroxide solution, both purchased from Sigma-Aldrich) at 50 °C. Substrate pieces were then rinsed with distilled Milli-Q water. This surface was considered as the reference and was the basis of all of the other types of surfaces. It is called "Reference" in the following sections of the paper (see Figure 1).

For the elaboration of amino-functionalized layers made of APTES, piranha-cleaned substrates were immersed in a 1 mM solution of 3-aminopropyltriethoxysilane (APTES, purchased from ABCR in Germany) in acetone (Sigma-Aldrich), overnight at room temperature in the dark. Samples were cleaned for 30 s in acetone under ultrasonic treatment (45 kHz) to remove the free silane fraction.[21] The same protocol was used for *N*-(6-aminohexyl)-aminopropyltrimethoxysilane (AHAPS, purchased from ABCR in Germany), respectively, in ethanol (Sigma-Aldrich). These two types of surfaces are named "APTES" and "AHAPS", respectively, in the further sections of the paper (see Figure 1, step1).

For the elaboration of the multistep-grafted surfaces, glutaraldehyde was used as a linker for grafting the biomolecules on AHAPS surfaces. For that purpose, AHAPS surfaces were activated by 2 h incubation in 10%-vol glutaraldehyde in Milli-Q water at pH 5−6 and at room temperature, as described elsewhere.[21] Samples were then rinsed several times with Milli-Q water to remove noncovalent bounded glutaraldehyde. In the further sections, these surfaces are called "AHAPS-GAD" (see Figure 1, step 2). The biomolecule immobilization was finally performed by grafting an amino acid, here glutamine, on AHAPS-GAD surfaces. Glutaraldehyde activated surfaces were immersed overnight in 1 mM glutamine solution in Milli-Q water at pH 5−6 and at room temperature before rinsing with Milli-Q water. These surfaces are called "AHAPS-GAD-glutamine" in the further sections (see Figure 1, step 3).

These substrates were voluntarily elaborated without any control of humidity conditions to reflect the common protocols used for elaborating molecular layers dedicated to further bio-interface studies.

X-ray Photoelectron Spectroscopy (XPS). The chemical composition of the surfaces was determined by XPS analysis. This analysis was performed with a Gammadata Scienta spectrometer, equipped with a monochromated Al K_α X-ray source (1486.6 eV) under ultrahigh vacuum and a takeoff angle of 90°. Survey and high-resolution spectra were recorded at a pass energy of 500 and 100 eV, respectively. For high-resolution experiments, the overall energetic resolution can be estimated to 0.45 eV. All spectra were analyzed and peak-fitted using CasaXPS 2.3.12 software (Casa Software Ltd., Teignmouth, UK, www.casaxps.com). All components were referenced according to the CHx component at 285.0 eV, and the full width half-maximum (fwhm) was constrained to be constant for all components in the same spectrum. The relative binding energy of all components was fixed and maintained constant for all peak-fitting procedures (Table 3). The evaluation of the organic layer thickness was done with eq 1[25] based on the Lambert−Beer law, assuming that this layer is homogeneous.

$$I_B = I_B^\infty e^{-d/[\lambda_A(E_B)\cos\theta]} \quad (1)$$

where d is the thickness of the organic layer A on the substrate B; λ_A is the inelastic mean free path as described elsewhere (for Si2p photoelectrons traveling in APTES layer, λ_{Si} is evaluated to 4.60 nm);[23,26] I_B^∞ is the corrected intensity of the reference; and I_B is the corrected intensity of the modified surface. The corrected intensity of a surface was calculated according to the conventional integration of the XPS signal (eq 2).

$$I_B = \frac{\text{Area}}{RSF \cdot T \cdot \lambda} \quad (2)$$

where Area is the raw area determined on the spectrum; RSF is the relative sensitivity factor (Scofield cross-section factors); T is the value of the transmission function at a given kinetic energy; and λ is the inelastic mean free path.

Table 1. Refractive Index Values Used for Modeling the Experimental Results Obtained by Ellipsometry

	air	water	SiO_2	organic layer	Si
refractive index	1	1.33	1.46	1.465	4.15

Simulation of the "Ideal"Spectrum. The ideal spectrum is calculated on the basis of the ideal structure depicted for each case. Each chemical environment is represented by a Gaussian−Lorentzian peak shape model located at a binding energy given by the literature. The expression of the component is given by eq 3.

$$\mathrm{GL}(x,E,w,r) = \exp\frac{\left(-4\ln 2\left(1-\frac{r}{100}\right)\left(\frac{x-E}{w}\right)^2\right)}{1+4\left(\frac{r}{100}\right)\cdot\left(\frac{x-E}{w}\right)^2} \quad (3)$$

where E is the binding energy (position) of the chemical environment considered; w is the full width at half-maximum of the component (this value is matched with the experimental one); and r is the percentage ratio of Gaussian/Lorentzian character (30% for our system).

Ellipsometry. The ellipsometer was equipped with a phase modulation multiskop from Physik Instrument (model M-O33K001) at 532 nm (HeNe laser) and an incident angle of 70°. The thickness of the chemical layers grafted on the samples was evaluated at room temperature both in air (named "ellipsometry in air" in the following sections) and in distilled water (named "ellipsometry in liquid" in the following sections). The positions of the polarizer and analyzer were chosen so that the signal of the laser tends toward zero. Values of Δ and ψ were measured on three different regions of the sample. The thickness of the oxide layer was determined on ungrafted silicon wafers (Reference surface). The model used for that purpose was composed of a layer of pure silicon with an overlayer of silicon dioxide. To determine the thickness of the organic layer, a third layer was added to the model while keeping parameters from silicon and silicon dioxide layers constant. Refractive indexes used for the calculation are presented in Table 1.

Water-Contact Angle Measurements (CA). For evaluating the wettability and the hydrophilic/hydrophobic character of the surfaces, water contact angles were measured. The static, advancing, and receding contact angles were measured at room temperature using a Krüss contact angle goniometer. A drop of 2 μL distilled Milli-Q (pH 5.8) was deposited, and the contact angle was determined by the sessile drop method.[27,28] Contact angles were obtained using a camera coupled to an image analyzer. The static contact angle was determined after a delay of 1 min to ensure the equilibration of the droplet. Measurements were done after each grafting step. Reported values are an average

Table 2. Experimental Results of the Atomic Composition, Water Contact Angle, Roughness, and Thickness Analysis for Each of the Model Surfaces, i.e., Reference, APTES, AHAPS, AHAPS-GAD, and AHAPS-GAD-glutamine

	XPS survey (%)				contact angle (deg)				thickness (nm)					zeta potential
	Si2p	C1s	N1s	O1s	θs	θa	θr	Ra (nm)	in vacuum[a]	in air[a]	in liquid[a]	theoretical	IEP[c]	ZP at pH 7 (mV)
Reference	67.5 ± 0.1	10 ± 1	0	23 ± 1	-[b]	-[b]	-[b]	0.2 ± 0.1	-	1.80 ± 0.02	19 ± 1	-	3.7	−15.0 ± 0.5
APTES	44 ± 7	32 ± 7	3 ± 1	21 ± 1	53 ± 2	55 ± 3	25 ± 3	0.3 ± 0.1	0.7 ± 0.2	1.7 ± 0.2	2.3 ± 0.1	0.8	4.4	−5.3 ± 0.3
AHAPS	54 ± 4	21 ± 3	2 ± 1	22 ± 2	28 ± 2	36 ± 2	12 ± 1	0.3 ± 0.1	1.1 ± 0.2	0.9 ± 0.2	1.5 ± 0.1	1.4	4.0	−6.7 ± 0.2
AHAPS-GAD	54 ± 4	22 ± 5	1 ± 1	22 ± 1	55 ± 2	60 ± 2	20 ± 5	0.4 ± 0.1	0.7 ± 0.1	0.5 ± 0.1	1.5 ± 0.1	2.1	3.2	−11.2 ± 0.3
AHAPS-GAD-glutamine	55 ± 3	21 ± 4	1 ± 1	22 ± 1	21 ± 1	40 ± 1	22 ± 1	0.6 ± 0.5	1.2 ± 0.2	0.5 ± 0.1	1.2 ± 0.3	2.6	5.1	−3.5 ± 0.2

[a] In vacuum: determined by XPS. In air and in liquid: determined by ellipsometry. [b] Complete moistening. [c] IEP corresponds to pH value at ZP = 0.

of measurements performed at three different regions on four different samples. The difference between advancing and receding contact angles provides the hysteresis, which is a quantitative indication of the surface homogeneity. Small values are a sign of a homogeneous surface, while large values imply a heterogeneous surface.[27]

Atomic Force Microscopy (AFM). Surface morphology and surface roughness were determined by AFM imaging. A NanoScopeIII/Dimension 3000 (Digital Instrument) equipped with a phosphorus-doped Si cantilever (k = 20−80 N/m) purchased from Veeco was used in tapping mode under ambient air, with a scan rate of 1 Hz and an image size of 2 μm^2. AFM images were further analyzed using the NanoScope 6.13R1 software (Digital instrument) for providing the mean roughness values (parameter Ra, the arithmetic average of the absolute height values). In the absence of differences between height and phase contrast images, only height images were considered for discussion.

ζ-Potential Measurements. ζ-Potential measurements were performed with a ZetaCAD device (CAD Instrumentation, Les Essarts le Roi, France). The streaming potentials were measured with a high impedance Keithley 2000 analyzer in the presence of 5 mM NaCl and were done at different pH values ranging from 3 to 10. The streaming potential values, $\Delta E/\Delta P$, were measured between two Ag/AgCl electrodes located on the opposite sides of the flow cell. The pressure difference ΔP between the two electrolyte compartments is varied with compressed air by increments of 30 kPa between −300 and +300 kPa versus the atmospheric pressure. An analyzing flow cell was specifically designed for samples based on silicon wafers, allowing the optimal conditions of measurement. The two silicon slides, coated with the layers of interest, were mounted parallel to each other in a plexiglass sample holder. They are separated by a 500 μm thick poly(tetrafluorethylene) (PTFE) spacer. The liquid was forced through the gap between the two identical wafers, with their functionalized surface facing each other. Five independent measurements were realized on one sample of each of the five surface types. The zeta potentials were calculated from the measured streaming potentials using the Smoluchowski equation (eq 4).

$$\zeta = \frac{\Delta E \eta \lambda}{\Delta P \varepsilon \varepsilon_0} \qquad (4)$$

where ζ, η, λ, and $\varepsilon\varepsilon_0$ are the ζ-potential, the solution viscosity, the solution conductivity, and the dielectric permittivity of water. Since the viscosity and the dielectric permittivity are temperature dependent, the temperature of the solution is regularly measured in situ, and its value is used to calculate temperature corrected values of ε and η. The solution conductivity is also measured in situ, and its value is used in the Smoluchowski equation.

Two particular values were extracted for each surface sample type: the zeta potential (which will be denoted by ZP in the following) value at physiological pH (∼pH 7) and the isoelectric point (IEP) that was determined on the ZP vs pH curves (see curves in Supporting Information, Figure 2). Both factors were presented in the results table (Table 2), but usually, only one of both was used for the discussion according to the necessity. In agreement with the Grahame equation,[29] low (i.e., less than 25 mV) ZP values were assumed to be proportional to the surface charge density.

Four different surface types ("APTES", "AHAPS", "AHAPS-GAD", "AHAPS-GAD-glutamine", Figure 1, steps 1, 2, and 3) based on silicon wafer substrate (Reference, Figure 1) were used for testing the two analysis approaches. For each type of surface, each analysis approach was repeated on three distinct samples.

RESULTS AND DISCUSSION

To appreciate the importance of each of the surface characterization techniques for highlighting potential defects of the layer, two characterization steps have been distinguished for analyzing the same samples. The related descriptions were compared with the theoretical/ideal surface.

The experimental results of the five different surfaces are summarized in Table 2, except the high-resolution XPS data that are presented in Table 3.

Reference Surface. Silicon wafers were used as a substrate for all of the further grafting.

An expected high Si2p signal was detected in the XPS survey spectrum, resulting from the silicon substrate, while the oxygen peak (O1s) indicated the presence of an oxide layer that is expected for a silicon surface in contact with the atmosphere. The low static contact angle, corresponding to a high hydrophilic character, is in agreement with the presence of this oxide layer. Furthermore, the weak value of the mean roughness Ra revealed a flat surface topography, without the presence of pores potentially due to the "piranha solution" etching. Finally some organic contaminations, which usually occur during the time delay between sample preparation and XPS analysis, were suspected due to the detection of a carbon peak (C1s). No specific details about the reactivity of the substrate/oxide layer were given by this first analysis approach.

Table 3. Experimental Results of the XPS C1s and N1s High-Resolution Analysis for Each of the Model Surfaces[a]

C1s		% area			
assignment	position (eV)	APTES	AHAPS	AHAPS-GAD	AHAPS-GAD-glutamine
C−Si	284.4	20	4	3	2
CH_x/C−C	285.0	50	71	63	56
C−COO	285.5	0	0	4	4
C−N	286.1	20	14	9	11
C−O	286.6	6	7	12	16
O=C−N/C=O	288.0	4	4	5	7
O−C=O	289.1	0	0	4	4
N1s		**% area**			
assignment	position (eV)	APTES	AHAPS	AHAPS-GAD	AHAPS-GAD-glutamine
N=C	398.4	0	0	3	5
C_2N−H/C−NH_2	399.6	17	19	25	17
N−C=O	400.1	0	0	0	38
NH_2H bonds	400.7	17	8	17	-
C−NH_3^+	401.8	66	73	55	40

[a] Due to the high intensity and proximity of the two neighbouring peaks, the deconvolution algorithm failed to converge to determine the intensity of the NH_2 H-bonded component in the case of the AHAPS-GAD-glutamine surface.

The thickness measured by ellipsometry in air and in liquid was approximately 2 nm, showing that the oxide layer was not completely removed by the piranha treatment. This result suggests that the piranha etching did not cause surface defects, which was confirmed by the homogeneity displayed by the AFM images (see Supporting Information, Figure 1a). This integrity of the surface, already suggested by the first approach, is of high importance for ensuring further controlled and homogeneous grafting. The surface description was completed by the negative surface charge (−15.0 ± 0.5 mV) determined at pH 7 by ZP measurement, which demonstrated the successful chemical activation of the surface. On the basis of this result, the hydroxyl groups that are necessary for further grafting were assumed to be present at the surface.

Finally, the first analysis approach was successful to state the presence of the oxide layer and to suggest the integrity of the surface. Nevertheless, the absence of any surface defects and the surface activation necessary for the further grafting were completely demonstrated by the second approach.

APTES Surfaces. APTES is a short amino-terminated organosilane that is used to introduce amine functions at the surface of the oxidized substrates. According to the literature, this silane is expected to provide a monolayer structure[30,31] as depicted in Figure 2a.

According to the XPS survey spectrum, binding energies corresponding to nitrogen (N1s), carbon (C1s), silicon (Si2p), and oxygen (O1s) were detected. Since APTES was the only possible source of nitrogen on this surface, the nitrogen amount was assigned to the grafted silane, which demonstrated its presence on the surface. The overlayer was also detected by the decrease of the signal coming from the substrate (Si2p) in comparison with the Reference surface, while the presence of the silane was confirmed by the static water contact angle (53 ± 2°) that corresponds to the values reported in the literature for amino-functionalized surfaces.[22,24,32] Finally, this analysis suggests the presence of an APTES layer grafted onto the substrate,

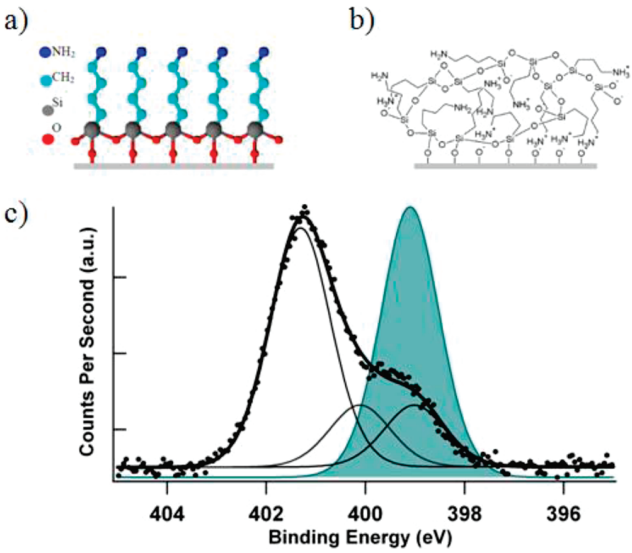

Figure 2. "Ideal" and "real" APTES layer. (a) Representation of the ideal molecular organization and layer structure expected for an APTES monolayer grafted on a silicon wafer substrate. (b) Representation of the real molecular organization and layer structure as described by the complete ("second approach") experimental analysis. The APTES coating forms a multilayer, especially due both to the short alkyl chains leading to small van der Waals forces and to the amine end group leading to sensitivity for polymerization. (c) XPS N1s high-resolution spectra expected in the ideal case (full curve) and in the real case (i.e., experimental results) (line curve). The ideal case is described by one component: NH_2.

which may be in agreement with the expected monolayer structure. However, the experimental amount of nitrogen (3%) is approximately 3 times higher than expected (1.1%) for a monolayer in the case of the ideal structure shown in Figure 2a (for theoretical atomic amounts, see calculation and data in

Supporting Information, Figure 3). The high amount of nitrogen on the sample allows us to assert that the experimental structure of the layer is very different from the expected monolayer. This is also supported by the high roughness error (100% of the mean value) that indicates the presence of topographical heterogeneities of the surface, although roughness mean values measured on the APTES layer (Ra = 0.4 ± 0.4 nm) and the cleaned substrate (Ra = 0.2 ± 0.1 nm) were not significantly different.

The XPS high-resolution spectrum of C1s showed typical binding energies that were assigned to C−Si, CHx/C−C,[33−36] C−N,[34,37] C−O,[33,35] and O═C−N/C═O.[36] The C−Si, CHx/C−C, and C−N functional groups were attributed to the silane, while the C−O, C═O, and O═C−N groups were certainly the result from chemical reactions between the amine groups and the atmospheric carbon dioxide (i.e., atmospheric contamination).[38] On the other hand, the decomposition of the N1s peak on the XPS high-resolution spectrum highlighted three components (Figure2c) that were assigned to C−NH_2 (and/or C−NH− that should not be present on this surface type),[39] C−NH_2 involved in hydrogen bonds,[40] and C−NH_3^+ according to the literature.[33] Nevertheless, only the C−NH_2 component was expected since APTES contains only free primary amines. The second component was probably due to H bonds between amino groups and silanol groups of the surface which should result in a component located at a higher binding energy than the free amines[40] as it was here observed. The third component that was assigned to the positively charged amine was hypothesized to result from electrostatic interactions between the NH_2-termination of the silane and the silicon substrate (C−$NH_3^+\cdots{}^-$OSi). Such side reactions, leading to the "head to foot" organization of a part of the molecules, may have been favored by the non-humidity-free conditions, responsible for weak van der Waals forces between the short length chains of APTES molecules. Head to foot molecular organization and lack of alkyl chains assembling should result in an unorganized, multilayer structure as depicted in Figure 2b. This representation is in agreement with the experimental thickness values obtained by ellipsometry since measurements in air (1.7 ± 0.2 nm) and in liquid (2.3 ± 0.2 nm) were much higher than the theoretical length of a single APTES molecule (0.8 nm[22,23]). The difference observed between the in-liquid in one hand and the in-air and in-vacuum (obtained by XPS) thickness values are attributed to the collapsing of the molecules under vacuum and in air compared to the layer swelling occurring in water. The presence of an unorganized structure was confirmed by the high value of the hysteresis that indicated an uneven surface topography and by the AFM images that showed defects in the coating layer (see Supporting Information, Figure1b). Concerning the surface charge, although an IEP value between pH 8 and pH 9 was expected for a complete packed layer of amine end groups,[41] the measurement led to pH 4.4, indicating that the chemical surroundings of the amino groups were complex. Such modification of the IEP value may be caused by the presence of various functional groups of the silane (like Si−OH), which is in agreement with the hypothesis of an unorganized multilayer.

In conclusion, the complete description demonstrated that the APTES surfaces realized in nonhumidity-free conditions present an unorganized, multilayer structure (Figure 2b), presenting not only C−NH_2 but also C−NH_3^+ groups on the top of the surface. Despite the high density of amino groups, which is an important factor for further grafting, the lack of structure control should strongly affect the efficiency of further grafting of biomolecules

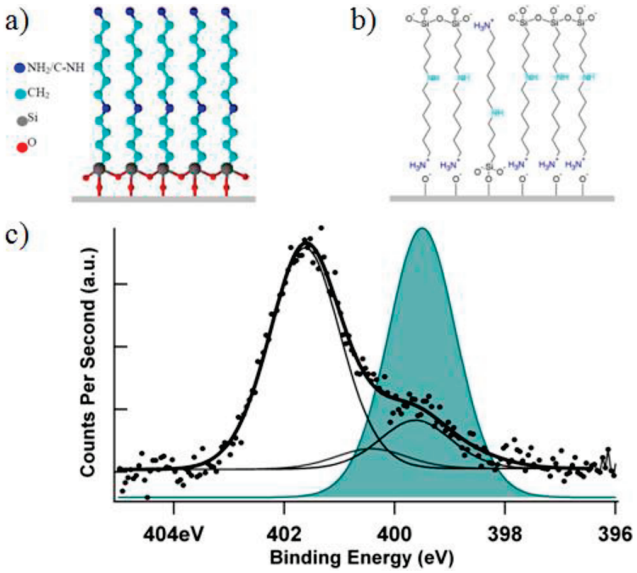

Figure 3. Ideal and real AHAPS layer. (a) Representation of the ideal molecular organization and layer structure expected for an AHAPS monolayer grafted on a silicon wafer substrate. (b) Representation of the real molecular organization and layer structure as described by the complete ("second approach") experimental analysis. The AHAPS coating forms a monolayer in which the large part of the silane molecules is adsorbed on the wafer's surface with a head to foot organization. (c) XPS N1s high-resolution spectra expected in the ideal case (full curve) and in the real case (i.e., experimental results) (line curve). The ideal case is described by a single component corresponding to NH and NH_2 chemical environments.

since the amino groups are hindered in the multilayer, thus reducing their accessibility. The poor control of the layer structure is also responsible for a lack of reproducibility as highlighted by the high standard deviation values of the positions and area of the C−NH_2 (position, 399.4 ± 0.3 eV; % area, 30 ± 11), C−NH_2 H-bonded (position, 400.5 ± 0.5 eV; % area, 25 ± 11), and C−NH_3^+ (position, 401.7 ± 0.3 eV; % area, 45 ± 22) components determined on the XPS high-resolution spectra.

Finally, while the first analysis approach only suggested some imperfections in the APTES layer, the second approach allowed us to highlight the real surface as a multilayer containing topographical surface heterogeneities and a poor surface accessibility of the reactive groups.

AHAPS Surfaces. Longer silanes like AHAPS (*N*-(6-aminohexyl)-aminopropyltrimethoxysilane) are expected to form better defined monolayers than APTES due to the increase in the van der Waals forces along the alkyl chains[42] (Figure 3a). Therefore, AHAPS was used to introduce amine functions at the surface of the oxidized substrates, attempting to form monolayer structures.

The XPS survey spectrum displayed a nitrogen peak (N1s) in agreement with the nitrogen-rich signal expected with a silane layer. Furthermore, the experimental amount of nitrogen (2 ± 1%) was very similar to the theoretical, expected value (2.3%, see calculation in Supporting Information, Figure 3), and the static water contact angle (28 ± 2°) indicated a hydrophilic surface in agreement with a silane layer. However, higher contact angle values are usually reported in the literature.[43,44] This can be attributed to a low packing of the molecules, but since the experimental nitrogen amount agrees with a packed layer, we rather

attributed the difference to the exposition of Si−OH groups at the surface of the packed layer. The Ra roughness (0.24 ± 0.02 nm) similar to the value determined for the reference surface suggested a uniformed surface topography compatible with a well-organized molecular layer. Finally, the first characterization approach seems to indicate a closely packed monolayer of AHAPS grafted onto the substrate in agreement with the representation in Figure 3a.

The XPS high-resolution spectrum of C1s (Supporting Information, Figure 4) showed binding energies corresponding to C−Si, CH_x/C−C, C−N, C−O, and O═C−N/C═O groups that were attributed to the silane and to chemical reactions between the amine groups and the atmospheric carboxylic acids as already evoked for the APTES surface analysis. Three nitrogen components were detected in the N1s high-resolution XPS spectrum (Figure 3c) that were assigned to primary ($C-NH_2$) and/or secondary (C−NH−) amines, primary amines involved in hydrogen bonds ($C-NH_2$ H-bonded), and protonated primary amines ($C-NH_3^+$), respectively. Since only primary and secondary amines were expected according to the AHAPS chemical composition, the presence of protonated primary amines was attributed to the probable physisorption of the silane molecules on the surfaces, with protonated primary amine groups facing the wafer, similarly to the situation described for APTES layer. As already discussed for AHAPS, the measurement of an IEP value (pH 4.0) that is significantly lower than expected (between pH 8 and pH 9) indicates that not only amino groups were present at the surface top. Such modification of the IEP value may be caused by the presence of SiO^- groups, which supports the hypothesis of a part of the silane molecules, orientated head to foot with amino groups in interaction with the surface Si atoms.

In spite of this molecular organization, the measurement of the silane layer thickness provided values (between 0.86 ± 0.01 nm and 1.5 ± 0.1 nm according to the environmental conditions of measurement) similar to the theoretical one (1.43 nm[44]), tending to demonstrate a monolayer structure of the coating, in which, as shown by the AFM images, rare topographical heterogeneities are present (see Supporting Information, Figure 1c). The presence of topographical or/and chemical heterogeneities is supported by the high value of contact angle hysteresis (24°). These features may be due to grafted molecules surrounded by adsorbed AHAPS molecules as depicted in Figure 3b.

Finally, even if the monolayer structure was suggested by the first approach, the second approach was necessary to reveal the uncontrolled orientation of the silane. Although the molecular assembling is better in the case of AHAPS in comparison with APTES molecules, the particular head to foot structure should significantly affect the accessibility of the amino groups and therefore also the further biomolecule grafting efficiency.

AHAPS-GAD Surfaces. Glutaraldehyde is frequently used as a linker between amino-functionalized surfaces and the amino groups of biomolecules. In the present study, it was reacted with the amino-functionalized AHAPS surfaces before an amino acid was grafted. The structure that is expected for this coating is represented in Figure 4a.

As expected, the XPS survey spectrum displayed nitrogen (N1s), silicon (Si2p), and carbon (C1s) peaks, which did not allow us to provide any specific information about the presence of GAD on the preformed AHAPS layer. As well, the weak difference between the Ra values measured on AHAPS-GAD (0.4 ± 0.1 nm) and AHAPS (0.3 ± 0.1 nm) surfaces was not

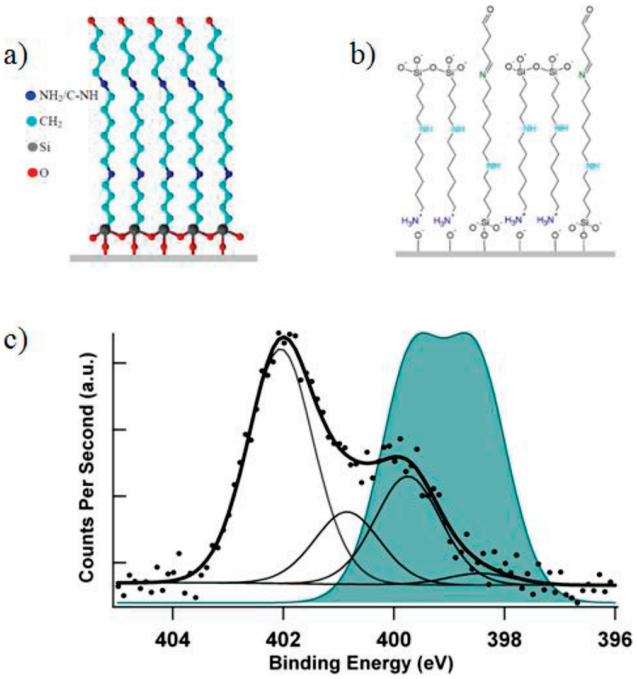

Figure 4. Ideal and real AHAPS-GAD layer. (a) Representation of the ideal molecular organization and layer structure expected for an AHAPS monolayer grafted on a silicon wafer substrate. (b) Representation of the real molecular organization and layer structure as described by the complete ("second approach") experimental analysis. The grafted amount of GAD is low due to the low density of amine groups and the high density of silanol groups present on the surface top. (c) XPS N1s high-resolution spectra expected in the ideal case (full curve) and in the real case (i.e., experimental results) (line curve). The ideal case is described by two components: NH and C═N.

sufficient to conclude about the success of the grafting. Finally, only the water contact angle that was higher on AHAPS-GAD surfaces than on AHAPS surfaces (55 ± 2° and 28 ± 2°, respectively) and in agreement with those expected for similar systems (59 ± 3° for APTES surfaces after glutaraldehyde derivatization[21]) suggested the grafting of GAD molecules.

The XPS N1s high-resolution spectrum (Figure 4c) showed four components that were assigned to imine (N═C), primary ($C-NH_2$), and/or secondary amines (C_2N-H), hydrogen-bonded primary amines ($C-NH_2$ H bonded), and primary protonated amine ($C-NH_3^+$). Due to the reaction between the amine groups present on the surface and the aldehyde groups of the GAD molecules (known as Shiff base reaction), imine groups were expected, signing the successful grafting of GAD molecules. The corresponding component in the XPS C1s high-resolution spectrum (the C═N component) is likely to appear at the same binding energy as C−O, but the exact energy is unknown. Besides, the presence of GAD was confirmed by the increase in intensity of the O═C−N/C═O peak compared to the C−N peak, while the presence of the C−O and the O−C═O[33,36] peaks indicated also that GAD molecules were present and, for a part, were hydrolyzed. However, the only slight increase in intensity of the O═C−N/C═O peak relative to the signal measured on AHAPS surfaces suggests only a low quantity of grafted GAD molecules. Furthermore, the quantity of imine groups (N═C) measured on AHAPS-GAD surfaces (3 ± 2 atom %) was significantly smaller than expected (50 atom %). This may

have resulted from a weak grafting reaction yield of GAD, and this hypothesis is supported by the high amount of primary protonated or unprotonated amine remaining after the GAD grafting and then showing the detection of the underlying AHAPS surface. This may also result from the hydrolysis of imine groups in secondary-amine groups, which may occur even in the case of high grafting yield, and was indicated by the $C_2\underline{N}-H$ group detection. Nevertheless, the layer thickness value was significantly higher in liquid (1.5 ± 0.1 nm) than in air (0.5 ± 0.1 nm) and vacuum (0.7 ± 0.1 nm) suggesting that the GAD molecules were grafted in a low density and collapsed on the AHAPS surfaces in air and vacuum conditions. This low density, that was probably due to the poor accessibility of AHAPS NH_2- or NH_3^+-termination available for the GAD molecules, was confirmed by the ZP value at pH 7 (-11.2 ± 0.3 mV) that was strongly lower than the neutral value expected for a complete GAD-grafted layer. After grafting of GAD, moreover, the balance between negatively and positively charged functional groups present at the surface top was affected, leading to a ZP value inferior to the value measured for AHAPS surfaces. Besides, the high water contact angle hysteresis (40°) and heterogeneities observed in the AFM images (see Supporting Information, Figure 1d) suggest that the few GAD molecules grafted on the AHAPS surface were present as approximately 2 nm high small aggregates, despite the grafted condition (pH < 7) that was chosen to limit GAD polymerization.[45]

Finally, aside from the presence of grafted GAD already suggested by the results of the first approach, the second approach demonstrated that the reaction yield of the GAD grafting on the AHAPS layer was low (Figure 4b), jeopardizing further grafting of biomolecules.

AHAPS-GAD-Glutamine. Glutamine was grafted on the GAD linker previously attached on the AHAPS-modified wafers according to the expected layer structure depicted in Figure 5a.

As evoked above for GAD grafting on AHAPS surfaces, the XPS survey spectrum, despite displaying binding energies that were assigned to silicon (Si2p), carbon (C1s), nitrogen (N1s), and oxygen (O1s), cannot assert the presence of glutamine molecules on AHAPS-GAD surfaces since no atomic component is specific for glutamine. Nevertheless, the reduction of the static water contact angle ($21 \pm 1°$) in comparison with the value measured on AHAPS-GAD surfaces ($55 \pm 2°$) and the increase in roughness observed in AHAPS-GAD-glutamine surfaces (Ra = 0.6 ± 0.5 nm) in comparison with AHAPS-GAD surfaces (Ra = 0.4 ± 0.1 nm) both indicate modifications of the surface in agreement with the hydrophilicity increase expected after glutamine grafting and with the glutamine molecule dimensions.

The N1s high-resolution spectrum shows four different binding energies that were assigned to imine ($\underline{N}=C$), primary ($C-NH_2$), and/or secondary amines ($C_2\underline{N}-H$), $O=C-\underline{N}$ component,[46] and protonated amine ($C-\underline{N}H_3^+$), while the binding energies observed in the C1s high-resolution spectrum were assigned to $\underline{C}-Si$ and $O=\underline{C}-N$. Aside from the signals resulting from the underlying AHAPS-GAD surface ($C_2\underline{N}-H$, $C-NH_2$, $C-\underline{N}H_3^+$, and $\underline{C}-Si$), the $O=C-\underline{N}$ and $O=\underline{C}-N$ amide peaks clearly indicated that glutamine molecules were present on the AHAPS-GAD surfaces. However, the quantification of the $C=\underline{N}$, $O=C-\underline{N}$, and $C_2\underline{N}-H$ group components resulted in an experimental $C=\underline{N}$:$O=C-\underline{N}$:$C_2\underline{N}-H$ ratio of 1:8:3, while a ratio of 2:1:1 was expected (Figure 5c), demonstrating that the glutamine layer was incomplete. This is confirmed by the

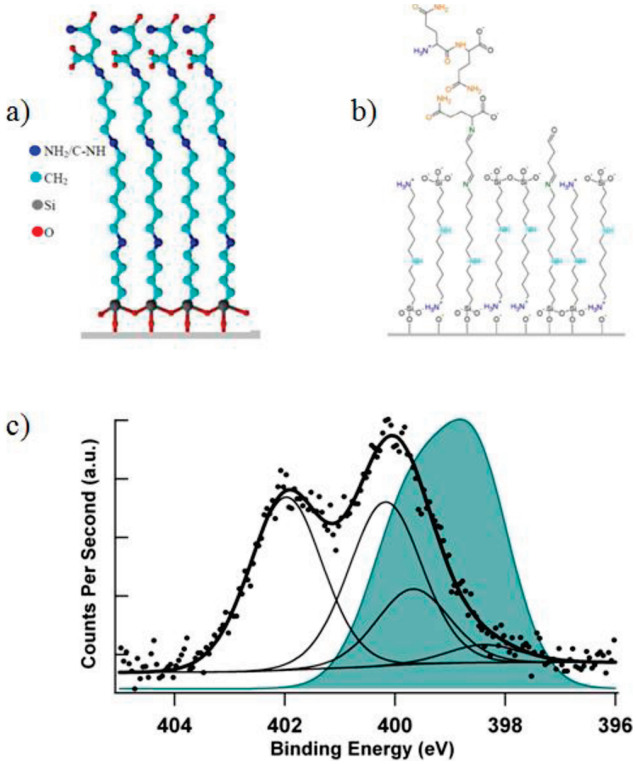

Figure 5. Ideal and real AHAPS-GAD-glutamine layer. (a) Representation of the ideal molecular organization and layer structure expected for an AHAPS monolayer grafted on a silicon wafer substrate. (b) Representation of the real molecular organization and layer structure as described by the complete (second approach) experimental analysis. The grafted amount of glutamine is low due to the low density and the aggregative organization of the linker (GAD) present on the surface top. (c) XPS N1s high-resolution spectra expected in the ideal case (full curve) and in the real case (i.e., experimental results) (line curve). The "ideal" case is described by three components: 25% NH, 50% $C=N$, and 25% $O=C-NH_2$.

AHAPS-GAD-glutamine layer thickness (1.2 ± 0.3 nm in liquid) that was significantly lower than those expected for a complete glutamine layer (3.1 nm for a fully extended layer with molecules adopting a *trans* conformation). Moreover, in agreement with the previously observed distribution of the GAD molecules, the AFM images (see Supporting Information, Figure 1e) suggest that the glutamine molecules reacted with aggregates of GAD molecules, leading to aggregates of immobilized glutamine (Figure 5b). However, the high $\underline{C}-N/\underline{C}H_x$ and $C-O/\underline{C}H_x$ ratios suggest that free aldehyde groups were still remaining on the surface, which may be due to the GAD aggregates that limited the accessibility for reacting with the glutamine molecules. A combination between aggregates and effects due to the glutamine molecular volume and charges may also have affected the ion mobility during ZP measurements as highlighted in the literature for nonhomogeneous molecular layers,[47] leading to significantly higher ZP values (-3.5 ± 0.2 mV) as expected.

Finally, while the presence of grafted glutamine was only suggested by the first approach, the second approach demonstrated that the grafting was successful but that the reaction yield of the glutamine on the AHAPS-GAD layer was very weak, probably resulting from both the low density and the in-aggregates orientation of the GAD molecules.

CONCLUSIONS

Using a multimodal approach to analyze the surface chemistry, we attempted to precisely describe different molecular layers leading to the grafting of a model biomolecule (glutamine) on silicon wafer substrates. In the first step, the characterization consisted of the XPS survey spectrum, static water contact angle, and mean roughness value since they are frequently the only data provided in the literature to prove the chemical modification of the surface. In the second step, the potential improvements resulting from XPS high-resolution spectra, ZP value at pH 7 and IEP, AFM images, and thickness values obtained by ellipsometry were studied. The ability of each of the techniques to complete the thorough description of the molecular layer was evaluated by analyzing APTES surfaces and each grafting step necessary to create AHAPS-GAD-glutamine surfaces.

This study demonstrated that the atomic composition, the mean surface roughness, and the hydrophilic/hydrophobic character of the surface provided by the first approach were in good agreement with the properties expected for the used model surfaces but that these data were insufficient for evaluating the efficiency of the grafting and the structure of the so-formed layer(s). Even some incorrect assumptions, especially concerning the mono- or multilayer character of the coating, were suggested by this first approach. On the contrary, the second step allowed us to precisely construct a "real" description of the surface layer, including especially molecular orientation, organization, and reactivity. In several model cases that were analyzed in this study, this complementary information was essential to evaluate the quality of the grafted layer, which is the crucial factor allowing us to ensure a good quality of further grafting of biomolecular layer or correct understanding of potential interactions with biological organisms. The APTES grafting and the AHAPS-based multistep biomolecular grafting were used as examples, allowing us to demonstrate that the first analysis step only allowed us to assert the presence of a chemical modification, without highlighting that the quantity of grafted molecule, the molecule organization, and the molecular layer structure were far from expected and led to surfaces of poor qualities. Due to the sensibility of biological objects (mammalian cells, bacteria, and biomolecules) to the density of immobilized molecules, this aspect of the surface elaboration for biological and biomedical applications should be considered carefully. Using brominated silane to prevent polymerization at the surface, modifying the conditions of surface elaboration by using the vapor phase instead of the liquid phase, for example, or adding an annealing step to the protocol to stabilize the monolayer structure are possible ways to improve the quality of such surfaces.

Finally, this study demonstrates the importance of a careful analysis for assessing the grafting quality of biomolecule on surfaces dedicated for biological studies.

ASSOCIATED CONTENT

Supporting Information. Four figures are presented, depicting the AFM height images of the model surfaces (Figure 1), Zeta potential vs pH curves for each of the model surfaces (Figure 2), scheme and calculation of the theoretical atomic composition that should be measured by XPS analysis for APTES and AHAPS model surfaces (Figure 3), and C1s peak fitting in the cases of experimental and "ideal" AHAPS-GAD substrates (Figure 4). This material is available free of charge via the Internet at http://pubs.acs.org.

AUTHOR INFORMATION

Corresponding Author
*E-mail: lydie.ploux@uha.fr.

ACKNOWLEDGMENT

We thank Philippe Fioux and Christian Ringwald for the XPS and zeta potential measurements, respectively, and the Region Alsace for their financial support.

REFERENCES

(1) Jane Andrew, D. R.; Hodges, A.; Voelcker, N. H. *Trends Biotechnol.* **2009**, *27* (4), 230–239.
(2) Pancrazio, J. J.; Whelan, J. P.; Borkholder, D. A.; Ma, W.; Stenger, D. A. *Ann. Biomed. Eng.* **1999**, *27*, 697–711.
(3) Velasco-Garcia, M. N.; Mottram, T. *Biosyst. Eng.* **2003**, *84*, 1–12.
(4) Blasco, C.; Picó, Y. *TrAC* **2007**, *26*, 895–913.
(5) Mello, L. D.; Sotomayor, M. D. P. T.; Kubota, L. T. *Sens. Actuators, B* **2003**, *96*, 636–645.
(6) Thevenot, D. R.; Toth, K.; Durst, R. A.; Wilson, G. S. *Pure Appl. Chem.* **1999**, *71*, 2333–2348.
(7) Lin, V. S. Y.; Motesharei, K.; Dancil, K. P. S.; Sailor, M. J.; Ghadiri, M. R. *Science* **1997**, *278*, 840–843.
(8) Asanov, A. N.; Wilson, W. W.; Odham, P. B. *Anal. Chem.* **1998**, *70*, 1156–1163.
(9) Lazcka, O.; Del Campo, F. J.; Muoz, F. X. *Biosens. Bioelectron.* **2007**, *22* (7), 1205–1217.
(10) Thévenot, D. R.; Toth, K.; Durst, R. A.; Wilson, G. S. *Biosens. Bioelectron.* **2001**, *16*, 121–131.
(11) Lim, S. H.; Kim, B. W. *Biotechnol. Bioprocess Eng.* **2004**, *9* (2), 118–126.
(12) Sadik, O.; Ngundi, M.; Yan, F. *Biotechnol. Bioprocess Eng.* **2000**, *5* (6), 407–412.
(13) Prucker, O.; Naumann, C. A.; Ruhe, J.; Knoll, W.; Frank, C. W. *J. Am. Chem. Soc.* **1999**, *121* (38), 8766–8770.
(14) Ruckenstein, E.; Li, Z. F. *Adv. Colloid Interfac Sci.* **2005**, *113* (1), 43–63.
(15) Zhao, B.; Haasch, R. T.; MacLaren, S. *J. Am. Chem. Soc.* **2004**, *126* (19), 6124–6134.
(16) Kim, J.; Seidler, P.; Sze, W. L.; Fill, C. *J. Colloid Interfac. Sci.* **2009**, *329* (1), 114–119.
(17) Cloarec, J. P.; Chevolot, Y.; Laurenceau, E.; Phaner-Goutorbe, M.; Souteyrand, E. *IRBM* **2008**, *29*, 105–127.
(18) Choi, S. H.; Zhang, N. B. *Surf. Sci.* **2006**, *600*, 1391–1404.
(19) Vericat, C.; Vela, M. E.; Benitez, G.; Carro, P.; Salvarezza, R. C. *Chem. Soc. Rev.* **2010**, *39*, 1805–1834.
(20) Fryxell, G. E.; Rieke, P. C.; Wood, L. L.; Engelhard, M. H.; Williford, R. E.; Graff, G. L.; Campbell, A. A.; Wiacek, R. J.; Lee, L.; Halverson, A. *Langmuir* **1996**, *12*, 5064–5075.
(21) Cottenye, N.; Teixeira, F., Jr.; Ponche, A.; Reiter, G.; Anselme, K.; Meier, W.; Ploux, L.; Vebert-Nardin, C. *Macromol. Biosci.* **2008**, *8* (12), 1161–1172.
(22) An, Y.; Chen, M.; Xue, Q.; Liu, W. *J. Colloid Interfac. Sci.* **2007**, *311*, 507–513.
(23) Cumpson, P. J. *Surf. Interface Anal.* **2001**, *31*, 23–34.
(24) Wei, Z. Q.; Wang, C.; Zhu, C. F.; Zhou, C. Q.; Xu, B.; Bai, C. L. *Surf. Sci.* **2000**, *459*, 401–412.
(25) Briggs, D.; Grant, J. T. *Surface Analysis by Auger and X-Ray Photoelectron Spectroscopy*; IM Publications and Surface Spectra Ltd: Chichester, UK, 2003.
(26) Jedlicka, S. S.; Rickus, J. L.; Zemlyanov, D. Y. *J. Phys. Chem. B* **2007**, *111* (40), 11850–11857.
(27) Kwok, D. Y.; Gietzelt, T.; Grundke, K.; Jacobasch, H. J.; Neumann, A. W. *Langmuir* **1997**, *13*, 2880–2894.
(28) Van Oss, C. J. *Annu. Rev. Microbiol.* **1978**, *32*, 19–39.

(29) Bütt, H. J.; Graf, K.; Kappl, M. *Physics and Chemistry of Interfaces*, second, revised and enlarged ed.; Wiley-VCH Verlag: Weinheim, 2006.
(30) Qian, W.; Xu, B.; Yao, D.; Lin, Y.; Wu, L.; Wang, C.; Yu, F.; Lu, Z.; Wie, Y. *Mater. Sci. Eng., C* **1999**, *8*, 475–480.
(31) Chopra, N.; Hinds, B. *Inorg. Chim. Acta* **2004**, *357*, 3920–2926.
(32) Nugaeva, N.; Gfeller, K. Y.; Backmann, N.; Düggelin, M.; Lang, H. P.; Güntherodt, H. J.; Hegner, M. *Microsc. Microanal.* **2007**, *13* (1), 13–17.
(33) Liu, H. B.; Venkataraman, N. V.; Bauert, T. E.; Textor, M.; Xiao, S. J. *J. Phys. Chem. A* **2008**, *112*, 12372–12377.
(34) Alila, S.; Boufi, S. *Ind. Crops Prod.* **2009**, *30*, 93–104.
(35) Hansson, K. M.; Tosatti, S.; Isaksson, J.; Wetterö, J.; Textor, M.; Lindahl, T.; Tengvall, P. *Biomaterials* **2005**, *26*, 861–872.
(36) Ko, Y. G.; Ma, P. X. J. *Colloid Interface Sci.* **2009**, *330*, 77–83.
(37) Chen, Y.; Kang, E. T.; Neoh, K. G.; Lim, S. L.; Ma, Z. H.; Tan, K. L. *Colloid Polym. Sci.* **2001**, *279*, 73–79.
(38) Cabilil, H. L.; Pham, V.; Lozano, J.; Celio, H.; Winter, R. M.; White, J. M. *Langmuir* **2000**, *16*, 10471–10481.
(39) Minier, M.; Salmain, M.; Yacoubi, N.; Barbes, L.; Methivier, C.; Zanna, S.; Pradier, C. M. *Langmuir* **2005**, *21*, 5957–5965.
(40) Zhang, F.; Srinivasan, M. P. *Langmuir* **2004**, *20*, 2309–2314.
(41) Lee, S. H.; Lin, W. C.; Kuo, C. H.; Karakachian, M.; Lin, Y. C.; Yu, B. Y.; Shyue, J. J. *J. Phys. Chem. C* **2010**, *114*, 10512–10519.
(42) Barbot, C.; Bouloussa, O.; Szymczak, W.; Plaschke, M.; Buckau, G.; Durand, J. P.; Pieri, J.; Kim, J. I.; Goudard, F. *Colloid Surf., A* **2007**, *297*, 221–239.
(43) Kazuyuki, H.; Nagahiro, S.; Hiroyuki, S.; Osamu, T.; Nobuyuki, N. *Ultramicroscopy* **2002**, *91*, 151–156.
(44) Hiroyuki, S.; Kazuyuki, H.; Nagahiro, S.; Nobuyuki, N.; Osamu, T. *Appl. Surf. Sci.* **2002**, *188* (3−4), 403–410.
(45) Rasmussen, K. E.; Albrechtsen, J. *Histochemistry* **1974**, *38*, 19–26.
(46) Ploux, L.; Anselme, K.; Dirani, A.; Ponche, A.; Soppera, O.; Roucoules, V. *Langmuir* **2009**, *25*, 8161–8169.
(47) Werner, C.; Körber, H.; Zimmermann, R.; Dukhin, S.; Jacobasch, H. J. *J. Colloid Interface Sci.* **1998**, *208*, 329–346.

Supporting information

Figure 1

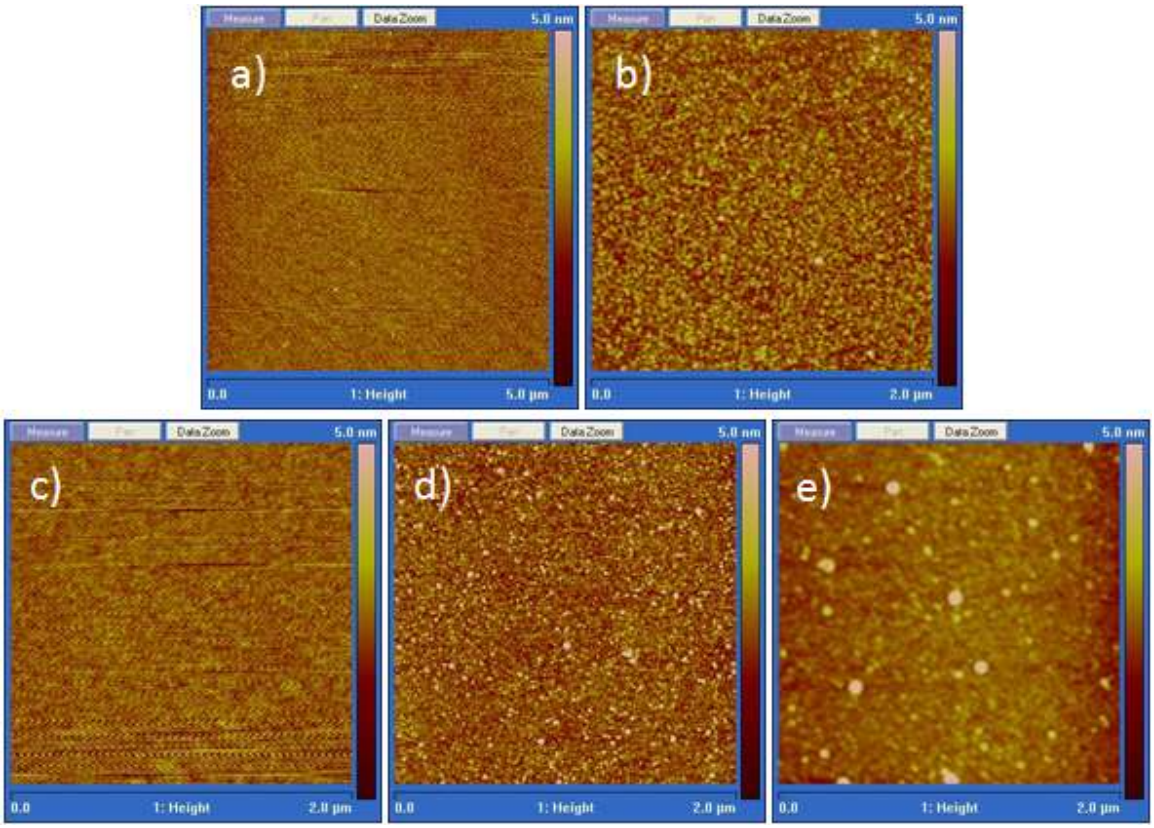

Figure 2

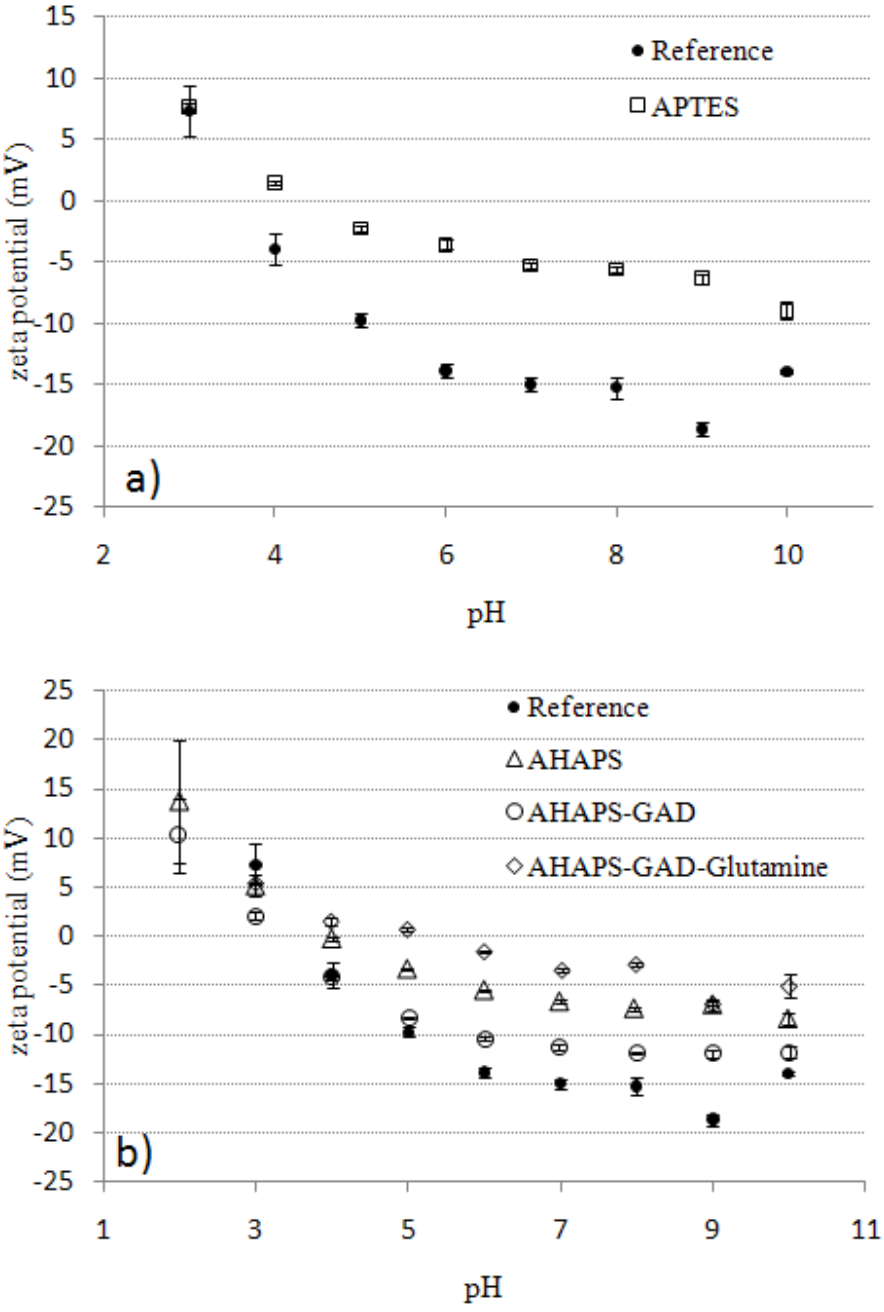
15
10
5
0
-5
-10
-15
-20
-25
zeta potential (mV)
Reference
APTES
a)
2
4
6
8
10
pH
25
20
15
10
5
0
-5
-10
-15
-20
-25
zeta potential (mV)
Reference
AHAPS
AHAPS-GAD
AHAPS-GAD-Glutamine
b)
1
3
5
7
9
11
pH

Figure 3

a)

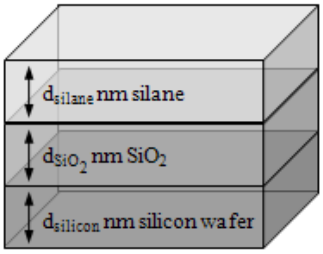

$\rho_{SiO_2} = 2.0$ g/cm^3
$M_{SiO_2} = 60.1$ g/mol
$\rho_{silicon} = 2.3$ g/cm^3
$M_{silicon} = 28.086$ g/mol

b)

$$N_{atoms_B} = \frac{\rho_B \cdot N_A \cdot V_B}{M_B}$$

c)

layer	atomic composition	Volume (nm^3)	N_{Si}	N_C	N_N	N_O
APTES	$NC_3H_8SiO_2$	0.8	5	15	5	10
siliconoxide	SiO_2	2.0	40	--	--	80
silicon	Si	6.2	306	--	--	--
∑			351	15	5	90
atomic %			76.1	3.3	1.1	19.5

layer	atomic composition	Volume (nm^3)	N_{Si}	N_C	N_N	N_O
AHAPS	$N_2C_9H_{21}SiO_2$	1.4	5	45	10	10
siliconoxide	SiO_2	2.0	40	--	--	80
silicon	Si	5.6	276	--	--	--
∑			321	45	10	90
atomic %			73.6	3.4	2.3	20.6

Figure 4

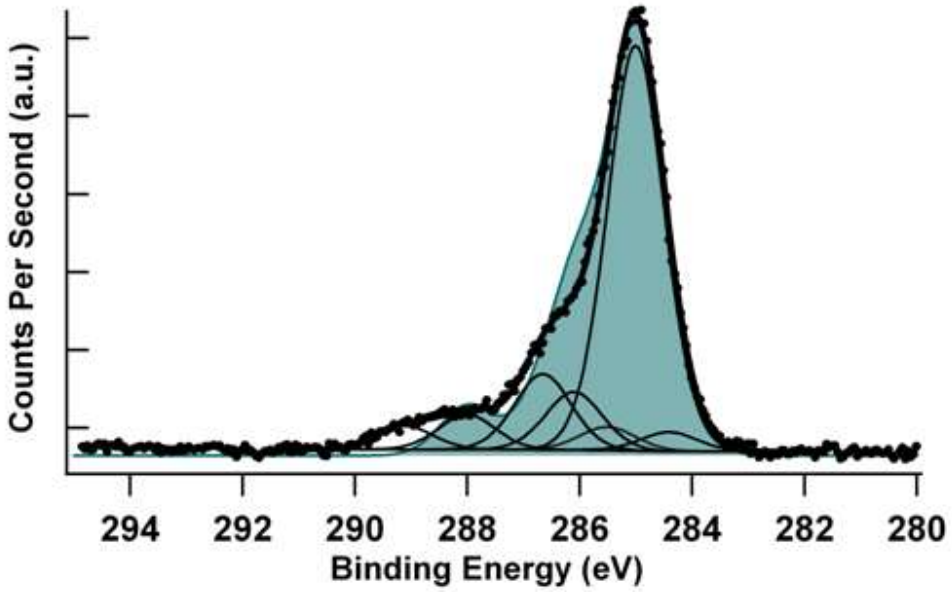
Counts Per Second (a.u.)
294
292
290
288
286
284
282
280
Binding Energy (eV)

Supporting Information.

Figure 1: AFM height images of the model surfaces. a) Reference surface displaying a flat topography in agreement with the common silicon wafer topography. b) APTES surface displaying a heterogeneous topography attributed to the polymerised, multilayer structure formed by the APTES molecules. c) AHAPS surface displaying a homogeneous topography in agreement with the monolayer, but not well-organised ("head to foot " molecular organisation) structure formed by the AHAPS molecules. d) AHAPS-GAD surface displaying small aggregates attributed to GAD aggregates grafted on the rare amine groups present on the surface top. The surface is not homogeneously and completely covered by a GAD layer. e) AHAPS-GAD-glutamine surface displaying larger aggregates attributed to glutamine grafted on GAD aggregates. The surface is not homogeneously and completely covered by a glutamine layer.

Figure 2: Zeta potential vs. pH curves for each of the model surfaces. The pH corresponding to the inflection point indicates the IEP value.

Figure 3: : Calculation of the theoretical atomic composition that should be measured by XPS analysis for APTES and AHAPS model surfaces. a) Layers model used for the calculation. b) Equation used for calculating the number of atoms detected in each layer and therefore the atomic ratios, where N_A is the Avogadro constant, ρ_B and M_B are respectively the density and the molecular weight of the B material, V_B is the volume of the B material (V_B = 1nm^2 X d_B nm, with d_B the thickness of the B material). c) Table giving the theoretical number of atoms (N) in each layer. N was calculated on the basis of an average grafting density of 5 molecules of silane per nm² as found in the litterature[1,2], and a probing depth of XPS of 9nm.

Figure 4 : C1s peak fitting in the case of experimental AHAPS-GAD substrates (line curve). The spectrum is decomposed in six components listed in table 3. The full curve is a representation of an « ideal » synthetic envelope in the case of a 100% yield of glutaraldehyde molecule grafting (7at% C-Si, 57at% CHx, 22at% C-N, 7at% C-O and 7at% C=O).

2.5 Supplementary Information

2.5.1 XPS analysis: Calculation of the thickness of a thin overlayer

In this paragraph it is shown in an example how of the thickness of a thin overlayer is calculated. The utilized principle is that the intensity of the substrate signal decreases when the layer is added to the substrate. The equation 2.4 of section 2.3.3.1 relates the pure and modified substrate with respect to the overlayer. The corrected area of the Si2p peak was used as intensity of the substrate (see equation 2.5) [118, 126, 127]. Cumpson *et al* demonstrated a way to calculate the mean free path ($\lambda(E_B)$) for molecule units: The methods was originally developed for polymers units [128] to calculate the thickness of an overlayer, with repeating molecular units. For example, here $\lambda_{Si_{APTES}} = 4.8\ nm$ is obtained, using the relation given in equation 2.9.

$$\lambda(E_B)[nm] = \frac{3.117({}^{o}\chi^{v}) + 0.4207N_{rings}}{N_{non-H}} + 1.104(E[keV])^{0.79}, \tag{2.9}$$

where ${}^{o}\chi^{v}$ is the index of repeat unit (APTES molecules), N_{rings} is the number of atomic six-member rings (for APTES $N_{rings} = 0$), N_{non-H} is the number of atoms in APTES excluding hydrogen atoms and E is the energy of the anode in keV (for Al K_α E = 1.4866 keV). The index ${}^{o}\chi^{v}$ depends on the electronic environment and the bonding configuration of the atoms in the molecules [117] and is given in equation 2.10. A ${}^{o}\chi^{v}$ value of 8.66 was estimated for APTES.

$${}^{o}\chi^{v} = \sum\nolimits_{non-H} \frac{1}{\sqrt{\delta^{(v)}}}, \tag{2.10}$$

where $\delta^{(v)}$ describes the valence connectivity, which expresses the electronic structure of the skeletal atoms in the molecule. The valance connectivity index counts all valence electrons and is described by equation 2.11.

$$\delta^{(v)} = \frac{Z^{(v)} - h}{Z - Z^{(v)} - 1}, \tag{2.11}$$

where $Z^{(v)}$ is the number of valence electrons in an atom, h the number of hydrogen atoms bound to it and Z is its atomic number, consequently is $Z - Z^{(v)}$ is the number of inter-shell electrons. The $\delta^{(v)}$ values of Si, C, N and O are listed in table 2.3.

Table 2.3: Values of valence connectivity index [128].

Atom	Si		C									N						O		
Hybridization	sp^3		sp^3				sp^2			sp		sp^3			sp^2		sp	sp^3		sp^2
N_H	1	0	3	2	1	0	2	1	0	1	0	2	1	0	1	0	0	1	0	0
$\delta^{(v)}$	1/3	4/9	1	2	3	4	2	3	4	3	4	3	4	5	4	5	5	5	6	6

2.5.2 XPS analysis: Calculation of the theoretical atomic composition

For a better interpretation of the survey spectra and the resulting atomic qualification, the atomic composition for an ideal monolayer of an APTES and an AHAPS surface were calculated, assuming five silanes per nm^2 grafted onto the silicon wafer [129, 130]. The model was simplified by setting on 3λ as 9 nm for all measurement. A three layer model was used to describe the system silane/SiO_2/Si_{wafer} as shown in figure 2.12. The first layer corresponds to the organic layer (grafted silane). The theoretical length for a fully extended silane was used for the height of this first layer (APTES=0.8 nm and AHAPS=1.4 nm). The second layer represents the oxide layer (SiO_2) of the wafer with a thickness of 2 nm, as determined by ellipsometry. The third layer finally correspond to the substrate, here the pure silicon. Through the assumption of an analysis depth of $h_{XPS} = 9$ nm, the thickness of the measured Si layer (d_{Si}) is consequently calculated by equation 2.12.

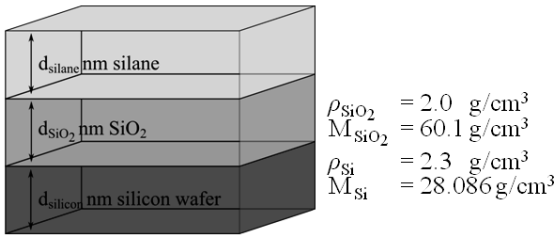

Figure 2.12: The three layer model describes the system used to calculate the theoretical atomic composition.

$$d_{Si} = h_{XPS} - d_{SiO_2} - d_{organic\,layer}, \tag{2.12}$$

where $d_{organiclayer}$ is the thickness of the concerning layer X.
The theoretical number of atoms in each of these three layers was calculated to estimate the final atomic ratio on the surface. In the organic layer, five silanes are considered per nm^2, hence the number of atoms of the silane was multiplied by five. The equation 2.13 was applied to calculate the theoretical numbers of atoms of the SiO_2 and Si layer.

$$N_{atoms_B} = \frac{\rho \cdot N_A \cdot V_B}{M_B}, \tag{2.13}$$

where N_A is the Avogadro constant, M_B and V_B are the molecular weight and the density of the material B (either SiO_2 or Si).
The volume is determined by an assumed area of 1 nm^2 and the thickness of the layer. Figure 3 in the supporting information of the article shows the estimated values of the atomic percentage on the two APTES and AHAPS surfaces. Here, N_X denotes for the number of the present elements, Si, C, N and O in each layer. The sum of each element within h_{XPS} was used to determine the ideal ratio.

2.6 Conclusion

We could demonstrate (in collaboration with the laboratory of Prof. Vincent Ball), in this second chapter, the importance of a thorough and careful characterization of model surfaces. The combination of different characterization techniques can allows a suitable description of the real model surfaces. To determine the most adequate combination of different techniques to reveal characteristics of the overlayer, frequently used amino terminated silanes (APTES and AHAPS) were used.

In this characterization process, the main technique was XPS. The experimental atomic ratios obtained by XPS have been compared to theoretical calculations. This allowed to highlight, for example, too high atomic content of nitrogen, indicating multilayer structure. High resolution spectra were also used. They allowed to obtain informations about the environment of each element and its electronic configuration, leading to highlight side reactions or unexpected electrostatic interactions that may lead to positively charged nitrogen, for example.
The chemical properties of the overlayer were also assessed by contact angle that are fast to perform and can be used to easily follow the change of the hydrophilic or hydrophobic character during a several step synthesis of the surface. Contact angle measurements were also exploited to prove dense packing of the grafting molecules. Furthermore, by considering hysteresis between advancing and receding angles, indications about the overlayer topography was obtained. Topography was especially further studied by AFM imaging.
The thickness of the grafted layer, determined by ellipsometry, was measured in air and in water and compared to thickness in vacuum assessed by XPS. The monolayer or multilayer structure was determined by comparing these obtained values with the theoretical ones. Furthermore, comparison between thicknesses measured in liquid and dry conditions allowed to identify a possible swelling or collapsing of the overlayer, since deposited and stable monolayer should lead to thickness similar whatever the conditions. Finally, zeta potential and IEP values were used to finally confirm the chemical composition of the overlayer.

The adequate combination of these indications allowed to highlight particular features of the layer on the contrary to the combination of techniques the most commonly reported in the biointerface literature. Precise descriptions of the layers could therefore be proposed, showing non-ideal structures and organizations. The combination of different characterization techniques is thus crucial to be able to interpret the obtained results correctly.

The results presented in this chapter show finally that a careful control of the real structure and stoichiometry of the overlayer is necessary for further biointerfaces studies. Beside, this work confirms that common aminosilane seems to not to allow this control and another route to gain reproducibility and control of SAMs of the final surface will be proposed in chapter 3.

Chapter 3

Model surfaces with well controlled densities

3.1 Introduction

The goal of this third chapter is to obtain well-defined and stable surfaces with different densities of amino groups in a CH_3 environment, for further studying bacterial adhesion on them. As it was shown in the second chapter of the thesis and in the article *"Necessity of a Thorough Characterization of Functionalized Silicon Wafers before Biointerface Studies"*, the amino terminus reacts with the silicon substrate and the head group of the silane, which results in multilayers (APTES) or unorganized layers (AHAPS). Aminosilanes are prone to oligomerization and it exists a competition between amine groups and silane for the interaction with the surface.

Thus, in this chapter, another strategy was proposed in which a silane with a terminal group that does not interact with the substrate is used. Conditions of preparation were carefully adapted to assure that layer was organized as a monolayer. Then, the functional group can be converted into an amine. As already shown in literature by several research groups [73,131–133], the bromine terminus can be (i) converted into an azide by nucleophilic substitution, and (ii) subsequently reduced to an amine. To optimize the grafting reaction and the conversion, different conditions of reaction were investigated. Further, the bromine silane can be combined with a second silane, a silane that contains an alkyl terminus. The two silanes can be used together and depending on their initial concentration in solution, mixed monolayers with the corresponding ratio of the bromine and alkyl silanes are obtained. Consequently, after the conversion of the bromine functional groups into amine groups, surfaces with different densities of amino groups backfilled from methyl groups are achieved.

Further in this chapter, different methods are described to graft a single amino acid. The objective was to assess if a surface fully covered with amine groups in close contact to each other keeps its reactivity despite the sterical hindrance in the vicinity of the surface. At first, three different homobifunctional linker were used to promote the grafting of the

amino acid glycine. In a second approach, glycine was directly grafted onto the substrate. The amino group of glycine was protected by fluorenylmethyloxycarbonyl (Fmoc), to avoid polymerization and 2-(1H-Benzotriazole-1-yl)-1.1.3.3-tetramethyluronium hexafluorophosphate (HBTU) was used as coupling agent. The surfaces were thoroughly characterized by XPS and the reaction yield was calculated based on the obtained results.

The chapter is based on two unpublished articles. Results that were not considered in the article were presented in the SUPPLEMENTARY INFORMATION that followed the concerned article.
The first article (2a) deals with the importance and the impact of the organization of model surfaces on bacterial adhesion and the realization and characterization of such model surfaces.
In the second article (2b), well-controlled amine terminated substrates were used to investigate various grafting possibilities of the amino acid glycine, via homobifunctinal linkers and the thoroughly characterization of the realized surfaces by XPS.

3.2 State of the art

3.2.1 Amino terminated self-assembled monolayers

In the second chapter, APTES and AHAPS were used as model surfaces to establish the characterization methodology of model surfaces on silicon wafers. However, neither APTES nor AHAPS appeared as adequate silanes to perform well controlled monolayers.
Therefore, to avoid side reactions and gain a better reproducibility, the choice of the silane plays a significant role. First, long-chain organosilane should be preferred to avoid multilayer structures [134]. Long chains favors Van der Waals interactions along the chain facilitating a more dense layer. Secondly, the functional groups must not compete with the head groups and interact with the surface [132]. In addition, the temperature and the solvent have to be adjusted to reduce the production of silane aggregates. The ideal temperature (T_i) for the deposition of controlled monolayers (silanes) depends on the chain length and the used solvent. T_i was found to be 0 °C for 10 carbon atoms in the main chain [73, 134]. The solvents are chosen on the basis of the main criteria: the solubility of the main chain [$(CH_2)_n$] and the head group. A good solubility is necessary to avoid micelle formation in solution [73, 132]. Consequently, to induce a well defined thin layer, trichlorosilanes with a non-nucleophilic functional group (as halide) are favorable. The advantage of halide functionalized silanes is the possibility of changing the halide group into another functional group by a nucleophilic substitution (S_N2) [131, 132, 135] and of avoiding an interaction with the surface.

In the 90ths Balachander and Sukenik [131] showed for the first time that S_N2 reactions can be used for the conversion of functional groups of monolayers. They investigated different

nucleophiles[1](Nu) like N_3^-, SCN^-, S^{2-} and S_2^-, and demonstrated that the monolayer structure can be preserved under adequate reaction conditions. Some years after, Fryxell *et al.* [132] highlighted that the S_N2 reaction is significantly retarded on surfaces compared to the reaction realized in solution. By increasing the surface-azide concentration, the S_N2 reaction slowed down.

The nucleophilic substitution reaction contains two reactions (see figure 3.1), the attack and the suppression of one functional group of the molecule that should be modified. A nucleophile reacts with a molecule that binds a nucleofuge[2] [136], which is ejected from the molecule by bond cleavage. In this process, the nucleophilic group provides an electron pair, while the binding electrons are retained with the leaving group (LG) [137]. The most important nucleophiles are Cl^-, Br^-, I^-, HO^-, RO^-, HS^-, N_3^-, all of them have a free electron pair that can attack a molecule. In general, the leaving groups (nucleofuges) are electron attractive and the bond between the carbon atom and the leaving group is polarized by the induction effect of the leaving group. Furthermore, the dissociation energy between leaving group and the carbon atom (C-LG) should not be too high, otherwise the bond is difficult to break. The less alkaline these groups are, the higher is the tendency that the bond breaks. The following leaving groups are typically found in literature: -Cl, -Br, $-OH_2^+$, $-NR_3^+$, sorted by energy bond. If the new connection is build simultaneously with the break of the bond between the carbon atom and leaving group, then the reaction is called a bimolecular nucleophilic substitution or S_N2. The nucleophile approaches a polarized bond of C-LG from the opposite direction (backside) of the leaving group and interacts with the carbon atom. Synchronously with the formation of a new Nu-C bond the distance of the C-LG bond increases. The S_N2 reaction goes through a transition state where the nucleophile is bonded loosely, and the leaving group is not yet totally suppressed (see figure 3.1). This transition state or complex has steric demands due to the penta coordinated carbon atom [137].

In SAMs the nucleophile must penetrate the monolayer to attack the C-LG bond from the backside. Therefore, the nucleophile has to be a small and strong nucleophile. There is a kinetic barrier, due to the fact that the monolayer is closely packed and in which the nucleophile must shed much or all of his solvent shell to be able to penetrate the monolayer. The success of a displacement reaction in SAMs depends strongly on the type of SAM and its defects [132].

Chemical reactions or modifications on solid surfaces are difficult to follow compared to organic reactions in liquid phase. However, it can be done by a thorough investigation by XPS [131–134], and additionally by measuring changes of the contact angle and layer thickness [131–133, 138] as will be demonstrated in this chapter [76].

[1] A nucleophile contains a free electron pair.
[2] A nucleofuge is a leaving group that retains the electron pair of a bond.

Nevertheless, it is crucial to adjust the reaction conditions to obtain controlled monolayers. Since trichlorosilanes are highly reactive and might tend to polymerize in the presence of water, controlled conditions must be carefully chosen to avoid side reactions [74].

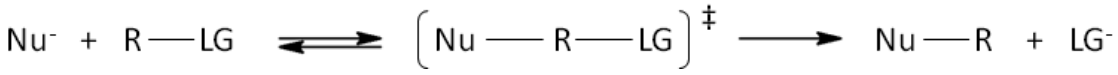

Figure 3.1: The general mechanism of a nucleophilic substitution (S_N2). The nucleophile is approaching the molecule, which contains a leaving group. A transition state (‡) is formed, where both the Nu^- and the LG are bound to the molecule. In a third step, the LG is suppressed and the Nu^- is bound to the molecule.

3.2.2 Mixed monolayers (MML)

Chemical gradients are of great interest for various studies and practical applications. On the basis of such surfaces with gradients, biomolecular interactions, cell motility and microfluidics can be investigated [138]. Another possibility are surfaces with different densities of one molecule species within another. The co-adsorption of two different surfactants, for example, leads to mixed monolayers. In general, two or more silanes with different terminal functionalizations are diluted in an adequate solvent. By immersion of the substrate in the solution, the silanes are adsorbed onto the surface (see figure 3.2 a). If the two silanes are similar in their physical properties (chain length, terminal functionalization etc.), the co-adsorption of both silanes is regarded as equal. Hence, it is expected that despite the different terminal groups of the silane a correlation exists between the concentration in solution and the concentration of the silanes on the surfaces [65, 98, 132]. It was further presumed by Fryxell *et al.* that the bromine and a methyl terminal group monomers are identical [132]. Hence, no segregating nor islanding is attended and the distribution of the molecules in solution is random [132, 139–141] (see figure 3.2 b) [132].

Mixed monolayers with designed surface composition allow us to control surface properties like surface energy, roughness and chemical reactivity [65, 142]. There are three different kinds of MMLs, not considering the head group of the surfactants e.g. silanes or thiolates. The first kind are mixed monolayers, caused by different (ω)-functionalized molecules, but with the equally chain lengths [10, 132, 133]. The resulting MMLs are quite flat and different wettability properties of the surface can be obtained. The second kind of MMLs is caused by molecules with different chain lengths, while containing the same functionality of the terminal group [139]. The obtained mixed SAMs are suited to investigate roughness effects. Finally, to get the third kind of mixed monolayers, molecules with different (ω)-functionalities and different chain lengths [10, 18, 77] are used.

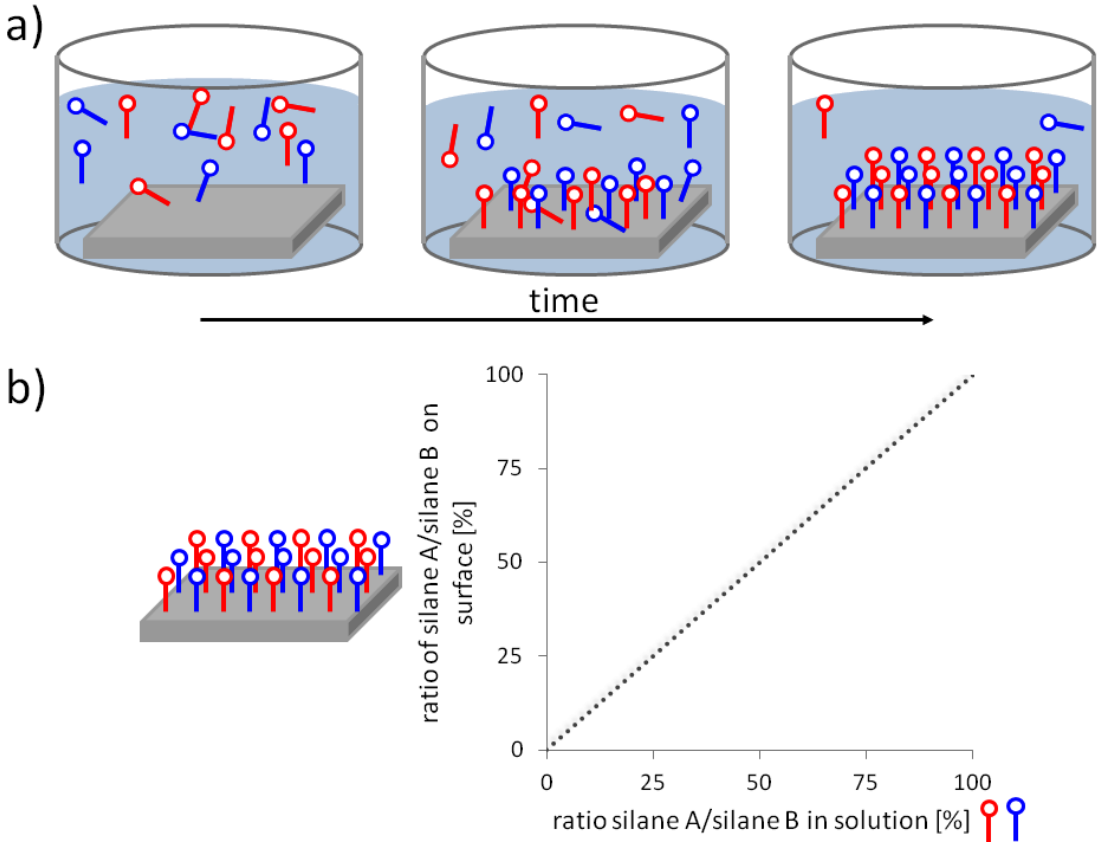

Figure 3.2: Fabrication of mixed monolayers. A co-adsorption of two different silanes takes place after immersion of the substrate in solution. In case the two silanes have comparable physical properties, a linear correlation between the silane in solution and on the surface is expected [132].

3.2.3 Biomolecule grafting

In the biomaterial and biomedical field, the grafting of biomolecules on a surface is frequently applied. On one hand, there is the non-covalent adsorption of the biomolecule and on the other hand the covalent linkage between the biomolecule and the surface. However, for the covalent grafting of biomolecules, functional groups of the surface are required to which the biomolecule can attach. Thereby, the surfaces are functionalized by alcohol-, alkene-, alkine-, amine-, carboxy-, hydroxy-, thiol-, or halide-groups [75, 143–147]. However, most of the studies in literature are concerned with the grafting of biomolecules on amine groups. Thus, an aim of this work was to achieve amine terminated surfaces. Surface grafting take place by aid of a linker molecule or via coupling agents. These coupling agents activate either the surface or the biomolecule. For a successful reaction between surfaces and biomolecule either the surface site or the biomolecule has to be activated. Thus the energy barrier of a reaction can be reduced and the reaction becomes faster. In literature, the combination of N-hydroxysuccinimide (NHS) and ethyl(dimethylaminopropyl) carbodiimide (EDC) is frequently used, to activate the carboxy group of biomolecule or

surface [144]. Another method is the activation of the carboxy group with hydroxybenzotriazole (HOBt), which enables the reaction with amine groups. However, if the biomolecule i.e. a protein is activated in solution, e.g. with HOBt, it is necessary to protect the amine functionalization of the biomolecule with for example 9-fluorenylmethyl succinimidyl carbonate (Fmoc-OSu) to avoid the polymerization.

In general, the biomolecule is not directly grafted onto the functionalized surface. Several parameters like sterical demands, activation barriers etc., have to be overcome before grafting. One solution is to use a linker molecule, also called a spacer, as a linkage between the surface and the biomolecule. Another advantage of the linker is to preserve biological activity of molecules, by moving the biomolecule away from the surface. The kind of linker depends on the functional group of the surface. An amine group can react with an aldehyde or a diisothiocyanate. Short or long, flexible or rigid, hydrophilic or hydrophobic molecules [144] may provide the linkage between the functional groups of surfaces and the functional group of the biomolecules. Linkers are either ring-opening-molecules, homofunctional or heterofunctional[3], regarding the reaction or functional groups they are carrying. These coupling agents or linkers can provide almost any functional groups at the surface and the desired or requested biomolecule [143, 144].

Typical homobifunctional linkers between two amino functionalities which are also used in this work are: glutaraldehyde (GAD), di-(N-succinimidyl)oxalate (DSO) and 1.4-phenylendiisothiocyanate (PDITC). GAD is a short homo-biofunctional coupling reagent, which is commonly used to graft biomolecules [148]. However, it is also known that GAD leads to a weak quantity of grafted molecules [149] and can polymerize on the surface [150]. By the reaction of the GAD-aldehyde group with an amino group, a Shiff base (C=N) is obtained. These bonds are very unstable and the reaction is reversible [85], hence the Shiff base has to be reduced with e.g. $NaCNBH_3$ to get a stable amide bond [151]. An alternative to GAD is a homobifunctional linker without aldehyde functionality like DSO and PDITC. DSO contains two leaving groups, which are suppressed by reaction with amine groups, which results in an amide bond. PDITC contains two thiocyanate groups and an aromatic ring system. Hence, PDITC, is able to react with an amine group, while its π-system in the aromatic ring provides its stacking [149]. An overview of commonly used methods of biomolecule grafting is shown in table 3.1. Generally, most of the grafting methods are based on amine or carboxy groups, due to their high amount in biomolecules, such as peptides or enzymes.

There are two preparation techniques to graft biomolecules by aid of a coupling agent, which are frequently used in literature. The first one is a one-step technique in which the surface, the coupling agent and the biomolecule are altogether and the reactions take places simultaneously. The problem of this technique is that the biomolecule may polymerize if the functional groups are not protected. The second technique is a multi-step method,

[3] A homobifunctional linker is a molecule with two reactive functional groups, while heterofunctional linkers contain different reactive groups [144].

where the surface is activated in a first step and the biomolecule is added in a second one. This technique avoids the polymerization of proteins and amino acids [143], but not polymerization of linker molecules, which can react with each other, like GAD and is also more time consuming.

In general, there are issues regarding the orientation and the mobility of the grafted biomolecule [152]. However, a not controlled grafting of biomolecules resulting in an unorganized layer may be lead to problems for some applications. For other devices, like biosensors, the loading capacity and the density of grafted biomolecules are crucial. Therefore, it is important to understand the reaction of an abiotic material and its affect on the biofunctionality of the biotic layer [153] to improve devices.

Table 3.1: Methods for the grafting of biomolecules [144].

functional group of surface	functional group of biomolecules	resulting chemical linkage
NHS-ester	amine	amide
aldehyde	amine	imine
isothiocyantate	amine	thiourea
epoxide	amine	aminoalcohol
amine	carboxy	amide

3.3 Material and Methods: Part 1

3.3.1 Grafting of silanes

In the following, two different silanes were used to provide SAMs, namely 11-Br-undecyltrichlorosilane and undecyltrichlorosilane. Both silanes were furnished by ABCR in Germany. They have the same chain lengths of CH_2 units and similar properties. Neither the terminal group Br nor CH_3 interact with the substrate. Thus, these silanes are expected to prone to well controlled (mixed) self assembled monolayers, due to their physical similarity. The protocol of grafting of the silane and optimization of bromine monolayer are described in detail in article 2a on page 85.

3.3.1.1 Optimization of silane grafting

The piranha activated substrates were immersed in a solution containing 1 mM silane in different solvents [s_o] for different reactions times [t_o] and at different temperatures [T_o]. The substrates were then rinsed either with or without an annealing step and an ultrasonic treatment (15 min in $CHCl_3$). In this process, three condition-sets were carefully investigated (see table 3.2). The three conditions are different in reaction time, temperature, solvent and final rinsing step.

The first condition-set, reflects a well investigated protocol [71] for the grafting of bromine-trichlorosilanes. The original protocol was established in the 90ths and apparently well-controlled monolayers were obtained. The second condition-set is a general protocol that was used for the grafting of silanes under no specific conditions. Therefore, these surfaces were elaboratted in hexadecane, at room temperature and overnight, followed by a short immersion in hot water and a 1 min sonication treatment in $CHCl_3$. Finally, the third condition-set considers a study of trichlorosilanes with similar lengths on various temperatures [73]. In the process of optimization, further experiments were carried out to establish the third condition set as final protocol. All three condition-sets were performed to obtain bromine monolayers. In the first and second condition-sets, the surfaces were rinsed after the grafting step, while in the third condition-sets an annealing step followed by 15 min ultrasonic treatment was added.

As mentioned above, different solvents (polar, apolar, mixture of two solvents), different temperatures (6 °C, 20 °C and 45 °C) and different reactions times (4 h, 5 h and 16 h) were used to optimize the monolayer. To obtain stable surfaces an additional annealing procedure was added in a first step. In a second step, different solvents were used for the desorption of the silane: $CHCl_3$, n-heptane, toluene and 30 % $CHCl_3$ in 70 % n-heptane (v/v). The most promising results were obtained with the solvent 30 % $CHCl_3$ in 70 % n-heptane, which was hence used for further optimization. The next parameter that was changed was the temperature. The experiments were conducted at 6 °C, 20 °C and

45 °C and a reaction temperature of 6 °C was finally selected. The surfaces are generally described by their expected surface coverage (e.g. 75 %Br). Therefore, the experiments were performed in 30 % $CHCl_3$ in 70 % n-heptane, at 6 °C for 4 and 16 h followed by a rinsing, an annealing step and finally an ultrasonic rinsing of 15 min.

Table 3.2: Controlled grafting of silanes.

parameter	1. condition	2. condition	3. condition
concentration	1 mM	1 mM	1 mM
solvent	hexadecane	hexadecane	heptane(70 %)/$CHCl_3$(30 %)
time	4 h	16 h	4 h
temperature	45 °C	room temperature	4 °C
rinsing	$CHCl_3$/ hot water	$CHCl_3$/ hot water	$CHCl_3$/ hot water
annealing	–	–	1 h at 105 °C
ultrasounds	–	–	15 min, 45 kHz

3.3.1.2 Variation of surface density

After the optimization of the reaction conditions for the grafting of bromine silane, the final protocol (third condition-set) was used to perform mixed monolayers. Different ratios of 11- bromoundecyltrichlorosilane and undecyltrichlorosilane were used to induce various densities of functionalized surfaces (see figure 3.3).
The final concentration of silane was set up to 1 mM in a solution of 30 % $CHCl_3$/70 % n-heptane (99 %, Carlo Erba) in volume. The five bromine densities 0, 25, 50, 75, 100 % Br were further investigated. The wafers were immersed over 4 h at 6 ± 0.8 °C in the silane solution with a concentration of the bromo silane according to the desired bromine density of the final surface, followed by a rinsing step with $CHCl_3$ and hot water and baking for 1 h at 105 °C. Afterwards, the wafers were thoroughly rinsed by 15 min ultrasonic treatment in $CHCl_3$ and dried under nitrogen stream.

3.3.2 Conversion of Br into NH_2

The conversion of bromine terminal groups into amine terminal groups takes place in two steps, depicted in figure 3.4. In a first reaction, the bromine is replaced by an azide and in the second reaction, the azide is reduced to an amine.

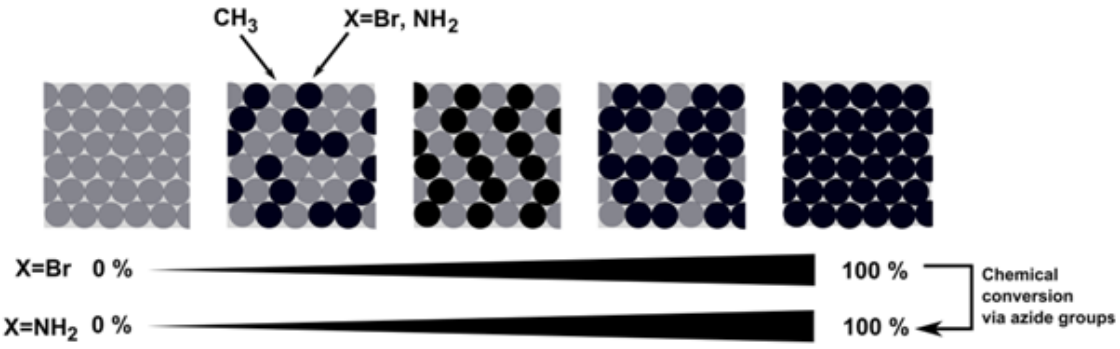

Figure 3.3: Various densities of Br in CH_3 were first introduced on the silicon wafers to obtain MMLs. Afterwards, the bromine was chemically converted into amine groups.

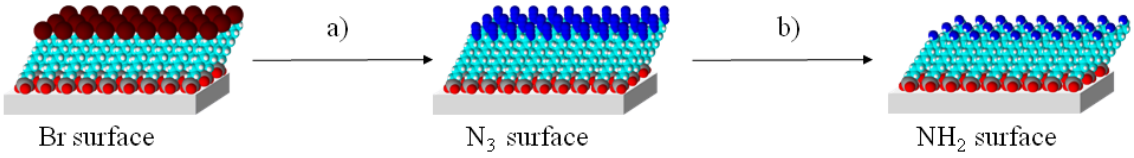

Figure 3.4: (a) The Br-groups of the obtained monolayer are converted by an S_N2 reaction in N_3-groups. (b) These N_3-groups are subsequently reduced in NH_2-groups.

3.3.2.1 From Br to N_3

Bromine-functionalized samples were immersed in a solution of 0.7 M NaN_3 in DMF (both purchased from Sigma-Aldrich), under shaking for 72 h and at room temperature. Afterwards, the samples were rinsed with MilliQ water and acetone and dried under nitrogen stream [131, 133].

3.3.2.2 The kinetics of the replacement reaction

The S_N2 reaction was performed in over saturated solution of NaN_3 in water and DMF. The reaction vessels were shaken at room temperature for several hours. XPS analysis was performed after 1, 6, 12, 24 and 72 h to verify the substitution reaction of Br^- by N_3^- and to determine the end of the reaction. A typical behavior for a kinetic reaction is expected, i.e. a fast increase (decrease) of N (Br) with time while the speed of the reaction slows down, as depicted in figure 3.5.

3.3.2.3 Reductive amination

Azide terminated samples were reduced overnight in a solution of 0.2 M $LiAlH_4$ (Sigma-Aldrich) in THF (Carlo Erba), followed by an immersion of the samples in THF for 12 h at

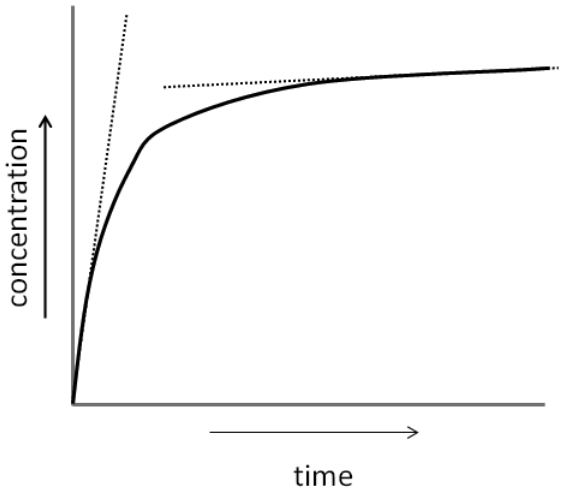

Figure 3.5: A S_N2 reaction is usually fast at the beginning, and slows down with time and increase of the product concentration.

room temperature. The lithium complexes formed on the surface were removed by hydrolysis. For that purpose, samples were immersed for 1 h in 10 % HCl (Sigma-Aldrich). Afterwards, the samples were rinsed with MilliQ water and EtOH (absolute, Sigma-Aldrich) and dried under nitrogen stream. Similarly to the lithium-complexes, the NH_2-groups on the surface were reduced to NH_3^+. To achieve NH_2-groups, the NH_3^+-groups were converted by immersion in triethylamine (TEA, 99.5 %, Sigma-Aldrich) during 24 h, at room temperature (see figure 3.4 b). Finally, the samples were rinsed several times with MilliQ water and EtOH and dried under nitrogen stream [131, 133].

3.3.3 Microbiology experiments on homogeneous amino terminated surfaces

Bacterial adhesion experiments were carried out to compare homogeneous 100 % amino terminated SAMs (APTES, AHAPS and 100 %NH_2) and the impact of their organization on bacterial adhesion. Bacterial adhesion studies are explained in detail in article 2a, page 89.

3.3.3.1 Bacterial strains

In the bacterial adhesion studies, the laboratory strain *E.coli* MG1655 [154], SCC1 [155] was used. This bacteria strain is auto fluorescent, through a genetic insertion [155], expresses curli and produces exo-cellular polymeric substances (EPS) [154].

3.3.3.2 Bacterial cultivation

Bacteria were cultured overnight in the selective M63G media at pH 6.8 at 30 °C, for detailed information about the media, the properties and provenance of the products see chapter 4. A second preculture was inoculated by the overnight culture (10 vol-% of the first culture), and was grown for 4 h at 30 °C. The final culture, used for performing the bacterial adhesion experiment, was inoculated with this 4 h preculture (10 vol-% of the second culture). The optical density at 600 nm (Abs_{600}) was adjusted to 0.1 (i.e. 10^6 bacterial/mL).

3.3.3.3 Static experiments

The substrates were sterilized by immersion in 70 % EtOH for 30 min and subsequently rinsed with sterile MilliQ water under a laminar flow. Finally, the substrates were dried and put into small petri dishes (ø 35 mm).
3 mL of the bacteria culture (Abs_{600} = 0.01) were added to the substrates. Bacteria were grown for 2 h at 30 °C on the samples. Subsequently, the samples were thoroughly and carefully rinsed with NaCl (150 mM), to remove non attached bacteria without creating an air-surface interface and to remove media from the Petri dish.

3.3.3.4 Observation of bacterial adhesion by confocal laser scanning microscopy

The samples were analyzed by taking images of the surface with an upright confocal laser scanning microscope (Carl ZEISS, LSM700). The *gfp* fluorescence of *E. coli* SCC1 was exploited for imaging in fluorescence mode with a laser wavelength of 488 nm for excitation. A reference experiment was conducted with a sterile piranha cleaned wafer (see section 2.3.1). The obtained images were analyzed by ImageJ 4.13 software and the number of bacteria was determined. Statistical T-Test analyses (excel) were done, and the bacterial adhesion behavior on one surface was compared to the bacterial adhesion behavior on another surface.

3.3.4 Surface analysis and treatment of results

AFM, zeta potential and ellipsometry were used to characterize surface modifications. XPS was used to determine the ratios of mixed monolayers and to evaluate surface reactions yield. For contact angle measurements, the surfaces and their modification were thoroughly analyzed and interpreted by XPS survey and high resolution spectra. For more detailed information see article 2a on page 88.

3.3.4.1 Additional information on XPS analysis

The same parameters as in the second chapter (see on page 28) were used to analyze the XPS spectra of the well-controlled monolayer and mixed monolayers. In addition, two more characteristic high resolution spectra (the Br3d of the bromine monolayer, and a second N1s spectra of azide signal) will be analyzed in this chapter.

For analysis of the survey spectra, the corrected area of the Br3d signal at ~ 69 eV (relative sensitivity factor (RSF): 2.84) was used for further treatments. In the high resolution spectra, the Br3d peak further contains two specific signals that are correlated to the spin orbit coupling of Br3d 5/2 at 69 eV (RSF of 1.68) and Br3d 3/2 at 70 eV (RSF of 1.16). An area constraint was set to 0.69 to obtain equal corrected areas for the both signals, while the fwhm constraint was fixed to be equal (see table 3.6.1).

During the conversion of the terminal group of the monolayers, an azide group ($^{-}N \equiv N^{+} - N-; ^{-}N = N^{+} = N-$) is obtained in the intermediary step. By XPS analysis of an azide group, a very characteristic high resolution signal can be obtained for the three different configurations of the nitrogen components ($N^{+}; N^{0}; N^{-}$). One of the nitrogen atoms is neutral, the second is negatively charged, while the third nitrogen atom is positively charged. Consequently, the emitted electrons hold different kinetic energies as a result of different nitrogen charges in the azide group. Hence two peaks are detectable at different binding energies with a separation distance of ~ 3.7 eV. The signal of the positively charged nitrogen is measurable at a higher binding energy than the other two nitrogen components. The neutral and negatively charged nitrogen signals (0.5 eV distance) are not fully separated due to energetic resolution but the area of this peak is double of the N^{+} previous peak. For the deconvolution of high resolution spectra three components were set up with the same fwhm and the area constraint was fixed to be equal (see figure 3.6).

3.3.4.1.1 Mixed monolayers

Further, the coverage of bromine, azide and amine of mixed monolayers was calculated. The coverage X_{Br,N_3,NH_2} [%] provides the information, whether the experimental ratio for pure (100 %) monolayers or mixed monolayers is in an agreement with the expected ratio (depending on the ratio of silanes in solution in the first grafting step, see section 3.3.1). There are two possibilities to determine the surface coverage: one is based on the data of the survey spectrum (see equation 3.1) and a second one is based on the high resolution spectra of C1s and Br3d or N1s for bromine or azide/amine surfaces, respectively. The coverage is given by the two following equation,

$$X = 11 \cdot \frac{A_{Br3d\ or\ N1s}}{A_{C1s}}, \tag{3.1}$$

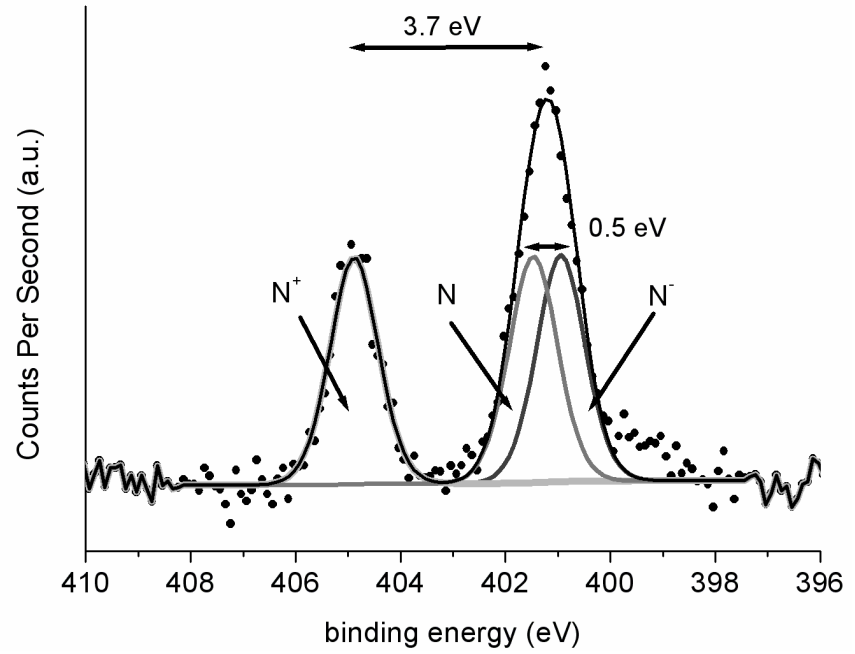

Figure 3.6: A characteristic XPS high resolution spectrum of an azide surface. Two peaks are detectable, containing three nitrogen components with the same corrected area.

$$X = 11 \cdot \frac{\frac{A_{Br3d\ or\ N1s}}{A_{CH_x}}}{1 + \frac{A_{Br3d\ or\ N1s}}{A_{CH_x}}}, \tag{3.2}$$

where $A_{Br3d\ or\ N1s}$ is the corrected area of the $Br3d$ or $N1s$ signal, A_{C1s} is the corrected area of the C1s and A_{CH_x} is the corrected area of the CH_x component in the C1s signal.

Equations (3.1) and (3.2) are based on the ratio of bromine or nitrogen atoms to carbon atoms. In case of equation (3.1), only the atomic concentration is considered, this atomic concentration can be determined from the survey spectrum. The ratio of Br:C is 1:11 atoms in the silane molecule. In case of equation (3.2), high resolution peak fitting is considered. Instead of using the C-Br (or C-N) component of the C1s spectra, it is then preferable to use the Br3d since the component determination is not the result of a complex peak fitting and Br3d is not influenced by neighboring components like C-Br one. Theoretically the corrected area of the pure element is in theory the same as the C-X component in the C1s spectra, which is confirmed by experimental data (examples are shown in table 3.3). These values are based on three different samples for the 1. and 2. condition-set and on two different samples for the 3. condition-step.

It is expected that the coverage is lower if calculated with equation (3.1), due to possible incertitudes on the baseline and determination of the background: The only source of the CH_x component and bromine or nitrogen is the silane and its conversion, respectively. All the used constraints and parameters for the analysis of XPS survey and high resolution spectra are shown in table 3.6.1 in the supporting information of this chapter.

Table 3.3: Comparison of the corrected areas of C-Br and Br3d 5/2 components.

surface	A(C-Br)	A(Br3d 5/2)
1 condition-set	47 ± 10	53 ± 10
2 condition-set	203 ± 19	222 ± 37
3 condition-set	14 ± 2	14 ± 1

3.3.4.2 Contact angle measurements

The wettability characteristics of the surfaces were analyzed by a DSA100 goniometer from Krüss. For static contact angle measurements, a droplet of 2 μL was placed onto the surface and θ_s was determined after 1 min, time enough for the system to be in a state of equilibrium. By adding and withdrawing liquid, advancing θ_a and receding θ_r angles were obtained, respectively. The flow rate of the liquid was 20 μL/min and values of θ were automatically collected each $\frac{1}{2}$ second.

The surface energy of the final amino terminated surfaces were additionally determined. This is essential when considering surface properties e.g. the area wetting/adhesion or surface modifications. The contact angle method is based on the assumption that the surface is homogeneous [156]. The mixed monolayers were regarded as homogeneous surfaces, since no aggregation or islanding was expected. Surface energies were obtained by the measurement of the contact angle of several different solvents, here diiodomethane, 1-bromonaphthalene and water were used. Contact angles are usually measured with polar and apolar liquids [157]. The dispersion forces of a solid-liquid system can be described by equation 3.3. Here, diiodomethane $\frac{\sqrt{\gamma_L^D}}{\gamma_L} = 0.137$ and 1-bromonaphthalene $\frac{\sqrt{\gamma_L^D}}{\gamma_L} = 0.15$, were used.

$$\gamma_L \cos\theta = -\gamma_L + 2\sqrt{\gamma_L^D \gamma_S^D} - \pi_e, \tag{3.3}$$

where γ_L is the surface tension of the liquid L, $\cos\theta$ is the contact angle, γ_L^D is the dispersion force of L, γ_S^D is the dispersion force of solid S and π_e is the equilibrium film pressure of adsorbed vapor on the solid. π_e is zero if $\gamma_L > \gamma_S$ [158].

The surface energy of a solid can be sufficiently determined with only one contact angle measurement by plotting of $\cos\theta$ versus $\frac{\sqrt{\gamma_L^D}}{\gamma_S^D}$. A straight line should be obtained with the origin at $cos\theta$ = -1 and with a slope of $2\sqrt{\gamma_S^D}$ [158].

3.4 Material and Methods: Part 2

3.4.0.3 Grafting of the amino acid glycine with aid of a homobifunctional linker

3.4.0.3.1 Linker 1: Glutaraldehyde (GAD)

The samples were immersed in a solution of 10 vol-% glutaraldehyde (25 %, grade I, Sigma-Aldrich) in MilliQ water, at pH between 5-6 for 1 h. Afterwards, the samples were rinsed with MilliQ water and dried under nitrogen stream. The glutaraldehyde activated surfaces were then immersed in a 20 mM glycine (purchased from Alfa Aesar in Germany) solution containing 50 mM $NaCNBH_3$ (Sigma-Aldrich) in MilliQ water (pH 5-6). The reaction was carried out overnight at room temperature. Afterwards, the samples were rinsed with MilliQ water [159] and dried under nitrogen stream. A reaction scheme is depicted in figure 3.7.

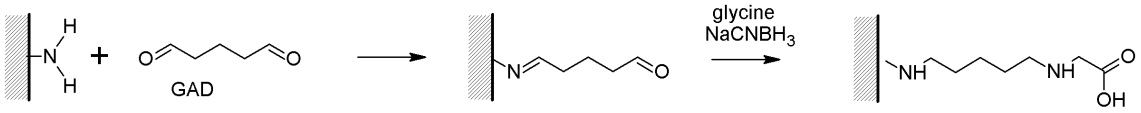

Figure 3.7: Scheme of the grafting of glutaraldehyde, followed by the glycine grafting.

3.4.0.3.2 Linker 2: Di-(N-succinimidyl)oxalate (DSO)

NH_2 terminated surfaces were immersed in a solution of 10 mM DSO purchased from Fluka in CH_2Cl_2 (Sigma-Aldrich) supplemented with TEA (1 vol-%) for two hours at 6 ± 0.8 °C. The surfaces were rinsed several times with CH_2Cl_2 and dried under a nitrogen stream. DSO-activated surfaces were directly used for surface analysis and for amino acid grafting. For the amino acid grafting, samples were immersed in a solution of glycine (1 mM) and kept 24 hours at room temperature. Afterwards they were rinsed with MilliQ water and EtOH and dried under nitrogen stream [149]. The reaction scheme of glycine grafting via DSO is depicted in figure 3.8.

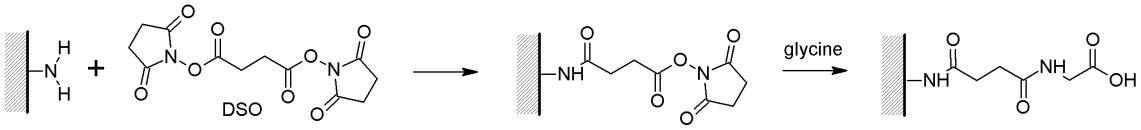

Figure 3.8: Reaction of DSO and NH_2-group of the surface, followed by the reaction of the DSO-activated surfaces and glycine.

3.4.0.3.3 Linker 3: 1.4-Phenylendiisothiocyanat (PDITC)

NH_2 terminated surfaces were activated with PDITC by immersion of surfaces in a solution of 10 mM PDITC purchased from Sigma-Aldrich in CH_2Cl_2 supplemented with 1 vol-% pyridine (Sigma-Aldrich) for 2 h at 6 ± 0.8 °C. Afterwards, the samples were rinsed several

times with CH_2Cl_2, dried under nitrogen stream and immediatly used for further amino acid grafting and the analysis of the surfaces. An 1 mM glycine/MilliQ water solution was prepared, in which activated surfaces were immersed. After 24 h at 4 °C the surfaces were rinsed with MilliQ water and EtOH and dried under nitrogen stream [149]. The schematic of glycine grafting via PDITC is shown in figure 3.9.

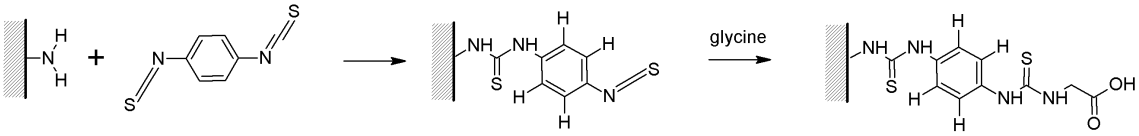

Figure 3.9: The isothiocyanate groups of the linker reacts first with an amine groups of the surface and, after adding of an amino acid, with their amino groups.

3.4.0.4 Grafting of an amino acid by protection and activation of glycine

3.4.0.4.1 Step 1: Synthesis of Fmoc-glycine

For the synthesis of Fmoc-glycine, 13.3 mM glycine and 26.7 mM Na_2CO_3 (Sigma-Aldrich) were dissolved in MilliQ water. The solution was added, drop by drop, into 1.4-dioxane (Sigma-Aldrich), containing 20 mM 9-fluorenylmethyl succinimidyl carbonate (Fmoc-OSu, Fluka). During the addition of glycine, the solution was stirred at 0 °C up to 1 h after glycine was completely added and let 12 h under stirring at room temperature.
The reaction medium was diluted with MilliQ water and extracted two times with AcOEt (Riedel-de Hoen). The organic phase was washed two times with a saturated Na_2CO_3 solution. Obtained water phases were combined and a pH of 1 was reached by adding HCl. Subsequently, the aqueous phase was rinsed three times with AcOEt. The resulting organic phases were dried by $MgSO_4$ (Fluka), filtered and concentrated by rotary evaporator. After removal of the solvent, a white, solid substance was obtained. Finally, the substance was washed with CH_2Cl_2 to remove traces of Fmoc-OSu. The obtained product was analyzed by ^{1}H-NMR and the reaction yield of the purified product was calculated. The protection mechanism of glycine with Fmoc-OSu is depicted in figure 3.10.

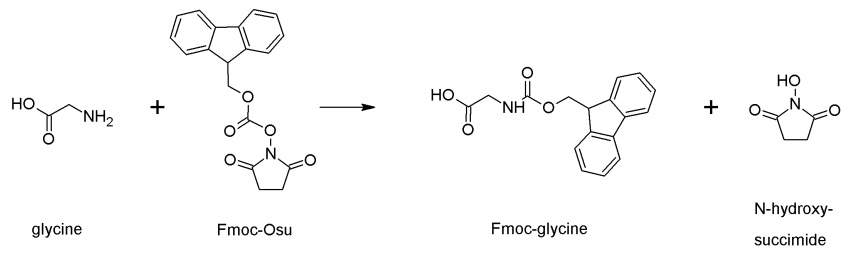

Figure 3.10: The amine groups of glycine is protected by Fmoc

3.4.0.4.2 ^{1}H-Nuclear Magnetic Resonance spectroscopy (^{1}H-NMR)

NMR spectroscopy techniques (^{1}H-, ^{13}C-, ^{15}N-NMR) are often used to determine the structure of organic products or biomolecular compounds. The techniques investigates the electronic environment of single atoms and interactions with neighboring atoms. The measurements take place in a main magnetic field with a vertical high frequently alternating field to the main field. An energy (ΔE) is absorbed by the sample from the alternating field and can be measured in a current strength (in case of resonance). ΔE corresponds to a certain frequency and depends on magnetic properties of the nucleus of the atom. It is also proportional to the outer magnetic field H_o. A spectrum is obtained with shifted frequencies of resonance versus their intensity compared to a reference (standard). The chemical shift of the resonance frequency depends also on the electron density of the corresponding proton. There is an influence of π-systems but as well of substituents. The magnetic shielding increases or decreases if the substituents are electron-acceptors or -donators, respectively. The shift is defined in equation (3.4), while the signals are split in multiple signals due to the J-coupling (indirect dipole-dipole coupling). These splittings have specific patterns and result from the interaction of different spin states through a chemical bond.

$$\delta[ppm] = \frac{\nu_{H(Probe)} - \nu_{H(Standard)}}{\nu_{H(Standard)}}, \tag{3.4}$$

where δ is the chemical shift of resonance frequency, $\nu_{H(Probe)}$ is the frequency of the sample and $\nu_{H(Standard)}$ the frequency of the reference.

3.4.0.4.3 Step 2: Grafting of glycine onto NH_2 functionalized surfaces

For the reaction, Fmoc-glycine, hydroxybenzotriazole (HOBt, Sigma-Aldrich), 2-(1H-Benzotriazole-1-yl)-1.1.3.3-tetramethyluronium hexafluorophosphate (HBTU, Sigma-Aldrich) and N,N-Diisopropylethylamine (DIPEA, Sigma-Aldrich) were added to a solution of DMF. During the reaction, DIPEA deprotonates the COOH of the Fmoc protected glycine. The deprotonated Fmoc-glycine reacts in a first step with HBTU, before forming an active ester with HOBt. Finally, the OBt-activated Fmoc-glycine reacts with the amino group of the surface. Figure 3.11 shows the reaction of Fmoc-glycine with the amino functionalized surface.

Three conditions of concentration were tested (C1, C2 and C3). They are shown in table 3.4. The reaction with NH_2 functionalized surfaces took place at room temperature and with different reaction times. To remove the Fmoc protection-group, the surfaces were immersed in a solution of piperidine (21 vol-%) in DMF for at least 12 h, followed by a rinsing with water and EtOH. Finally the samples were dried under nitrogen stream.

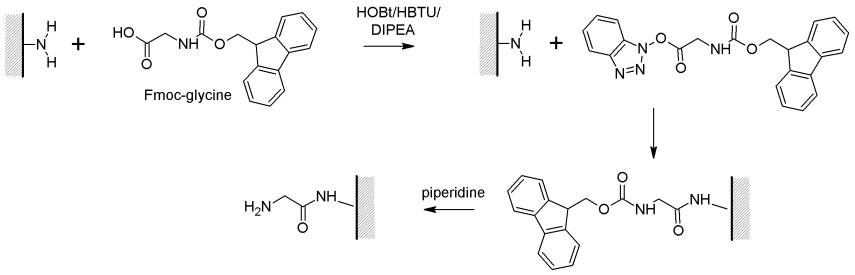

Figure 3.11: The carboxy group of Fmoc-glycine is activated by HBTU, before reacting with the amine group of the SAM surface. The protecting group is removed by piperidine.

Table 3.4: Different conditions of amino acid grafting.

	C_1	C_2	C_3
Fmoc-gly	8.3 μM	33.7 μM	3.3 mM
HOBt	8.3 μM	33.7 μM	3.3 mM
HBTU	33.0 μM	8.3 μM	3.3 mM
DIPEA 67	3 μM.17	6 μM.	6.7 mM
solvent		in DMF	
time of reaction	137 h	143 h	200 h

3.4.1 Amino acid grafting on amine reactive surfaces

Amine functional SAMs were used as substrate to graft an amino acid such as glycine via a homobifunctional linker. A summary of the coupling agents used in this chapter is given in table 3.5.

3.4.2 Analyses of surfaces

All surfaces were analyzed by XPS. The reaction yield was determined by use of the survey and high resolution spectra (see section 3.4.2.1). In addition, contact angle measurements, ellipsometry and AFM were performed on several surfaces, as described before in the second chapter.
Additional information about XPS analysis are given in article 2b on page 116.

3.4.2.1 Additional Information about XPS analysis

The reaction yields of the grafting of amino acids were determined after evaluation of the XPS data analysis. The yield was calculated through (i) the experimental ratio of N1s to C1s compared to the ideal ratio and (ii) after deconvolution of C1s spectra. Thereby, the

Table 3.5: Summary of coupling reagents for amino acid grafting.

Short name	Name IUPAC	Molecular formula	Purpose
GAD	pentane-1.5-dial	$C_5H_8O_2$	Linker homobifunctional, flexible between two NH_2 groups
DSO	N,N'-Disuccinimidyl oxalate	$C_8H_4N_2O_8$	Linker homobifunctional, flexible between two NH_2 groups
PDITC	1.4-phenylene diisocyanate	$C_{10}H_8N_2S_2$	ring-opening molecule; homobifunctional, rigid between two NH_2 groups
Fmoc-Osu	9-fluorenylmethyl succinimidyl carbonate	$C_{19}H_{14}N_1O_5$	Activation of amino acid
HOBt	N-Hydroxybenzo-triazol	$C_6H_5N_3O$	activation of COOH-groups of amino acid
HBTU	O-(Benzotriazol-1-yl)-N,N,N',N' -tetramethyluronium hexafluorophosphate	$C_{11}H_{16}F_6N_5OP$	coupling additive

differences of the chemical composition of C1s of initial and final surfaces were compared to the ideal ones. However, the components had to be normalized by the CH_x component of the same spectrum to be able to compare different analysis of XPS. The yield of (ii) was calculated according to the following equation 3.5:

$$yield\,\% \;=\; \frac{(\frac{A_X}{A_{CH_x}})^{final}_{exp} - (\frac{A_X}{A_{CH_x}})^{initial}_{exp}}{(\frac{A_X}{A_{CH_x}})^{final}_{ideal} - (\frac{A_X}{A_{CH_x}})^{initial}_{ideal}}, \tag{3.5}$$

where A_x is the corrected area of the component X of C1s, A_{CH_x} is the corrected area of the CH_x component of the experimental and ideal surfaces, subscripted *exp* and *ideal*, respectively. The ratio of the substrate is called *initial*, while the ratio after the reaction is named $final$.

Besides the calculation of the yield by comparing the experimental and ideal ratios of concentrations (areas), the surface structure was interpreted by evaluation of the decrease/increase and disappearance/appearance of C1s components.

3.5 Results and Discussion of Part 1

3.5.1 Article 2a: "Well-controlled platforms to study the role of functional groups accessibility at bacteria / material biointerfaces"

Article by Judith Böhmler, Arnaud Ponche, Karine Anselme, and Lydie Ploux, in preparation.

Well-controlled platforms to study the role of functional groups accessibility at bacteria / material biointerfaces

Judith Böhmler, Arnaud Ponche, Karine Anselme, Lydie Ploux[§]
Institut de Science des Matériaux de Mulhouse (CNRS LRC7228), Mulhouse, France

[§] Corresponding author:
Dr Lydie Ploux, Institut de Science des Matériaux de Mulhouse (CNRS LRC7228), 15 rue Jean Starcky, BP2488, 68057 Mulhouse cedex, France; Lydie.Ploux@uha.fr

Abstract
Well-controlled mixed molecular layers are crucial to study the role of material surface chemistry in biointerfaces such as bacteria and subsequent biofilm on biomaterials. Although self-assembled monolayers (SAMs) based on silanes with non-nucleophilic functional groups are promising due to their low sensitivity to side-reaction, their well-control in terms of surface chemistry, as well as layer structure and organization has never been evidenced. Here, we report a comprehensive synthesis and analysis of undecyltrichlorosilane and 11-bromoundecyltrichlorosilane based mixed SAMs on silicon substrate. Role of several reaction conditions on the control of surface chemistry, layer structure and organization was investigated by survey and high resolution X-ray photoelectron spectroscopy analysis, wettability measurements and ellipsometry. Aiming at providing well-controlled yet easily made platforms for biointerface studies, the most appropriate conditions were determined for elaborating pure 11-bromoundecyltrichlorosilane SAMs of high reproducibility. We demonstrated that control is maintained on more complex surfaces i.e. surfaces revealing various chemical densities that were obtained with different ratios of undecyltrichlorosilane and 11-bromoundecyltrichlorosilane as well as after bromine was converted to amine groups via S_N2 bromine-to-azide conversion. Appropriateness for biointerface studies of such amino and methyl group revealing platforms (NH_2-X % / CH_3) was proved by higher reproducibility of bacterial adhesion on NH_2-100 % / CH_3 SAMs compared to commonly reported SAMs of theoretically similar surface chemistry, yet less control of quality.

Keywords: SAM, surface analysis, high resolution XPS, surface chemistry, biointerface, bacterial adhesion

1. INTRODUCTION

Biointerfaces have become a crucial field of the material science, being involved in application fields as different as microfluidic systems, biosensors and biomaterials. Interfaces between materials and biological objects are therefore more and more investigated attempting to improve the fundamental knowledge in this area [1,2]. A typical example, crucial topic for better understanding biomaterials-related infections, concerns whether bacteria - material interfaces may be controlled by the material surface chemistry through affectation of bacterial adhesion and biofilm formation [3,4]. Chemical heterogeneity of the surface, accessibility or orientation of (bio)molecule adsorbed or grafted at this interface are some of the parameters potentially relevant for bacterial response to surface. To study such aspects, however, material tools are rare. Surfaces should be as ideal as possible to avoid coupling of effects resulting from different surface characteristics (typical, frequent coupling of surface topography and surface chemistry). They must be very well-controlled and well-known i.e. well-described surfaces, to know the exact surface in contact with the studied biological system (bacteria for example) [4].

The best controlled surfaces currently suitable for fundamental study at biointerfaces are probably self-assembled monolayers (SAMs) [5-7]. Aside from, in principle, well-controlled structure and architecture of the molecular layer [8,9], they can reveal a large diversity of functionalities by choosing the adequate molecular candidates [8], can be further grafted through various ways with biomolecules for example [10], and are stable enough to envisage their use in long term aqueous aging conditions or in vivo mimicking experimental set-ups like bioreactors or flow cells [11-13]. If realized on silicon wafer, their high substrate smoothness is an additional advantage to achieve platforms for biointerface studies, avoiding any undesired effect of the surface topography even at the nanoscale. Many studies at biointerfaces have been reported with SAMs, providing number of relevant results in particular in the surface - bacteria interface field [11-13].

Based on the principle of SAMs, chemically mixed monolayer can be achieved. They allow to envisage studying the role of chemical heterogeneities and molecular accessibility in bacterial and cell adhesion to surfaces. M. Wiencek and M. Fletcher proposed promising SAMs of mixed chemical composition with which they investigated bacteria behaviors in response to surface chemistry [14,15]. E. Burton *et al.* developed mixed monolayer revealing gradients of chemical density that they used for studying bacteria and cell response to chemical surface properties [16]. Nevertheless, despite the indisputable interest of these mixed surfaces, the difference in length of the molecules used to create the molecular layer may have led to side effects due to topographical features at the molecular scale or chemical groups carried by the molecular chain. In other words, the biological response observed on such surfaces may be the result of several added or coupled effects [15].

Heise *et al.* proposed to exploit silanes with non-nucleophilic functional group like bromine and methyl terminated trichlorosilanes for creating mixed monolayer with reduced risk of polymerization and homogeneous length of the silanes [17,18]. Further in situ transformation (S_N2 reaction) allows to convert the bromine groups into azide groups [19] to finally obtain amino mixed monolayer [20,21] suitable for further grafting of (bio)molecules. Very promising platforms were obtained, providing in particular control of chemical group density, which was stated by the quasi-linear relationship between monolayer composition and composition of silanization solution [17]. However, the surface coverage by bromine groups, and subsequent amine groups, of the monolayers was much lower than expected, being inferior to 60 % and 40 % for pure bromine-revealing (Br 100 %) and pure amine-revealing (NH_2 100 %) monolayers respectively. Values may be erroneous due to the degradation of C-Br bond during XPS analysis with a non-monochromatic source, as it was already stated by Fryxell *et al.* [19]. This can also be attributed to the presence of solvent or other contaminants that may be inserted in the molecular layer. Incomplete or uncertain description of the layer, as well as the presence of unknown and unexpected additional components both prevent the use of such monolayers for studying the role of subtle surface chemical properties on biological objects. Nevertheless, adequate changes in the reaction conditions and careful analysis of the surface properties should allow to improve monolayer quality and knowledge about surface composition, structure and organisation. This was provided in the present study.

As we showed previously [22], thorough surface analysis must be supplied to provide the necessary insurances about surface chemical nature and layer architecture and structure, including the presence of defects such as impurities intercalated in the layer or undesired chemical side reactions. The common association of contact angle (sessile drop analysis), thickness (ellipsometry) and elementary chemical composition (X-ray photoelectron spectroscopy survey spectra analysis) measurements mainly failed to highlight such defects. Typically, additional analysis with high resolution XPS and zeta potential measurements were essential to show silane polymerization disturbing molecular layer architecture and failure in the orientation of molecules in SAMs based on 3-aminopropyltriethoxysilane (APTES) and N-(6-aminohexyl)-aminopropyltrimethoxysilane (AHAPS) respectively [22]. Until now, similar thorough analysis of mixed monolayers, mainly based on high resolution XPS, was not reported in the literature and experimental evidence of well-control of their structure and architecture has never been supplied.

In the present work, we provide comprehensive investigations of the synthesis and characteristics analysis of mixed monolayers based on trichlorosilanes with bromine and methyl groups as non-nucleophilic functional groups. Besides, we report evidence that this strategy of mixed monolayer elaboration supplies very well-controlled and reproducible platforms for biointerface studies.

First, different reaction conditions like concentration, solvent, temperature, reaction time, rinsing and annealing are screened for elaborating full covered (i.e. Br 100 %) bromine

surfaces. Changes so-induced in the coating properties, i.e. surface chemical composition, layer structure and architecture, are comprehensively analysed. High resolution XPS analysis is used in particular to evaluate not only the chemical composition of the layer surface but also the structure and the organisation of the layer. Variability in layer characteristics is determined aiming at evaluating whether such platforms may be elaborated in high number without losing the control of the surface chemical composition, and layer architecture and structure. Secondly, mixed monolayers are synthesised using the reaction conditions that allowed to obtain the most controlled layer characteristics. They are completely analysed to confirm the control of surface chemical composition, layer structure and organization, as well as reproducibility. Conversion of bromine/methyl- to amino/methyl-revealing surfaces is also investigated. Finally, by comparing adhesion of bacteria on such full amino-covered platforms (NH_2 100 %) and on similarly amino-covered APTES and AHAPS SAMs, we evaluate whether these platforms may constitute an advantage to provide new and more relevant results in biointerface studies.

2 MATERIAL AND METHODS

2.1 Surface substrate

Silicon wafer (100), purchased from MCR (Germany), one side polished, was used as a substrate for further chemical modification and cut into pieces of 1 cm x 1 cm. Substrate pieces were ultrasonically (frequency 45 kHz) cleaned for 10 min in $CHCl_3$ (Sigma-Aldrich) to remove organic contamination, followed by 30 min of cleaning in Piranha solution (30:70 vH_2O_2 25 %:vH_2SO_4 99 %, both purchased by Sigma-Aldrich) at 50 °C. Samples were then rinsed with MilliQ water.

2.2 Chemical modifications: NH_2 terminated SAMs

2.2.1 3-aminopropyltriethoxysilane (APTES) and N-(6-aminohexyl) aminopropyltrimethoxysilane (AHAPS) based SAMs.

For the elaboration of amino-functionalized layers made of APTES, piranha-cleaned substrates were immersed in a 1 mM solution of 3-aminopropyltriethoxysilane (APTES, purchased from ABCR in Germany) in acetone (Sigma-Aldrich) overnight at room temperature in the dark. Samples were cleaned for 30 s in acetone under ultrasonic treatment (45 kHz) to remove the free silane fraction.

The same protocol was used for N-(6-aminohexyl)-aminopropyltrimethoxysilane (AHAPS, purchased from ABCR in Germany) in ethanol (Sigma-Aldrich). These two types of surfaces are named "APTES" and "AHAPS", respectively, in the following sections of the paper.

2.2.2 SAMs based on silane with non-nucleophilic functional group.

11-bromoundecyltrichlorosilane based SAMs.

Freshly cleaned substrates were immersed for 4 h in a solution of 70 % n-heptane (n-C_7H_{16}, Carlo Erba) and 30 % chloroform ($CHCl_3$, Sigma-Aldrich) at 4 °C containing various molar ratios of undecyltrichlorosilane and 11-bromo-undecyltrichlorosilane (ABCR, Germany)

according to the desired bromine density i.e. Br/CH_3 surface ratio.
Freshly prepared, piranha-activated wafers were immersed in 1 mM solution of 11-bromo-undecyltrichlorosilane (ABCR, Germany). Several solvents (hexadecane, $CHCl_3$, heptane, toluene and 30 % $CHCl_3$ in heptane), temperature (6 °C, 20 °C and 45 °C) and immersion time (4 h and 16 h) were tested (table 3.6 and Supporting Information, tables 3.8 to 3.11). Samples were then rinsed by immersion in $CHCl_3$ and hot water, before drying under nitrogen stream. Improvement of stability potentially resulting from an additional annealing and ultrasonic treatments step was tested. For that purpose, functionalized samples were baked for 1 h at 105 °C, and subsequently ultrasonically rinsed for 15 min in $CHCl_3$ to remove residual silanes.
The final surfaces are named "Br 100 %" in the following sections.

Table 3.6: Definition of the three different reaction conditions sets considered for Br 100 % surfaces fabrication.

Parameters	1. Condition-set	2. Condition-set	3. Condition-set
Concentration silane	1 mM	1 mM	1 mM
Solvent	hexadecane	hexadecane	70 % n-heptane/ 30 % $CHCl_3$
Time	4 h	16 h	4 h
Temperature	45 °C	20 °C	6 °C
1. Rinsing	$CHCl_3$/hot water	$CHCl_3$/hot water	$CHCl_3$/hot water
Annealing	None	None	1 h at 105 °C
2. Rinsing	None	None	15 min sonication in $CHCl_3$

Conversion of bromine to amino termination.
S_N2 nucleophilic substitution and subsequent reductive amination were performed on Br 100 % surfaces to convert them in azide terminated surfaces (N_3 100 %) and finally in amine functionalized surfaces (NH_2 100 %) [18,20] (figure 3.12). To convert bromine to azide functional groups, bromine-functionalized samples were immersed in a 0.7 M solution of sodium azide (NaN_3, Fluka) in dimethylformamide (DMF, Sigma-Aldrich) under shaking for 72 h at room temperature. Samples were then rinsed with MilliQ water and acetone before drying under nitrogen stream. Subsequently, azide-revealing samples were reduced overnight by immersion in a 0.2 M solution of lithium aluminium hydride ($LiAlH_4$, Sigma-Aldrich) in tetrahydrofuran (THF, Carlo Erba), before being immersed in THF over 12 h at room temperature. Lithium-complexes on the surface were removed by hydrolysis by immersion for 1 h in 10 % solution of hydrochloric acid (HCl , 37 %, Sigma-Aldrich). Samples were then rinsed with MilliQ water and ethanol (C_2H_5OH, 99.9 % absolute anhydrous, Carlo Erba) before drying under nitrogen stream. Finally, the resulting NH_3^+ groups were converted in NH_2 groups by immersion in triethylamine (TEA, Sigma-Aldrich) during

24 h at room temperature. Samples were finally rinsed with MilliQ water (pH between 5.0-5.8) and ethanol before drying under nitrogen stream. The final surfaces are called "NH_2 100 %" in the following sections.

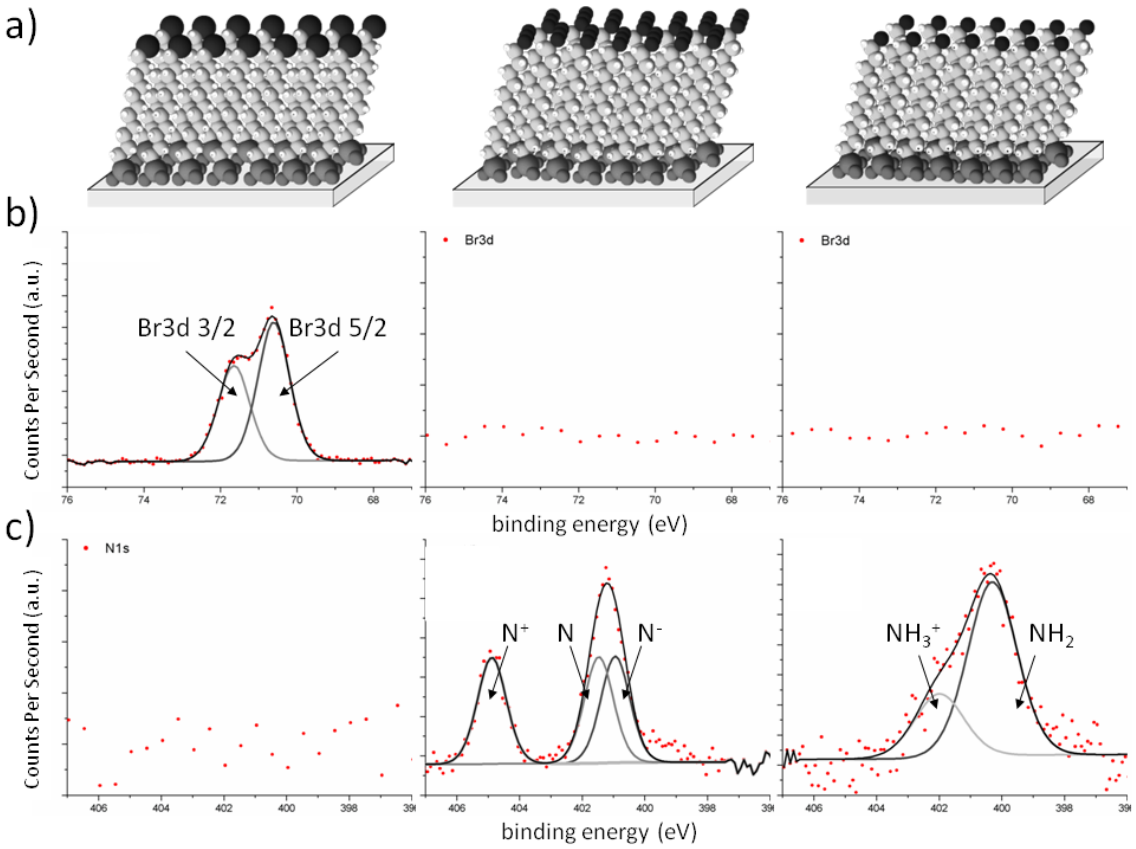

Figure 3.12: (a) Scheme of the conversion of bromine-revealing to amino-revealing surfaces: bromine groups are converted by a S_N2 reaction to azide groups that are subsequently converted to amino groups. (b) Br3d high resolution XPS spectra associated to Br 100 %, N_3 100 % and NH_2 100 % surfaces respectively (from left to right). (c) N1s high resolution XPS spectra associated to Br 100 %, N_3 100 % and NH_2 100 % surfaces respectively.

2.3 Chemical modifications: Br/CH_3 and NH_2/CH_3 mixed self-assembled monolayers (MML)

Freshly cleaned substrates were immersed for 4 h in a solution of 70 % n-heptane (n-C_7H_{16}, Carlo Erba) and 30 % chloroform ($CHCl_3$, Sigma-Aldrich) at 4 °C containing various molar ratios of undecyltrichlorosilane and 11-bromo-undecyltrichlorosilane (ABCR, Germany) according to the desired bromine density i.e. Br/CH_3 surface ratio. Five ratios of bromine surface coverage were considered: 0, 25, 50, 75 and 100 Br % (figure 3.13). The final concentration of silane in solution was constant and equal to 1 mM. Samples were rinsed with chloroform and shortly immersed in hot water. Subsequently, they were baked for 1 h at 105 °C before rinsing for 10 min in chloroform under ultrasonic treatment. In the

following sections, these final surfaces are named "Br X %", according to the expected surface coverage in bromine. A Br 100 % surface is expected to exhibit only Br groups at the extreme surface.
Br X % surfaces were further converted to so-called NH_2 X % surfaces by using the same procedure as described in paragraph 2.2.2 (figure 3.12). As each molecule of silane contains one nitrogen atom, NH_2 X % surface is expected to reveal a NH_2 to CH_3 functional groups ratio of X %.

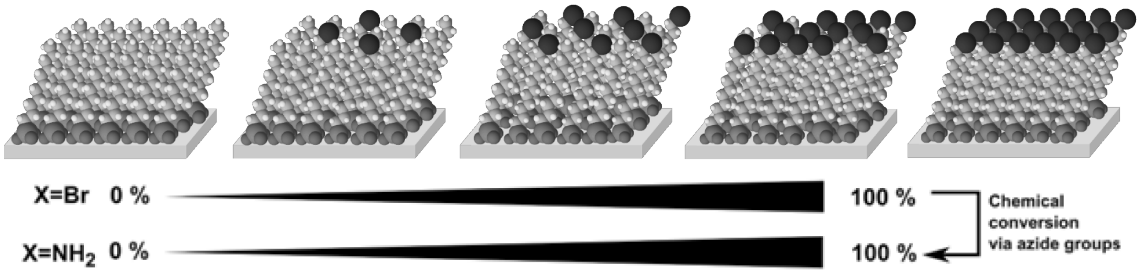

Figure 3.13: Aim of mixed monolayer fabrication. Five flat, chemically well-controlled surfaces with five different coverages (0, 25, 50, 75 and 100 %) with Br group (respectively NH_2 group after S_N2 conversion and further amino reduction) in a CH_3 group environment.

2.4 Surface characterization

Survey and high resolution X-ray photoelectron spectroscopy (XPS), ellipsometry, atomic force microscopy (AFM) and contact angle measurements were used to determine the chemical composition, the structure and the organization of the layers.

X-ray photoelectron spectroscopy (XPS).

XPS analysis was used to determine the chemical composition of the surface layers. It was performed with a Gammadata Scienta spectrometer equipped with a monochromated Al Kα X-ray source (1486.6 eV) under ultrahigh vacuum (base pressure $< 10^{-9}$ mbar) and a takeoff angle of 90 °. Survey and high-resolution spectra were recorded at pass energy of 500 and 100 eV respectively. For high-resolution experiments, the overall energetic resolution is estimated to 0.45 eV. All spectra were analyzed and peak-fitted using CasaXPS 2.3.12 software (Casa Software Ltd., Teignmouth, UK, www.casaxps.com). All components were referenced according to the CH_x component at 285.0 eV, and the full width half-maximum (fwhm) was constrained to be constant for all components in the same spectrum. The relative binding energy of all components was fixed and maintained constant for all peak-fitting procedures. For quantification purpose and area corrections, Scofield sensitivity factors were used ($Br3d_{5/2}$: 1.68, $Br3d_{3/2}$: 1.16, C1s: 1.00 and N1s: 1.80). To evaluate the most efficient reaction conditions, reproducibility of atomic composition and Br surface

coverage were used. After calculation of the area ratio of N1s or $Br3d_{5/2}$ /CH_x components on high resolution, the experimental Br or NH_2 coverage was evaluated by the equation 3.6.

$$X(\%) = \frac{11.\frac{A(N1s)orA(Br3d5/2)}{A(CH_x)}}{1+\frac{A(N1s)orA(Br3d5/2)}{A(CH_x)}}, \tag{3.6}$$

where $A(N1s)$ is the corrected area of N1s, $A(Br3d5/2)$ is the corrected area of $Br3d_{5/2}$ and $A(CH_x)$ is the corrected area of the CH_x component in the C1s spectra.
Equation 1 originates from the stoichiometry of the two silanes used for mixed monolayers. In an ideal case and for each surface coverage, the ratio of corrected area of NH_2:CH_x XPS components are the following: 100 % - 1:10, 75 % - 3:41, 50 % - 2:42, 25 % - 1:43. The sensitivity of the spectrometer allows for the separation of the CH_x (285.0 eV) and C-Br (286.0 eV) components. The peaks that are the most intense and less sensitive to peak fitting conditions, i.e. CH_x and Br3d5/2 components, were used for coverage calculation.

Contact angle measurements.
Water contact angles were measured for assessing wettability and hydrophilic/hydrophobic character of the surface layers. Static, advancing, and receding contact angles were measured as described elsewhere [16] at room temperature with a contact angle goniometer (Krüss) coupled to a camera and an image analyzer. The static contact angle was determined after a delay of 1 min to ensure the equilibration of the droplet (2 μL distilled Milli-Q, pH 5.8). Reported values are an average of measurements performed at three different regions on four different samples. Hysteresis, defined as the difference between advancing and receding contact angles, was used as a quantitative indication of surface homogeneity. In general, small and large values are a sign for homogeneous and heterogeneous surface properties [23].

Ellipsometry.
Ellipsometry was used to determine the thickness of the layers as described elsewhere [16]. Briefly, measurements were done at 532 nm (HeNe laser) and incident angle of 70 °, with an ellipsometer equipped with a phase modulation multiskop from Physik Instrument (M-O33K001). Thickness of the chemical, grafted layers was evaluated at room temperature both in air (named "thickness in air") and in distilled water (named "thickness in liquid"). Δ and ϕ values were measured on three different regions of each sample. Thickness of the oxide layer was determined on ungrafted silicon wafers cleaned as described in section 2.1. Models were composed of two (pure silicon and oxide layer) or three layers (pure silicon, oxide layer and organic layer) for ungrafted and grafted silicon wafers, respectively. Refractive indices were those reported previously [16].

Atomic force microscopy (AFM).
AFM was used to determine surface morphology and surface roughness. A NanoScopeIII/Dimension 3000 (Digital Instruments) equipped with Si cantilever (k=42 N/m, Pointprobe, Nano World) was used in tapping mode under ambient air, with scan rate of 1 Hz and image size of 2 μm^2. AFM micrographs were analyzed with the

NanoScope 6.13R1 software (Digital Instruments) for providing mean roughness values (R_a, arithmetic average of the absolute height values). Height and phase contrast micrographs being similar, only height images are considered for discussion.

2.5 Biointerface experiment

The relevance of better control of not only the surface chemical composition but also the structure and organization of the layer was tested by investigating the repeatability of bacterial adhesion on three different NH_2 terminated surfaces (APTES, AHAPS and Br based NH_2 100 %).

Bacterial strain and bacteria culture.

Bacterial experiments were conducted with *Escherichia coli* (*E. coli*) MG1655 [24]. -80 °C frozen bacteria were cultured overnight on Luria Bertani (LB purchased from Sigma-Aldrich) agar plate at 30 °C. A first pre-culture was then prepared with one colony in LB and incubated overnight at 30 °C. A second pre-culture (10 % of the first pre-culture) was prepared in M63G selective medium [24] and incubated overnight at 30 °C. A third pre-culture (10 % in M63G of the second pre-culture) was incubated for 4 h before centrifugation for harvesting bacteria. Bacteria were then re-suspended in M63G to reach an absorbance of 0.01 at 600 nm.

Bacterial adhesion test.

Three different types of NH_2 100 % surfaces (APTES, AHAPS and Br based NH_2 100 %) were inoculated with the bacterial suspension at 0.01 of 600 nm absorbance. Hence, bacteria were cultured for 2 h on the samples before non-adherent bacteria were removed by 3 subsequent gentle rinsings with sterile NaCl 9 g/L solution. Visualization of bacteria was performed by fluorescent confocal microscopy (Zeiss Upright LSM700) after bacteria staining with Syto9® (Molecular Probes, 1 μL/mL of a 5 mM Syto9® stock solution). Bacteria were observed directly in the last rinsing solution using a 9 mm long focal objective (Zeiss LD Epiplan Neofluar 50X). The experiment was repeated 3 times. Two samples of each type were used for one experiment. Ten zones per sample were microscopically imaged. On each micrograph, the adherent bacteria number was determined through image analysis by using ImageJ V.1.44d software with LSMtoolbox V4.0g plugins [25], allowing to calculate adherent bacteria number average and standard deviation for each sample. Bacterial adhesion was statistically analyzed by student's test (T-Test) to determine differences of bacterial adhesion on one surface compared to all the other surfaces.

3. RESULTS AND DISCUSSION

3.1. Control of monolayer chemical composition, layer structure and organization

The functionalization of silicon wafer with organosilane-based SAMs should allow to control the surface chemical functionality with molecular precision without adding any roughness side-property [9]. Such SAMs should lead to well-organized and long-term stable 2-dimensional polysiloxane networks, thanks to numerous Van der Waals interactions along

the main chains and dehydration between adjacent Si-OH groups [8,9]. Nevertheless, silane must display necessary, yet insufficient, specific characteristics, to permit the fabrication of well-defined monolayers: Functional groups have to be sterically small enough [19] to allow close packed assembling [26]; Organosilane main chain must be long enough to lead to well-order, while short silane form multilayers [27]; Functional groups should not be able to compete with the head groups for the interaction with the surface [19,22]. Additionally, the reaction conditions are crucial: temperature, reaction time, solvent(s) and additional annealing for example have been reported for their influence. As pure SAMs, chemically mixed monolayers with well-control chemical group density and layer structure and organization can be envisaged on this basis. The most successful mixed monolayers reported in the literature probably displayed the expected monolayer structure as shown by the thickness measurements. Moreover, the relationship between the composition in silane of the monolayer and the content in silane of the silanization solution was quasi-linear, stating a good control of the surface chemical composition [18]. However, the coverage of the monolayers in bromine groups was much lower than those expected for pure layers of undecyltrichlorosilane and 11-bromoundecyltrichlorosilane as used in the study. Instead of 100 % expected for a pure bromine-revealing monolayer (Br 100 %), the coverage was inferior to 60 %, which may have resulted from the intercalation of solvent and other contaminants in the silane layer or/and from the underestimation of coverage value due to the silane layer degradation during XPS analysis with a non-monochromatic source. In addition, the absence of survey spectra and atomic Br to substrate (Si) percentage prevented both to confirm the monolayer structure of the coating which was uncertain as shown by some spots-like aggregates, and to indicate the close-compactness of the grafted silanes. Finally, solvent insertion leading to uncertain chemical composition as well as low coverage and uncertain structure prevent the use of such mixed monolayer as platforms for biointerface studies.

Based on some literature about SAMs [19,28], we introduced adequate changes in the reaction conditions to improve the monolayer quality while keeping a protocol easy to use in biointerface study environments (room temperature or low positive temperature as reached by refrigerator for example). Moreover, surface and layer characteristics such as chemical composition, structure and organization were determined through a comprehensive approach of analysis.
Three reaction conditions were considered for a thorough analysis of Br 100 % layers (table 3.6). As a reference, we considered the reaction conditions used in the published work having provided the most successful of such mixed monolayers (so-named "1. Conditions-set"). By analogy with the protocols commonly used for synthesizing APTES-based SAMs, a protocol, easy to be applied in non-specialist environments, was proposed by introducing room temperature and overnight reaction time (so-named "2. Conditions-set"). Further parameters including solvent, temperature, annealing and ultrasonic post-treatment were added or/and modified for the so-named "3. Conditions-set". The most appropriate con-

ditions to reach the highest quality of SAMs were chosen after specific investigations that are described in Supporting Information.

Briefly, annealing and subsequent ultra-sonic post-treatments were added in order to improve the monolayer stability for further biological experiments in aqueous, long-term conditions. Expected to remove small quantity of silane molecules that are not directly linked with the substrate, and to convert physisorption of the silanes to the silicon substrate to chemisorption, by removing the water molecule layer present at the silane-substrate interface [29,30], annealing allowed to slightly decrease the monolayer thickness without reducing Br coverage (eq. 3.6) (see Supporting Information, table 3.8). By this process, enhancement of the monolayer stability for experiments in liquid medium, as used in biological experiments, is expected. This was shown by the higher Br3d / SiO_x ratio measured after annealing and ultrasonic treatment. Solvent was also adapted to improve the silane solubility. Among five solvents tested (hexadecane, chloroform, heptane, toluene, chloroform/heptane mixture), chloroform/heptane mixture allowed to improve both Br coverage ($\sim$ 100 %) and layer thickness (1.2 $\pm$ 0.0 nm measured in air) (see Supporting Information, table 3.9). The slight difference with the theoretical thickness value (1.4 nm) was probably the result from a well-structured and solvent- and contaminant-free monolayer yet presenting an insufficiently dense packing of the assembled silanes. Improvement of the compactness was obtained by decreasing reaction temperature to 4 °C (see Supporting Information, table 3.10), which was empirically reported by Brozska *et al.* to provide the optimized conditions for forming monolayers with silanes of 11 carbon main chains [26,27,30]. Time reaction was reduced to 4 h, which was shown not to degrade the layer quality yet facilitating the protocol (see Supporting Information, table 3.11).

Results of the 3 reaction conditions are presented in table 3.7. 1. Conditions-set led to results significantly different than those reported by Heise *et al.* [18]. In particular, Br coverage was much higher than estimated from the published results ($\sim$ 100 % compared to $\sim$ 60 %) and any spots-like aggregates were observed on the surfaces (data not shown). However, thickness values, measured in air or in liquid, were 10 times higher as expected, which demonstrates the non-monolayer structure of the surface. Additionally, the contact angle hysteresis was sufficiently high to suggest the presence of topographical defects at the extreme surface.

Modifications in temperature and time reaction applied to 1. Conditions-set to obtain 2. Conditions-set moderately affected the quality of the layer, leading in general to slight improvements. Br coverage as measured on high resolution spectra was not changed (107 $\pm$ 2 % for 1. Conditions-set; 106 $\pm$ 6 % for 2. Conditions-set). However, Br3d / SiO_x ratio significantly decreased, indicating the reduction of the Br-containing layer. This was further confirmed by the layer thickness values (10.5 $\pm$ 2.8 nm for 1. Conditions-set; 7.0 $\pm$ 1.4 nm for 2. Conditions-set) that significantly decreased, yet remaining 5 times higher than expected (1.4 nm). 2. Conditions-set thus allows to prepare thinner layers than 1. Conditions, however without achievement of well-structured monolayers.

On the contrary, 3. Conditions-set allowed to highly improve the layer quality. The layer thickness was 1.6 ± 0.2 nm, in very good agreement with the theoretical value (1.4 nm), which demonstrates that silanes were structured in a monolayer. In addition, as expected, the high Br coverage value (105 ± 5 %) and the high value of contact angle (86 ± 1 °) in agreement with published values (80-89 ° according to Aswal *et al.* [10]) insure that the improvement of the layer structure was not accompanied by a degradation of the dense packing of silane. The 3. Conditions-set was demonstrated to allow the synthesis of well-structured and well-packed Br 100 % SAMs.

Table 3.7: Characteristics of Br 100 % layers obtained in the three different reaction conditions sets described in table 3.6.

	1. Condition -set	Sample number	2. Condition -set	Sample number	3. Condition -set	Sample number
Br coverage [%]	107 ± 2	3	1066 ± 6	4	105 ± 5	3
HR spectra						
Br coverage [%]	95 ± 3	3	87 ± 6	4	91 ± 5	3
Survey spectra						
Br3d/SiOx	0.42 ± 0.05	3	0.26 ± 0.05	4	0.15 ± 0.02	3
θs [°]	88 ± 2	3	84 ± 6	5	86 ± 1	4
θa [°]	102 ± 2	3	92 ± 2	4	94 ± 1	3
θr [°]	70 ± 2	3	64 ± 8	4	72 ± 3	3
θH [°]	32		28		22	
Thickness air [nm]	11.7 ± 3.6	3	5.8 ± 2.1	5	1.5 ± 0.2	6
Thickness liquid[nm]	10.5 ± 2.8	3	7.0 ± 1.4	3	1.6 ± 0.2	5

3.2. Mixed Monolayers

The possibility to reach well-structured and well-packed Br mixed monolayers based on the 3. Condition-set of reaction conditions, while maintaining well-control of Br coverage, was tested by a similar characterization than above.

As shown in figure 3.14, the Br solution content vs. Br coverage relationship was quasi-linear, which indicates that the chemical properties of the surface in terms of coverage can be easily controlled by simply proportionally adapting the content in Br of the solution. This aspect was improved through the new reaction conditions proposed in the present paper. Indeed, no preferential adsorption of Br- versus CH_3-terminated silane was observed on the contrary to results obtained with 1. Conditions-set and reported in literature [18]. Significantly higher Br coverages were achieved compared to literature as already noted above for Br 100 %, indicating excellent purity and close packing of the grafted layer as well as non-destructive XPS analysis. Well-control of the chemical content of the surface and purity of the grafted layer were confirmed by the hydrophilic character of the surface (figure 3.15) that directly increased with the increase of Br content and was in the 85-110 ° range as expected according to literature [18]. This especially proves the absence of any

interactions of the water drop with the underlying silicon substrate during contact angle measurements and demonstrates therefore that layers are highly densely packed. Despite the high silane packing, however, a monolayer structure was maintained whatever the Br to CH_3 coverage ratio, as shown by the good agreement of the thickness values with the theoretical one (figure 3.15).

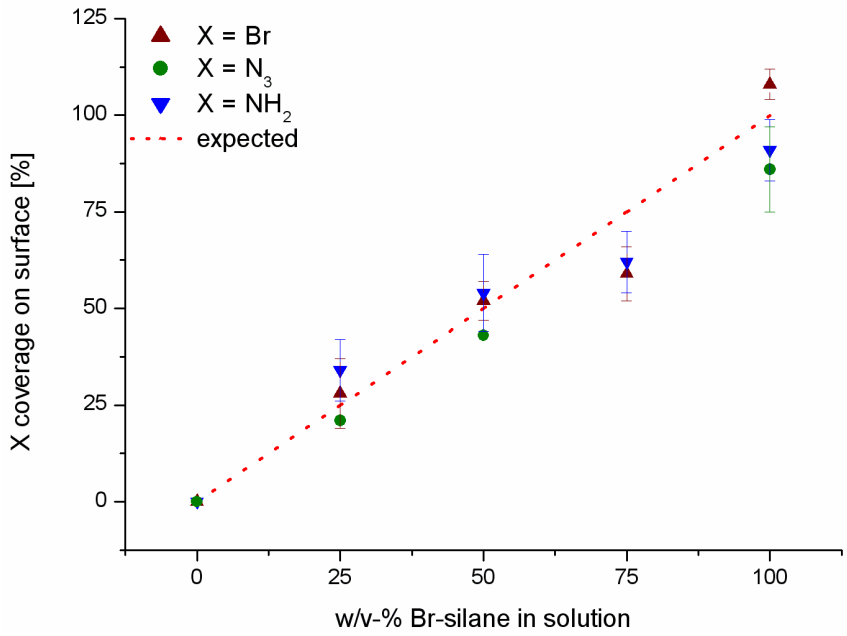

Figure 3.14: Surface coverages of Br, N_3 and NH_2 for surfaces revealing the five various, theoretical Br/CH_3, N_3/CH_3 and NH_2/CH_3 coverages (0, 25, 50, 75 and 100 %) versus the concentration of bromine silane in solution.

3.3. Conversion of bromine termination to amino groups

Further conversion of Br/CH_3 to NH_2/CH_3 mixed surfaces was performed via S_N2 bromine-to-azide conversion as depicted in figure 3.12 a. Efficiency of the conversion steps was determined on high resolution XPS spectra. Typically, as shown in figure 3.12 b and figure 3.12 c respectively, conversions of Br to N_3, and of N_3 to NH_2, led to the total disappearance of Br and N_3 respectively. Quantitatively, high resolution XPS spectra analysis allowed to highlight that the linear relationship between Br surface coverage ratio and initial Br content of the solution was conserved after the first (from Br to N_3) as well as the second (from N_3 to NH_2) conversion step (figure 3.14). Nevertheless, bromine and amine content were equal but azide surface coverage was systematically lower than bromine or amine content. This is attributed to the probable chemical reduction of azide groups during XPS analysis, which however has no impact on the preparation of the amine surfaces. Conversion led finally to create NH_2/CH_3 mixed monolayers that displayed the expected chemical properties as further attested by the contact angle measurements (figure 3.15). The monolayer structure and the organization of the silane in a dense layer were not modified by the conversion steps. Indeed, thickness values were not modified by the chemical process, and, as

discussed in the above paragraph, the good accordance between contact angle values and expected ones [10] certifies the compactness of the monolayers (figure 3.15). Importantly, the good reproducibility was maintained, shown by the low standard deviation values on each of the indicative characteristics (coverage rate, contact angle value, thickness value), throughout the conversion from Br to NH_2 functional groups. As depicted in figure 3.16 b for a NH_2 100 % surface, the real structure and organization of the mixed monolayer are estimated to be close to the expected, ideal structure (figure 3.16 a). The presence of NH_3^+ functional groups (20 at. %), as shown in the high resolution XPS spectrum of N1s peak (figure 3.16 e), may result from the incomplete reduction of the functional groups during the post-conversion treatment with triethylamine. Ejection of photoelectrons from the material during the XPS analysis may also have induced additional positive charges at the surface.

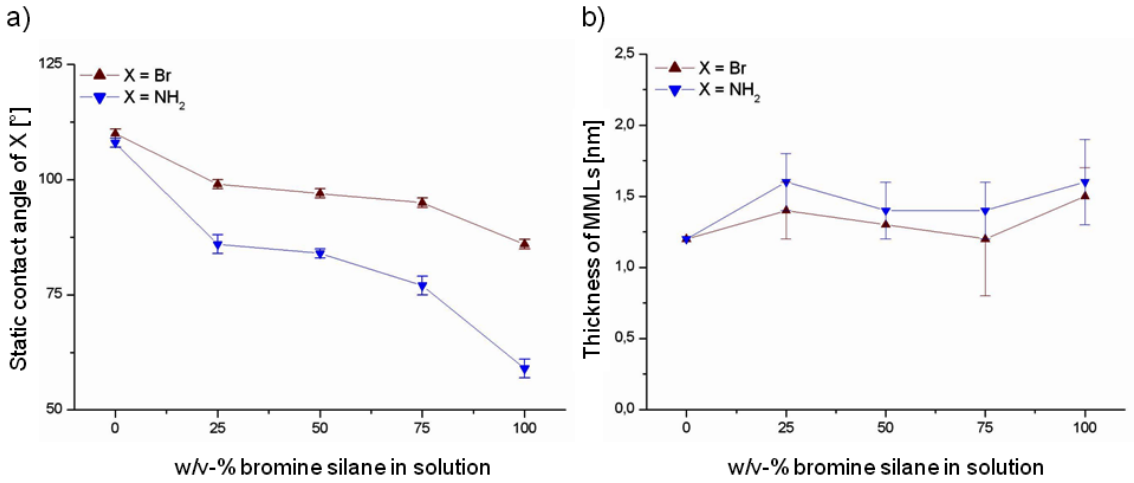

Figure 3.15: Contact angle values (a) and thicknesses (b) for surfaces revealing the five various, theoretical Br/CH_3, N_3/CH_3 and NH_2/CH_3 coverages (0, 25, 50, 75 and 100 %).

3.4. Relevance of the Br based NH_2/CH_3 platforms for biointerface studies

SAMs, chemically homogeneous or mixed monolayers, have been already frequently used either under static or dynamic conditions for analyzing the influence of surface chemistry on bacterial adhesion and biofilm development. Ploux *et al.* used homogeneous NH_2 and CH_3 terminated layers on silicon wafers for studying the adhesion and proliferation of *E. coli* under static conditions in a time space from 4 h to 2 weeks [13]. They demonstrated that despite similar colonization at 2 h, considered as bacterial adhesion, NH_2 and CH_3 surfaces can reveal significantly different kinetics of biofilm formation as well as biofilm structure. Katsikogianni *et al.* used CH_3, NH_2 and OH terminated surfaces on glass substrate to investigate the adhesion of *S. epidermidis* on different surface chemistry after 2 h of culture under various hydrodynamic shear rates [11,31]. They reported that the number of adherent bacteria decreased following the rank $CH_3 > NH_2 >$ OH (pure glass slide). Through the use of OH/CH_3 mixed monolayers on gold substrates under hydrodynamic

conditions of bacterial culture, Wiencek *et al.* showed that the bacteria attachment to detachment balance also leads to more bacterial attachment on CH_3 surfaces than on OH surfaces for *Pseudomonas sp.*. Besides, bacterial colonization to OH/CH_3 surface relationship was linear [14,15]. Although these different SAMs enabled to provide relevant results in the bacteria/material biointerface field, the absence of a comprehensive analysis of their structure and organization leads to wonder whether possible structure and organization failures may have altered biological responses. Hence, sensitive effects that surface chemistry may induce in bacterial response to surface, such as those related to functional group accessibility and chemical heterogeneity, may be screened. The assurance of well-controlled surface chemistry, structure and organization of the Br-based NH_2/CH_3 mixed monolayers should therefore offer new opportunities of relevant results in the biointerface field.
To test the relevance of better controlling surface chemical composition, layer structure and organization for material/bacteria biointerface studies, we compared the repeatability of bacterial adhesion on Br based NH_2 100 % with those measured on other NH_2 100 % terminated surfaces that were shown not to reveal well-structured and well-organized layers on the contrary to Br-based NH_2 100 % surfaces (figures 3.16 b, 3.16 c, 3.16 d) [22]. APTES and AHAPS were chosen since we recently demonstrated defects in the layers despite characterization results in apparent agreement with expected.

The averaged numbers of adherent bacteria observed on APTES and AHAPS NH_2 100 % surfaces were not significantly different (114 $\pm$ 35 and 132 $\pm$ 32 respectively) but differed from the weaker average value determined on Br based NH_2 100 % (102 $\pm$ 14). This first result demonstrates that layer structure and organization can affect the result of material/bacteria biointerface studies, confirming that their control must be a crucial topic of the elaboration of dedicated platforms. Differences in colonization probably results from the few quantity of NH_2 groups revealed at the APTES and AHAPS NH_2 100 % surfaces, what is expected for a fully packed, well-structured and well-organized layer. Besides, a remarkable result concerns the deviation of the adherent bacteria numbers determined for each type of NH_2 100 % surfaces throughout the experiment replicas. As shown by the atomic percentages of nitrogen determined on XPS survey spectra (2.7 $\pm$ 1.1, 1.7 $\pm$ 0.7 and 1.1 $\pm$ 0.4 for APTES, AHAPS and Br-organosilane-based NH_2 100 % respectively), the differences in bacterial adhesion on APTES, AHAPS and Br-organosilane-based NH_2 100 % should not be attributed to the variation and reproducibility of nitrogen amount in the silane layers. However, the significant differences in the structure and organization that were highlighted in a previous [22] and in the present study (figures 3.16 b, 3.16 c, 3.16 d) lead to significant differences in the functional group accessibility at the extreme surface of the silane layers. Furthermore, insufficient control of APTES and AHAPS layer structure and organization leads to probable high variation of the functional group amount present at the extreme surface of the layer. These variations between APTES and AHAPS samples of one series are probably the main reason of both the slight differences in the adherent bacteria number average and the high differences in the reproducibility of the bacteria

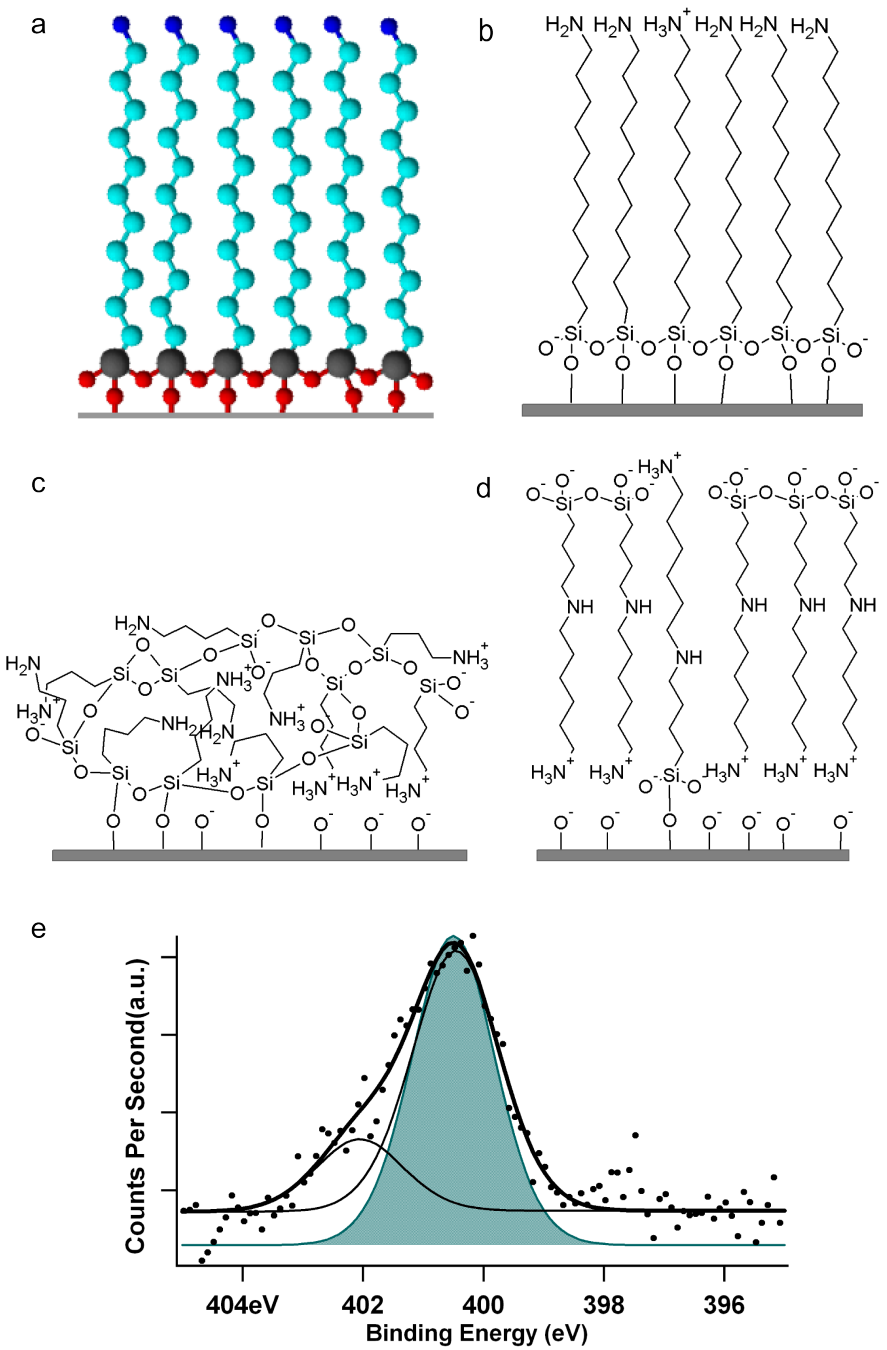

Figure 3.16: (a) Representation of the "ideal" layer structure and molecular organization of Br-organosilane-based NH_2 100 % terminated surfaces. Representations of the "real" layer structure and molecular organisation of NH_2 100 % terminated surfaces based on Br-organosilane (b), APTES (c) and AHAPS (d) ((c) and (d) reprinted with the permission from [22], Copyright 2010 American Chemical Society). (e) XPS N1s high-resolution spectra expected for the ideal case (full curve) and in the real case (i.e., experimental results) (line curve) of Br-organosilane-based NH_2 100 % terminated surfaces.

adhesion test (figure 3.17). Nevertheless, variations of the adherent bacteria number on AHAPS surfaces are less than on APTES surfaces in agreement with the higher control of both structure and organization observed for AHAPS in comparison to APTES layers (figures 3.16 c, 3.16 d).

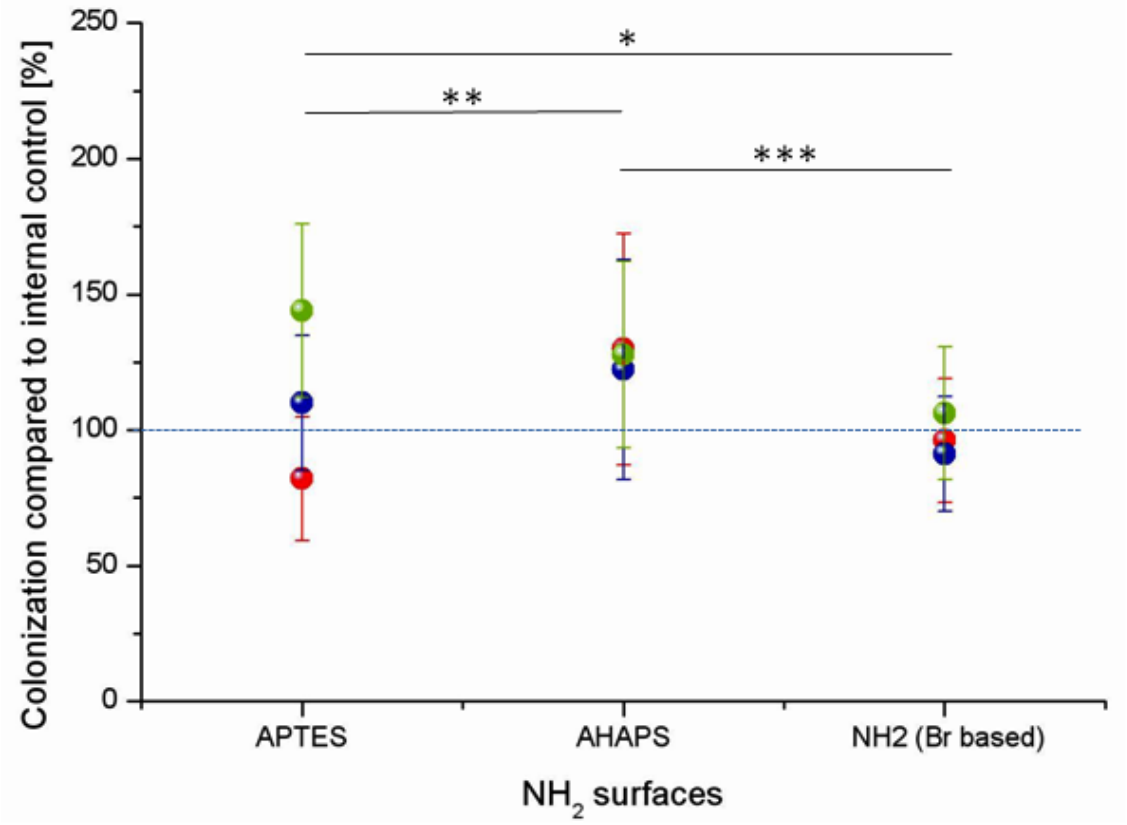

Figure 3.17: Amount of *E. coli* K12 (MG1655 [24]) bacteria adhered on the three different types of NH_2 100 % surfaces (APTES, AHAPS and Br-organosilane-based surfaces) on six different samples for each type of surface. Number of bacteria was compared to the colonization on internal control (i.e., cleaned, ungrafted silicon wafers; 100 = 6.1x10^5 *pm* 5.3x10^4 bacteria/cm^2). *: Significant difference (p > 95.0 %); **: Significant difference (p > 99.0 %); ***: Significant difference (p > 99.9 %).

4. CONCLUSION

Based on a comprehensive analysis of Br-organosilane-based mixed monolayers and the development of an adequate protocol, we achieved the well-control of chemically well-defined and well-structured monolayers. In particular, Br / CH_3 and NH_2 / CH_3 surface coverage rates were perfectly controlled by the chemical content of the initial Br-organosilane solutions. S_N2 bromine-to-azide and further azide-to-amine conversions did not affect the chemical well-control. The molecules that were structured in a monolayer were densely packed and organized as expected for SAMs. The relevance of such well-controlled surfaces was evaluated by comparing bacterial adhesion on NH_2-terminated surfaces obtained

by the Br-organosilane way and APTES and AHAPS ways. The quantity of adhered bacteria on Br-organosilane-based monolayer throughout several experiment replicates was very significantly less dispersed than on both the other SAMs types, showing the high importance of the functional group accessibility in the adhesion or the retention of bacteria at the interface. Therefore, we believe that the platform quality that was achieved in this work may offer new opportunities for studying in a comprehensive way behavior and biological response of microbiological and eukaryotic cells at the biointerfaces. Through further grafting of biomolecules, this platform may provide promising tools for the study of the still unknown impact of the accessibility of biomolecules immobilized on biomaterials.

5. ACKNOWLEDGMENT

We thank Philippe Fioux for the XPS measurements, and the Region Alsace for their financial support.

REFERENCES

1. Anselme, K., et al., in Comprehensive Biomaterials, D.H. P. Ducheyne, K. Healy, J. Kirkpatrick, Editor. 2011, Elsevier p. 235-256.
2. Boonaert, C.J.P., et al., in Encyclopedia Environmental Microbiology, G. Bitton, Editor. 2002, Wiley: New York. p. 113-132.
3. Katsikogianni, M. and Y.F. Missirlis, European Cells and Materials, 2004. **8**: p. 37-57.
4. Ploux, L., et al., Journal of Adhesion Science and Technology, 2010. **24**: p. 2165-2201.
5. Ponche, A., et al., Journal of Adhesion Science and Technology, 2010. **24**: p. 2141-2164.
6. Margel, S., et al., Journal of Biomedical Materials Research, 1993. **27**(12): p. 1463-1476.
7. Mrksich, M., Acta Biomaterialia, 2009. **5**(3): p. 832-841.
8. Gooding, J.J. and S. Ciampi, Chemical Society Reviews, 2011. **40**: p. 2704-2718.
9. Sullivan, T.P. and W.T.S. Huck, European Journal of Organic Chemistry, **2003(1)**: p. 17-29.
10. Aswal, D.K., et al., Analytica Chimica Acta, 2006. **568**(1-2): p. 84-108.
11. Katsikogianni, M. and Y. Missirlis, Journal of Materials Science: Materials in Medicine, 2010. **21**(3): p. 963-968.
12. Nilsson, L.M., et al., Molecular Microbiology, 2007. **65(5)**: p. 1158-1169.
13. Ploux, L., et al., Colloids and Surfaces B: Biointerfaces, 2007. **57**: p. 174-181.
14. Wiencek, K.M. and M. Fletcher, Journal of Bacteriology, 1995. **177(8)**: p. 1959-1966.
15. Wiencek, K.M. and M. Fletcher, Biofouling, 1997. **11(4)**: p. 293-311.
16. Burton, E.A., et al., Langmuir, 2009. **25(3)**: p. 1547-1553.
17. Heise, A., et al., Thin Solid Films, 1998. **327-329**: p. 199-203.
18. Heise, A., et al., Langmuir, 1997. **13**: p. 723-728.
19. Fryxell, G.E., et al., Langmuir, 1996. **12(21)**: p. 5064-5075.
20. Balachander, N. and C.N. Sukenik, Langmuir, 1990. **6(11)**: p. 1621-1627.
21. Shyue, J.-J., et al., Langmuir, 2004. **20(20)**: p. 8693-8698.
22. Böhmler, J., et al., Journal of Physical Chemistry C, 2011. **115(22)**: p. 11102-11111

23. Kwok, D.Y., et al., Langmuir, 1997. **13(10)**: p. 2880-2894.
24. Vidal, O., et al., Journal of Bacteriology, 1998. **180(9)**: p. 2442-2449.
25. Rasband, W., U. S. National Institutes of Health, Bethesda, Maryland, USA. 1997.
26. Brzoska, J.B., et al., Langmuir, 1994. **10(11)**: p. 4367-4373.
27. Barbot, C., et al., Colloids and Surfaces A: Physicochemical and Engineering Aspects. **297(1-3)**: p. 221-239.
28. Brzoska, J.B., et al., Langmuir, 1994. **10(11)**: p. 4367-4373.
29. Angst, D.L. and G.W. Simmons, Langmuir, 1991. **7**(10): p. 2236-2242.
30. Silberzan, P., et al., Langmuir, 1991. **7(8)**: p. 1647-1651.
31. Katsikogianni, M.G. and Y.F. Missirlis, Acta Biomaterialia, 2010. **6(3)**: p. 1107-1118.

Supporting Information

Table 3.8: Characteristics of Br 100 % layers obtained in the 2. condition-set of reaction conditions (named "A" condition set) (see table 3.6) with supplementary post-treatments including annealing step and further rinsing under sonication (named "B" condition set) (see Material and Methods).

	Thickness in air (in liquid) [nm]		Br coverage HR spectra [%]		Br coverage Survey spectra [%]		Br3d/ SiOx	
A	5.8 ± 2.1	5	106 ± 6	4	87 ± 6	8	0.26 ± 0.05	4
	(7.0 ± 1.4)	3						
B	4.7 ± 0.6	3	106 ± 7	3	87 ± 3	2	0.30 ± 0.05	2
	(5.6 ± 3.2)	2						

Table 3.9: Characteristics of Br 100 % layers obtained in the B condition set and modified by changing the solvent ($CHCl_3$, heptane, toluene and 30 % $CHCl_3$ in heptane for the so-called "C", "D", "E" and "F" condition-sets respectively) (see Material and Methods).

	Thickness in air (in liquid) [nm]	Nr	Br coverage HR spectra [%]	Nr	Br coverage Survey spectra [%]	Nr	Br3d/ SiOx	Nr
B	4.7 ± 0.6	3	106 ± 7	3	87 ± 3	2	0.30 ± 0.05	2
	(5.6 ± 3.2)	2						
C	2.4 ± 0.3	1	82	1	83	1	0.11	1
D	4.3 ± 0.4	1	128	1	106	1	0.61	1
	(6.6 ± 0.1)	1						
E	2.9 ± 0.4	1	81	1	72	1	0.22	1
	(3.0 ±0.3)	1						
F	1.2 ± 0.0	1	109	1	90	1	0.16	1

Table 3.10: Characteristics of Br 100 % layers obtained in the F condition set and modified by changing the reaction temperature (20 °C, 45 °C and 6 °C for the so-called "F", "G", and "H" condition sets respectively) (see Material and Methods).

	Thickness in air [nm]	Nr	Br coverage HR spectra [%]	Nr	Br coverage Survey spectra [%]	Nr	Br3d/ SiOx	Nr
F	1.2 ± 0.0	1	109	1	90	1	0.16	1
G	1.4 ± 0.0	1	93	1	74	1	0.24	1
H	1.5 ± 0.0	1	115	1	101	1	0.19	1

Table 3.11: : Characteristics of Br 100 % layers obtained in the H condition set and modified by changing the reaction time (16 h and 4 h for the so-named "H", and "I" condition sets respectively) (see Material and Methods).

	Thickness in air (in liquid) [nm]	Nr	Br coverage HR spectra [%]	Nr	Br coverage Survey spectra [%]	Nr	Br3d/ SiOx	Nr
H	1.5 ± 0.0	1	115	1	101	1	0.19	1
I	1.5 ± 0.2	6	105 ± 5	3	93 ± 5	3	0.15 ± 0.02	3

3.6 Supplementary Information of Part 1

3.6.1 Additional information on XPS analysis

For the background determination, a Shirley equation was used. Parameters like positions and constraints to analyze the XPS survey and high resolution spectra are shown in the tables beyond. Table 3.12 shows the parameters for the survey spectra. In comparison to chapter 2 only the bromine signal at a binding energy of $\sim$ 71 eV was added to analyze the survey spectra. The Br3d signal is deconvoluted in two peaks Br3d 3/2 and Br3d 5/2, which arises from the spin orbit coupling. Here, an area constraint is needed to adjust the peaks and finally to obtain the same corrected area of Br3d 3/2 and Br3d 5/2 for one surface. In the ideal case, the C1s high resolution spectra should only contain the signals of CH_x assigned at 285.0 eV and C-Br assigned at 286.0 eV. However, a third component has to be added at 286.65 eV (C-O) for an adequate peak fitting. The attribution of this component is unclear, but has no impact on the yield calculation.

Table 3.12: Parameters and constraints for XPS analysis.

survey spectra						
	Br3d	Si2p	C1s	O1s		
position [eV]	71	99	285	533		
±						
RSF	2.84	0.817	1	2.93		
High resolution of Br3d and C1s						
	Br3d 5/2	Br3d 3/2		CHx	C-Br	C-O
position [eV]	70.6	71.6		285	286	286.65
±	0.0	0.0				
position constr.	A	A + 1		A	A + 1	A + 1.65
area constr.	A	A · 0.69				
FWHM constr.	A	A · 1		A · 1	A · 1	A · 1
RSF[4]	1.68	1.16		1	1	1

In tables 3.12 and 3.13, the parameters for the deconvolution of the N1s high resolution signal of the azide surface (see table 3.13) are presented. The parameters for the C1s high resolution spectrum are the same as shown in the supporting information of chapter 2 in table 2.1.

Table 3.13: High resolution spectra of azide surfaces.

High resolution of N1s			
	N	N^-	N^+
position [eV]	401.4	400.9	404.9
±	0.1	0.1	0.1
position constr.	A	A - 0.5	A + 3.5
area constr.	A	A · 1	A · 1
FWHM constr.	A	A · 1	A · 1
RSF	1.8	1.8	1.8

3.6.2 Optimization of the Br-silane grafting

As shown in the article 2a: *"Well controlled platforms to study the role of surface chemistry at biointerfaces"*, the choice of the solvent is crucial to obtain well-controlled monolayers. By using hexadecane as solvent, a multilayer is achieved. The signal of bromine is then more intense in XPS survey spectrum in the case of a multilayer structure than for a monolayer. Consequently, the survey spectrum of a multilayer differs from a spectrum of a monolayer. For instance, the peak of the substrate (Si2p) decreases compared to the C1s and Br3d signals. Additionally to the Br3d signal, the signal of Br3s (at 257 eV) is more distinctive. In general, a low concentration of the substrate may already indicate that a multilayer was formed on the surface. In figure 3.18, two survey spectra are shown, (a) was prepared in hexadecane and a multilayer was obtained, while the use of $CHCl_3$ leads to a monolayer (b).

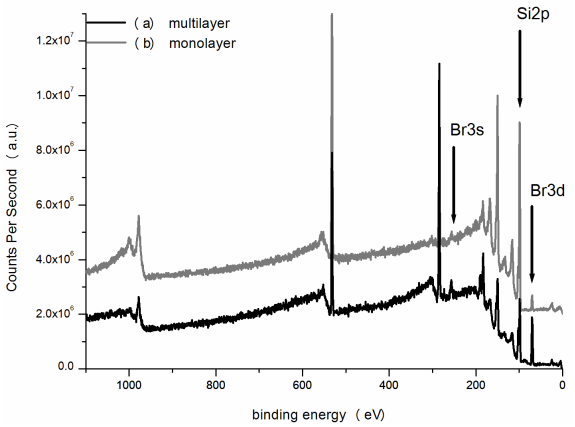

Figure 3.18: The survey spectra of a multi- and a monolayer differ from each other. (a) Spectrum from a multilayer, the substrate signal of Si2p is less intense than in a monolayer (b). Through the high amount of Br, the Br3d and Br3s signals are more intense than in case of a monolayer.

3.6.3 Br terminated mixed monolayers

Surfaces with different percentages of atomic concentration of bromine were obtained according to the ratio of Br silane in the solution. The density of Br groups in a CH_3 environment was demonstrated in the article 2a. Further, the variation of the density reflected by the Br3d signal, is depicted in figure 3.19 a. The wettability character of the surfaces was analyzed by dynamic contact angle measurements. Therefore, a water droplet was deposited on the surface, and by the increase of the drop volume, the advancing contact angle could be obtained, while the receding contact angle was measured by reducing the volume of the droplet.

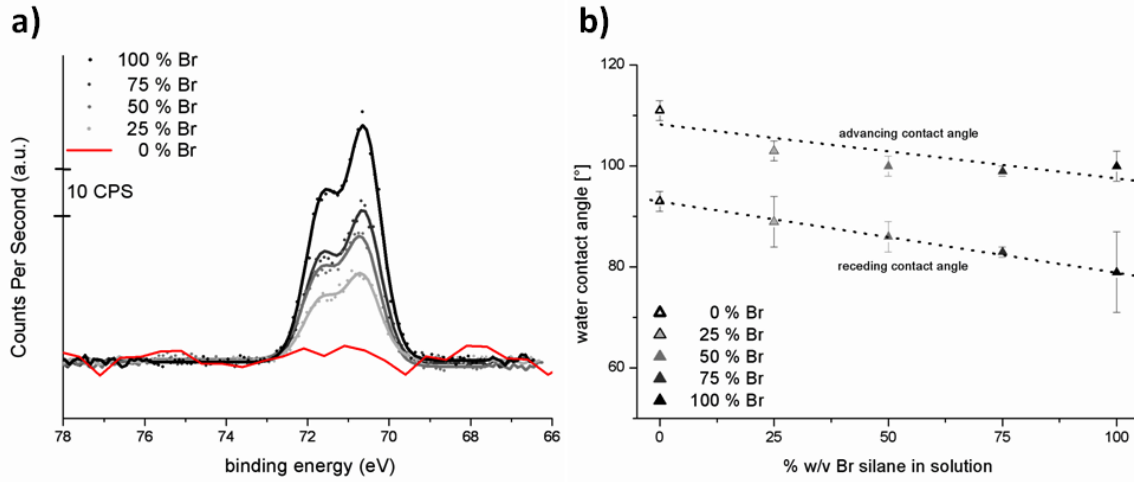

Figure 3.19: Br terminated mixed monolayers can be easily identified by Br3d high resolution spectra of XPS (a) and contact angle measurements (b). Through different ratios of the Br silane and CH_3 silane, various densities of Br on the surface can be obtained. In (a) is shown that the signal of Br increases with the % w/v of Br silane in solution. (b) the change of the wettability character of the surface, is correlated with the increase of Br silane in solution, the surfaces become less hydrophobic than CH_3 terminated surfaces.

In figure 3.19 b, the advancing and receding contact angles were plotted for the surfaces with different densities of bromine, revealing a linear correlation. As expected the CH_3 terminated surface shows the most hydrophobic character (highest advancing and receding contact angle), while the bromine terminated surface shows the most hydrophilic character (lowest advancing and receding angle) of the investigated surfaces. The difference between the advancing and the receding contact angle is the hysteresis. A small hysteresis indicates a homogeneous surface, while a high hysteresis indicates a heterogeneous surfaces. For the investigated surfaces hysteresis values between 14 and 27 were obtained. In which the 0 %Br:ΔH=18, 50 %Br:ΔH=14, 75 %Br:ΔH=16 showing a hysteresis beyond ΔH=20. These hysteresis values are in agreement with flat surfaces. For the mixed

monolayers 50 %Br and 75 %Br surfaces, the lowest values of hysteresis were obtained while for 25 %Br and 100 %Br an elevated hysteresis was obtained ΔH=27 and ΔH=22, respectively. Despite, the flat surfacesn the hysteresis is elevated for the mixed monolayers. However, this can be explained by the inluence of the different chemical functionalities on the surface and their impact on the contact angle.

3.6.4 Conversion of bromine into amine

3.6.4.1 Kinetics of the S_N2 reaction

Investigations of the conversion reaction from bromine to azide were performed in DMF and in water. DMF favor the bimolecular nucleophilic substitution reaction. Hence, no reaction took place in water, while the bromine was successfully substituted by the reaction in DMF. As mentioned in literature [132], the conversion is quite fast at the beginning. As depicted in figure 3.20 a, over 50 % of the bromine is already converted into azide after 6 h. The following displacement reaction takes more time and after 72 h more than 95 % of the bromine are converted into amine. XPS analyses of amine surfaces showed no residual bromine, therefore the reaction is considered as complete after 72 h. Further, the atomic concentration of N_3 is three times the atomic concentration of Br (on the substrate), therefore the S_N2 reaction is assumed to be quantitative.

3.6.4.2 Reduction: from azide to amine

The reduction from azide to amine is characterized by the loss of nitrogen signal and the change of the peak shape in the N1s spectrum. The azide contains three differently charged nitrogen atoms, a positively charged, a negatively charged and a neutral nitrogen. Therefore, three signals areas can be assigned to the azide. NH_2 groups are achieved, by reduction of azide with $LiAlH_4$. However, a treatment in acid solution is necessary to remove lithium complexes on the surface. Hence, the amine groups is protonated, and has to be deprotonated in a subsequent step by reaction with TEA. As expected the shape of the peak changes by comparison of azide and amine terminated surfaces, as depicted in figure 3.21. The reduction reaction is quantitative after 14 h, confirmed by the nitrogen concentration, that is three times higher for azide than for amine. Nevertheless, a small quantity of NH_3^+ (around 18 %) was always detectable on amine terminated surfaces. One explanation could be that this small amount of NH_3^+ is stablized by the NH_2 environment and therefore was not deprotected by TEA. However, no counterion was detected. A second explanation is the evolution of positive charge of the surface during XPS analysis, due to the photoelectrons ejection.

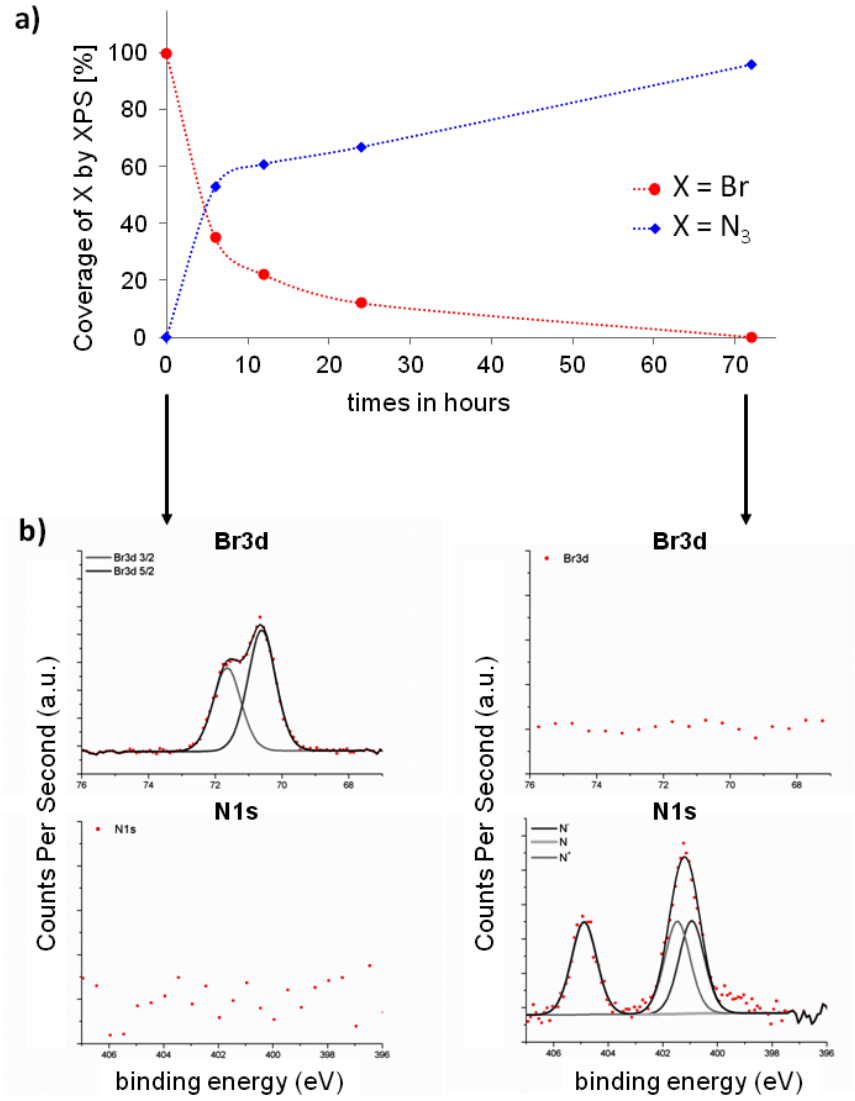

Figure 3.20: During the reaction of the surfaces reacted with NaN_3, XPS measurements were done after 6, 12, 24 and 72 h. (a) The obtained coverage of bromine is plotted against the reaction time (red curve). It decreases with time while the coverage of nitrogen increases (blue curve). (b) XPS measurements at t=0 h (left) and t=72 h (right) show that at the beginning of the reaction only a signal of Br3d but no nitrogen was detectable. After 72 h the signal of Br3d disappeared, while a new signal of N1s appeared.

3.6.4.3 Amino functionalized surfaces

The equation of Israelachvili (equation 3.7), which is adequate for mixed monolayers, can be used to demonstrate a correlation between the contact angle and the different densities of one functional group (NH_2) among another (CH_3) [160].

$$(1 + \cos\theta)^2 = f_1 \cdot (1 + \cos\theta_1)^2 + f_2(1 + \cos\theta_2)^2 , \tag{3.7}$$

$$1 = f_1 + f_2 \tag{3.8}$$

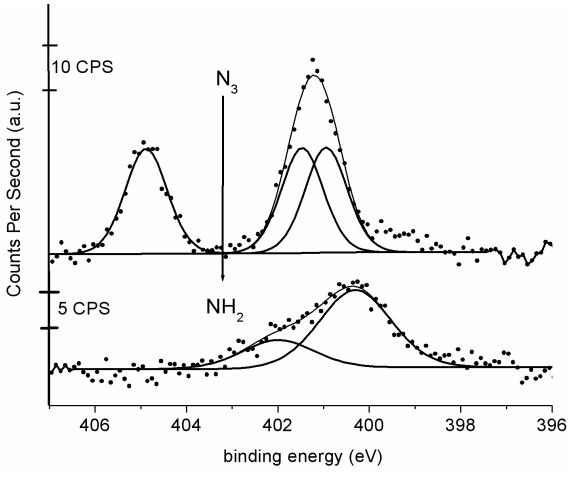

Figure 3.21: The N1s spectra show the differences between the signal of N_3 and the signal of NH_2. The three components of azide becomes united in one signal containing the two components NH_2 and NH_3^+. The decrease of the NH_2 signal is due to the loss of nitrogen atoms ($N_3 \rightarrow N$).

where $\cos\theta$ is the experimentally obtained contact angle, f_1 and f_2 are the mole fraction of the first component NH_2 backfilled with a second component CH_3 and added up to 1 (see equation 3.8), here 0.75 NH_2 = 0.25 CH_3. θ_1 is the contact angle of the SAM with 100 % of grafted component 1 and θ_2 is the contact angle of the 0 % grafted component 1 i.e. of the 100 % grafted component 2.
Based on the following equation 3.9, $(1+cos\theta)^2$ can be plotted versus f_1 and as mentioned above, there is a linear correlation between $(1+cos\theta)^2)$ and f_1.

$$(1 + \cos\theta)^2 = f_1 \cdot ((1 + \cos\theta_1)^2 - (1+\cos\theta_2)^2) + (1 + \cos\theta_2)^2 , \qquad (3.9)$$

where $((1 + \cos\theta_1)^2 - (1+\cos\theta_2)^2)$ is the slope and represents the contact angle of 100 % NH_2, and $(1 + \cos\theta_2)^2$ is the y-intercept, which represents the contact angle of 100 % CH_3. For example, the advancing contact angle of a 100 % NH_2 surface is 77 ° (111 ° 100 % CH_3), and by using the slope of equation 3.9, an angle of 78 ° (112 °, for CH_3) is assessed. The linear correlation between $(1+cos\theta)^2$ and the NH_2 concentration of the surfaces, implies a chemical heterogeneity at molecular or atomic scale [160]. Further, the Cassie equation was applied however, no linear correlation was obtained. Hence, the silanes with different functional groups are well distributed at the surface, without forming domains of one component within the other.
In addition, the surface energy was estimated through the contact angle of different polar and apolar solvents. Figure 3.22 b shows the obtained surface energies of the mixed monolayers. The hydrophilic NH_2 terminated surface has a higher energy than the hydrophobic CH_3 terminated surface.

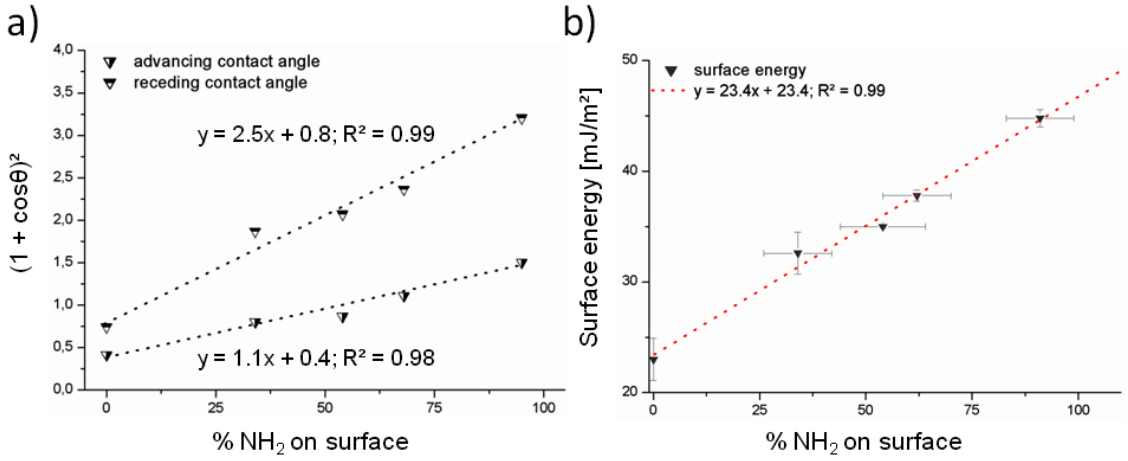

Figure 3.22: A linear behavior of the contact angle of mixed monolayers is well described by equation 3.7 that takes into account different group contributions. (a) shows the linear correlation between the advancing and receding angle $(1 + cos\theta)^2$ and the NH_2 mixed monolayers. (b) shows the surface energy of the mixed monolayers obtained by water contact angle measurements. The surfaces energy increases with the hydrophilic character of the surfaces.

3.6.4.4 Zeta potential

As in the second chapter, the IEP of the mixed monolayers was determined by zeta potential measurements (see figure 3.23). An IEP between pH 8 and pH 9 was expected for closely packed NH_2 terminated SAMs [76]. However, table 3.14 shows that the values of the IEP for the mixed monolayers and the substrate are similar.

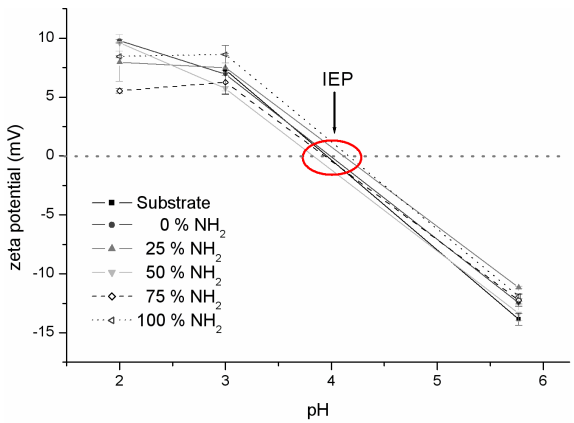

Figure 3.23: A pH titration was carried out, to determine the IEP of the amine terminated surfaces. However, the values of the surfaces are similar to the cleaned substrate.

Nevertheless, it was demonstrated by XPS, contact angle, and AFM analysis that well organized SAMs were obtained. In contrast, the values of the IEP are equal to the IEP of the substrate. Values of the zeta potential are measured due to the charge transport

between the Stern and the diffuse layer. However, the Stern layer is not only represented by the ions on the top of the layer but also on the entire surface. It is not surprising that the structure has small defects, which can appear in form of nano channels. These nano channels might be large enough for the small cations in solution (Na^+, H+) to pass through the monolayer down to the silicon substrate. At the same time, these nano channels might be small enough that they are not visible by other applied characterization techniques like AFM and (macroscopic) contact angle measurements. Consequently, the charge of the silicon substrate becomes predominant compared to the charge of the monolayer on top of the surface.

Table 3.14: IEP values of mixed monolayers.

	substrate	0 % NH_2	25 % NH_2	50 % NH_2	75 % NH_2	100 % NH_2
IEP [pH]	3.7	3.4	3.5	3.4	3.4	3.5

3.6.4.5 Atomic force microscopy

After the deposition of the silanes and the conversion from Br terminated silanes into NH_2 terminated silanes, AFM measurements were done. As expected, no aggregation or islanding was detected by the visualization of the surfaces. Figure 3.24 represents the phase contrast AFM images of five surfaces with different amounts of NH_2 backfilled with CH_3. In addition, the height contrast images (not shown) show a homogeneous and smooth surface.

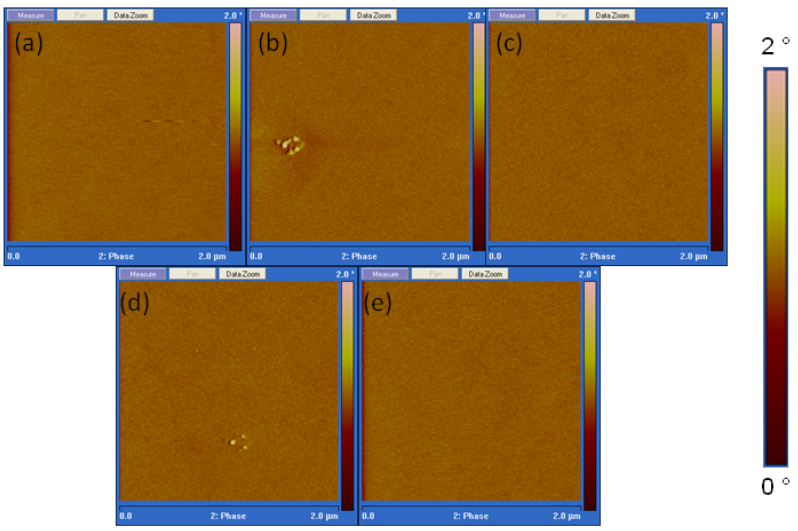

Figure 3.24: The mixed monolayers were characterized by height and phase contrast AFM. (a) shows the AFM phase contrast images of a 100 %NH_2 surface, (b) of a 75 %NH_2 surface, (c) of a 50 %NH_2 surface, (d) of a 25 %NH_2 surface and (e) of a 0 %NH_2 surface.

3.7 Results and Discussion of Part 2

3.7.1 Article 2b: "XPS evaluation of the influence of a linker on the grafting yield of glycine on aminofunctional self assembled monolayers"

Article by Judith Böhmler, Lydie Ploux, Karine Anselme, and Arnaud Ponche, in preparation.

XPS evaluation of the influence of linkers on the grafting yield of glycine on aminofunctional self assembled monolayers.

Judith Böhmler, Lydie Ploux, Karine Anselme, Arnaud Ponche[§].
Institut de Science des Matériaux de Mulhouse (CNRS LRC7228), Mulhouse, France

[§] Corresponding author:
Dr Arnaud PONCHE, Institut de Science des Matériaux de Mulhouse (CNRS LRC7228), 15 rue Jean Starcky, BP2488, 68057 Mulhouse cedex, France, arnaud.ponche@uha.fr

Abstract :
The chemical yield of classical surface reactions destinated to graft biomolecules has been estimated using X-ray photoelectron spectroscopy. We show that high resolution peak fitting of C1s spectrum is necessary at each step to evaluate efficiency of the chemical reaction at the surface of a biomaterial. Dense amino-functional self assembled monolayers have been elaborated and serve as chemical platform to graft small biomolecules like glycine with bifunctional linkers. Common glutaraldehyde linker has been evaluated and appears to be grafted under oligomer form. Isothiocyanate and succinimide linkers solve the problem of oligomerization but the reaction is still limited to approximately 50 % of yield. Systematic evaluation of efficiency of surface reactions gives a better insight on the real structure of the organic layer and will then improve efficiency of biomaterial modification.

Keywords: XPS, C1s, linker, glutaraldehyde, isothiocyanate, succinimide, glycine grafting

Introduction:
In 2008, M. Mrksich pointed out the difficulty to characterize a reaction yield at the surface of a material[1]. Whereas common characterization techniques are operated in liquid conditions to follow organic reaction (NMR, liquid and gaz chromatography), all these

techniques (except NMR) are usually unavailable for surface characterization. It is then necessary to use physical techniques like X-xay photoelectron spectroscopy (XPS), infrared spectroscopy, quartz crystal microbalance (QCM) or mass techniques like matrix assisted laser desorption ionization (MALDI-ToF) or surface enhanced laser desorption ionization (SELDI ToF)[2,3]. However, if users want to determine a reaction yield, for instance, the technique has to be quantitative and XPS remains one of the most used techniques.
Surface chemical reactions are used to confer specific chemical properties to a substrate[4]. The latter usually gives the mechanical resistance whereas chemical reactivity is induced by a molecule grafted at the surface. In that case, chemical informations about organic top layers are important to verify the presence of the molecule and to ensure that the topography of the layer is in accordance with the ideal scheme[5]. It is particularly critical for biomaterial applications, where a complete control of the structure of the layer is required to achieve a good enhancement of the final properties. Biomaterial chemical modification in the field of biosensors[6], implants[7,8] or microarrays[9,10] is usually a multi-step procedure and if the yield of each step is not carefully optimized, the final structure of the grafted layer will definitely move away from the target result and can dramatically reduce the sensitivity of a biosensor for example.
A lot of grafting procedures exist in the literature via multiple techniques[11]. We are interested in self assembled monolayers for their simpleness and control provided over the final layers[10]. Yet, when trying to elaborate organic layers via Self Assembled Monolayers (SAMs), we have already shown that a careful characterization of the surface was necessary in order to investigate the grafting efficiency. A lot of secondary reactions[12] occurs with reactants or compounds of atmosphere making the real chemical structure of the final layer deviate from the ideal representation. In particular, the ideal monolayer is very difficult to achieve with commonly used aminosilane for bioconjugation like aminopropyltriethoxysilane. Short aminosilanes are prone to polymerization as well as interaction with the surface giving a non controlled final structure. Bromo-functionalised silane offers the opportunity to avoid this interaction and a more ideal structure is obtained. Such SAMs can be easily converted into aminofuntional SAMs via a nucleophilic reaction (S_N2) with NaN_3 and reduction of azide goups in amines[13,14]. It gives a more controlled structure with aminogroups located away from the surface and avoids all polymerization side reactions. At the end, the surface is fully covered with amine groups which serve as anchor to graft biomolecules[15]. If the direct immobilization is possible, the surface or the biomolecule has to be activated with a coupling reagent. To favor the reaction with amine groups, N-hydroxysuccinimide esters are common. This step is crucial and is justified by lower reactivity of functional groups close from the substrate[4]. Aside from coupling reagents, bifunctional linkers are commonly used to immobilize biomolecules. The role of the linker is to push aside the biomolecule from the surface to ensure that it will keep its biological activity with a sufficient mobility[16]. In the choice of a bifunctional linker, it is important to favor quantitative and stable reaction. With amine groups, isocyanate[17,18] or isothiocyanate[9,19] are often used as well as glutaraldehyde for example[4,20–22].

In the following study, different reactions were performed to obtain immobilized single amino acids on NH_2 functionalized silicon wafer. The advantage to study the immobilization of a single amino acid and not large biomolecules like protein is that the amino acid has a smaller size and sterical hindrance plays a minor role. Yet amino acid can be considered as a probe to evaluate the reactivity of amino functional SAMs via the use of a linker.

The main objective of this study is to evaluate the potentiality of XPS to calculate surface reaction yield after peak fitting of C1s spectrum. Using only one photoelectric peak for quantitative study avoid the problem of evaluation of mean free path and transmission function of the spectrometer. These parameters are indeed known to contribute largely to the uncertainties or systematic errors of quantitative study by XPS[23,24]. This study will be focused on well controlled SAMs elaboration with maximum density of amine groups followed by coupling of glycine with three classical homobifunctional linkers. Glutaraldehyde (GAD) is a commonly used linker between two amino groups. However, research groups mentioned a low yield and the risk of polymerization and bridging[25]. Di-(N-succinimidyl)oxalate (DSO) is a linker that contains two leaving groups. The split off of the leaving groups happens by the reaction of DSO with amine group[26,27]. DSO is larger and requires more place than GAD. The last homobifunctional linker is 1.4-Phenylendiisothiocyanate (PDITC), where the isothiocyanate group reacts with an amino group[19,27]. PDITC contains an aromatic ring system, which would allow a stacking of PDITC through interactions of the aromatic rings and result in a second organized layer at the top of the monolayer. It is also a more rigid molecule and this characteristic can limit the reaction with the surface. In this article, we will study the influence of three linkers with different physico-chemical properties on the grafting yield of the smallest amino acid: glycine. These linkers will be grafted on self assembled monolayers on silicon, giving a high density of amine groups at the surface. These monolayers have been described elsewhere but, to our knowledge, have never been used for biomedical applications. As a surface sensitive and quantitative technique, X-ray photoelecton spectroscopy will be used to determine yield of reaction by extensive analysis of high resolution C1s spectra.

Material and Methods:

Preparation of NH_2 terminated substrates:

As substrate for the SAMs, silicon wafers were used. The silicon wafers (N-Phosphorus doped, orientation (100), one side polished, resistance 1-30 $\Omega{\cdot}cm^{-1}$, Mat technology, France) were cut into 1 x 1 cm^2 pieces and cleaned by an ultrasonic treatment in chloroform ($CHCl_3$ pure, Carlo Erba) followed by a piranha cleaning step, as described elsewhere[5]. Subsequently, the wafers were thoroughly rinsed with MilliQ water. Cleaned wafers were immediately used for silanization. The silanization took place in small glass vessels containing 1 mM of 11-Br-undecyltrichlorosilane (98.5 %, ABCR) in $CHCl_3$/n-heptane (3:7) solution. Silicon wafers were immersed in the silane solution for 4 h at 6 $\pm$ 1 °C[28]. Afterwards, the substrates were cleaned by short immersion in $CHCl_3$ and hot water. The

substrates were baked at 105 °C for 1 h to stabilize the monolayer. Residual ungrafted silanes were removed by an ultrasonical rinsing step of 15 min in $CHCl_3$. Finally, the substrates were dried under a nitrogen stream.
Amine terminated SAMs were obtained by conversion of the bromine functionalization into an amine[14,29](see Supplementary informations: figure 3.32). Thereby, the bromine terminated substrates were immersed in an over saturated solution of 0.7 M sodium azide (NaN_3, 99.5 %, Sigma-Aldrich) in dimethylformamide (DMF, 99.9 %, Sigma-Aldrich) over 72 h at room temperature. Afterwards, the substrates were rinsed with water and acetone and dried under a nitrogen stream. An azide functionalization was obtained through this S_N2 reaction. The azide groups were reduced by immersion in a 0.2 M solution of lithium aluminum hydride ($LiAlH_4$, 95 %, Sigma-Aldrich) in tetrahydrofuran (THF, 99.9 %, Carlo Erba) for 12 h, followed by an immersion of the substrate for further 12 h in THF. The substrates were treated for 1 h with 10 % HCl, to remove the lithium complexes on the surface[13,14]. Finally the surfaces were deprotonated by immersion of the substrate in triethylamine (TEA, 99.5 % Sigma-Aldrich) for 24 h. The amine functionalized substrates were rinsed with ethanol (EtOH, absolute, Carlo Erba) and dried under a nitrogen stream. Amine substrates were immediately used for further experiments.

Glycine grafting by GAD.
Amine terminated SAMs were immersed in a solution of 10 % v/v GAD in MilliQ water, for 1 h at a pH between 5 and 6. The samples were thoroughly rinsed by MilliQ water and dried under a nitrogen stream. GAD activated surfaces were subsequently immersed in a 20 mM solution of glycine, containing 50 mM $NaCNBH_3$ in MilliQ water. $NaCNBH_3$ reduces the imine group to an amine. Ideal representation of the glycine surface after each chemical step is given in figure 3.25.

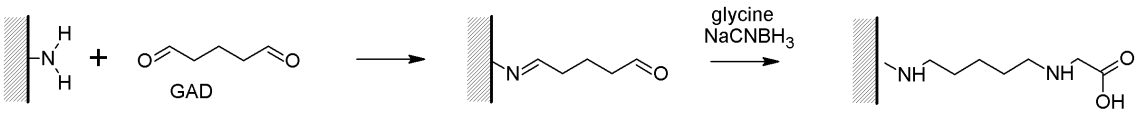

Figure 3.25: Ideal representation of the chemical steps necessary for elaboration of NH_2-GAD-Glycine surface.

Glycine grafting by DSO.
The amino terminated substrates were immersed in a solution of DSO (10 mM) in CH_2Cl_2 supplemented with TEA (1 % v/v) for 2 h at room temperature[19]. Afterwards, the samples were rinsed several times by CH_2Cl_2 and dried under nitrogen. The DSO activated surfaces were immersed in a solution of 1 mM glycine in MilliQ water for 24 h at 6 °C. The samples were rinsed with MilliQ water and EtOH and dried under a nitrogen stream. Chemical steps and ideal stoechiometry of the surface are given in figure 3.26.

Glycine grafting by PDITC.
The amino terminated substrates were immersed in a solution of PDITC (10 mM) in

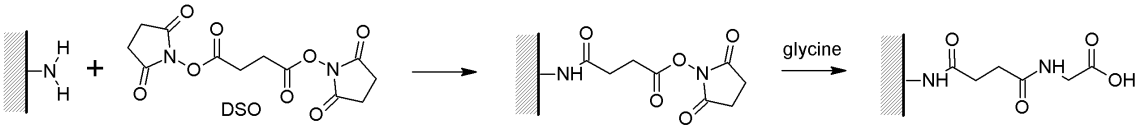

Figure 3.26: Ideal representation of elaboration of NH_2-DSO-Gly surfaces.

CH_2Cl_2 supplemented with pyridine (1 %, v/v) for 2 h at room temperature[19]. Afterwards, the samples were rinsed several times by CH_2Cl_2 and dried under nitrogen. The PDITC activated surfaces were immersed in a solution of 1 mM glycine in MilliQ water for 24 h at 6 °C. The samples were rinsed with MilliQ water and EtOH and dried under a nitrogen stream. Chemical sketches of surfaces are drawn in figure 3.27.

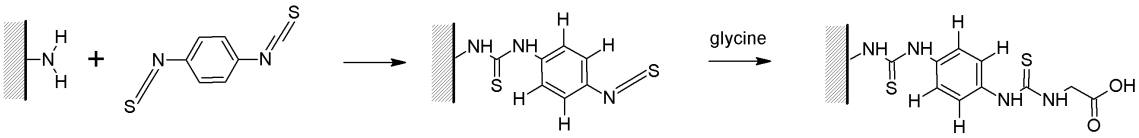

Figure 3.27: Ideal representation of elaboration of NH_2-PDITC-Gly surfaces.

Characterization by X-ray Photoelectron Spectroscopy (XPS).
The chemical composition of the surfaces was determined by XPS analysis. The analysis was performed with a Gammadata Scienta spectrometer, equipped with a monochromated Al Kα X-ray source (1486.6 eV) under ultra high vacuum and a take off angle of 90 °. Survey and high resolution spectra were recorded at pass energies of 500 eV and 100 eV, respectively. For the high resolution experiments, the energetic resolution was estimated to 0.45 eV. All spectra were analyzed and peak-fitted using CasaXPS 2.3.12 software (Casa Software Ldt, Teignmouth, UK, www.casaxps.com). All components were referenced according to the CH_x component at 285.0 eV. The full width half maximum (fwhm) of the fitted peaks in high resolution spectra was constrained to be constant for all components in the same spectrum. The areas given in the article are corrected areas, calculated with a Shirley background and modified by the value of the transmission function of the spectrometer at the selected energy and inelastic mean free path.

Yield calculation
Several parameters were analyzed to follow surface modification and calculate reaction rates.
(i) The experimental ratio of the N1s and C1s regions was compared to the ideal ratio.
(ii) The following equation (see equation 3.10) was used to calculate the yield of a reaction. The equation is based on the difference of experimental ratio of carbon components before and after chemical reaction compared to the ideal one. For example, if glutaraldehyde is

characterized by C=O component, the yield is calculated as follows:

$$Yield(\%) = \frac{(\frac{A(C=O)}{A(CH_x)})^{NH_2-GAD}_{exp} - (\frac{A(C=O)}{A(CH_x)})^{NH_2}_{exp}}{(\frac{A(C=O)}{A(CH_x)})^{NH_2-GAD}_{ideal} - (\frac{A(C=O)}{A(CH_x)})^{NH_2}_{ideal}}, \quad (3.10)$$

where A(C=O) and A(CH_x) are the corrected area of C=O and CH_x C1s components. Upperscript NH_2-GAD denotes the surface after glutaraldehyde grafting and NH2 the initial amino-functional SAMs surface. To normalize all values and avoid every problem of X-ray intensity over two different analysis, the area of CH_x component has been used as a reference.
(iii) The direct evolution of one component (appearance or disappearance), characteristic of the chemical reaction was considered.

Results and Discussion:
XPS is a quantitative characterization technique, hence the yield of a reaction can be calculated by the ratio of components and regions. In this study, survey spectra have been acquired as well as high resolution C1s. For high resolution analysis, a peak fitting model based on the stoichiometry of the ideal surface has been used in order to follow the chemical modifications.

Peak fitting model for XPS characterization
Survey spectrum of amino functional self assembled monolayers exhibits characteristic photoelectron peaks of substrate and organic layer: Si2p at a binding energy of 100 eV, O1s at 533 eV, C1s at 285 eV and N1s at 400 eV. Silicon and oxygen from the substrate represent 60 at% and 18 at% respectively of the volume probed, the rest being characteristic of the thin organic layer. In a first approach, it is possible to evaluate the presence or not of a biomolecule by inspecting the evolution of the area ratio of each atom. According to the stoichiometry given in figure 3.25, the ideal N/C ratio for NH_2 SAMs is N/C=1/11=0.09, N/C=1/16=0.0625 for NH_2-GAD samples and N/C=2/17=0.12 for NH_2-GAD-Glycine. Experimental ratio are systematically lower than the ideal value: 0.071, 0.03 and 0.05 respectively. This indicates that the amount of carbon probed by XPS technique is higher than expected. The higher content of carbon on the reference NH_2 samples can only be due to contamination. Effectively, if SAMs were under the form of multilayers, the N/C ratio would not be modified and the value would be close to 0.09. The only piece of evidence of such a multilayer will be the reduction of the substrate signal and in particular Si2p transition. It can also be noticed that after GAD grafting, the amount of carbon is two times higher than expected and even more after glycine immobilization. Assuming that contamination is the same for all steps and occurs during storage of the samples, it seems that glutaraldehyde in solution is sensitive to polymerization and consequently the ratio of glutaraldehyde over amine on the surface is higher than one.

To go further into details about the chemistry of the layer, it is necessary to analyze high resolution spectra of the photopeak C1s. An example of C1s spectra for the three steps of elaboration of glycine grafted with glutaraldehyde is presented on figure 3.28. The binding

energy and interpretation of the components for all samples are the following: the first component at lower binding energy is attributed to aliphatic carbon (CH_x, 285.0 eV) and is the energy reference for all peaks, the second component is related to carbons adjacent to a carboxylic group (C-COO, 285.5 eV) and is constrained by definition to have the same atomic quantification than carboxylic groups or esters (COO, 289.1 eV). Carbons atoms linked to nitrogen are located at a binding energy of 286.1 eV (C-N, 286.1 eV). The two last components are related to carbons linked to oxygen via a simple bond (C-O, 286.65 eV) and carbons doubly bonded to oxygen (C=O) where appear aldehydes and also amides (NC=O). The analysis of the data of the high resolution spectra let assume that the C-O and the C=N component can be both assigned to a binding energy of 286.65 eV. Hence in the following, the carbon of the C=N and the C-O component are considered to have the same binding energy. We can also notice that the central carbon atoms in the glycine molecule (NH_2-CH_2-COOH) are similar to C-N (286.1 eV) but are submitted to an extra binding energy shift of 0.5 eV (C-COO) due to the adjacent position of carboxylic acid. As binding energy shifts are cumulative, central carbons atoms of glycine will appear at a binding energy of 286.6 eV and then be counted in the C-O (286.65 eV) component.

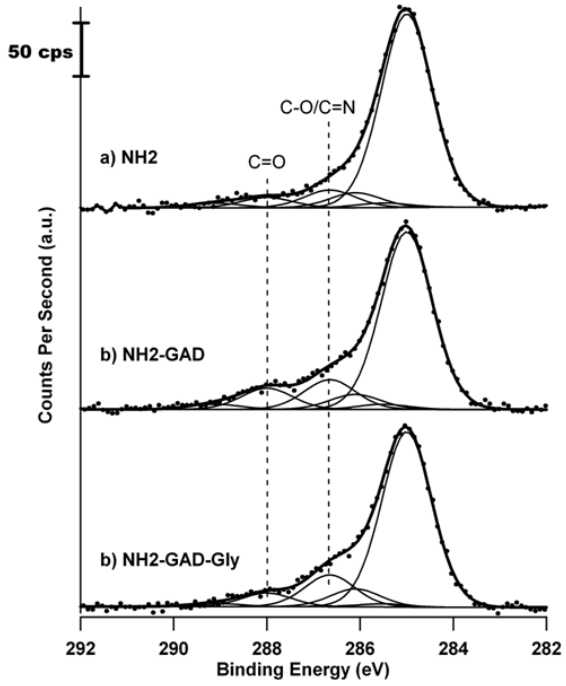

Figure 3.28: Evolution of C1s lineshapes for (a) amino-functional SAMs, (b) glutaraldehyde grafted surface and (c) after immobilization of glycine.

NH_2-GAD

After the glutaraldehyde grafting on NH_2 terminated SAMs, two carbon components showed significant differences compared to the substrate (table 3.15). The first component is C-O/C=N and the second component is C=O /N-C=O at a binding energy of

286.65 eV and 288 eV, respectively. If glutaraldehyde is grafted ideally on the NH_2 surface, amine group reacts with one aldehyde of GAD to give an imine, while the second aldehyde function of GAD is free at the surface. This ideal grafting has been simulated as described elsewhere[5] on the basis of the experimental NH_2 surface C1s spectrum and adding contribution of the aliphatic carbons of glutaraldehyde as well as C=O at 288 eV and C=N at 286.65 eV (figure 3.29). As expected for the GAD grafting, the experimental XPS data show an increase in the corrected area of those two components. The area of C-O/C=N increased from 10.4 up to 26.5 (Δ = 16.1) and C=O from 6.15 up to 19.0 (Δ = 13.15). A similar evolution was expected if GAD is grafted via an ideal mechanism. The fact that the experimental spectrum deviates from the simulated spectrum (see figure 3.29) at a binding energy attributed the component C-O/C=N, indicates that a small amount of GAD molecules react with both terminal aldehyde groups on the substrate. Consequently few bridges of GAD are formed on the monolayer. We can estimate the number of glutaraldehyde molecules which make a bridge with amine groups of the surface to be approximately 10 % of the total number of glutaraldehyde molecules. Nevertheless, the increase of those components indicates that GAD was successfully grafted on the substrate. Two ways are possible to determine the yield of glutaraldehyde grafting, one compare the increase of area of C=N component (with reference to CH_x) compared to the ideal increase and the second one the increase of C=O compared to the ideal one. On the basis of equation 3.10, it is possible to calculate a yield which take into accounts the contamination present on all the surfaces. Reaction yield of 98 % and 87 % could be obtained for the grafting of GAD on NH_2 terminated SAMs. The difference of 10 % is due to the existence of bridging molecules which reacts via the two aldehyde moieties. The almost quantitative yield told us that one aldehyde is present per amine group of the initial SAMs surface. Nevertheless, the first part of the characterisation showed that the number of carbons probed by XPS was higher than the ideal. It can not be excluded that oligomers of glutaraldehyde are attached to the surface. Polyglutaraldehyde is formed via aldol condensation reaction of glutaraldehyde monomer. The polymerization process results in soluble and insoluble polymer but the reaction is favored in basic conditions[25]. With the synthesis conditions used in this study (pH 6, 10 % solution and reaction time 1 h), unsoluble polymers (of high mass) are unlikely to appear but from the molecular point of view of the surface dimers or trimers can not be excluded[25].

Table 3.15: NH_2-GAD-glycine: corrected areas of C1s components.

	CHx	CCOO	C-N	C-O/C=N N-CH_2-COO	C=O/ N-C=O	COO
NH_2	120.0	2.3	9.7	10.4	6.2	2.3
NH_2-GAD	157.8	4.6	13.5	26.5	19.0	4.6
NH_2-GAD-Gly	153.9	2.8	15.7	27.9	12.0	2.8

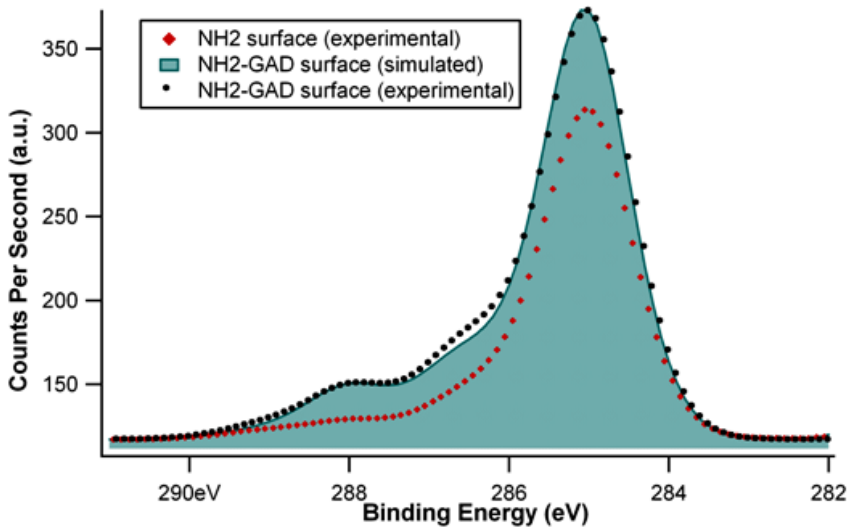

Figure 3.29: Comparison between experimental and simulated spectra for NH_2-GAD surfaces.

NH_2-GAD-Glycine

The ratio of the nitrogen and the carbon signals obtained from survey spectra results in a value of 0.058. This value is lower than the expected value for ideal ratio of GAD surface. Again, the excess of carbon due to glutaraldehyde oligomerization prevent from calculating the yield of reaction. Consequently, peak fitting and analysis of components of high resolution spectra is necessary to avoid miscalculation.

After glycine grafting, the main evolution in lineshapes is the decrease of the component attributed to C=O (288.0 eV, figure 3.26 c). This trend is explained by the disappearance of aldehyde moieties upon reaction with glycine to give first an imine (C=N), which is further reduced to secondary amine by the $NaCNBH_3$ treatment. In summary, the C1s modification obtained after grafting of glycine are:

- The disappearance of imine C=N and C=O to the profit of secondary amine (detected in the C-N component at a binding energy of 286.1 eV).
- The gain of one carbon atom (central atom of the glycine molecule) detected, as previously seen in the C-O component (286.65 eV).
- The gain of one carboxylic acid carbon (COO, 289.1 eV).

The yield obtained with the disappearance of aldehyde compounds is 36 %. This yield is certainly a maximum value. The reducing treatment with $NaCNBH_3$ can have an impact on aldehyde and carboxylic groups. In acidic conditions, both can be reduced to alcohols. The pH of glycine solution in MilliQ water was measured to be 5.8, hence the conversion of aldehyde into alcohol must be limited. Acidic conditions and several hours are necessary (pH 3-4) to obtain adequate reduction rates. In neutral conditions, cyanoborohydride is

practically inert toward aldehyde. This is also confirmed by the very low increase of C-O C1s component reflecting alcohols. By using equation 3.10 and area of the C-O component, the yield obtained is 24 %, lower than the previous value, as expected (see table 3.17 in supporting information).

Influence of linkers

In an attempt to evaluate the reactivity of other molecules, we have grafted two other classical linkers: di-(N-succinimidyl)oxalate (figure 3.26) and phenylendiisothiocyanate (figure 3.27). Both linkers avoid the possibility of polymerization, the first is flexible whereas the second incorporates a phenylene group giving a high rigidity. The high resolution peak fitting procedure has been applied as discussed above, except for the COO component. As a DSO molecule contains a modified ester with succinimide, the binding energy should be lower than 289.1 eV (binding energy for classical ester). To take this into account, the binding energy was not constrained to a fixed value.

Analysis of survey spectrum gives only limited information. The grafting can be confirmed by the increase of carbon content (C1s) or decrease of substrate signal (Si2p). But the estimation of the yield is very difficult, the stoichiometry of the surface being very close before and after glycine immobilization. The use of high resolution peak fitting of C1s spectrum is again requested.

NH_2-DSO-Gly Lineshapes of C1s for NH_2DSO and NH_2-DSO-Gly are presented in figure 3.30. The major difference between the two lineshapes is the shift of the carboxylic component toward lower values of binding energy (288.7 eV vs 289.1 eV). This shift is due to the presence of succinimidyl groups that induce a lower positive charge of the carbon atom in the carbonyl group. After glycine immobilization, only one component appears (289.1 eV): the difference of binding energy between the two components is too low (in the order of the energetic resolution of the spectrometer) and only one peak is kept by the software. The two previous characteristic peaks are then unusable for yield calculation. Nevertheless, glycine grafting on DSO is characterized by an increase of C-O (as previously the central atom of glycine is related to the component C-O) as well as an increase of the amide peak. When a glycine molecule is grafted, a succinimidyl group (detected at 288.7 eV) is leaving and an amide bond is established (and counted in the 288.0 eV C=O component). Then, based on increase of C=O or C-O components, the grafting yield can be evaluated. Interestingly, these two components provide similar values of 42 % and 44 % respectively.

NH_2-PDITC-Gly The sulfur element is characteristic of the PDITC and can be used as a marker. Unfortunately, silicon surfaces and in particular Si2p and Si2s transition exhibits loss plasmon peaks which superimpose with the sulfur 2p transition. The presence of sulfur could then not be confirmed owing to the small amounts present and to its low atomic sensitivity factor. Using C1s peak fitting, this system only allows the determination with C-O component (related to the central atom of glycine) and carboxylic groups (figure 3.31,

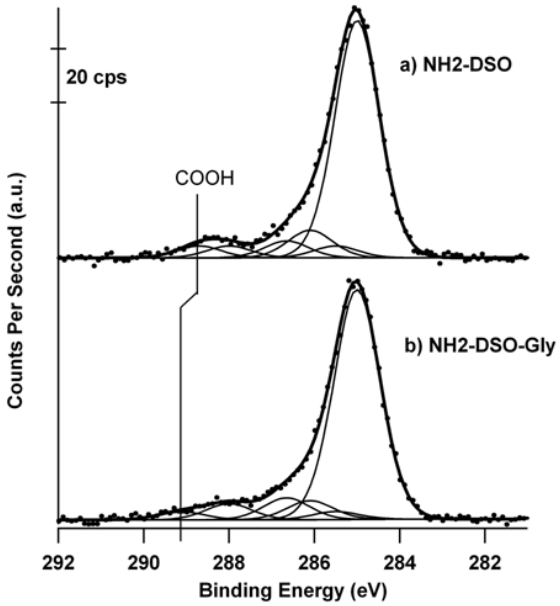

Figure 3.30: Evolution of C1s lineshapes for (a) NH_2-DSO surfaces and (b) NH_2-DSO-Gly.

286.6 eV and 289.1 eV). Using equation 3.10, the two values are both close to 46 %.

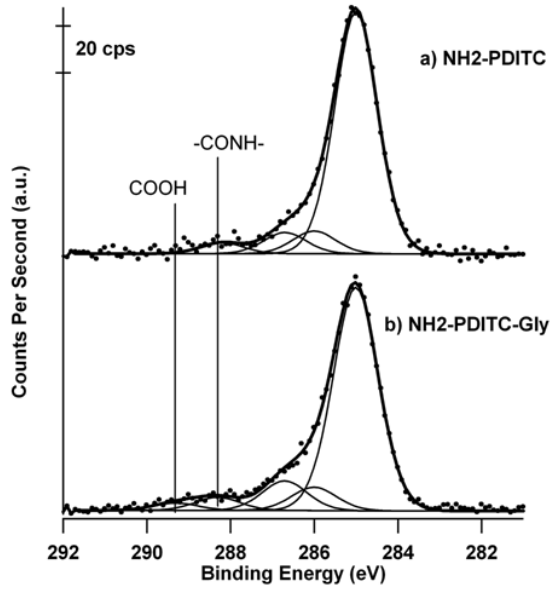

Figure 3.31: Evolution of C1s lineshapes for (a) NH_2-PDITC surfaces and (b) NH_2-PDITC-Gly.

All yields determined in this article are summarized in table 3.16. We can notice that PDITC and DSO linkers give very similar value, lower to 50 %. The reaction seems to be limited by the size of the glycine molecule and no difference can be made for the flexible or rigid linker. For glutaraldehyde, the yield attained hardly 30 % with the chemical

conditions used. This can be due to the structure of the glutaraldehyde layer, known to polymerize or, at least oligomerize, inducing bridging phenomenon between two amine groups of the surface or limited accessibility to the free aldehyde in the layer.

Table 3.16: Glycine grafting: yields obtained with three linkers (GAD, DSO, PDITC).

Linker	C1s component	grafting yield of glycine	remarks
GAD	C-N	29 %	Conversion of imine in secondary amine
	C-O	24 %	Specific signature of the central carbon of glycine
	C=O	36 %	Overestimated due to the possibility of reduction of aldehyde by $NaCNBH_3$
DSO	C-O	44 %	Specific signature of the central carbon of glycine
	C=O	42 %	Conversion of succinimidyl-group into amide
PDITC	C-O	46 %	Specific signature of the central carbon of glycine
	COOH	46 %	Specific signature of carboxylic group

Conclusion Going into details of high resolution peak fitting of C1s, we have estimated surface reaction yield as a function of three common linkers used for biomaterial modifications. The comparison between ideal stoichiometric ratio and area ratio determined by XPS allows the calculation of surface reaction yield. As expected, the surface reaction, in normal condition, is often limited by the vicinity of the surface. No differences have been made between rigid and flexible linker, the yield being limited in both case around 45 %. For glutaraldehyde, the yield was even lower (around 25 %) and this reduction is probably due to oligomerisation property of glutaraldehyde which give a complex structure, probably less accessible even for a small amino-acid like glycine. We believe that these informations are crucial when surfaces are put in contact with biological materials. If not controlled, chemical and structural heterogeneities, induced by limited reaction rates, will add errors to the intrinsic variability of biological experiment and can result in misinterpretation. The procedure described in this article allow precise quantification without chemical derivatization. Variable angle XPS analysis can, nevertheless, add supplementary informations to the knowledge of the structure layer and also give even more surface sensitive analysis.

Acknowledgment.
We thank Philippe Fioux for the XPS measurements and the Region Alsace for financial support.

References

(1) Mrksich, M. *ACS nano* **2008**, 2, 7-18.
(2) Ponche, A.; Ploux, L.; Anselme, K. *Journal of Adhesion Science and Technology* **2010**, 24, 2141-2164.
(3) Kasemo, *B. Materials Science* 451-459.
(4) Kim, J.; Cho, J.; Seidler, P. M.; Kurland, N. E.; Yadavalli, V. K. *Langmuir* **2010**, 26, 2599-608.
(5) Böhmler, J.; Ploux, L.; Ball, V.; Anselme, K.; Ponche, A. *The Journal of Physical Chemistry C* **2011**, 115.
(6) Libertino, S.; Scandurra, a; Aiello, V.; Giannazzo, F.; Sinatra, F.; Renis, M.; Fichera, M. *Applied Surface Science* **2007**, 253, 9116-9123.
(7) Davis, D. H.; Giannoulis, C. S.; Johnson, R. W.; Desai, T. a *Biomaterials* **2002**, 23, 4019-27.
(8) Schuler, M.; Owen, G. R.; Hamilton, D. W.; de Wild, M.; Textor, M.; Brunette, D. M.; Tosatti, S. G. P. *Biomaterials* **2006**, 27, 4003-15.
(9) Peelen, D.; Smith, L. M. *Langmuir 2005*, 21, 266-71.
(10) Senaratne, W.; Andruzzi, L.; Ober, C. K. *Biomacromolecules* **2005**, 6, 2427-48.
(11) Gooding, J. J.; Ciampi, S. *Chemical Society Reviews* **2011**, 40, 2704-2718.
(12) Sullivan, T. P.; Huck, W. T. S. *European Journal of Organic Chemistry* **2003**, 17-29.
(13) Heise, A.; Menzel, H.; Yim, H.; Foster, M. D.; Wieringa, R. H.; Schouten, A. J. *Langmuir* **1997**, 13, 723-728.
(14) Fryxell, G. E.; Rieke, P. C.; Wood, L. L.; Engelhard, M. H.; Williford, R. E.; Graff, G. L.; Campbell, A. A.; Wiacek, R. J.; Lee, L.; Halverson, A. *Langmuir 1996*, 12, 5064-5075.
(15) Wong, L. S.; Khan, F.; Micklefield, J. *Chemical reviews* **2009**, 109, 4025-53.
(16) Perlin, L.; MacNeil, S.; Rimmer, S. *Soft Matter* **2008**, 4, 2331.
(17) Perzyna, A.; Zotto, C. D.; Durand, J.-O.; Granier, M.; Smietana, M.; Melnyk, O.; Stará, I. G.; Starý, I.; Klepetárová, B.; Šaman, D. *European Journal of Organic Chemistry 2007*, **2007**, 4032-4037.
(18) Tucker-Schwartz, A. K.; Farrell, R. A.; Garrell, R. L. *Journal of the American Chemical Society* **2011**, 133, 11026-11029.
(19) Benters, R.; Niemeyer, C. M.; Wöhrle, D. *Chembiochem* **2001**, 2, 686-94.
(20) Libertino, S.; Giannazzo, F.; Aiello, V.; Scandurra, A.; Sinatra, F.; Renis, M.; Fichera, M. *Langmuir* **2008**, 24, 1965-72.
(21) Cottenye, N.; Teixeira, F.; Ponche, A.; Reiter, G.; Anselme, K.; Meier, W.; Ploux, L.; Vebert-Nardin, C. *Macromolecular Bioscience* **2008**, 8, 1161-1172.
(22) Dettin, M.; Herath, T.; Gambaretto, R.; Iucci, G.; Battocchio, C.; Bagno, A.; Ghezzo, F.; Di Bello, C.; Polzonetti, G.; Di Silvio, L. *Journal of biomedical materials research. Part A* **2009**, 91, 463-79.

(23) Powell, C. J.; Jablonski, A. *Journal of Electron Spectroscopy and Related Phenomena* **2010**, 178-179, 331-346.
(24) Margel, S.; Rembaum, A. *Macromolecules* **1980**, 13, 19-24.
(25) Xiao, S.-jun; Brunner, S.; Wieland, M. **2004**, 16508-16517.
(26) Caminade, A.-marie; Maraval, A. *Synthesis* **2006**, 901-914.
(27) Brzoska, J. B.; Azouz, I. B.; Rondelez, F. *Langmuir* **1994**, 10, 4367-4373.
(28) Natarajan, B.; Chaim N., S. *Langmuir* **1990**, 6, 1621-1627.

Supporting Information

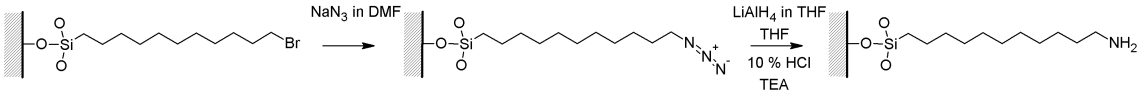

Figure 3.32: Chemical scheme of conversion of bromine surfaces into amine functionalized surfaces

Table 3.17: NH_2-GAD-glycine: yield of reaction.

b	$\frac{C-O/C=N}{CHx}$	$\frac{C=O}{CHx}$	$\frac{C-N}{CHx}$
NH_2-GAD	98 %	87 %	–
NH_2-GAD-Gly	24 %	36 %	29 %

3.8 Supplementary Information of Part 2

Amino acid grafting via Fmoc-glycine

Additionally to the used homobifunctional linkers GAD, DSO and PDITC (see article2b *"XPS evaluation of the influence of linker on the grafting yield of glycine on amino functional self assembled monolayers."*), one further experiment was carried out, in which the functional group COOH was activated before reaction with a NH_2 group. Therefore, the amine group of glycine was protected by reaction with Fmoc-OSu, followed by the activation of the COOH of glycine by HBTU. After reaction of the activated glycine with the NH_2 terminated substrate, the Fmoc protection group was suppressed by piperidine.

Preparation of Fmoc-glycine

In a first step, the amine group of glycine was protected by the Fmoc-protection group. The obtained Fmoc-glycine was purified by extraction in DCM. Given that the educt Fmoc-OSu is much more soluble in DCM than Fmoc-glycine, the educt and product could be separated. After the purification 1.15 g Fmoc-glycine were obtained, which is equivalent to a yield of 30 %. The Fmoc-glycine was analysed by H^1-NMR. The assignment of the protons of the product to the chemical shift is shown in figure 3.33:

δ=7.77 ppm; d; 2H; H; ^{3}J=7.6 Hz. δ=7.60 ppm; d; 2H; H; ^{3}J=7.6 Hz. δ=7.40 ppm; t; 2H; H; ^{3}J=7.6 Hz. δ=7.31 ppm; t; 2H; H; ^{3}J=7.6 Hz. δ=5.25 ppm; s large; 1H; NH. δ=4.43 ppm; d; 2H; CHCH_2OCO; ^{3}J=6.8 Hz. δ=4.24 ppm; t; 1H; $C_{aromat.}$CHCH_2; ^{3}J=6.8 Hz. δ=4.06 ppm; d; 2H; NHCH_2; ^{3}J=5.6 Hz.

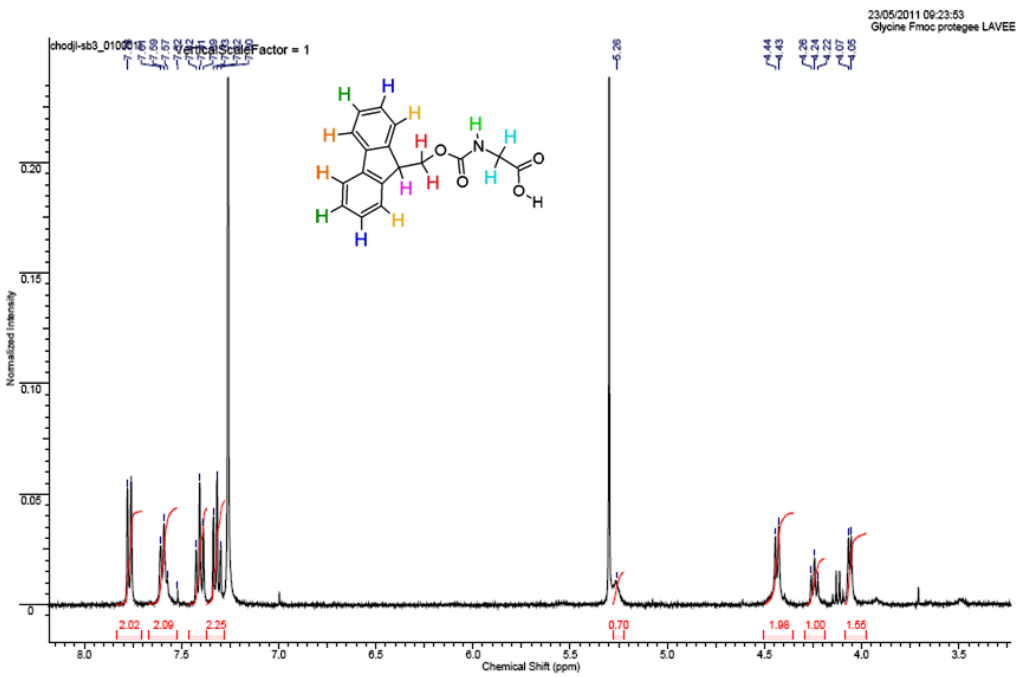

Figure 3.33: The shifts of the frequencies in the H^1-NMR spectra can be assigned to the different hydrogen environments.

3.8.0.0.1 Grafting of Fmoc glycine

The amino terminated substrates were immersed in 2500 equivalents (eq.) of Fmoc-glycine (C1) and afterwards deprotected. The samples were analyzed by XPS. Each step of the glycine grafting was evaluated by comparison of the ideal N1s/C1s ratio with the experimental one (see table 3.18).

Table 3.18: Reaction yield of glycine grafting

	ratio $\frac{N1s}{C1s}$ experimental	ratio $\frac{N1s}{C1s}$ ideal	yield [%]
NH_2-glycine-Fmoc	0.070	0.074	94
NH_2-glycine (C1)	0.067	0.154	43

After the grafting of Fmoc-glycine onto NH_2 functionalized substrate, the value of the N1s/C1s ratio should decrease, through the addition of 17 carbon atoms and only 1 nitrogen atom per grafted Fmoc-glycine. Indeed, the C1s peaks increases slightly compared to the substrate, while the nitrogen peaks decreases (see figure 3.34). Considering the ideal value of N1s/C1s ratio as a total grafting reaction of Fmoc-glycine, a yield of the reaction of 94 % was achieved. In the next step, the Fmoc protection group was removed, and hence 15 carbon atoms are suppressed. Consequently, the value of the N1s/C1s ratio is expected to increase. Finally the deprotection of glycine results in a reaction yield of 43 %.

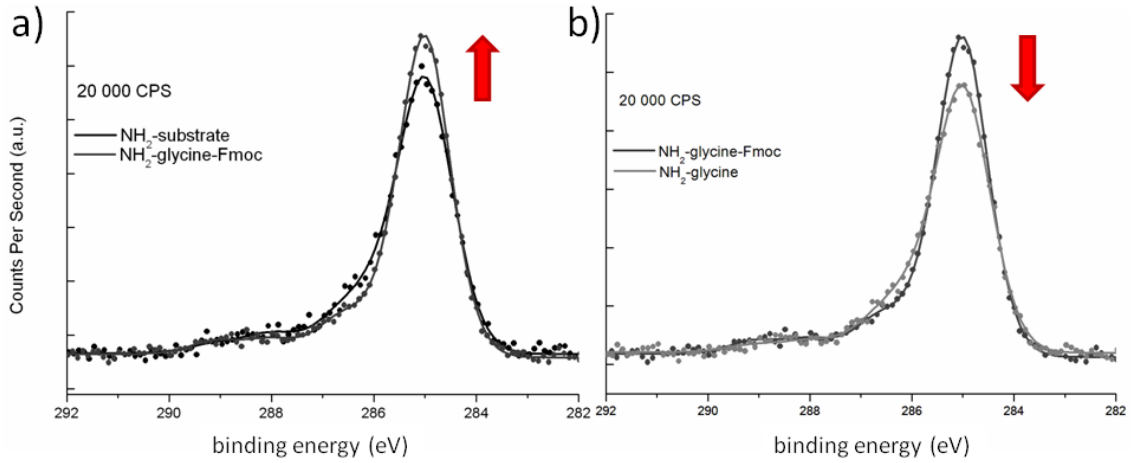

Figure 3.34: Surface modifications can be monitored by XPS. Here, attention was payed to the changing of the C1s signal after grafting of Fmoc-glycine onto the substrate (a) and after the deprotection of glycine (b).

In addition to XPS measurements, the final surface was characterized by AFM, ellipsometry and contact angle measurement. The AFM height contrast images show a flat and

homogeneous surface with few, very small aggregates on it (see figure 3.35). The presence of these aggregates is confirmed by the thickness of the surface, which increased of about 3.6 nm, while an increase of the thickness about 0.8 nm was expected. Further, the heterogeneity of the surface is indicated by the high hysteresis of $\Delta H = 57$, obtained by contact angle measurements.

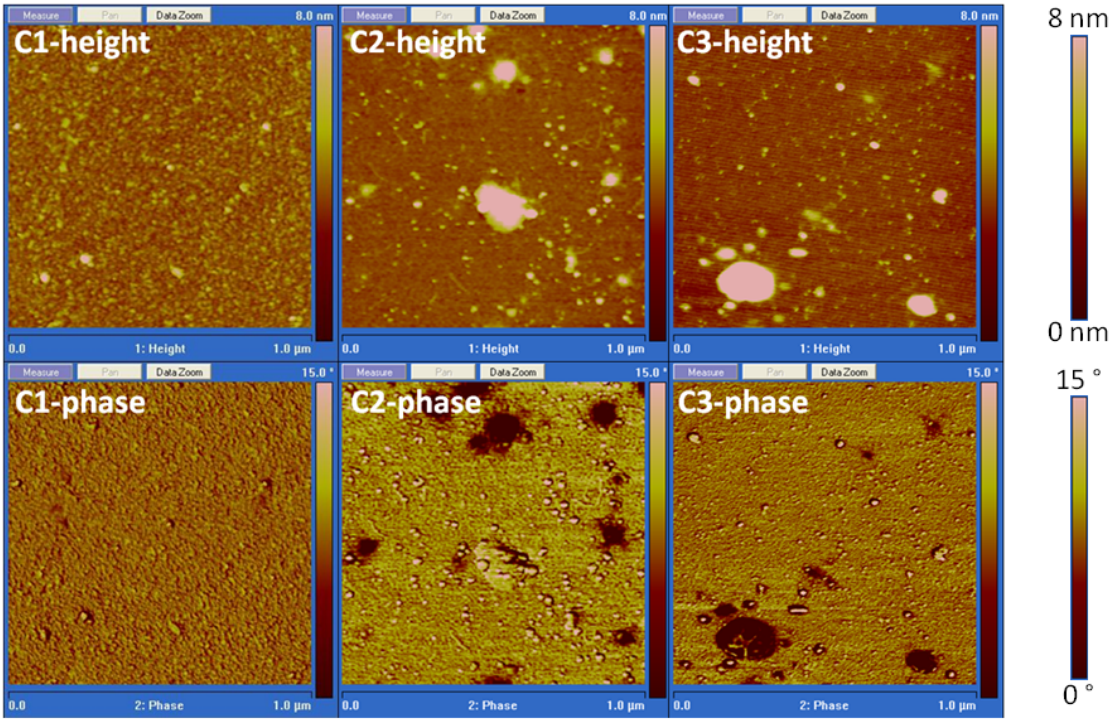

Figure 3.35: The AFM height and phase contrast images of the surfaces were analyzed. C1 (10 000 eq. Fmoc-glycine) shows almost no modification of the surface, only few small aggregates are visible. The AFM contrast images of C2 (2 500 eq. Fmoc-glycine) show several aggregates and different phase of the aggregates deposited on the surface. C3 (1 000 000 eq. Fmoc-glycine) contrast images are similar to the results of C2, there are some aggregates, with different phases.

Here it was found that a surface modification took place; aggregates are deposited on the surface which influence the topography, the contact angle and the thickness. Further, these aggregates seem to be the source of the additional carbon detected by XPS. Results are summarized in table 3.19. These aggregates may result of side reactions like polymerization, or crystallization of the used products.

Influence of the concentration

The concentration of Fmoc-glycine was increased to 10 000 eq. (C2) and 1 000 000 eq (C3), to increase the possibility of the glycine grafting. As before, the yield was estimated based on the N1s/C1s ratio obtained by XPS and the ideal ratio (N1s/C1s) for grafted glycine. The yields are slightly higher, with 47 % and 52 %, for 10 000 and 1 000 000 eq.

respectively, compared to the first reaction yield of 43 %.
Interestingly, with the increase of the Fmoc-glycine concentration, the thickness approaches the theoretical value of around 2.3 nm (see table 3.19). The hysteresis increases from $\Delta H = 33.3$ for the substrate up to $\Delta H = 48$ and for C2. Similar to C1, AFM height contrast images of C2 show several large aggregates on the substrate (see figure 3.35).
In contrast, for C3 a lower hysteresis $\Delta H = 42.1$ was obtained. By the increase of the concentration of Fmoc-glycine, a homogeneous surface modification was obtained.

Table 3.19: Grafting of Fmoc-glycine.

Condition	equivalent Fmoc-gly.	$\frac{N1s}{C1s}$	yield [%]	θ_s [°]	θ_a [°]	θ_r [°]	thickness [nm]
NH_2-substrate				65 ± 2	77 ± 1	44 ± 1	1.4 ± 0
C1	2500	0.067	43	73 ± 2	83 ± 3	20 ± 2	5.1 ± 1
C2	10000	0.081	47	69 ± 1	81 ± 5	33 ± 1	3.6 ± 3
C3	1000000	0.073	52	73 ± 2	83 ± 1	41 ± 0	2.4 ± 0
theoretical		0.154	100	–	–	–	2.3
C3-blind	0	0.080		75 ± 2	85 ± 1	41 ± 1	2.3 ± 1

Side reactions
The substrate was immersed under the conditions of C1 and C3 (see table 3.4 in Material and Methods), but without Fmoc-glycine, called C1-blind and C3-blind respectively, to investigate possible side reactions. After analyzing the sample C1-blind, the surface showed no change of chemical composition. In contrast, the ratio N1s/C1s increased from 0.065 for the NH_2 substrate up to 0.08 for C3-blind and the ratio of N1s/SiO_2 increases from 0.15 (substrate) up to 0.26. Similarly, the C1s/SiO_2 ratio increased from 2.4 up to 3.2. Consequently, carbon and nitrogen components were deposited on the amino terminated substrate. Nevertheless, the profile of C1s was the same, except for the intensity (see figure 3.36 a). In contrast, the N1s spectrum of C3-blind (figure 3.36 b) indicates positively charged nitrogen at a binding energy of 402.5 eV.

A possible side reaction is the reaction of HBTU with an amine group, which results in a tetramethylguanidine [161]. This side reaction could explain the increase of the area of the nitrogen component and the carbon component on the substrate. Nevertheless, on the N1s high resolution spectra the new component at 402.5 eV is higher than expected for a N^+, which usually is assigned to a binding energy of 401.8 eV. Besides the XPS analysis,

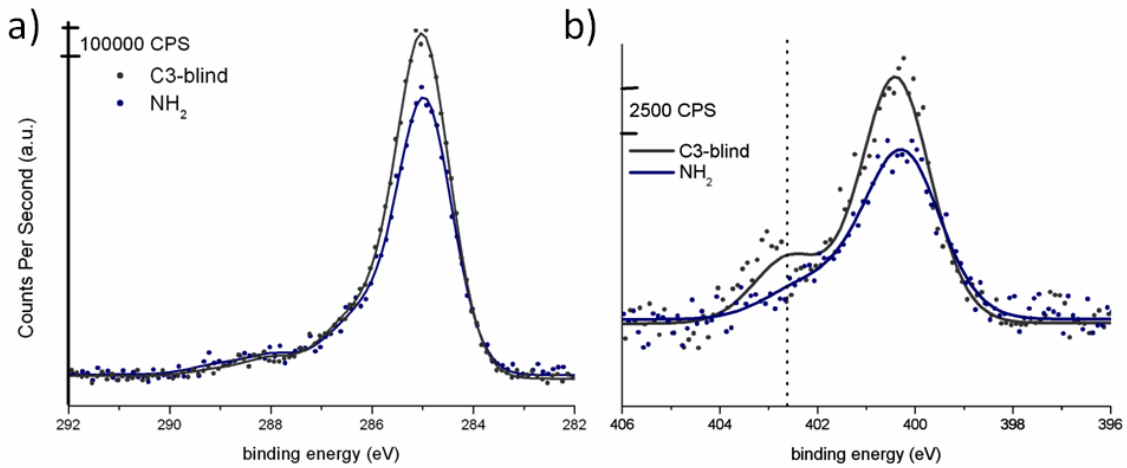

Figure 3.36: The profile of C1s (a) and N1s (b) high resolution spectra changed after immersion in solution of C3. (a) shows the same profile, hence the interpretation of a new surface modification is difficult. (b) shows the N1s spectra with a new component at 402.5 eV that appeared, which indicates that a surface modification took place.

the static and advancing contact angles and the thickness increased slightly compared to the substrate.

3.9 Conclusion

The aim of this chapter was to create well-controlled surfaces that can be used as substrates for the immobilization of biomolecules and for biointerface studies.
As showed in the chapter before, amine terminated silanes were used to establish the thoroughly characterization of SAMs on silicon wafer. The thorough surface characterization and analysis demonstrated that amine terminated silanes in the used conditions lead to surfaces, which are not controlled. Consequently, a different types of silane was used to obtain well-controlled amine-terminated surfaces. This silane contains a bromine termination, hence does not interact with silanol groups of the substrate and the other silanes, it is also slightly longer, compared to AHAPS and contains 11 carbon atoms (instead of 9 for AHAPS). Through the longer chain, the Van der Waals forces and consequently the probability of an organized overlayer increases. Moreover, the bromine terminus hold the possibility to react in a nucleophilic substitution reaction, in order to obtain an amine terminus.
The preparation of the bromine-silane base monolayers was based on literature that reported layers made of this silane; however without proving the monolayer structure and the well organization of silane. Various parameters as the solvent, the temperature and the reaction time were adapted to achieve optimal silane grafted and the assembling on the silicon wafer. An annealing step was used to stabilize the overlayer and therefore to provide adequate substrates for biointerfaces studies, which are performed in liquid conditions.
Finally, a protocol was defined that leads to well controlled bromine monolayers, using a mixture of two solvents, a reaction time of 4 h and a reaction temperature of 6 °C. In the following process, the bromine terminus was successfully converted into an azide and subsequently into an amine terminus. Hence, amino terminated well-controlled surface (100 %NH_2) was obtained, which led to ideal amino-terminated surfaces, on the contrary to APTES and AHAPS surfaces. The fact that APTES and AHAPS are less organized, was used to investigate the impact of the organization of theoretically "ideal" substrate (amino terminated SAMs) on bacterial adhesion. The results of the bacterial adhesion experiments shows that there is a significant impact of the organization of the substrate. The reproducibility increasing with the quality of the substrate organization, i.e. the chemical "purity" of the overlayer showing that bacterial adhesion is sensible to subtle chemical heterogeneities of the surface.

Furthermore, mixed monolayers were obtained by the use of a second silane with methyl termination. Different concentrations of bromine on the surfaces, backfilled with methyl groups, were achieved by the immersion of the substrate in a solution containing adequate ratios of the two silanes. The successful fabrication of the mixed monolayers was mainly confirmed by XPS, ellipsometry and contact angle measurements. Further, the characterization by height and phase contrast AFM imaging showed no islanding of one silane in the other.

In the next step the bromine/methyl mixed monolayer were transformed into amine/methyl mixed monolayers. XPS measurements showed the increase and decrease of the nitrogen signal according to the percentage of amine terminated silane, i.e. the bromine terminated silane. Furthermore, it could be verified that, as expected, the relationship between the contact angle and the amount of nitrogen follows the Israelachvili equation.

In conclusion, well-controlled amine/methyl mixed monolayer were obtained, which were used as substrates for bacterial adhesion investigations. These investigations will be described in the following chapter.

Aiming at investigating the possibility to use such surfaces to prepare biomolecule-revealing model surfaces of different densities, we studied the grafting efficiency of amino acid (glycine) on well-controlled amine monolayer. Thereby, 100 %NH_2 terminated monolayers were used as substrates, prepared as previously described. Different ways were attempted to achieve a high concentration of glycine grafted onto surfaces. At first three homobifunctional linker (GAD, DSO and PDITC) were used to graft the amino acid on the substrate. The yield of the grafting evaluated by XPS measurements was similar for the three homobifunctional linkers with 30-46 %. However, the linkers themselves are quite different. This shows that, on a fully covered surface with NH_2 groups in close contact, it is not possible to graft one glycine for one NH_2 group. Another possibility of grafting, without the use of any linker was investigated (in collaboration with Delphine Josien). In this process, the grafting protocol was adapted to graft an amino acid onto a solid substrate. A reaction yield around 47 % was obtained. Moreover, several coupling reagents were shown to react with the surface, leading to uncontrolled grafting of amino acids. Finally, the four strategies tested, failed to achieve a yield of grafting higher than 50 %. The expected consequence for achieving mixed monolayers revealing different densities of amino acid is the restriction of the range of coverage that will be possible to reach. Nevertheless, optimizing of the amino acid grafting protocol may allow to improve the loading capacity of the subtrate with amino acid.

In addition, it was demonstrated that the grafting of an amino acid could be monitored and evaluated by thorough analysis of each step by XPS.

Chapter 4

Bacterial response to well controlled model surfaces

4.1 Introduction

This chapter aims at investigating bacterial behavior resulting from chemical surface properties existing at the nano- and molecular-scale. It is separated in two parts. The first part deals with the ability of bacteria to, actively or not, differentiate surfaces, according to subtle and neglected differences in their chemistry. For that purpose, the well-controlled mixed monolayers (MMLs) from the third chapter are used to analyze the bacterial adhesion and hence the possible ability of bacteria to distinguish between the surfaces, containing different densities of NH_2 backfilled with CH_3. The second part of this chapter deals with the ability of bacteria to sense and/or response specifically to these surfaces by expressing different genes, thus with the change of their metabolism. Two different bacteria strain, the gram-negative *E. coli* and gram-positive *S. epidermidis*, which both cause serious health problems, were used. Aside from the differences in their envelope, structure and composition *E. coli* is rod shaped and quite mobile due to appendages on its membrane. In contrast, the *S. epidermidis* strain is coccus shaped and known for the production of the polysaccharide intercellular adhesion (PIA), which has been recognized as a virulence factor.
For all microbiological experiments conducted in this work, MMLs with different densities of NH_2 backfilled with CH_3 were used as substrate. Since the substrates have been thoroughly characterized and are fairly smooth, topographical and other uncontrolled features of the surface are minimized. "Gradients" of mixed functionalities were achieved over several surfaces (see figure 3.3) which allows to study the accessibility of a functional group without coupling another surface property.

The first part of the chapter consistes in bacterial adhesion experiments that were conducted in batch and real-time experiments for a short incubation time (2 h) (see figure 4.1 step 1). Experiments were done in simple and well-defined saline solution (9g/L NaCl) to

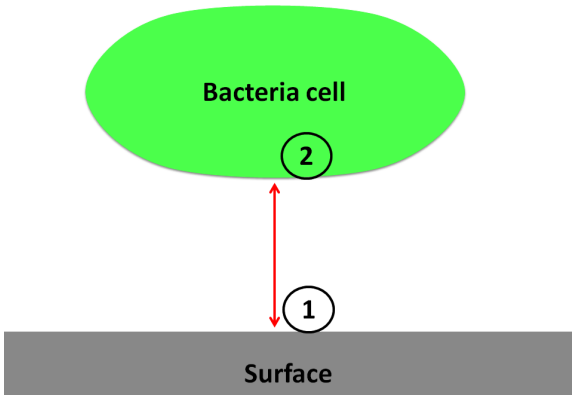

Figure 4.1: The first part of the chapter deals with interactions between the surface and bacteria (1). In the second part, the changes of the metabolism resulting from adhesion were investigated (2).

limit unknown influence of surrounding parameters. Nevertheless, batch experiments with *E.coli* SCC1 were also performed in the minimal media M63G-B1 to investigate potential modifications of bacterial behavior coming from surroundings. For real-time experiments on non-transparency materials, an upright confocal laser scanning microscope (CLSM) allowing fluorescent and reflexion examination was used as well as flow cell and protocol specifically developed for that purpose. For both batch and real-time experimental conditions bacterial adhesion and proliferation analyses were either in fluorescence or in reflexion mode according to the bacteria species. Plot of numbers of adherent bacteria on the surface, versus the amount of NH_2 of the surface provided, bacterial adhesion rate and proliferation rate were used as indicators of the bacterial behavior on the surface.

In the second part of this chapter, investigation of the metabolism of bacteria and its change depending on the surfaces on which they adhere were aimed to visualize (see figure 4.1 step 2). However, the study of changes in the metabolism, which is influenced by the surface was and remains quite challenging. In this work, RT-PCR was used to investigate the expression of *icaA* and *icaD*, two genes that are involved in the production of PIA and in the biofilm formation of *S. epidermidis* [162]. In parallel, the results of the RT-PCR were confirmed by CLSM observation after bacteria and PIA fluorescent staining. A second approach based on staining of membrane proteins and analysis of these proteins in a 2D gel-electrophoresis was envisaged, aiming at determining changes in the bacterial membrane proteins as an indicator of the capacity of a bacterium to sense subtle properties of the surface. The number of adherent bacteria in bacterial adhesion experiments is usually rather low. Consequently, the material of protein or nucleic acids, which can be used to examine bacterial metabolism in response to the surface, is low. This leads to difficulty or even impossibility to extract suitable experimental data from proteomic and genomic techniques. Thus, difficult adaptions were needed to be within the detection range of the used characterization techniques.

The chapter is separated in two parts. The microbiology results of the first part are mainly given in form of an article *"The role of chemical heterogeneities of surfaces in the adhesion and proliferation of bacteria"*. Additional results of this part are given in Supplementary Information. The second part is written in a classical form with a Results and Discussion section.

4.2 State of the art

4.2.1 Biofilm

A biofilm is a structured community of sessile (attached) bacteria on a surface, enclosed in a self-polymeric matrix [1]. The advantage of biofilm formation for bacteria is their protection against several external stresses, as antibiotics, changes in temperature, dehydration or detergents [1, 3]. Further, the matrix of the biofilm stores nutriments and is able to restrict the diffusion of molecules within the biofilm. The biofilm is therefore highly favorable for the survival of bacteria in hostile media. Various factors are involved in the biofilm formation, like the cell wall properties [3, 163] and external conditions, like temperature, pH, shear stresses etc. [7–9]. Diverse macromolecules on the bacteria surface can interact with the material surface and with other bacteria cells. Such macromolecules are generally lectins [164, 165], flagella [166–168], pili [51, 54, 164, 169, 170], other fimbriae, and proteins [171] and polysaccharides [172–174] (see paragraph 4.2.1.3). Among them, material properties have been recognized to play an important role [3]. Material properties i.e. the topography and the surface chemistry, are known to influence bacterial adhesion. Several articles are published in literature, addressing the impact of surface topography on bacterial adhesion, as reviewed in reference [3]. Bacteria adhere for example, on surfaces with topographical features, rather on the bottom than of the top such features [175]. A higher number of bacteria colonies was found on site with surfaces defects [176–178]. Further, bacterial adhesion seems, most likely to be influenced by specific functional groups on the surface, hydrophobic or hydrophilic surface character, surface energy and surface charge. Functional groups can lead to receptor/ligand interactions between bacteria and the surface [3]. Bacterial adhesion studies on hydrophilic/hydrophobic surfaces lead to controversial results (see paragraph 4.2.2) [3, 13, 14, 19, 163, 179, 180]. Aside from functional groups and the wettability character of the surface, the surface energy and the surface charge were studied. It is assumed that the surface charge plays an important role due to attractive or repulsive attractions, by the mainly negatively charged bacterial envelope (at physiological pH) and charged surfaces (see paragraph 4.2.2) [47, 78, 181]. Finally, the surface free energy was considered in the process of bacterial adhesion. However, no obvious relationship appeared between the bacterial adhesion and the surface free energy [20, 48, 182–184], which may due to the envelope of bacteria that is rarely considered [3].

4.2.1.1 Formation of a biofilm

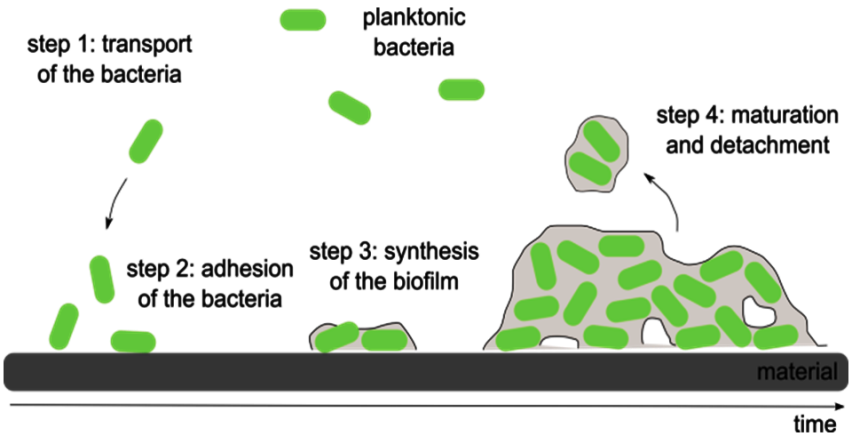

Figure 4.2: The biofilm formation consists in four steps, that may more or less overlap depending on bacteria species and external conditions. At first, planktonic bacteria are transported close to the surface, with which they interact in the second step. Finally, the bacteria irreversibly adhere on the surface and build up a 3D structure by proliferating and starting to produce exopolysaccharide substances. This biofilm matures, some bacteria detach from the biofilm and are transported as planktonic bacteria to other regions. (Illustration from Ploux *et al.* [3])

The formation of biofilm can be described in 4 steps, as depicted in figure 4.2. The steps may more or less overlap each other.

Step 1: Bacteria transport near the surface

In the first step, bacteria are passively and/or actively transported to the living or abiotic surface [185]. In the passive transport, long-range forces like gravitational or brownian forces play an important role. In addition, hydrodynamic forces, when present, take part in the transport. In the active transport, depending on species and strains, proteinic organelles like flagella are involved [3].

Step 2: Adhesion of bacteria on the surface

The adhesion of bacteria consists in two separate stages. First, bacteria reversibly attached to the surface before they irreversibly adhere to the surface. Different physico-chemical interactions between the surface and bacteria are involved in these two stages [3, 185] (see paragraph 4.2.2 for more details) as well as diverse cell surface structures according to bacteria species and strains [163]. Interestingly, after sensing the surface during the initial adhesion phase, the expression of specific genes can be switched on governing for example the synthesis of fimbriae involved in the bacterial attachment to surface [50, 53, 54] or of the biofilm matrix [1, 186, 187].

Step 3: Synthesis of matrix and proliferation

In the third step, adherent bacteria start to proliferate and to synthesize a matrix that mainly consists of exopolysaccharide substances (EPS) [188–190]. Sessile bacteria are then embedded in a 3D matrix forming the biofilm [1]. Appendages, like flagella and fimbriae, pili, curli are assumed to also play a crucial role in this step [3].

Step 4: Maturation of the biofilm and detachment
Biofilm has a complex structure with pores and channels for the nutrition transport [3, 185]. These characteristics evolve with the time and external conditions. Within the biofilm, bacteria communicate with each other via chemical and electrical signals. Gene expressions of sessile bacteria in a biofilm and of planktonic bacteria can significantly differ. For example, 38 % of the genes are differently expressed in *E.coli* biofilms compared to planktonic state [54]. Mature biofilms are known to grow up to a certain point, at which bacteria that are farest from the surface and nearest from the surrounding escape from the biofilm. These newly planktonic cells become able to colonize other surfaces [185].

4.2.1.2 The envelope of bacteria

The outermost cell surface plays a crucial role in bacterial adhesion, since it constitutes the direct contact with material surfaces. Its chemical composition and structural arrangement surface is extremely complex due to the presence of a large variety of chemical components and surface appendages of different lengths [12, 191].
Bacteria can be separated in two different groups due to their envelope structure: gram-positive and gram-negative bacteria, distinguished by the gram-staining. As depicted in figure 4.3, the composition of the cell wall of Gram-positive and Gram-negative bacterial differs considerably. On top of the cytoplasmic membrane, gram-positive bacteria have a thick and rigid peptidoglycan layer, whose density varies throughout the layer within 20 % [191, 192]. In contrast, the peptidoglycane layer of gram-negative bacteria is much thinner and sandwiched between two phospholipid membranes, i.e. the inner and outer membrane. The outer membrane contains aggregated proteins, which form pores of various types [193,194] to facilitate the transport of molecules through the membrane. A characteristic component of the outer membrane of gram-negative bacteria, is the lipopolysaccharide (LPS). LPSs contain mainly saturated fatty acids, which are linked to a glucosamine disaccharide backbone. On this backbone and on sugar residues many negatively charged groups are present [193]. LPS was also found to bind divalent cations. Furthermore, the physical structure of LPS depends on the nature of such cations [193, 195, 196].
Bacterial cell surface is highly complex and differs strongly from surfaces of non-biological colloids, such as polystyrene particles [192]. Therefore, description of bacteria surface properties through global values of charge, hydrophobicity/hydrophilicity etc. must be carefully considered. However, some general trends can be stated: (i) The bacterial surface is charged due to the dissociation and protonation of several functional groups contained in polysaccharides, proteins, peptidoglycan, teichoic acids and phospholipids on the cell envelope, such as carboxyl, phosphate and amine groups. At a physiological pH (pH $\sim$7) most bacteria are negatively charged, as the number of carboxyl and phosphate groups exceeds the number of amine groups [192]. (ii) The hydrophobicity of bacterial cell wall varies according to the bacteria species, and is influenced by the growth medium and the age and the surface structure of the bacteria [163]. (iii) The stiffness and the thickness of the cell

envelope can significantly change with environment conditions, like the pH [197–199].

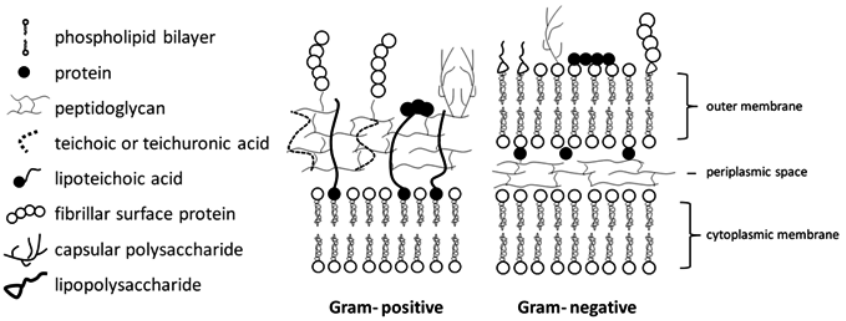

Figure 4.3: Schematic model of the surface of gram-negative bacteria (like *E. coli*) and gram-positive bacteria (like *S. epidermidis*) adapted from reference [192].

4.2.1.3 Factors involved in biofilm formation

It is assumed that several membrane-anchored or extracellular, macromolecules produced by bacteria (for example their flagella, pili and other fimbriae or exopolysaccharide), play an important role in the motility, the attachment of bacteria on the surface and the biofilm formation [3, 200].
Pili, also named fimbriae, are filamentous appendages on the bacterial surfaces, which are often no more than 4 to 7 nm in diameter and 0.2 up to 20 nm in length [163]. These pili are rigid, straight and of a polymer nature. They are composed by identical subunits [201]. From 100 up to 1000 pili may be present on the outer surface of the outer membrane and may reach considerable distances beyond the outer membrane. They are most prominent in gram-negative bacteria [163], as *E. coli*. As example, in *E. coli*, the most common and well studied fimbriae is called Type I pili/fimbriae, which is long and rod-shaped [200]. Physical interactions between Type I fimbriae and a solid surface have been shown to lead to structural changes in the outer membranes of attached *E. coli*, which is reflected by the reduction in the expression level of outer membrane proteins [51, 200]. The adhesion mediated by fimbriae has been proposed to vary with the hydrophobicity of the substrate, due to the increase of the hydrophobicity of the envelope of fimbriaeted bacteria [202].

Beside fimbriae, other heteropolymeric, filamentous appendages like curli are also able to influence the adherence properties of several biofilm-forming *E. coli* strains [203]. Curli were shown to be involved in bacteria-surface interactions [204]. They are involved in irreversible attachment, formation of microcolonies, early development of the biofilm architecture and maturation of the biofilm [200].
Beside the extracellular slime, composed of EPS and that were shown to favor the attachment of some species of bacteria [163,205] (see next section), some species possess capsules outside of the cell wall, which may also favor adhesion to abiotic surfaces. They can exist

in gram-negative and gram-positive bacteria [163]. Capsules consist of firmly adherent and discrete covering layer and that depending on its properties, changes the hydrophobicity of the bacteria surfaces [163].

4.2.1.4 Excursus: The role of PIA in *S. epidermidis* biofilm formation

By investigation of *S. epidermidis* strains, which caused several serious infections on catheters in the 80ths, a slime layer was identified by staining with alcian blue. This material was assumed to be a polysaccharide [206]. Since then, many different saccharides that are involved in the biofilm formation of *S. epidermidis* were discovered (reviewed in [185]).

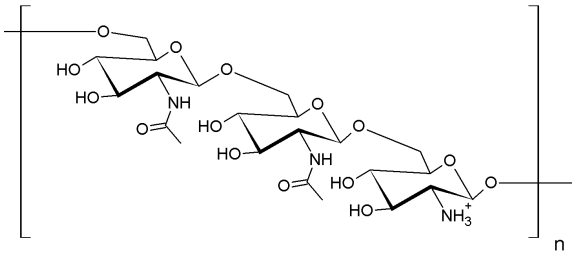

Figure 4.4: PIA is a linear homoglycan. It is composed of β-1,6-linked N-acetyl-glucosamine residues. Around 20 % of the residues are deacetylated and hence positively charged. Illustration adapted from reference [207].

Among them, one exopolysaccharide is important for the formation of cellular aggregates and is a virulence factor in the pathogenesis of foreign body infection: the **p**olysaccharide **i**ntercellular **a**dhesin (PIA) [162]. PIA is a linear β 1-6 N-acetyl-D-glucosaminylglycan, depicted in figure 4.4, which is expressed by the *icaADBC* operon [207]. The *ica* operon is depicted in figure 4.5.

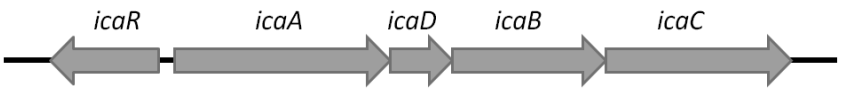

Figure 4.5: The synthesis of PIA is expressed by the genes of the *ica* operon in *S. epidermidis*. *icaADBC* are regulated by *icaR* and result in PIA. For the RT-PCR, the expression of *icaAD* was examined, *icaAD* are usually coexpressed when PIA is produced [207].

icaA and *icaD* are coexpressed, since *icaA* is responsible for a transmembrane protein that requires the product of *icaD* for its optimal activity. The products of *icaA* and *icaD* are N-acetyl-glucosamine oligomers, which reach a maximal length when they are coexpressed with *icaC*. Finally, IcaB is attached to the surfaces and is responsible for the deacetylation

of the poly-N-acetylglucosamine molecule [208, 209]. The role of the formation of cell aggregates, depicted in figure 4.6 was also demonstrated by Dunne *et al.* [185].

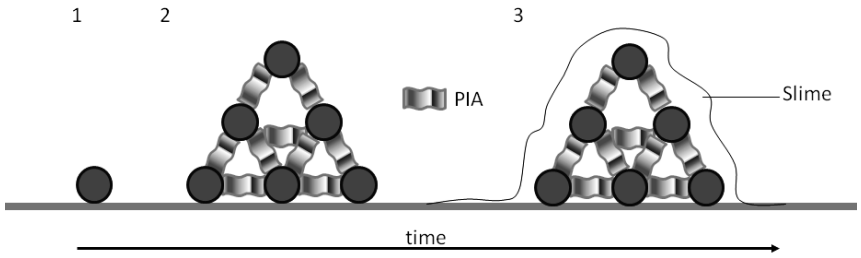

Figure 4.6: The cell aggregation of *S. epidermidis* is promoted by the exopolysaccharide PIA. Hence, the biofilm formation of *S. epidermidis* is generally described in 3 steps: 1. The bacterial adhesion; 2. The accumulation of cells, promoted by PIA; and 3. the synthesis of another slimy exopolysaccharide. Adapted from reference [185].

4.2.2 Bacterial adhesion

Bacterial adhesion depends on the physico-chemical properties of the material and bacterial surfaces. The typical attractive interaction leading to the reversible adhesion mainly results from the balance between repulsive and attractive, electrostatic, van der Waals and hydrophobic/hydrophilic interactions (see figure 4.7) [3].

In general, it is assumed that, the bacteria with hydrophobic properties prefer to adhere on hydrophobic materials and bacteria with hydrophilic properties prefer hydrophilic materials. Additionally, the amount of adhered bacteria is higher on hydrophobic surfaces than on hydrophilic ones [163]. Aside from the wettability character of the cell envelope and the material surface, their charges are also considered to be important for the interaction with material surface. As already evoked in paragraph 4.2.1.2 most bacteria are negatively charged at physiological pH (pH$\sim$7). Bacterial surface charge can be assessed by isoelectric point, zeta potential and electrophoretic mobility [163]. Importantly, whatever their charges, bacterial and material surfaces are frequently ionized in aqueous systems. Therefore they attract dissolved ions, resulting in a charged double layer at the surfaces, which is expected to highly impact the bacteria/material interface [192].

4.2.2.1 Theories to describe bacterial adhesion

Two theories are reported in literature to attempt to describe the adhesion of a bacterium to the surface: the thermodynamic theory and the DLVO-based theory [205].

Bacterial adhesion based on thermodynamic theory

The thermodynamic theory describes the approach of two surfaces, resulting in adhesive

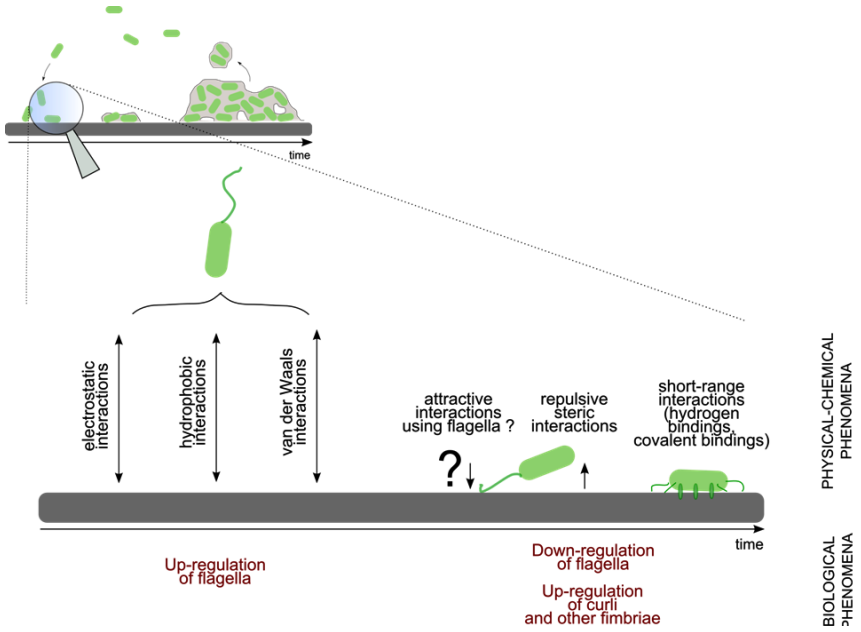

Figure 4.7: The adhesion of bacteria is imprinted by different long and short distance interactions between the bacteria cell and the surface. (Illustration from Ploux *et al.* [3]).

molecular interaction, in which adsorbed water must be displaced. If the surface is highly hydrated, such water displacement is energetically unfavorable and may be impossible to overcome by counteracting attractive interactions [48]. The thermodynamic theory is based on the surface free energy of the solid-bacteria, the bacteria-liquid, and the solid-liquid interface. Briefly, the bacterial adhesion is favored if the free energy is negative [205].

DLVO based theory of bacterial adhesion

The DLVO (Derjaguin-Landau-Verwey-Overbeek) theory describes the interaction between a particle and a surface, since bacteria and particles are frequently assumed to behave similar, due to their comparable size. The total interaction is then calculated by the sum of the Van der Waals forces and Coulomb interactions [205,210]. In case the particle is close to the surface, the Van der Waals forces are predominant, while when increasing the distances between particles and surface, the Coulomb interactions becomes predominant. In solution, ion double layers are commonly formed on charged surfaces and particles, i.e. bacteria that are mainly negatively charged at physiological pH. Hence, a repulsive electrostatic energy is caused by the overlap of the electrical double layer of bacteria and the substrate [205,211–214].

In the process of bacterial adhesion, bacterium approaches the surface by its motility or brownian motion and adheres first reversibly. Adherent bacteria can now overcome the energy barrier by a linkage through nanofibers (e.g. pili and flagella) or EPS between bacteria and surface (irreversible attachment). Thereby, the ionic strength of the solution and the distance between bacteria/particle are crucial parameters for a successful adhesion of the bacteria/particle on the surface [205].

In summary: The adhesion behavior of bacteria on surfaces is also often described by the DLVO theory [215], the extended DLVO theory [216] or the extended DLVO theory with steric effects [214]. The DLVO theory is based on the Van der Waals and electrostatic interactions of colloids, while the extended DLVO considers such hydrophobic/hydrophilic and osmotic interactions, as in the thermodynamic theory [205,216]. The extended DLVO theory with steric effects considers the steric repulsions between bacteria and surface [3, 192].

The main limitation of theories to describe bacterial adhesion is common to thermodynamic and DLVO theories. In both cases, bacteria are highly simplified. Bacteria are regarded as particles, but they are not always spherical as assumed for particles [3]. On the contrary, the real envelope of bacteria is elastic and porous and may change in terms of its protein composition [193]. Bacteria cells have also various appendages, like pili, curli, etc. as described above, which may specifically interact with the surface and are responsible for bacterial movements. Further, the cell shape varies depending on bacteria species and strains. Another issue, results from the bacteria stereotypes that are used in theories and does not consider the capability of bacteria to sense the surface and to change their metabolism, like for example the composition of their envelope, in response to this surface [217]. These specific modifications are still not fully understood and, hence, can hardly be described in the theory of bacterial adhesion.

Finally, the thermodynamic theory assumes only reversible adhesion that however, is rarely the case [205]. Nevertheless, this approach helps to explain the previously described observation that: Bacteria with hydrophobic surface character prefer to adhere on surfaces with also hydrophobic character, while bacteria with a hydrophilic surface character adhere preferentially on surfaces with hydrophilic character [163,205].
The extended DLVO-theory seems to predict better the bacterial adhesion, which is based on strong acid-base interactions than the classical DLVO-theory [205].

4.2.2.2 Impact of surface chemistry on bacterial adhesion

Aside from surface topographical features, surface chemistry is the most frequent topic of articles concerning bacterial adhesion. The three following topics are mainly addressed: the wettability of the surfaces [12,14,19,49,180,218–220], the charge of the surface [11,47] and more generally the influence of chemistry [10,13,18,20,48,221].

It is assumed that the attachment of bacteria is influenced by the hydrophobicity/hydrophilicity and the surface charge of the substrate, beside the impact of bacterial characteristics, as previously addressed in paragraph 4.2.1.2, which is also affected by ionic strength and pH [221]. These influences have been recently extensively reviewed in literature [163]. Briefly, it was found that hydrophilic materials might be more resistant to bacterial adhesion than hydrophobic ones [10,14,163]. Wiencek and Fletcher used mixed

monolayers (OH backfilled with CH_3) to study the effect of various substrate wettability on bacterial adhesion [10, 49]. Observation showed that with the increase of the hydrophobic character of a substrate, the initial bacterial adhesion rate and the net number of adherent bacteria also increased, while the attachment/detachment rate decreased. They concluded from their results that the detachment rate rather than the attachment rate determines the net number of adherent bacteria, suggesting that interfacial forces, which are responsible for the initial binding of bacteria are greater on hydrophilic than on hydrophobic surfaces. Hence, more bacteria changes from reversible to irreversible adhesion with the increase in CH_3-groups on the surface. Interestingly, they also suggested but did not amplify the possibility that OH terminated surfaces have only a limited number of attachment sites that influence the number of attached bacteria [10, 49]. While Wiencek and Fletcher studied one bacterial strain on different surfaces [10, 49], Cerca *et al.* investigated the bacterial adhesion of several *S. epidermidis* strains on one hydrophilic and one hydrophobic substrate [14]. Most of the bacteria strains adhered preferentially on the hydrophobic substrate than on the hydrophilic one. However, they observed no correlation between the bacteria hydrophibicity and the extent of the initial binding to either hydrophilic or hydrophobic substrate [14]. Other studies, which considered the impact of the wettability revealed that the surface energy on bacterial adhesion is conflicting [13, 19, 48]. For example, Katiskogianni and Missirlis studied the bacterial adhesion of two *S. epidermidis* stains on mainly CH_3, NH_2 and OH terminated surfaces with different ionic strengths and different shear rates [48]. Both bacteria strains showed the same adhesion tendency, i.e. most bacteria adhered on $CH_3 > NH_2 >$ OH terminated surfaces. They suggested that the enhanced bacterial adhesion on CH_3 and NH_2 terminated surfaces is due to the increase of the ionic strength and hence the minimization of repulsive electrostatic interactions. They concluded that zeta potential and electron donor properties of the material influences bacterial adhesion [48]. Moreover, they compared the results of bacterial adhesion with the predictions of the thermodynamic theory, the DLVO and the XDLVO theory. They found that the DLVO and XDLVO were more adequate to predict bacterial adhesion results under low ionic strengths than the thermodynamic theory. Furthermore, the XDLVO described, the adhesion results, obtained under higher ionic strength better than the DLVO theory, because the surface chemistry and the ionic strength are encountered in the XDLVO theory [48]. In contrast, Tegoulia *at el.* observed no differences in the bacterial attachment on CH_3, COOH and OH terminated surfaces under low shear rates [13]. However, under high shear rates, the bacteria adhered the most on CH_3 terminated surfaces, then on the negatively charged COOH and the least on the OH terminated surface. They expected repulsive interactions between the negatively charged *S. aureus* and the negatively charged COO^- (at physiological pH) surfaces, which was however, not observed. The hydrophobic CH_3 surface was more preferable than the hydrophilic OH surface [13].

Some studies investigated the surface properties and their influence on the mobility of bacteria [19] and the morphology of the formed biofilm [16]. Ploux *et al.* demonstrated that the number of attached bacteria on NH_2 and CH_3 terminated surfaces are similar

after 4 h of incubation. However, the kinetics of biofilm formation was quite different on the two substrates. Further, they observed that the morphology of the biofilm is changing depending on the substrate properties. A similar effect, the change of the cell shapes depending on the substrate detected by Parreira *et al.* [21].

Boks *et al.* [19] studied the residence time on hydrophilic and hydrophobic surfaces. The attachment and detachment rate of bacteria significantly differed on hydrophobic and hydrophilic surfaces. They found that the hydrophobic character of the surface strongly influences and increases the dynamic behavior of adherent bacteria [19]. Adherent bacteria were moving on hydrophilic surfaces, while their were quite immobile on hydrophobic ones. In their article, four different bacterial adhesion modes were proposed (see figure 4.8). A bacterium arrives on a surface and either detaches, attaches or slides on it. Depending on the sliding speed of the bacterium on the surface, the bacterium is considered to interact with the surface (slow sliding) or not (fast sliding). Finally, the bacterium attaches irreversibly on the surface or detaches from the surface. However, these results are opposite to some other publications [3,10,49]. They also observed that detachment is promoted by the hydrophilic character of the substrate [16].

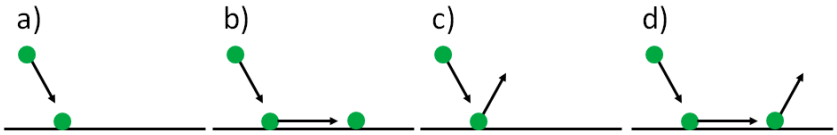

Figure 4.8: Different modes of adhesion distinguished in the paper of Boks *et al.* (a) Bacterium arrives and attaches on the surface without sliding, until possible detachment. (b) Bacterium arrives, attaches and slides along the surface in the direction of the flow until it finds its final adhesion site or it detaches. (c) Bacterium arrives on surface and detaches. (d) Bacterium arrives, attaches and slides along the substrate and finally detaches. Illustration adapted from Boks *et al.* [19].

As mentioned above, surface charge seems to strongly influence bacterial adhesion. Several research groups investigated the impact of charged surfaces on bacterial adhesion [11,47, 78,180,181,222–224]. Many results demonstrate that positively charged surfaces appear to promote bacterial adhesion, probably due to the attractive electrostatic interactions between the global, negatively charged bacterium and the positive charge on the surface. Furthermore, bacterial adhesion is discouraged on negatively charged surfaces, which may be due to the repulsive electrostatic interactions [47,224,225]. However, it was also shown in literature that bacteria preferentially adhere on surfaces with a similar zeta potential [78]. Bacterial adhesion behavior in response to charged surfaces have been also considered with the point of view of the electrokinetic theory. Bacteria cells as soft particles, with a hydrodynamically permeable layer surrounding the particle. However, the application of the theory remains difficult because of the heterogeneous character of microbial suspension but also of heterogeneities in bacteria envelope and its substructures. [222]

The prediction of bacterial adhesion on basis of attractive and repulsive electrostatic interactions often seems to be in accordance with the literature. Nevertheless, most of the studies focus on the first stage of bacterial adhesion. However, bacterial adhesion and further e.g. proliferation behavior on the surface can significantly differ. Typically, Gottenbos *et al.* demonstrated such differences in bacterial adhesion and proliferation behavior of two gram-negative *E. coli* and *P. aeruginosa* and two gram-positive *Staphyloccocus* bacteria strains on three charged surfaces: +12 mV (+), -12 mV(-) and -18 mV (–) [47]. The results showed that the initial adhesion rate was highest for *Staphyloccocus* and generally increased as the substrate became less negatively charged. They grew on all substrates, although preferably on less negatively charged surfaces (-) than on negatively (–) and positively (+) charged surfaces. The gram negative bacteria were proliferating only on negatively charged surfaces. Thereby, the number of *E. coli* cells on the surfaces increased slower than *P. aeruginosa* caused by a high desorption rate. The desorption rate of gram negative bacteria was in general higher from negatively charged surfaces. Gottenbos *et al.* suggested that the adhesion and the growth on surface may be oppositely affected by the substrate charge. Bacteria adhesion is enhanced thanks to the electrostatic interaction of the negatively charged bacterium and the positively charged substrate. However, the growth is reduced or even absent for gram negative bacteria on positively charged substrates. This absence may be explained by the inhibition of the elongation of attached bacteria caused by strong electrostatic interactions. Though, the elongation of bacteria cells is crucial for the cell division, hence the proliferation. The strong inhibition effect may be due the envelope properties of the bacteria cells, gram positive bacteria being less affected by the surface charge than gram negative bacteria [47].

The surface charge of substrate surfaces are finally considered to influence bacteria adhesion. However, it seems to depend on the bacteria strain and in particular on characteristic features of the bacterial envelope if electrostatic interactions interactions are a predominant parameter in bacteria adhesion process [181, 222].

In summary, the surface properties like the wettability and as well as surface energies seems to influence bacterial adhesion in different ways resulting is several bacterial adhesion theories as mentioned in paragraph 4.2.2.1. The surface properties of the substrate are able to influence the different dynamic behaviors of the bacteria on the surface, the cell morphology of attached bacteria or even the process of the biofilm formation. Many parameters, as the wettability character of the surface, the acid-base interactions between bacteria and surfaces, the surface charge etc. have to be considered, and yet not all of them are fully understood [13, 20]. Thus the interpretation of physical-chemical features of the surface and their impact on bacterial adhesion is still challenging.

4.2.2.3 Is there a correlation between bacterial adhesion and the accessibility of functional groups?

In literature, few articles report a correlation between bacterial adhesion and the accessibility of functional groups. Most of them are based on mixed monolayers (MMLs), creating different densities of one functionality, backfilled with another [10,18,49,77].

Qian *et al.* [77] used six different mannoside ligands backfilled with tri(ethylene glycol) (EG3) functionalized alkanethiol to study the inhibition of bacterial adhesion. The investigation was based on the specific interaction between mannose and the pili Type I of *E. coli*. As expected the type of mannoside influences bacteria adhesion and moreover, bacterial adhesion can be successfully inhibited [77]. Hence, influenced by the surface chemistry, the pili Type I seems to be crucial for bacterial adhesion. The influence of mono-and oligo-mannose (tri, hexa and nona) on bacterial adhesion, under batch and dynamic conditions, was investigated in another study [90]. In contrast to Qian *et al.* no MMLs were used but polycationic-g-PEG/PEG-mannoside polymers, which spontaneously assembled on Nb_2O_5 substrates. Thereby, the mono-mannoside was linked to the polymer either by an EG3 unit or a propyl unit, while the oligo-mannosides were linked to the polymer only by EG3. Bacterial adhesion experiments, in batches showed six times more bacteria adhered on surfaces with tri-mannose and mono-mannose-propyl residues than on surfaces with mono-mannose-EG3 and on nona-mannose residues. The specific interaction between the pili Type I and the mannose was shown by the inhibition of bacterial adhesion caused by α-Me-mannose. The pili Type I, has a specific mono-mannose binding site. Next to this site another pocket is expected that enables the binding to oligo-mannose. In case of the tri-mannose the interaction between the three mannose units and the pocket seems to be enhanced by further stabilizing interactions. Hexa- and nona-mannose seems to be too complex for a high affinity [90]. Hence, a specific interaction between the *E. coli* strain and the surface chemistry, mannose units and linker, was observed. Similarly to the study of Qian *et al.* [77], Burton *et al.* used two types of MMLs with EG3 to study the biofilm formation of *E. coli* on surfaces with different bioinertness: MMLs (CH_3 with backfilled EG3) and MMLs (OH also backfilled with EG3) [18]. EG is known to exhibit strong resistance to protein adsorption. In both series of MMLs, bacteria adhered preferentially on surfaces with a high amount of EG3. The lowest adhesion was found on surfaces with OH/EG3 than on surfaces with CH_3/EG3. Interestingly, a linear correlation was found between the biofilm formation and the decrease of EG3 on the surfaces. It should be mentioned that the experiments were performed in nutrition rich culture medium LB. Hence, the culture medium may have an influence on the surface chemistry or/and on the bacterial behavior itself. Furthermore, the EG3 terminated surfactant is longer than either the CH_3 or OH terminated surfactant and the resulting roughness effect may also have, beside the surface chemistry, an influence on the bacterial adhesion [18]. Wiencek and Fletcher [10] used also mixed monolayers to obtain surfaces without roughness effect and varying wettability character. They studied the effect of the hydrophobicity of the surface on the initial adhe-

sion, the attachment and detachment rate and the residence time of bacteria on surfaces. The impact on the stability of bacteria on the surface were discussed, and hydrophilic surfaces showed higher attachment and detachment rates. Furthermore, a tendency of the initial adhesion rate was obtained, that decreased with the increase of OH groups on the surface [10, 49].

The research groups, mentioned above, used the density of functionalities to study diverse questions, like the inhibition effect [77, 90] and the bioinertness [18] of surfaces or the impact of the wettability on bacterial adhesion [10, 49] and even, a linear correlation was found between the concentration of a functionality and bacterial adhesion [18]. However, the question of the impact of accessibility of functionalities did not directly arise even if, Wiencek *et al.* assumed that their surface have only limited attachment sites [10].

The knowledge of the impact of accessibility of functionalities on bacterial adhesion, may be crucial on surfaces modified by biomolecules or macromolecules. Such large molecules mainly contain various functional groups of different densities. If bacteria are able to sense such functional groups on the surface and adhere in respect to them, a macroscopic description of the surface may lead to wrong interpretations of the interaction between the bacteria and the surface. Hence, MMLs seems to be an ideal tool to investigate, a hypothetic correlation between functional groups and the bacterial adhesion on simple surfaces. Moreover, there may be a (linear) correlation between the concentration and bacterial adhesion, but further investigations are required.

They may also answer the question how important is the accessibility of a functionality to change the response of the bacteria, concerning the adsorption/desorption behavior or their metabolism.

4.2.3 Characterization of biofilms

Biofilms are usually visualized with microscopic techniques such as light, scanning electron or transmission electron microscopy [185]. When, the examination of biofilms is provided by scanning electron microscopy, the biofilm is dehydrated with various graded solvents [217]. Initially, the matrix of the biofilm contains up to 95 % water and is gelatinous. However, during the dehydration, the samples are modified and artefacts are created [185, 217]. With transmission electron micrsocopy, the nature of polysaccharides of biofilms and their association with the cells can be investigated through the use of several specific stains [217]. Electron microscopy is therefore suitable to characterize biofilm due to its high magnification. Nevertheless, it has several limitations like the need of dry samples and the resulting modifications of biofilm characteristics [185,217].

In the 80 ths, confocal laser scanning microscopy (CLSM) was used for the first time to analyze biofilms [217]. The main advantage of examination with CLSM and epifluorescence microscopy, is the possibility to perform it *in situ*. However, the resolution is worse com-

pared to scanning electron microscopy. The use of CLSM and epifluorescence microscopy often requires staining with special molecules labeling cells and matrix [217]. Some examples of frequently used stains are Syto9® and wheat germ agglutinin conjugates (WGA), that were used in the present PhD work. The first is Syto9®, which is green fluorescent and penetrates cells with intact or damaged envelopes. WGA is used to probe EPS, like PIA by binding to N-acetylglucosamine and N-acetylneuraminic residues [226]. Used together, Syto9® and WGA allow to quantify bacterial cell number to determine their behavior and to assess the production of EPS by attached bacteria.

Another approach is the insertion of genes expressing fluorescent proteins, like GFP, in the genome of bacteria. Hence, the bacteria produce a fluorescent molecule either constantly or initiated by a promotor, as antibiotics for example [18, 155, 227, 228]. Then no staining is needed and biofilm can be analyzed *in situ* without influencing the bacteria by adding staining molecules during the experiment.

In absence of staining, micrographs offer less contrast, leading to difficult analysis to extract data [10, 19, 49]. However, many authors reported relevant results with this method, even presenting satisfying standard derivation on the results [10, 49]. Besides the visualization of biofilms, the removal of biofilms or biofilm associated organism from substrates is frequently used for the quantification of biofilm cells as a measurement of total biofilm accumulation [217]. The bacteria cells are detached from a surface by sonication, vortexing or with a brush or a swab. Afterwards, cells are plated and counted [20, 217, 229]. Additionally, the weight of detached bacteria can be determined and thus the biofilm or the growth of bacteria can be assessed [230]. These techniques are commonly used for the characterization and quantification of infected implants. However, the localization of the bacteria on the substrate remains unknown [217].

Biofilms can also be analyzed by optical measurements after adequate staining. For example, the total amount of proteins, or the staining of bacteria can be assessed with crystal violet before measuring the absorbance at 490 nm [166, 231].
Some original, uncommon methods were also developed like time of flight- secondary ion mass spectrometry (TOF-SIMs), used to identify the correlation of bacterial location with chemical features on surfaces [232].

4.2.4 Characterization of bacterial adhesion

Adhesion of bacteria is usually studied by microscopy, in batches [14, 16] or in real-time experiments [10, 11, 49]. In particular, real-time experiments which are examined in situ allow to analyze several specific characteristics of bacterial adhesion. Generally, the adhesion rate, i.e. attachment of cells per time unit is investigated. Sometimes, attachment and detachment rates are distinguished and residence time of bacteria on surfaces can be determined [10, 11, 13, 19, 233, 234].

Techniques like micromanipulation, optical tweezer and AFM with special modified tips were also used to study bacterial adhesion and the adhesion force of bacteria on the surface [235]. Bacterial adhesion can also be monitored by quartz microbalance (QCM) [50]. However, these last methods do not allow to visualize, bacteria on surface.

4.2.5 Characterization of bacterial metabolism

As mentioned above, bacteria are able to adapt their metabolism in response to a surface. Thus changes in gene expression result in changes in protein production [236]. During the process of biofilm formation, some proteins and genes are of particular interest like those involved in the production of EPS, pili or curli, or in the synthesis of the biofilm matrix. However, publications about bacterial metabolism modification in response to surface are rare [54, 55, 237–239]. This rareness is mainly due to the sensitivity of the available analysis methods, for proteomic or genomic evaluation. A minimal quantity of cell is required and the investigation of bacterial cells in the first phase of the initial adhesion is a challenge. Alternatively, other methods have been proposed to examine bacteria metabolism. Dried bacteria can be analyzed by XPS [191, 225, 240–242] and IR [225], to obtain certain information about cell surface composition. However, the cause of such changes and the location remains unknown. Then more sensitive techniques are needed to be able to interpret environmental conditions effect on the individual bacterial response and metabolism. Finally, most of the established techniques requires dry samples for the characterization. Cell surfaces being sensitive to dehydration, the bacteria envelope may change during the drying process [197].

4.2.5.1 Proteome analysis

In general, proteins are examined with blots or 2-D gel electrophoresis. Proteins are stained and commonly detected by colorimetry and fluorescence techniques, by using either organic or silver based stains [243]. The detection limit depends on the used dyes: the range is between 1-100 ng for colorimetric dyes and between 0.005-30 ng for fluorescent dyes [244]. In addition, membrane proteins can be labeled and examined separately [51,238]. Specific stains can also allow to distinguish phosphoproteins and glycoproteins for example [244]. Additional 2-D gel-electrophoresis approaches can be combined with Maldi-TOF MS [245] or N-terminal sequencing [53] to obtain more detailed information, like the sequences, on the spots in the 2-D gel and on the proteins.

4.2.5.2 Investigation of gene expression using RT-PCR

Proteins are produced when a gene or gene sequence is expressed. If the protein and the corresponding gene sequences are known, real time-polymerase chain reaction (RT-

PCR) [246–248] can be performed to examine the potential over-expression of the genes. Another possibility is to introduce the *lacZ* gene into a certain gene cluster [50], which mutants can be identified by expression of *lacZ* [54].

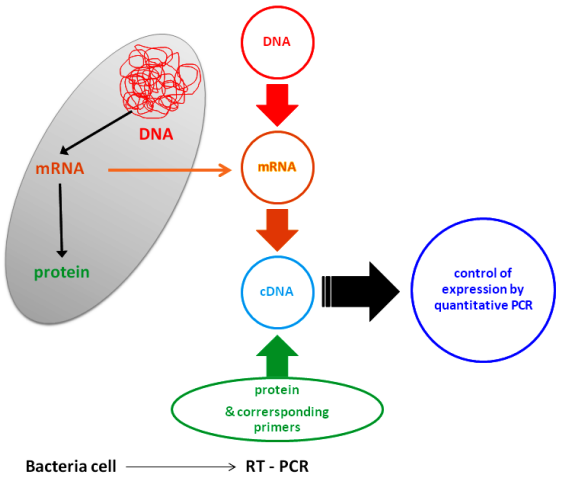

Figure 4.9: The mRNA is a short living messenger indicating which proteins are under production. After this mRNA have been isolated, cDNA can be synthesized. By the aid of PCR and the use of the defined primer of a certain gene, these cDNA fragments further indicate if this gene was produced.

RT-PCR is a quantitative real-time PCR (see figure 4.9) and is divided in two separate steps. The first step consists in a reverse-transcription (RT) of the messenger RNAs (mRNAs) isolated from bacteria cells, leading to synthesize single strand copy DNAs (cDNAs). mRNAs are short-living single strand sequences and indicate which genes are expressed at the time of the investigation. The second step is a quantitative polymerase-chain reaction (q-PCR), i.e., the amplification of the cDNAs fragments. PCR is conducted with designed primers for a certain gen and its expression is investigated. In addition, the use of an inner standard guarantees a relative quantification of the gene expression. The q-PCR is also named real-time PCR, due to the fact that the quantification of the PCR product takes places during the amplification cycles. In this process, the fluorescent dye SYBER® green (Applied Biosystems) binds at double strained DNA, emits green light at a wavelength of $\lambda_{max} = 521$ nm and adsorbs blue light at $\lambda_{max} = 494$ nm. Based on the intercalation, the fluorescence intensity signal of SYBER® green increases with the number of copies of double stranded DNA synthesized during the PCR.

4.3 Material and Methods: Part 1

4.3.1 Strains and cultivation

The used *Escherichia coli (E. coli)* and *Staphylococcus epidermidis (S. epidermidis)* bacteria strains (see table 4.1) were long-term stored either in liquid nitrogen at -200 °C or in a freezer at -80 °C. *E. coli* were purchased by Miao *et al.* and *S. epidermidis* by the Centre de Ressources of Pasteur Institute.

Table 4.1: Used bacteria strains.

Bacteria strain	properties	ATCC no/ reference
Escherichia coli SCC1	MG1655 with chromosomal insertion of $P_{A1/04/03/-}$*gfp*mut3* Cm^R	Miao *et al* 2009 [155]
Staphylococcus epidermidis (RP62A)	slime producing coagulase-negative-staphylococci Met^R, $Clin^R$, Ery^R, Gen^R CM^S, Tet^S	ATCC 35984 Christensen *et al* 1982 [206] Christensen *et al* 1983 [249]

4.3.1.1 Cultivation

4.3.1.1.1 *Escherichia coli* K12 SCC1

E. coli SCC1 bacteria cells were streaked on LB petri-dishes and cultivated at 30 °C. One colonie of *E. coli* SCC1 was used to inoculate freshly prepared LB medium. Bacteria were grown in LB medium for 14 h at 30 °C. 10 %-vol of this preculture were used to inoculate a second tube of LB culture medium. Bacteria of the second preculture were grown for 4 h at 30 °C, before they were centrifugated at 4 °C and 3500 rpm.
The obtained bacteria pellet was resuspended in either 150 mM sterile NaCl solution (saline solution), or in the minimal medium M63G-B1 (see table 4.2), depending on the experiment. The bacteria solution was diluted either with saline solution or M63G-B1 equal to an absorbance at 600 nm (Abs_{600}) of 0.01 (i.e. 10^6 bacteria/mL) for batch experiments or equal to an Abs_{600} of 0.1 for real-time experiments.

4.3.1.1.2 *Staphylococcus epidermidis* ATCC 35984

S. epidermidis ATCC 35984 were inoculated in Brain-Heart-Infusion (BHI, purchased from Sigma-Aldrich) medium for 18 h at 37 °C. For the preculture, 10 % of the overnight culture were inoculated in BHI medium. Afterwards bacteria were centrifugated at 3500 rpm, for

20 min at 4 °C.
For batch experiments, the bacteria pellets were then resuspended in saline solution and diluted equal to an Abs_{600} of 0.01. For real-time experiments, bacteria pellets were resuspended in saline solution and diluted with saline solution equal to an Abs_{600} of 0.1.

Table 4.2: M63G-B1.

KH_2PO_4	0.1	M
$(NH_4)_2SO_4$	20	% wt
$FeSO_4$	0.1	% wt
$MgSO_4$	20	% wt
KOH	6	M
$(agar$	1.5	% wt, optional)
	adjust to pH 6.8	
	autoclave for 20 min at 120 °C	
$VitaminB1$	0.05	% wt
$glucose$	10	% wt

4.3.2 Bacterial adhesion experiments

4.3.2.1 Substrates for bacterial adhesion experiments

The well-controlled and well-characterized MML achieved in the frame of the work and described in the third chapter, were used as substrates, for bacterial adhesion experiments in batch and real-time conditions. Batch bacterial adhesion were performed three times, each time in a double determination. In each series a reference was used to normalize bacterial adhesion. Thus, bacterial adhesion was averaged out of six surfaces. Real-time experiments were performed twice for each surface and bacteria strain. Therefore one sample was placed in one flow cell.

4.3.2.2 Sterilization

Substrates were incubated in 70 % EtOH (absolute ethanol, diluted with sterile and distilled water) for 30 min followed by thorough rinsing with sterile MilliQ water. Tips, pipettes, flow cells, tubes, bubble traps and liquids were autoclaved for 20 min at 120 °C. Cover glass slides to close the flow cell and not autoclavable parts of the flow cell system, were sterilized 30 min by UV light.

4.3.2.3 Batch experiments

The sterilized substrates were placed in small petri dishes (ø 35 mm) and covered with 3 mL bacteria suspension (Abs_{600} = 0.01) in the designated media. After 2 h at the experimental temperature (T_E) (*E. coli* 30 °C and *S. epidermidis* 37 °C), the substrates were thoroughly rinsed five times with saline solution, to remove the residual, non adherent bacteria. The rinsing procedure was carefully performed, so that bacteria were not removed by a surface/air interface. *S. epidermidis* were stained with Syto9® (Molecular Probes), purchased from Invitrogen. The adherent bacteria on the substrate were analyzed by confocal laser scanning microscopy (CLSM).

4.3.3 Real-time experiments

A flow cell was designed in IS2M for a direct use under the confocal microscope and was fabricated by the Technical University of Denmark, Lyngby, that also provided the bubble trab. The chamber of the flow cell is suitable for the use of different materials and samples. The volume of the chamber is 4.68 cm^3 i.e., larger than usually reported in the literature. These dimensions allow for a laminar flow (tested for a 1 mm thick silicon wafer, see paragraph 4.6.1) and avoid border-effects of the flow [250]. Interestingly, very low shear rates at the substrate surface can be reached due to the chamber dimensions. The flow cell was designed in such a way that the set-up can be easily adapted to changing parameters and conditions, e.g. with closed and open flow system, change of medium etc. The system (flow cell, tubes, valves, bubble trap) was immersed overnight in 10 %-v/v NaOCl solution and thoroughly rinsed with MilliQ water before autoclaving. Except for the valves, all parts of the system can be autoclaved for sterilization.

In this work the set-up for the closed system was used (see figure 4.10). For that purpose, the different parts of the flow cell were connected by Tygon® tubing, under the clean bench and it was tested with saline solution if there were some leaks. Parts, which are connected to the environment, were equipped with 0.2 μm filters from Millipore. These procedure was also performed, in a sterile environment under a clean bench. Then the closed and sterile system, filled with saline solution was installed under the CLSM in a thermostatic box (from OKOlab). The experimental temperature, T_E, depends on the used bacteria, as describe before. A peristaltic pump (Ismatch IP multichannel peristaltic pump) was running at least 1 h with the corresponding flow rate at T_E before the experiment started to ensure the stability of the system in terms of temperature.

10 mL of bacteria suspension was injected with the same flow rate (injection mode) as for the experiment, i.e. at 2.6 mL/min (i.e. a shear rate of 0.47 s^{-1}). After injection, the system was closed for 5 min so that bacteria could be distributed in the whole system

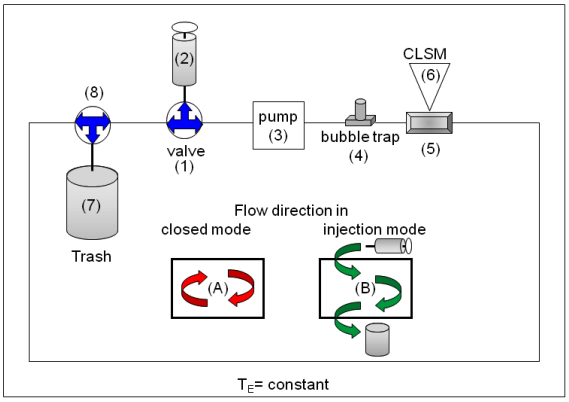

Figure 4.10: Scheme of the flow cell system in closed mode (A). Start point is a three way valve (1) to inject (bacteria, or rinsing media (2)) or to close the system. The bacterial or saline solutions are pumped (3) with a constant flow rate. To remove bubbles from the system, a bubble trap (4) is inserted between the pump and the flow cell (5). The flow cell itself is installed under the CLSM (6). Just before the first valve, another three way valve is present (7) to open the system in injection mode (B). To keep the volume constant during the rinsing step for example, this valve is connected to a trash container (8).

("closed mode of flow cell"). Images were taken by the CLSM during the whole experiment. The experimental procedure is summarized in table 4.3.

Table 4.3: Injection mode of flow cell.

Nr	System	Time [min]	Step
1	open	3.8	bacteria injection
2	closed	5.0	distribution
3	open	4.6	rinsing with saline solution
4	open	4.6	rinsing with saline solution
5	closed	120.0	bacterial adhesion in closed system

4.3.4 Analysis of bacterial adhesion

4.3.4.1 Confocal laser scanning microscopy (CLSM)

Bacterial adhesion was observed in fluorescent and reflexion mode by a confocal laser scanning microscope (Zeiss, LSM700) equipped with an 9.1 mm working distance focal objective (Zeiss LD EC "epiplan neofluar" 50X/055 DIC M27). The excitation wavelength of 488 nm in combination with a pinhole of 1 *AU*, was used for the GFP producing *E. coli* SCC1 and *S. epidermidis* stained by Syto9®, while the excitation at a wavelength of 405 nm and a pinhole of 0.5 *AU* was used for the reflexion mode. The images of the CLSM

were treated with Zen2009 software (Zeiss).
For batch experiments, images were taken from ten different regions of each sample in fluorescent and reflexion mode. Images were taken every 2 min for real-time experiments performed in fluorescent mode, while during experiments performed in reflexion mode, images were taken every 1 min.

4.3.4.2 Tracking and counting adherent bacteria

The bacteria were counted with CellC [251], on images of bacterial adhesion from batch and real-time experiments. Bacterial adhesion was statistically analyzed by excel student's test to determine differences on bacterial adhesion behavior on surfaces with different chemistries.
Additionally they were tracked with ImageJ Particle Tracker software [252] on images from real-time experiments. Real-time experiments conducted with *S. epidermidis*, however, only and the adherent bacteria number were manually assessed. To analyze bacterial behavior of real-time experiments, the counted numbers of bacterial cells on the surface were plotted per frame or time. From the resulting slopes, the bacterial adhesion rate and the proliferation rate were calculated. These rates were used to compare the experiments on surfaces with different chemistries (see paragraph 4.6.3).

4.4 Material and Methods: Part 2

4.4.1 Real-time experiments of *S. epidermidis* and subsequent RT-PCR of its genome

Confocal analysis and RT-PCR experiments of *icaA* and *icaD*, of *S. epidermidis* were done after 2 h in a parallel plate flow chamber (PPFC) and under different flow conditions at the Patras University (Greece) in collaboration with Prof. Yannis Missirlis, Dr. Maria Katsikogianni, Antigoni Foka and Prof. Iris Spiliopoulou. Each real-time experiment was performed 4 times. Two experiments were used for confocal analysis (staining of cells and EPS), while two experiments were used for further genomic analysis. For this last analysis, the bacteria were detached after 2 h and mRNAs isolated for RT-PCR. Confocal experiments were performed with an inverse confocal microscope from Nikon, thus transparent substrates were required. Therefore, the same mixed monolayers as introduced in chapter 3 were used but on glass slides as substrate instead of silicon wafers.

4.4.1.1 Real-time experiment: Parallel plate flow chamber (PPFC)

A parallel plate flow chamber (see figure 4.11) [253], placed in a thermostatic box, was used to perform real-time experiments of *S. epidermidis* [253]. After cultivation of bacteria in

BHI medium and centrifugation, the bacteria were resuspended in saline solution and diluted to an Abs_{550} value of 1.7. Real-time experiments were performed for 2 h with a flow rate of 5 mL/min or of 0.5 mL/min. Several flow cells were used in parallel, each flow cell containing one sample.

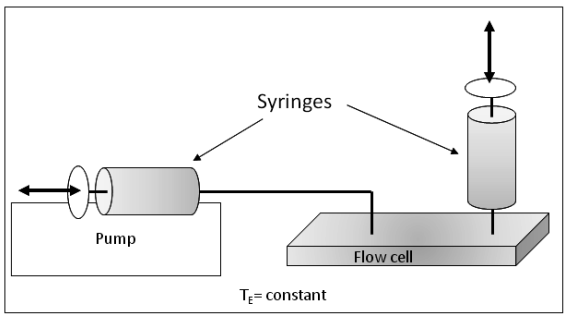

Figure 4.11: The parallel plate flow chamber was connected with two syringes, containing the bacteria suspension. One of the syringes was fixed to a pump to produce a steadily flow (injection and withdrawing).

4.4.1.2 Staining and analysis of adherent bacteria and PIA

4.4.1.2.1 Fixation of adherent bacteria cells and confocal analysis

After 2 h of PPFC experiments, samples were carefully rinsed in the flow cells with saline solution, with the same flow rate as used for the experiment, to remove non-adherent bacteria. Subsequently, cells were fixed with a 4 % paraformaldehyde solution, with the same flow rate for 30 min. Flow cells were removed from the pump and the thermostatic box before opening under laminar flow bench. The paraformaldehyde solution was carefully removed from the flow cells with a pipette. 1 mL of TexasRed® aliquot was added to the samples. Flow cells were kept in the dark for 30 min. Samples were rinsed with 1 mL of PBS, thereby the solution was two times withdrawn from the sample. PBS was added and samples were kept in the dark for 5 min. Finally, the solution was removed from the flow cells and 1 mL of saline solution, containing 2 μL Syto9® was added before samples were kept in the dark for 30 min. Afterwards, the solution with Syto9® was removed and samples were rinsed two times with saline solution. Samples were kept for 5 min in dark, saline solution was removed and added again, before samples are kept again in the dark for 5 min. Finally, saline solution was removed and surfaces with fixed and stained bacteria, were removed from the flow cells. A cover slip was hold on each surface with mounting oil, and samples were analyzed with an inverted confocal microscope (Nikon D-eclipse C1, ECLIPSE TE-2000U). Five different regions of the samples were captured by confocal microscopy.

4.4.1.3 RT-PCR

RT-PCR was performed for planktonic and adherent bacteria. Planktonic bacteria in syringes and planktonic cells in the flow chamber were gathered in a Falcon tube. Adherent bacteria were detached from the samples and also transferred in a Falcon tube.

4.4.1.3.1 Detachment of bacteria cells

For the mRNA isolation of adherent bacteria cells, the flow cell was opened. The planktonic cells were removed with pipette and gathered in a Falcon tube. 1 mL trypsin was added to the sample in the flow cell, to remove adherent bacteria. Samples were immersed for 5 min at 37 °C in the trypsin solution. Subsequently, bacteria cells were removed with a cell scratcher and the solution was harvest with a pipette. The bacteria-trypsin solution was neutralized by adding of 2.5 mL fetal bovine serum (FBS).

4.4.1.3.2 mRNA isolation

Gathered planktonic and adherent bacteria were centrifuged for 15 min at 4 °C and 3500 rpm. The supernatant was discarded and the bacteria pellet was resuspended in 1 mL DEPC water (see 4.4.1.3.7) and centrifuged for 15 min at 4 °C and 13000 rpm. After centrifugation, the supernatant was discarded and the pellet was resuspended in 100 μL TE-buffer (see 4.4.1.3.8), containing 2 mg lysozyme, to lyse the bacteria cells. After 10 min at 37 °C, 1 mL trizol® (Applied Biosystems) was added and the samples were incubated for 30 min at 30 °C. Then, 200 μL of $CHCl_3$ were added and the solution was carefully homogenized. Samples were kept 30 min at -20 °C, but vortexed each 5 min to homogenize the solution.

To separate the nucleic acid from cell fragments and proteins, samples were centrifuged for 15 min at 4 °C, resulting in three separate phases. The clear upper phase contains RNA. This phase was transfered to a new Eppendorf tube and 500 μL isopropanol was added. Tubes were gently turned to mix the samples and kept 30 min at -20 °C. Afterwards they were centrifuged for 10 min at 4 °C and 13000 rpm. The supernatant was removed and the nucleic acid pellet was washed with 70 % ethanol. 50 μL of RNase-free water were added, gently mix with tip and incubated for 10 min at 55-60 °C.

To finally destroy the DNA and only keep mRNA, 0.6 μL DNase (AmpI provided by Invitrogen) were added and incubated for 45 min at 37 °C. mRNA solution was stored at -20 °C. The purity of mRNA was tested by a PCR (PCR, TECHNE GENIUS) of a housekeeping gene *lin* (see table 4.4) and the adsorption ratio of $\frac{A_{260}}{A_{280}}$ [254]. Nucleic acids generally adsorbs at a wavelength of 260 nm, while proteins, phenol (or other contamination) absorbs at or near 280 nm. The ratio $\frac{A_{260}}{A_{280}}$>1.7 can indicate whether the nucleic sample is "pure" or contaminated by proteins etc. The absorption ratio depends thereby, on the kind of nucleic acid, DNA or RNA, and external parameters like the used water, pH etc. [254].

An agarose gel (see section 4.4.1.3.6) was charged with the PCR product. The expected length for the *lin*-fragment is around 420 bp. The control PCR is a negative control consequently, if there is no band visible at 420 bp, the DNA in the samples is supposed to be digested. A good quality of mRNA is obtained, if the adsorption ratio $\frac{A_{260}}{A_{280}}$ is higher than 1.7 [254].

Table 4.4: Schema of volume & conditions used for control-PCR.

	10x RT-buffer	5.0	μL
	$MgCl_2$ 50 mM	1.5	μL
	Primer lin$'$	1.0	μL
	Primer lin $''$	1.0	μL
	dNTPs	0.4	μL
	Taq-Polymerase	0.4	μL
	DEPC-H_2O	35.7	μL
	RNA	5.0	μL

Nr	Step	time	temp.
1	Denaturation	3 min	96 °C
2	Denaturation	1 min	95 °C
3	Annealing	30 sec	55 °C
4	Extension	30 sec	72 °C
5	Final extension	5 min	72 °C
6	Cooling down	∞	4 °C
	Cycles 2-4	40 x	

4.4.1.3.3 cDNA

Isolated and purified mRNA was used for a reverse transcription (see table 4.5) and the corresponding cDNAs were synthesized (SuperScriptIII Kit of Applied Biosystems). These cDNAs were finally used as a template for the quantitative PCR. Likewise, a control PCR of *lin* was carried out (see table 4.4). Since *lin* is a housekeeping gene, it is constantly produced, hence the mRNA of *lin* is always present. The experiment was performed with a GeneAmp® PCR system 9700 from Applied Biosystems. The successful synthesis of cDNA was confirmed by the PCR product *lin*.

Table 4.5: Conditions of cDNA preparation.

RNA (0.5 ng)	*	μL
random primer	1.0	μL
dNTPs	1.0	μL
DEPC-H_2O	8.0 - *	μL
Final volume	10.0	μL
	5 min	65 °C
	5 min	on ice
10x RT-buffer	1.4	μL
$MgCl_2$ 25 mM	2.9	μL
DTT 0.1 M	1.4	μL
RNaseOut	0.7	μL
DEPC-H_2O	3.6	μL
Incubation	2 min	25 °C
SuperScript III RT	1.0	μL
	10 min	25 °C
	50 min	42 °C
	15 min	70 °C
	5 min	one ice
RNase H	1.0	μL
	20 min	37 °C
kept at -20 °C		

4.4.1.3.4 Used primers

The primers corresponding to *icaA, icaD* and the housekeeping gene *lin* are listed in table 4.6.

Table 4.6: Used primers for PCR.

Gene	Sequence of primer′	Sequence of primer″
lin	5′ cttatctcccccaagagt 3′	5′ tctcgaactaaggacagctc 3′
icaA	5′ tctcttgcaggagcaatcaa 3′	5′ tcaggcactaacatccagca 3′
icaD	5′ atggtcaagcccagacagag 3′	5′ cgtgttttcaacatttaatgcaa 3′

4.4.1.3.5 quantitative-Polymerase-Chain-Reaction (q-PCR)

With the obtained cDNAs as templates, a quantitative-PCR (table 4.7) was performed for the genes of *icaA, icaD* and the housekeeping gene *lin* as an inner standard. For the q-PCR, a PCR device of Rotorgene RG 3000 from Corbett Research was used. During the PCR procedure double strand DNA of *icaA* and *icaD* genes is synthesized. The quantifications was assessed by the intercalation of SYBER® green, which was detected at a wavelength of $\lambda_{max} = 521$ nm. Obtained data were analyzed by the Rotorgene 6 software.

Table 4.7: Conditions of quantitative-PCR *icaA*, *icaD* and *lin*.

Sybergreen	12.5	μL
Primer′	1.0	μL
Primer″	1.0	μL
DEPC-H_2O	5.5	μL
cDNA	5.0	μL

Step	time	temp.
1	2 min	50 °C
2	5 min	95 °C
3	20 sec	95 °C
4	20 sec	* °C
5	20 sec	** °C
6	aquiring	*** °C
7	5 min	**** °C
Cycles 3-5	45 x	

	icaA & *icaD*	*lin*
*	58 °C	53 °C
**	72 °C	68 °C
***	74 °C	84 °C
****	72 °C	68 °C
gain	5	9.33
Melt: 60 °C → 90 °C		
2 sec/step; 0.2 °C/step		

4.4.1.3.6 Gel-electrophoresis

The PCR products of the different steps during the mRNA isolation until the RT-PCR were analyzed by gel-electrophoresis. An 1 % agarose-gel was used and prepared with TBS buffer (see 4.4.1.3.9). The gel was loaded by 10 μL of sample. Afterwards, the gel was stained by ethidiumbromid (EtBr) and analyzed with a transilluminator.

4.4.1.3.7 Diethylpyrocarbonate (DEPC) water

DEPC water is used to inactivate RNase enzymes in solution, and hence to protect the mRNA. 0.1 % v/v DEPS, were added to 500 mL distilled water, incubated overnight at 37 °C and sterilized by autoclaving.

4.4.1.3.8 Preparation of TE-Buffer

Tris-HCl	10	mM
EDTA	1	mM
	adjust to pH 8.0	
	sterilize by autoclaving	

4.4.1.3.9 Preparation of TBS-buffer

Tris-HCl	20	mM
NaCl	150	mM
	sterilize by autoclaving	

4.4.2 Analysis of (membrane) proteins of *E.coli* SCC1

4.4.2.1 Detachment of bacteria cells and protein extraction

Additionally to the RT-PCR, we aim at investigating potential changes of the membrane proteins content of adherent bacteria on surfaces NH_2 0 % and NH_2 100 %. For that purpose, preliminary experiments were done. A batch experiment was conducted with *E.coli* SCC1 for 2 h on the surface in M63G-B1. Unlike in the previous btach experiments, a bacterial concentration of Abs_{600}=1.0 was used. Triple experiments were conducted for 2 h at 30 °C on silicon wafer, NH_2 0 % and NH_2 100 %. After the experiment, the surfaces were rinsed 6 times thoroughly and carefully with sterilized MilliQ water and transferred to a new petri dish. Surfaces were then covered with 1.5 mL of sterilized MilliQ water and cells were detached by ultrasonic treatment, 3 x 15 min with a 5 min break and a frequency of 25 kHz. Afterwards, cells were scratched from the surfaces and the water with bacteria cells gathered in tubes. Finally, surfaces were rinsed again with 0.5 mL sterilized MilliQ water and water was added to the already detached cells. The absorption of the solution was determined at 600 nm.

Bacteria suspensions were centrifuged and the resulting pellets were resuspended in 2 mL of IEF buffer. Cells were disrupted by thermal shock (from -24 °C to 20 °C) followed by ultrasonication at 4 °C (30 W; 15 pulses of 2 s separated by 2 s breaks). The protein extracts were centrifuged (10000 g, 10 min) to eliminate cell debris [55].

4.4.2.2 Two-dimensional gel electrophoresis

The first dimension gel separation was carried out with Immobiline Dry Strips (18 cm, pH 3-10, nonlinear, Amersham Pharmacia Biotech). 200 μg of protein was loaded in 400 μL of isoelectric focusing (IEF) buffer (see 4.4.2.2.1). Gel electrophoresis was performed using the following parameters: 150 V for 1 h, 350 V for 15 min, 750 V for 45 min, 1.5 kV for 1 h, and 3.5 kV for 17 h (1 mA, constant). The second dimension consisted of SDS-PAGE using 12.5 % (wt/vol) polyacrylamide resolving gels (width: 16 cm; length: 20 cm; thickness: 0.75 mm). After migration, proteins were visualized by silver nitrate staining (developing time: 45 min) [55].

4.4.2.2.1 Preparation of IEF-Buffer

Urea	5	M
Thiourea	2	M
3-[3(cholamidopropyl)dimethylamino]-propanesufate	2	%
tributyl phosphine	2	mM
dithiothreitol	10	mM
carrier ampholytes (pH 3.5-10; Sigma-Aldrich	2	% v/v
Coomassie blue	0.4	% wt/v

4.5 Results and Discussion

4.5.1 Article 3: "The role of chemical heterogeneities of surfaces in the adhesion and proliferation of bacteria"

Article by Judith Böhmler, Hamidou Hadaira, Karine Anselme and Lydie Ploux, in preparation.

The role of chemical heterogeneities of surfaces in the adhesion and proliferation of bacteria

J. Böhmler, H. Haidara, K. Anselme, L. Ploux[§]
Institut de Science des Matériaux de Mulhouse (CNRS LRC7228), Mulhouse, France

[§] Corresponding author:
Dr Lydie Ploux, Institut de Science des Matériaux de Mulhouse (CNRS LRC7228), 15 rue Jean Starcky, BP2488, 68057 Mulhouse cedex, France; Lydie.Ploux@uha.fr

Abstract
Fonctionalization of materials has a broad application spectrum in the biomedical field for implants and biosensors, mainly aiming at controlling eukaryotic cell or bacteria response or retention. In this context, an essential parameter is surely the accessibility and the heterogeneity of the functional groups that are strongly related to the density of molecules immobilized on the surface. Aiming at improving the understanding of the impact of functional group density and chemical heterogeneity on bacteria adhesion and development on surfaces, we investigated the colonization by *Escherichia coli* K12 and *Staphylococcus epidermidis* RP62A strains of versatile, well-controlled and well-described silicon wafer platforms revealing various NH_2/CH_3 densities. A particular attention was focused on the chemical composition, layer structure and molecular organization. Through static and dynamic, real-time investigations under confocal microscope, we demonstrated for the first time that bacteria behavior on surfaces is affected by chemical heterogeneities of a surface at the molecular scale, probably in relation to the chemical heterogeneity of the bacterial cell wall. Relationships between NH_2/CH_3 surface fraction and bacterial adhesion or bacterial adhesion rate were non-linear and significantly dependent on the composition of the surrounding liquid medium and the hydrodynamic condition of culture. "Plateaus" and transition zones were especially highlighted. This bacterial behavior was related to the range of NH_2/CH_3 surface fraction offering stability or sharp variation in bacterium/surface interactions. This was attributed to the crucial influence of electrostatic, repulsive interactions occurring at the molecular scale. In particular the rare positive charges (relatively

to the high quantity of negative charges), which are revealed by proteins or other peptides of the bacterial envelope might play an important role in the interaction. A correlation between their discrete distribution at the cell envelope and a specific distribution of positive charges on the material surface probably induces the transition zone. Besides, the crucial and sensitive role of the environment or/and the growth conditions in the bacterial response to surface chemistry was confirmed.

Introduction

Despite many efforts of research since three decades, biofilm formation still remains a major source of problem and limitation in the biomedical field. In particular, infections developing on implants are the frequent cause of implant removal due to the difficulty and almost the impossibility to treat biofilm-related infections by systemic antibiotic treatments. Moreover, the use of implants that are coated with biomolecules to favour the integration in human body may still increase the risk of infections by enhancing bacterial adhesion, in addition to that of eukaryotic cells. Therefore, a comprehensive understanding of the role of the large variety of factors likely to intervene and control bacterial adhesion is crucial, deserving dedicated research efforts.

Material properties like surface topography (Whitehead *et al.* 2005; Whitehead and Verran 2006; Anselme *et al.* 2010), mechanical properties (Cottenye *et al.* 2010) and chemistry (Katsikogianni and Missirlis 2004; Ploux *et al.* 2010) are known to affect bacterial adhesion. So far, however, the complex relationships between bacterial adhesion and surface properties remain largely unknown. In the field of material surface chemistry in particular many studies exist that report the influences of the hydrophobic/hydrophilic and surface charge character on bacterial adhesion (An and Friedman 1998; Bakker *et al.* 2004; Roberts 2004; Terada *et al.* 2005), or the impact of various chemical functionalities (Ploux *et al.* 2007; Krsko *et al.* 2009; Katsikogianni and Missirlis 2010). Some particular yet sometimes contradictory trends have been revealed (Ploux *et al.* 2010). However, investigations fail so far to provide a general, integrative view of the already available results. Aside from an obvious role of the large variety of properties that are revealed by bacteria and the large diversity of experimental approaches used to realize the studies, an important cause of this scientific hurdle might be arise from an insufficient consideration of the material surface properties at the molecular scale. In other words, while effects are usually attributed to macroscopic, hydrophobic/hydrophilic or charge characters of the surface, chemical heterogeneities of the surface and accessibility of the chemical functional groups are likely to govern the interface between bacteria and the surface.

Only a few publications have addressed the influence of chemical heterogeneities of surfaces on bacterial adhesion (Wiencek and Fletcher 1995; Wiencek and Fletcher 1997; Qian *et al.* 2002; Barth *et al.* 2008; Burton *et al.* 2009). The influence of various mixtures of functional groups was considered by using self-assembled-monolayers (SAMs)-based model surfaces that allowed to control the relative amounts of each functional group at the surface. Despite the undisputable interest of the results reported by these studies, SAMs-coated

surfaces suffered from incomplete descriptions. Moreover, a common limitation was due to a weak yet real, and potentially essential, difference of length of the different molecules that constituted the molecular layers. As evoked by Wiencek and Fletcher (Wiencek and Fletcher 1997), the resulting molecular topography may make accessible to bacteria some chemical functionalities of the side-chain, different from the terminal functional groups. Side-chain effects may also be induced by additional molecules like PEG that are sometimes used as a linker between substrate and molecules of interest, and may be accessible to bacteria, as reported by Barth *et al.* (Barth et al. 2008). Chemical surface properties and therefore molecular accessibility are then incompletely controlled. Consequently, effects due to terminal functional groups, side-chain groups and molecular topographical properties cannot be clearly decoupled.

Aware of the difficulty to perfectly control the accessibility of chemical functionalities on SAMs-coated surfaces (Böhmler *et al.* 2011), we recently demonstrated the relevance of well-controlled and, importantly, well-described SAMs-based platforms for bacterial adhesion studies (Böhmler *et al.*). Made of mixed SAMs of two silanes with methyl and bromine end groups respectively (Figure 4.12 a), these surfaces provide smooth (topography-free) platforms that are further transformed to amino/methyl groups (Figure 4.12 b). These surfaces were thoroughly analyzed to provide a comprehensive description of their chemical composition, layer structure and molecular organization. The comparison of bacterial adhesion on NH_2-terminated surfaces obtained by this Br-organosilane approach on the one hand, and the direct grafting of 3-Aminopropyl-triethoxysilane (APTES) or N-(6-Aminohexyl)-3-aminopropyltrimethoxysilane (AHAPS) on the other hand showed the quantity of adhered bacteria on Br-organosilane-based approach was much less dispersed. This shows the need of "controlled" surfaces to prevent potential unexpected side-effects of surface properties on bacterial adhesion or retention by conducting biointerface investigations on substrates with perfectly controlled and described accessibility of the functional groups.

In the present work, we exploited the well-structured and well-described Br-organosilane-based mixed monolayers for studying the impact of chemical heterogeneities of surfaces on the behavior of bacteria during and following their adhesion to these surfaces. In order to address the variety of chemical composition of bacterial outer membrane, especially owing to the gram negative or gram positive class, two different bacteria species (*Escherichia coli* and *Staphylococcus epidermidis*) were considered. Moreover, we investigated the potential, additional impact resulting from specific, surrounding culture conditions. Two parameters were varied, both likely to interfere with the physical and chemical interactions between surface and bacteria: the liquid medium (selective growth medium versus NaCl 9 g/L solution) and the hydrodynamic flow (dynamic versus static condition) used during the adhesion experiment. Microbiological investigations were conducted with real time observations.

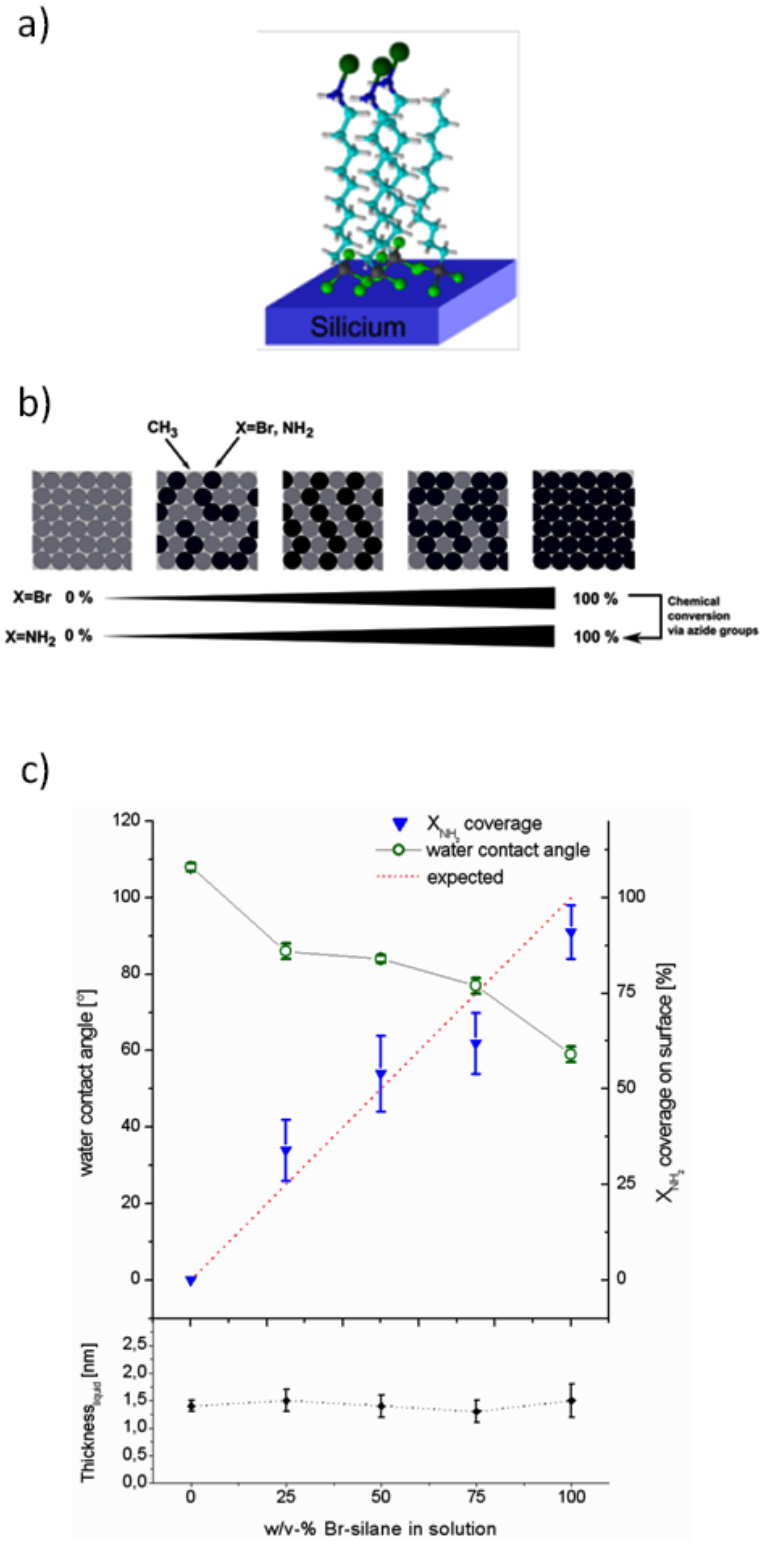

Figure 4.12: Description and characteristics of the chemically mixed model surfaces. (a) Simplified representation of a mixed monolayer. Three molecules of 11-Br-undecyltrichlorosilane and one of trichloroundecylsilane are grafted on silicon wafer. (b) Simplified top view of the five mixed monolayers revealing various densities of Br or NH_2 backfilled with CH_3. Initial Br / CH_3 surfaces are converted in NH_2 / CH_3 surfaces via N_3 / CH_3 surfaces. (c) Characteristics of the five final NH_2 / CH_3 surfaces in terms of NH_2 % content, water contact angle and thickness.

Material and Methods

Mixed monolayer preparation.

Preparation of the model surfaces was done as previously described (Böhmler *et al.*), by following protocols adapted from Heise *et al* (Heise *et al.* 1997), Balachander and Sudenik (Balachander and Sukenik 1990) and Brzoska *et al* (Brzoska *et al.* 1994). Briefly, silicon wafers (100), purchased from Mat Technology (France), one side polished, were cut into 1 cm x 1 cm pieces and cleaned by 10 min immersion in $CHCl_3$ (Sigma-Aldrich) and ultrasound treatment (frequency 45 kHz). Such cleaned, non-functionalized silicon wafers were used as internal control. For further mixed monolayer preparation, samples were then immersed in Piranha (1:3 H_2O_2:H_2SO_4, both purchased by Sigma-Aldrich) solution for 30 min at 50 °C, thoroughly rinsed with MilliQ water, dried under nitrogen stream and immediately immersed in silane solutions. Various ratios of 11-Br-undecyltrichlorosilane and trichloroundecylsilane (ABCR, Germany) in 30 % $CHCl_3$ in n-heptane (n-C_7H_{16}, Carlo Erba) were used to create SAMs-coated surfaces of five different Br/CH3 coverage ratio (0, 25, 50, 75 and 100 %). Final concentration of silane in solution was constant and equal to 1 mM. Samples were rinsed in chloroform and shortly immersed in hot MilliQ water. They were post-treated by annealing (1 h at 105 °C) and further rinsing for 15 min in chloroform under ultrasonic treatment to remove non-grafted silane molecules. The terminal bromine groups were commuted into azide by nucleophilic substitution reaction in a (0.7 M) NaN_3/DMF solution (NaN_3 and DMF purchased by Fluka and Sigma-Aldrich respectively). Azide-terminated samples were rinsed and dried under nitrogen stream. Subsequently, azide-to-amine reduction was performed by immersing samples in a (0.3 mM) $LiAlH_4$ (Sigma-Aldrich) in tetrahydrofuran solution (THF, Carlo Erba) before further immersion in THF over 12 h at room temperature. Lithium-complexes on the surface were removed by hydrolysis by immersion for 1 h in 10 % solution of hydrochloric acid (HCl , 37 %, Sigma-Aldrich) before rinsing in MilliQ water and ethanol (C_2H_5OH, 99.9 % absolute anhydrous, Carlo Erba) and drying under nitrogen stream. Positively charged amine groups (NH_3^+) were converted in NH_2 groups by immersion in triethylamine (TEA, Sigma-Aldrich) during 24 h at room temperature. Samples were finally rinsed with MilliQ water (pH between 5.0-5.8) and ethanol before drying under nitrogen stream. Before microbiological experiments, grafted surfaces were sterilized by immersing for 30 min in 70 % ethanol in MilliQ water solution, before rinsing sterile MilliQ water.

Mixed monolayer characterization.

The mixed monolayers were thoroughly characterized and analyzed elsewhere [Böhmler[a] *et al.*, in preparation]. The characterization aimed at providing the comprehensive description and knowledge of the mixed monolayers. Briefly, surface coverages with both functional groups grafted on the surface, layer structures and molecular organization in the grafted layer were evaluated at each grafting and chemical conversion step. For that purpose, XPS (survey and high resolution spectra) measurements and analysis using CasaXPS 2.3.12 software (Casa Software Ltd., Teignmouth, UK, www.casaxps.com) were done to determine atomic concentrations and chemical environments. A DSA100 geniometer was used

for static and dynamic water contact angle measurements. Ellipsometry (M-O33K001) at 532 nm provided thickness measurements of the grafted layers in both air and liquid conditions.

Bacteria species and culture.
Bacterial experiments were conducted with two bacteria species: the fluorescent, slime- and GFP-producing *Escherichia coli* (*E. coli*) SCC1 (Miao *et al.* 2009) and the slime-producing *Staphylococcus epidermidis* (*S. epidermidis*) ATCC35984 (purchased by Prof I. Spilioupoulo, Patras, Greece). -80 °C frozen bacteria were cultured overnight at 30 °C on Luria Bertani (LB purchased from Sigma-Aldrich) agar plate and at 37 °C on Brain-Heart-Infusion (BHI purchased from Sigma- Aldrich) agar plate for *E. coli* and *S. epidermidis* respectively. First pre-cultures were prepared with one colony of *E. coli* and *S. epidermidis* in LB or BHI respectively and incubated overnight (about 18 h) at 30 °C and 37 °C respectively. Second cultures were prepared with 10 % of the overnight cultures in LB or BHI for *E. coli* and *S. epidermidis* respectively. Bacteria were harvested by centrifugation. According to experiment (see the next session), bacteria pellets were re-suspended either in NaCl (150 mM) solution or in the so-called M63G-B1 *E. coli*-selective medium (Vidal *et al.* 1998). Bacterial suspensions were adjusted to an absorbance at 600 nm (A_{600nm}) of 0.01 and 0.1 for static and dynamic experiments respectively

Microbiological experiments in batch conditions.
Two surfaces with various NH_2 / CH_3 coverage ratio (0, 25, 50, 75 and 100 %) were immersed in 0.1 A_{600nm} *E.coli* suspensions, prepared in NaCl 9 g/L or M63G-B1 medium, or a 0.1 A_{600nm} *S. epidermidis* suspension, prepared in NaCl 9 g/L. As internal control, a cleaned, non-functionalized silicon wafer was used (20 min immersion in $CHCl_3$, ultrasound treatment at 45 kHz frequency, and sterilization by 30 min UV exposure). Surfaces were incubated for 2 h at 30 °C and 37 °C for *E. coli* and *S. epidermidis* respectively. Surfaces were thoroughly and carefully rinsed six times with NaCl 9 g/L solution to remove non-attached bacteria without creating air-surface interface. *S. epidermidis* adhered on substrates were fluorescently stained by adding 1 μL.mL^{-1} of a 5.10^{-3} M Syto9® (Invitrogen) stock solution to the last NaCl rinsing solution. Surfaces were directly observed in the last rinsing solution by using a fluorescence/reflection mode upright confocal microscope (LSM700, Carl ZEISS) equipped with a long working distance objective (9.1 mm). On each surface, micrographs were randomly taken on 10 different locations. Micrographs were analyzed by CellC (Selinummi *et al.* 2005) and ImageJ V.1.44d software with LSM-toolbox V4.0g plugins (Rasband 1997) for determining the quantity of adhered bacteria. Results were normalized to the internal control surfaces (i.e., cleaned, non-functionalized silicon wafers). Experiments were repeated three times. Relationships between number of adherent bacteria ($N_{AdhBact}$) and NH_2 / CH_3 surface coverage (NH_2 / CH_3 ratio) were fitted by using SciDAVis 0.2.4 software (http://scidavis.sourceforge.net/).

Microbiological experiments in real-time conditions.
A specific flow cell was designed for experiments conducted under a Zeiss LSM700 confocal

microscope (laminar flow at sample surface was tested on 1 mm thick silicon wafer with polystyrene particles of ø 2-3 μm), as described elsewhere (Cottenye *et al.* 2012). Flow cells were made with the support of the Technical University of Denmark, Lyngby, Denmark (Coico *et al.* 2005). Flow cell and accessories were sterilized by overnight immersion in 10 %-v/v NaOCl, thorough rinsing with MilliQ water and autoclaving. Flow chamber, Tygon® tubings (ø 1.52 mm), bubble trap (Technical University of Denmark, Lyngby, Denmark (Coico *et al.* 2005)), peristaltic pump (Ismatech IP multichannel peristaltic pump), medium and trash bottles closed with auto-cleavable caps equipped with filters (0.2 μm, Millipore), and connectors including one three ways connector allowing injections were connected together in sterile conditions to form a closed flow setup (see Supporting Information, Figure 4.12). The complete setup was placed under the confocal microscope in a thermoregulated chamber (Okolab, Germany) allowing a constant temperature of 30 °C for *E.coli* and 37 °C for *S. epidermidis*.

A flow rate of 2.6 mL.min^{-1} (i.e., shear rate of 0.47 $^{s-1}$) was used throughout the experiment (filling and stability test, injection and bacteria adhesion, rinsing, bacteria proliferation). The pump was run for at least 1 h to fill the system with NaCl 9 g/L solution and ensure flow and temperature stability. 10 mL of bacteria suspension (A_{600nm} of 0.1) were injected during 3.8 min before closing the system for 5 min. Non-adhered bacteria were rinsed twice during 4.6 min with NaCl 9 g/L solution under open system (see Supporting Information, Figure 4.12). The system was then closed and pictures were taken every 2 min during 150 min. The fluorescence and reflection microscopic modes were used to visualize *E. coli* and *S. epidermidis* respectively (see Supporting Information, Figure 4.21 for example of corresponding micrographs). Resulting images were analyzed by the Particle Tracker of ImageJ V.1.44d software with LSMtoolbox V4.0g (Rasband 1997) and particle tracking (Sbalzarini and Koumoutsakos 2005) plugins. Since study in dynamic conditions needs long-lived experiments for each individual material surface sample, statistical reproduction has been fixed at 2 replicates per condition.

Results & Discussion

Well-described mixed monolayer model surfaces.

The mixed monolayers were obtained by mixing two silanes with methyl and bromine end groups respectively (Figure 4.12 a), and by further in situ transformation including S_N2 reaction to convert bromine to amino nucleophilic groups (Figure 4.12 b) (Böhmler *et al.*). Their thorough analysis was mainly based on the determination of Br / SiO_x, Br / CH_3 and NH_2 / CH_3 surface coverage rates, layer thickness, layer compactness and wettability. As previously reported (Böhmler *et al.*), High-Resolution XPS analysis of the elaborated surfaces revealed a good correlation between the Br-organosilane content of the solution used for the surface elaboration, and the Br concentration detected on the surface. Similar XPS analysis conducted on the azide and amine surfaces after S_N2 bromine-to-azide and azide-to-amine conversions respectively showed a similar relationship between Br-organosilane solution content and azide or amine concentration detected on the surface, showing the control of the conversion. This finally demonstrates the possibility to control

the NH_2 / CH_3 surface coverage rate by simply controlling the initial Br-organosilane solution content as showed in Figure 4.12 c.

Thickness of the grafted layers was measured by ellipsometry in a range of 1.3-1.8 nm in liquid (Figure 4.12 c) and 1.3-1.7 nm in air, in very good agreement with the expected thickness (1.6 nm). This result demonstrates the monolayer structure of the coating whatever the NH_2 / CH_3 coverage of the surface. The monolayer structure was further confirmed by the low Br3d / SiO_x surface coverage that was determined by High-Resolution XPS analysis (0.15 ± 0.02 compared to 0.42 ± 0.05 for a typical multilayer (Böhmler *et al.*)), with SiO_x signal coming from the native silicon oxide layer present under ambiant conditions at the surface of all silicon substrates. Moreover, the good agreement between wettability measurements (59 ± 2 ° and 108 ± 1 ° for NH_2 100 % and NH_2 0 %, respectively) (Figure 4.12 c) and expected values (Aswal *et al.* 2006) demonstrated that silane molecules were densely packed and organized as expected for SAMs, which was also indicated by the similarity of thickness measured in air and liquid. Finally, a comprehensive description of layer structure, molecular organization and chemical composition of the extreme surface of the chemically mixed coating could be provided on the basis of these results. It allows to assure, first, that NH_2 and CH_3 groups were the only, accessible functional groups at the extreme surface, and secondly, that NH_2 and CH_3 groups were present at the surface in the quantity that are expected due to the Br-silane solution used for surface elaboration.

Relationship between bacteria adhesion and chemical surface content in batch conditions of culture.

E. coli and *S. epidermidis* bacteria strains were cultured in static conditions i.e., without any hydrodynamic stress, on mixed monolayer model surfaces of five different NH_2 / CH_3 surface coverages. When experiments were carried out in NaCl 9 g/L (Ionic Strength, IS = 0.15 M), *E. coli* and *S. epidermidis* bacteria strains both significantly and preferentially adhered on NH_2 0 % (i.e., CH_3 100 %) than on NH_2 100 % surfaces. Furthermore, CH_3-rich surfaces were in general more colonized than surfaces revealing less quantity of CH_3 groups (Figures 4.13 a and 4.13 b). Such general, direct decreasing trend of relationship between number of adherent bacteria ($N_{AdhBact}$) and NH_2 / CH_3 ratio is in agreement with already reported results. In particular, Wiencek and Fletcher (Wiencek and Fletcher 1995) and Burton *et al.* (Burton *et al.* 2009) observed higher adhesion on CH_3-rich surfaces than on more hydrophilic surfaces (OH-rich surfaces in both studies) by using mixed OH/CH_3 monolayers. However, differences in bacteria strains (*Pseudomonas sp.* and *E. coli* RP437 respectively) and medium (Instant Ocean Marine salts, IS = 0.48 M, and Luria-Bertani medium, IS = 0.18 M, respectively) compared to the present study prevents to come to a conclusion about common phenomenon. Using identical *S. epidermidis* bacteria as in the present study but chemically homogeneous yet non model surfaces, Katsikogianni *et al.* (Katsikogianni and Missirlis 2010) also reported similar general trend of surface colonization: surfaces that mainly revealed CH_3- , NH_2- and OH-groups were respectively colonized with decreasing bacteria amounts, in phosphate-buffered saline (PBS) of various

ionic strength (0.01 M, IS = 0.17 M, and 0.1 M, IS = 1.7 M). This general trend is usually interpreted as the result of the hydrophobic/hydrophilic and apolar/polar characters of the surfaces that may favor van der Waals interactions between CH_3-rich surface and bacterium, which may be on the contrary prevented on NH_2-rich surfaces due to a layer of adsorbed water (Wiencek and Fletcher 1995; Hermansson 1999; Hori and Matsumoto 2010). However, attractive electrostatic interactions between negatively-charged bacteria (Poortinga *et al.* 2002; Roy *et al.* 2009) and positively-charged NH_2-rich mixed surfaces are expected to compete with repulsive electrostatic interactions between some positive charged NH_3^+ on the bacteria envelope and the quantity of NH_3^+-groups present at the surface. Therefore, a reduction or even a cancellation of the differences in colonization between NH_2-poor and NH_2-rich surfaces is expected.

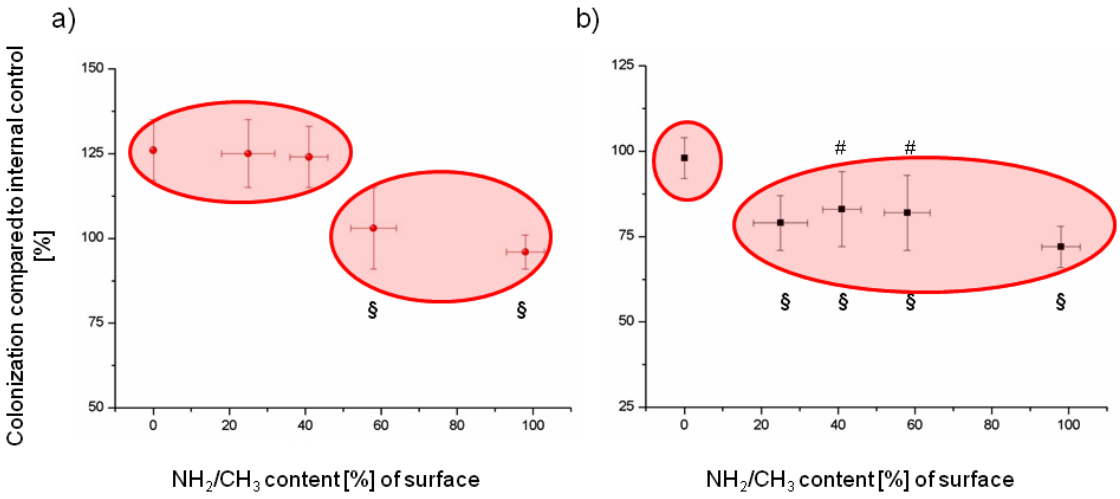

Figure 4.13: Number of *E. coli* (a) and *S. epidermidis* (b) bacteria adhered on mixed monolayers in NaCl 9 g/L medium and batch culture conditions. §: Significant difference (p > 99.9 %) compared to NH_2 0 %; #: Significant difference (p > 99.5 %) compared to NH_2 100 %. Number of bacteria was compared to the colonization on internal control (i.e., cleaned, ungrafted silicon wafers; *E. coli*: 100 = $6.1x10^5 \pm 5.3x10^4$ bacteria/cm^2 and *S. epidermidis*: 100 = $6.1x10^5 \pm 5.3x10^4$ bacteria/cm^2).

Yet, the present study shows for the first time a non-linear relationship between $N_{AdhBact}$ and NH_2 / CH_3 ratio. In contrast to the linear relationships reported by Burton *et al.* (Burton *et al.* 2009) and Wiencek and Fletcher (Wiencek and Fletcher 1995) in static and dynamic conditions respectively, $N_{AdhBact}$ versus NH_2 / CH_3 ratio relationships possess "plateaus" and transition zones (Figure 4.13). These zones are related to different ranges of NH_2/CH_3 surface coverage and are differently marked for both *E. coli* (Figure 4.13 a) and *S. epidermidis* (Figure 4.13 b). As shown in Figure 4.13, experimental curves for both bacteria strains can be fitted by functions similar to those describing acid/base titrations, clearly highlighting zones of stability besides transition zones. As noted above, this original result does not scale gradually with the modification of the surface property (i.e.,

surface charge, hydrophilicity/hydrophobicity or surface energy) which is expected to vary depend on the microscopic scale with the surface content in CH_3- or/and NH_2 groups. In other words, the simple addition of the contribution of the chemical heterogeneities of the material surface would induce a straight evolution of $N_{AdhBact}$ with the NH_2 / CH_3 ratio. The non-linear relationship rather suggests that interactions occurring between bacterium and surface at the scale of the chemical heterogeneities may significantly and non-linearly contribute to the overall bacterium/surface interaction. The transition zones evidence the existence of specific, threshold-like values (ca. 60 % of NH_2 / CH_3 for *E. coli*, ca. 12 % for *S. epidermidis*) of the surface content in chemical groups that delimitate two different behaviors of bacteria in term of their adhesion to the surface. For both bacteria species, adhered bacteria amounts were reduced to about 20 % for NH_2 / CH_3 surface content higher than the critical thresholds mentioned above.

The most probable hypothesis is schematized in Figure 4.14. On NH_2 0 % i.e., CH_3 100 % surfaces (Figure 4.14 b), only hydrophobic and van der Waals attractive interactions exist between the bacterium membrane and the hydrophobic, apolar and uncharged material surface. Nontheless, competition for the surface between bacterium membrane and aqueous medium is favorable to close bacterium/surface contact, although the compound layers of adsorbed water and counter-ions surrounding the charged, hydrophilic membranes of both bacteria strains used in this study (Ploux *et al.* 2007; Katsikogianni and Missirlis 2010) and (Poortinga *et al.* 2002) may induce sterical hindrance and consequently, slightly limit this contact. Close bacterium/surface contact leads to stronger van der Waals interactions, and therefore to stable adhesion of bacterium to 100 % CH_3 (NH_2 0 %) surfaces in static culture conditions, i.e. in absence of any external constraints on the bacterium/surface contact other than Brownian forces (Basu *et al.* 1997). On NH_2 X % ($X \neq 0$) surfaces, electrostatic interactions between the commonly negatively-charged bacterial membrane at physiological pH (Poortinga *et al.* 2002) and positively-charged NH_3^+ surface groups lead to additional attractive electrostatic interactions between bacterium and surface. Adhesion of bacterium to NH_2 X % ($X \neq 0$) surfaces is therefore expected to be stronger in comparison to NH_2 0 % (CH_3 100 %) surfaces. However, close bacterium/surface contact is limited by the presence at the surface of a layer of adsorbed water molecules due to the hydrophilic and polar characters of the NH_2-rich surfaces.

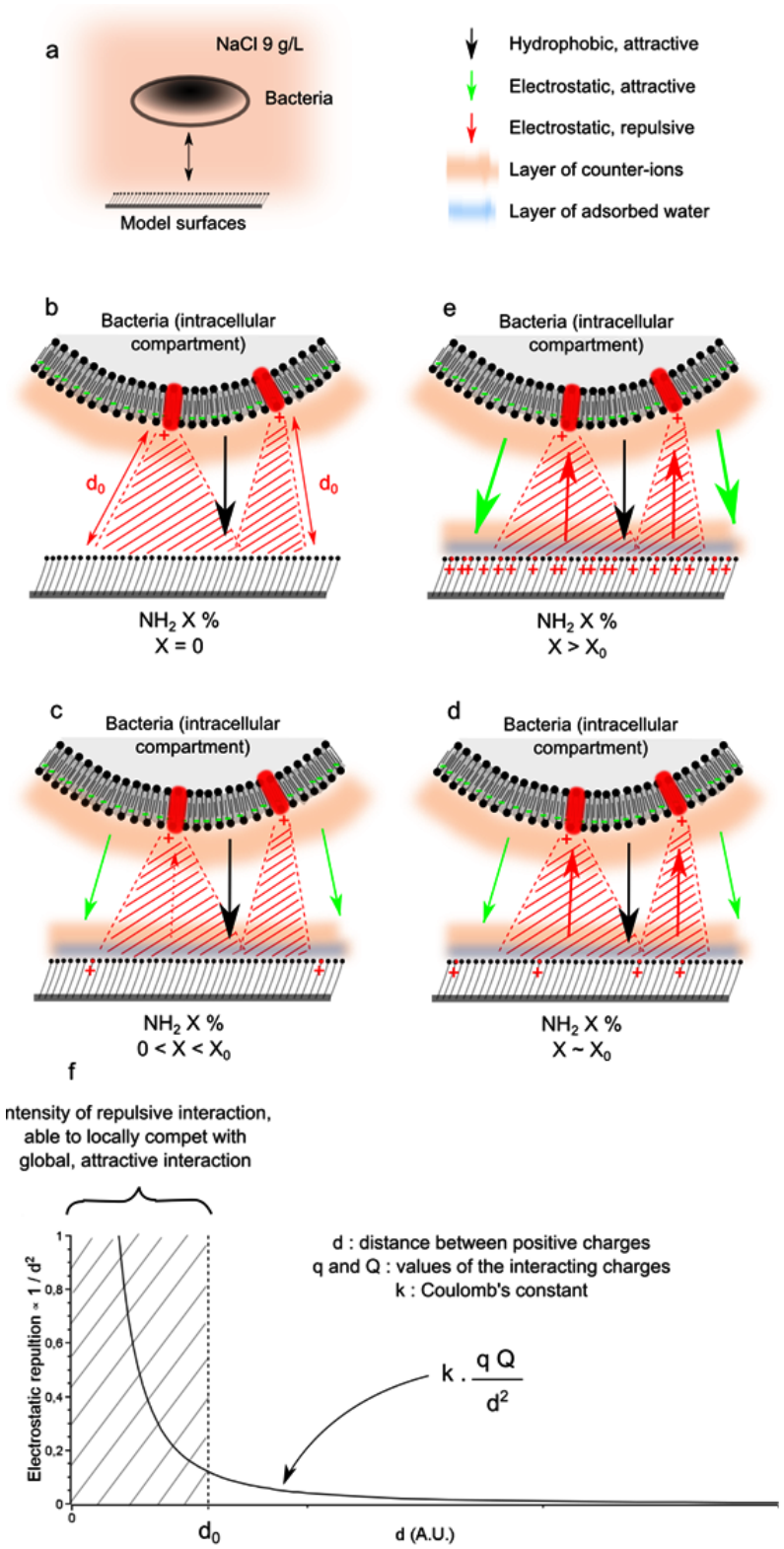

Figure 4.14: Scheme depicting interactions between the bacterial membrane and the material surface in batch conditions. A membrane of gram-negative bacteria is schematized by only depicting the phospholipid bilayer (negative charge in green) and two membrane proteins (positive charge in red).

Layers of counter-ions (due to electrostatic interactions between the positively-charged surface - NH_3^+ at pH $\sim$ 7 - and ions present in the surrounding liquid) (Hermansson 1999; Poortinga *et al.* 2002) also limit close bacterium/surface contact by sterical hindrance. More importantly, they may be the cause of an efficient screening of the material surface and bacterial membrane charges, reducing the attractive electrostatic bacterium/surface interactions by increasing the distance between both objects. However, these effects of sterical hindrance, osmotic pressure and screening of attractive electrostatic interactions due to the compouud layers of hydration and counter-ions, which reduce the bacterial adhesion on NH_2 X % (X $\neq$ 0) surfaces compared to NH_2 0 % surfaces should lead to a reduction of $N_{AdhBact}$ when the NH_2 /CH_3 surface content increases. Therefore, additional interactions which are probably repulsive since they enhance the decrease in $N_{AdhBact}$ with NH_2 / CH_3 surface content are suspected to non-linearly impact the bacterium/surface interface.

The intrinsic chemical heterogeneity of the bacteria outer membrane is certainly involved in this process (see Supporting Information, Figure 4.22). Whatever the species of bacteria, the main components of the outer wall of gram-negative bacteria like *E. coli* are phospholipids that provide, through phosphate groups, the most important contribution to the total negative charge of the bacterial outer membrane at physiological pH (Harkes *et al.* 1991; Poortinga *et al.* 2002). Besides other negatively charged groups like carboxylic acids, amino groups resulting from the proteins of the cell envelope are also present at the bacterial surface, and are responsible for the positive charges at the membranes surface at physiological pH. Cell wall of gram-positive bacteria like *S. epidermidis* is composed of a peptidoglycan macromolecule containing a large quantity of attached molecules like teichoic acids, teichuronic acids and polyphosphates (Navarre and Schneewind 1999). Therefore, whatever the gram-class of the bacteria, phosphate groups of the membrane provide at physiological pH a quasi-continuous distribution of negative charges since they represent the largest amount (highest density) of accessible groups on bacteria membranes. On the contrary, positive charges, originated from the sparse, peptidic structures in both gram-negative and gram-positive bacteria membranes, result in a discrete distribution of positive charges on the envelope at physiological pH. We therefore assume that specific conditions of bacterium/surface contact exist in which these positive (amino) envelope charges, and the ammonium (NH_3^+) of the supporting surface can create, beyond a certain surface fraction of NH_2/CH_3, repulsive electrostatic interactions which increase in intensity and start to balance the attractive and stable bacterium/surface contact.

This hypothesis is depicted in Figure 4.14 c,d,e. Electrostatic interactions at the bacterium / material surface are the result of the competition between (i) the overall, attractive interaction between the continuous distribution of negative charges of the bacterial envelope and the positively charged, amino groups of the material surface, and (ii) local and discrete, repulsive interactions between positively-charged chemical groups, sparsely distributed at the bacterium surface, and the positively charged amino groups of the material surface.

Due to the decreasing intensity of the repulsive Coulomb force with the inverse square of the distance between the interacting charges, only positively charged groups of the material surface that are within a finite lateral size r around the normal distance (d_0) to the positive charge of the bacterial surface ($d \leq d_0$, $r = r\ \rho$, Figure 4.14 b) may interact with the positive charge of bacterium, and contribute to the repulsive electrostatic interaction (Figure 4.14 f). The distance r defines a critical area on the material surface facing a positive charge of the bacterial surface, and a critical interaction distance $d \leq d_0$, through the solid angle ρ, $r = r\ \rho$. We propose therefore that, due to the discrete distribution of the positive charge in a quasi-negatively charged continuum at the bacterium surface, a critical density of positive charges on the material surface (X_0) exists, above which at least one positive charge of the material surface is located within the interacting area of each positive charge of the bacterial envelope. This specific situation where the density of interacting positive charges on material and bacterium surfaces ($X \sim X_0$, Figure 4.14 d) increases and becomes important can lead to a repulsive contribution that is able to compete with the overall attractive electrostatic interaction between bacterium and material surface. Up to X_0 (Figure 4.14 c), only very rare positive charges of the material surface may be located close to positive charges of the bacterium surface. Therefore, the overall, resulting, repulsive interaction at bacterium scale does not significantly contribute to the overall bacterium/material surface interaction. As soon as the surface density of positive charges on material surface allows at least one or more of these charges to be within the interacting area with the positive charges of the bacterial envelope ($X \sim X_0$, Figure 4.14 d) on bacteria/material contact, the overall, attractive interaction between bacterium and material surface is significantly reduced. For $X > X_0$ (Figure 4.14 e), the repulsive interaction intensity that involves one bacterial positive charge at $X \sim X_0$ increases proportionally to the number of positive charge of the material surface involved in the interaction. However, due to the probably small dimension of the critical area matching with the interaction range of the positive charge of bacterial surface, the quantity of positive charges of the material surface that contributes an increase of the electrostatic repulsive force between bacterium and material surface is therefore finite. The quantity of adhered bacteria observed on surfaces with different NH_2 coverage ratios, all higher than X_0, is consequently found to be roughly constant for both bacteria (Figure 4.14 e). Obviously, additional effect should be expected from the layers of counter-ions formed on positively charged material surfaces. The thickness of these layers increases with the density of positive surface charges, and hence might affect the distance between the bacteria envelope and the surface. This might therefore result in a shifting of the range of the transition zone as observed for the two bacterial species (Figure 4.14 f).

Indeed, although "plateaus" and transition zones were observed for both *E. coli* and *S. epidermidis* bacteria, some differences were observed. In particular, the transition zones correspond to different ranges of NH_2 / CH_3 coverage (Figure 4.13 a and 4.13 b). This might be related to the differences in distribution and quantity of positive charges that exist on the bacterial outer membranes of both bacterial species. In particular, higher N/C

ratios have been reported for gram-positive microorganisms, especially for Staphylococci compared to *E.coli* (Harkes *et al.* 1991). Although nitrogen of *Staphylococci* also results from amide bonds of peptidoglycan (Harkes *et al.* 1992), the presence of a high quantity of amino residues, i.e. peptides linked to the glycan chains (Navarre and Schneewind 1999), in probable higher quantity than proteins at the *E.coli* surface, may explain that X_0 ($\sim$ 12 %) of *S. epidermidis* is significantly smaller than of X_0 ($\sim$ 60 %) of *E.coli*.

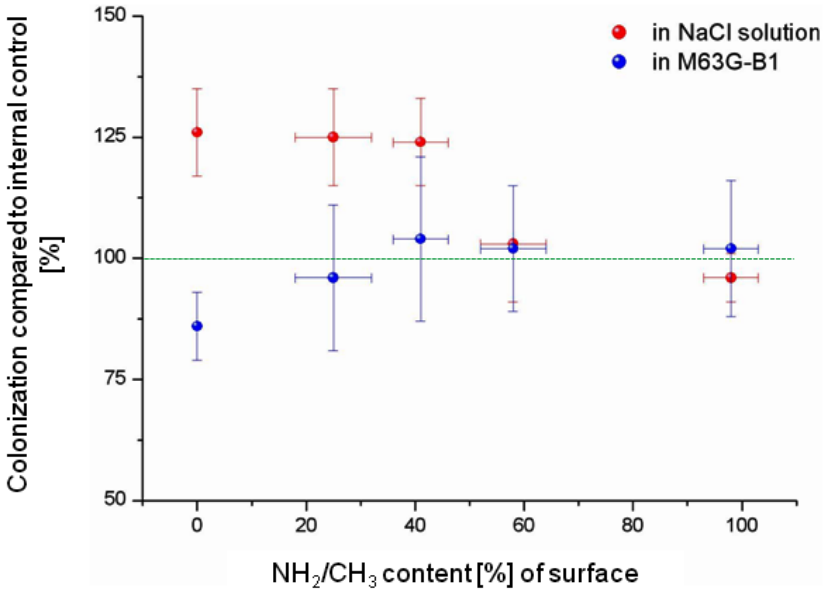

Figure 4.15: Number of *E.coli* bacteria adhered on mixed monolayers in NaCl 9 g/L and M63G culture medium (Vidal, Longin et al. 1998), and batch culture conditions. Number of bacteria were compared to the colonization on an internal control (i.e. clean silicon wafer. *E. coli* in NaCl: 100 = $6.1\text{x}10^5 \pm 5.3\text{x}10^4$ bacteria/cm^2, *E. coli* in M63G-B1: 100 = $6.1\text{x}10^5 \pm 5.3\text{x}10^4$ bacteria/cm^2) : Significant difference (p > 99.9 %) between M63G and NaCl 9 g/L conditions.

So far, no published work has reported, or even addressed, evidence of a critical density of (or critical distance between) surface functional groups that may be involved in non-specific bacterium/surface interactions. More generally, very little is known regarding the critical density of (or distance between) grafted molecules that may govern specific or unspecific adhesion of bacteria at the molecular scale. On the contrary, distance between ligand molecules grafted on surfaces has been highlighted as controlling binding force of adherent eukaryotic cells (Walter *et al.* 2006). The distance between Arginine-Glycine-Aspartic acid peptides (RGD peptides), well-known to be involved in cell adhesion to surfaces, was shown to determine the separation of individual integrins and thus the assembly of the integrin clusters that were only stable when ligands were spaced below a critical value (Deeg *et al.* 2011). Finally, the development of stable focal adhesions, their number, and size as well as the cellular adhesion strength was proved to be influenced by the local more

than the global ligand density. The ability of bacteria to bind single molecules at the surface of biological tissues through ligand/receptor interaction (Casadevall and Pirofski 2000) leads to expect similar involvement of the individual functional groups of a material surface: Variations at the molecular scale in the surface distribution of grafted molecules like carbohydrate residues may influence bacterial adhesion. The multivalence character of bacteria/mannose specific interactions, involving FimH adhesins located on *E. coli* pili (Disney *et al.* 2004), is an example of bacteria/host interactions in which the binding strength is probably highly impacted by the distance between mannose residues. This is also suggested by the higher affinity of bacteria for branched oligomannosides of specific size (Barth *et al.* 2008).

Effect of the culture medium on the relationship between bacteria adhesion and chemical surface content.

The number of adhered *E. coli* bacteria on mixed monolayer model surfaces of five different NH_2 / CH_3 surface coverage were compared in static conditions in two different liquid media (NaCl 9 g/L, IS = 0.15 M; M63G, IS = 0.20 M). A significant difference in the $N_{AdhBact}$ vs. NH_2/CH_3 coverage relationships was observed. Contrary to what was observed in NaCl 9 g/L, $N_{AdhBact}$ increases regularly, though only slightly, with NH_2 / CH_3 coverage in M63G medium (Figure 4.15). Interestingly, $N_{AdhBact}$ measured on surfaces with high NH_2 / CH_3 coverage ($X \leq 60$ %) were similar in NaCl 9 g/L and M63G media, while $N_{AdhBact}$ on low NH_2 / CH_3 coverage surfaces ($X < 60$ %) was significantly lower in M63G medium than in NaCl 9 g/L.

Three phenomena may be involved in this result. Firstly, as depicted in Figure 4.16 a and Figure 4.16 b, counter-ion layers at the bacterium and charged material surfaces should have various thickness in NaCl 9 g/L and M63G mainly due to the size of the ions present in the media (100 mM of K^+ and NH_4^+, and 10 mM of PO_4^{3-} and SO_4^{2-} in M63G), since valence of the main ions and IS were similar. Adhesion of bacteria was probably affected by this difference in thickness, which reduced the close contact between bacterium and material surface in M63G compared to NaCl 9 g/L. On surfaces containing NH_2 groups (NH_2 X %, $X \neq 0$), electrostatic interactions were therefore probably slightly reduced, which should a priori affect both attractive and repulsive interactions in a similar way, leading to insignificant modification of adhered bacteria number on changing the liquid medium. On CH_3 100 % surfaces (0 % NH_2), the increase of bacterium/material surface distance should have reduced close contact, resulting by the absence of attractive electrostatic between bacterium and material surface. It thus appears that a bacterium approaching a surface is highly sensitive to tiny external perturbations, resulting here in less stability of the bacterial adhesion, and finally to less immobilization of bacteria in M63G than in NaCl 9 g/L. Secondly, the mobility or flexibility of the macromolecular, polymeric substances that are present at the bacterial surface (fimbriae, lipopolysaccharide, etc) probably play a role in the bacterium / surface interaction. Their conformation, and thereby length, flexibility

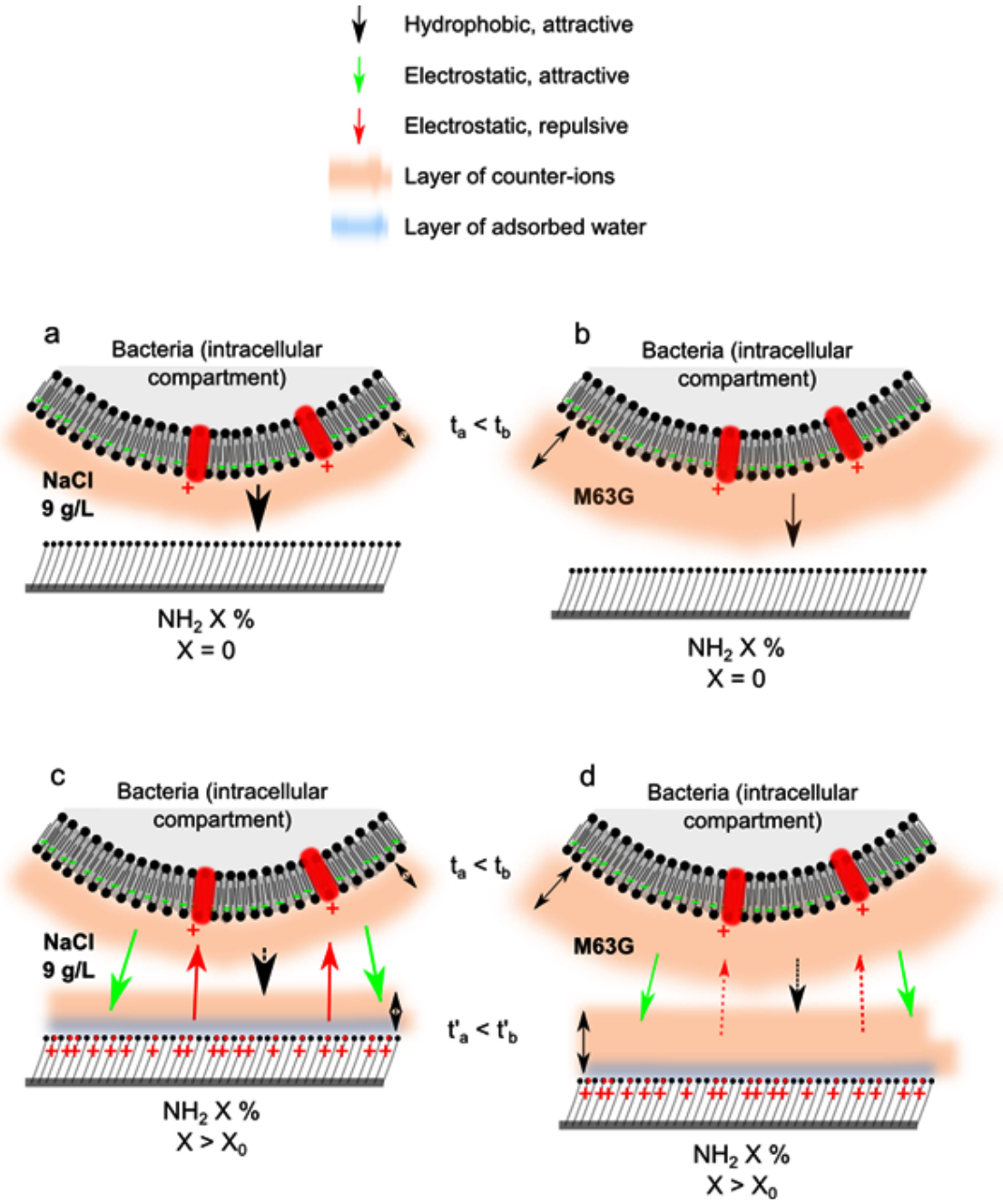

Figure 4.16: Scheme depicting interactions between the bacterial membrane and the material surface in batch conditions: Comparison between NaCl 9 g/L and M63G (Vidal et al. 1998). A membrane of gram-negative bacteria is schematized by only depicting the phospholipid bilayer (negative charge in green) and two membrane proteins (positive charge in red).

and the physico-chemical properties in potential contact with the material surface, may vary with the chemical, especially ionic, composition of the medium. Moreover, their synthesis by bacteria may vary according to medium and its nutrition- or starvation-favorable properties leading to different quantity of such structure at the bacterium surface.

Consequently, due to changes in their conformation or in their quantity, their interaction with the material surface is probably affected by the medium. Caused by differences in nutrition/starvation properties, ions transport through bacterial envelope is significantly different in M63G compared to NaCl 9 g/L mediun. Especially, changes of the overall bacterial surface charge induced by the adaptation of bacteria to environment have been reported (Briandet *et al.* 1999; Roy *et al.* 2009), which can be supposed to significantly affect further adhesion to a surface. Aiming at determining whether NaCl 9 g/L and M63G media differently affected conformation or mobility of the polymeric membrane structure, or bacterial surface charge related to ion transport, electrophoretic mobility of the used *E. coli* bacteria was determined in both media as described by (Dague *et al.* 2006). However, these preliminary experiments failed so far to account for any of these observed differences in bacterial behavior (data not shown).

Table 4.8: Hydrodynamic conditions of the bacterial experiments performed in the main reference studies, compared to the present work.

	Burton et al. (Burton, Simon et al.)	Wiencek and Fletcher (Wiencek and Fletcher 1995)	Kasikogianni et al. (Kasikogianni and Missirlis 2010)	Present work
Culture conditions	static	Dynamic	Dynamic	Static/Dynamic
Flow rate (mL/min)	– –	2.0	from 1.0 to 40.0	2.6
Shear rate s^{-1}	– –	57	from 50 to 2000	0.47
Reynolds number	– –	2.3	from 1.0 to 40.0	1.6

Relationship between bacteria adhesion and chemical surface content in real-time conditions of culture.

As shown in Table 4.8, hydrodynamic conditions used in published studies mentioned above (Wiencek and Fletcher 1995; Burton *et al.* 2009; Katsikogianni and Missirlis 2010) highly differed from a study to another. When hydrodynamic flow was applied (Wiencek and Fletcher 1995; Katsikogianni and Missirlis 2010), the shear stress was high enough to significantly affect the bacterial metabolism through direct flow-related stress (Liu and Tay 2001). In the present study, the flow chamber was designed to produce low, yet laminar and well-controlled shear stress on the surface. This prevents from flow-related modifications of the bacterial metabolism and therefore allows to study the unique effect of shear stress

on the adhesion and proliferation of bacteria to surfaces. This methodological precaution is rendered essential by the potentially strong sensitivity of bacterial behavior to very weak changes that are expected to arise from slight variations of the material surface chemical composition. *E. coli* and *S. epidermidis* bacteria strains were cultured in NaCl 9 g/L under a shear rate of 0.47 s^{-1} on the mixed monolayer model surfaces of the five different NH_2 /CH_3 coverages.

Bacterial adhesion rate and colonization rate were chosen as indicators for comparing bacterial behavior on surfaces of different NH_2 /CH_3 contents, rather than the absolute value of adhered bacteria as for static condition experiments. Adhesion rate was calculated for the first 20 min of experiment (Figure 4.17 a) which is a time range with quasi-linear evolution of the adhered bacteria number. Adhesion rate is therefore proportional to the number of adhered bacteria at a given time. This finally allows to compare trends obtained in dynamic and static conditions.

Figures 4.17 b and 4.17 c show that adhesion rate, versus NH_2 /CH_3 surface content relationships do not have identical transition zones in the dynamic and static conditions, both for *E. coli* and *S. epidermidis* bacterial species. Nevertheless, two common particularities of these relationships deserve being underscored:
(i) Some ranges of NH_2 /CH_3 surface content are related to sharper variations of the bacterial adhesion rate, similarly to the transition zone observed in static culture conditions. This supports the general results and conclusion of the experiments that were conducted in static culture conditions, showing that chemical heterogeneities of material surface affect and modify in a rather complex way the bacterial adhesion. In particular, while high concentrations of the density of chemical groups are unable under certain conditions to significantly affect bacterial adhesion, other but low concentrations of this density can lead to sharp and drastic modifications of the adhesion rate.

(ii) Although these relationships are far from linear, the general trend of the adhesion rates versus NH_2 /CH_3 surface content is a positive attachment which globally increases with NH_2 /CH_3 surface content, contrary to the behavior observed under static culture conditions. These two opposite trends can be explained as follows. The behavior of an adhering or already attached particle, and in particular, of a bacterium under shear-flow can be accounted for essentially by two competing forces: (i) an attaching or resisting force arising from the (bacterium/substrate) attractive forces, or the establissed adhesion of the bacterium to the underlying substrate and, (ii) a shear force arising from the hydrodynamic flow (Mougin *et al.* 2001). On pure CH_3 surface (0 %NH_2), the resisting adhesive force is provided only by the VDW and hydrophobic interactions between the bacterium and the support. Moreover, it is not the whole adhesion force that resists the hydrodynamic shear, but only its tangential component, the adhesive frictional force F_f, which is related to the normal adhesion force $F_n^{adh.}$ through the apparent frictional coefficient μ^* of the interface, $F_{f\sim}\mu * (F_n adh. + L_{bact.})$, $L_{bact.}$ being the load of the bacterium in the

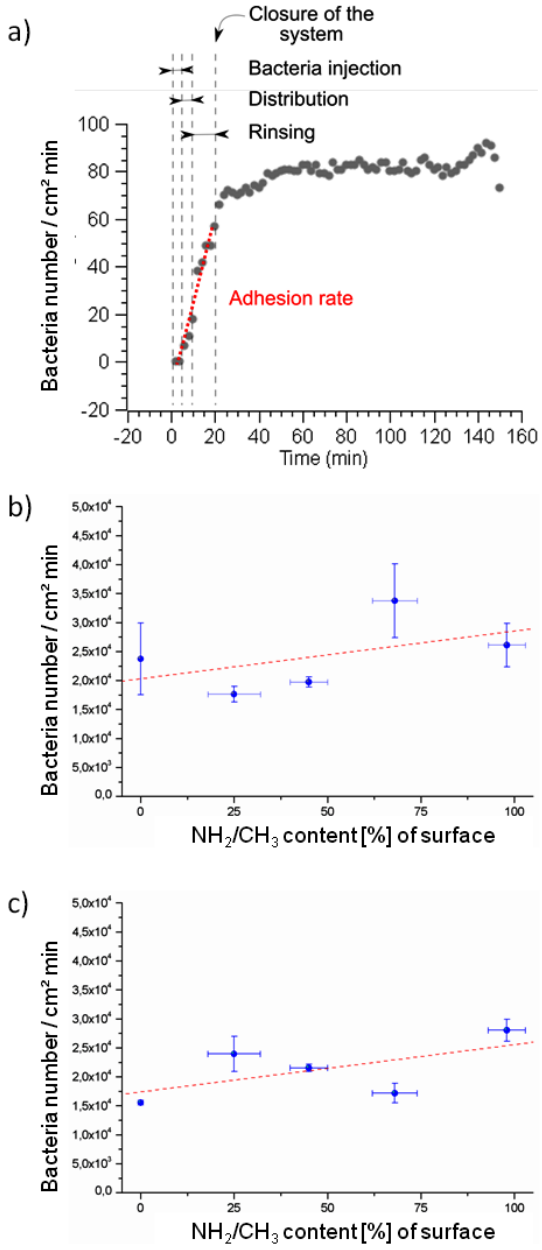

Figure 4.17: (a) Definition of the so-named "adhesion rate" parameter that was calculated for the 20 first minutes of experiment; (b) Adhesion rate of *E. coli* bacteria in NaCl 9 g/L medium ; (c) Adhesion rate of *S. epidermidis* bacteria in NaCl 9 g/L medium.

culture medium (Mougin *et al.* 2001). Dimensionally, when reported to the square of the bacterium/surface contact area $(C.A)$, this is equivalent to a tangential resisting adhesive pressure (stress), $P_{adh.} \sim F_f(C.A)^2$, which directly compares with the driving hydrodynamic shear (Mougin *et al.* 2001). And one can reasonnably imagine that the adhesion arising from these attractive but low strength physical forces may be insufficient to resist the driving (detaching) shear force produced by the hydrodynamic flow. Therefore, the probability for the bacterium to be detached and forced to slide (or roll off) at the surface

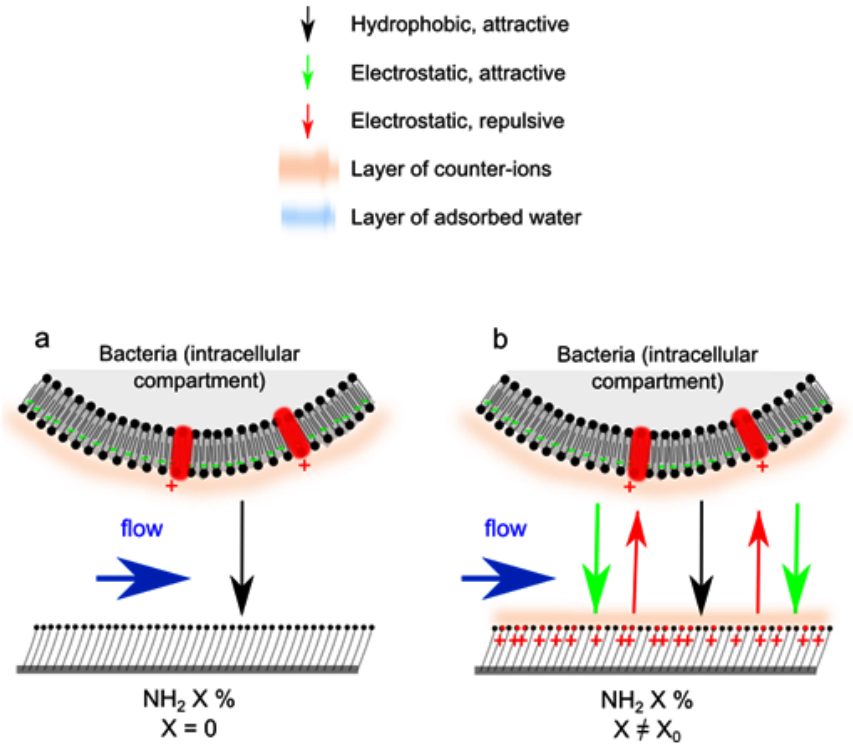

Figure 4.18: Scheme depicting interactions between the bacterial membrane and the material surface in real-time conditions. A membrane of gram-negative bacteria is schematized by only depicting the phospholipid bilayer (negative charge in green) and two membrane proteins (positive charge in red).

is high, leading consequently to a low probability of immobilization and low adhesion rate of the bacterium on the material surface (Figure 4.18 a). On NH_2 X % (X $\neq$ 0) surfaces, attractive electrostatic interactions additionally contribute to increase the attractive and resisting forces, achievin,g a level that can balance the driving/detaching shear-force. The overall result in this case is a decreased probability for bacterium detachment and its sliding (or rolling) entrainement in the flow (Figure 4.18 b). Therefore, one expects bacterium to be more easily immobilized on such surfaces, and their adhesion to be more stable against flow. This is well-confirmed by the high attachment and detachment rates (frequency), and the high total number of bacteria that were mobile throughout the experiment on CH_3-rich surfaces (Figures 4.19 a and 4.19 b). This result demonstrates that the mobility of bacteria was higher, and stability of their adhesion much less on CH_3-rich surfaces, compared to NH_2-rich surfaces. Finally, due to dynamic conditions that hamper the formation of counter-ion layers contrary to static culture conditions, electrostatic interactions may be stronger here than in static culture conditions. Dynamic conditions can be therefore considered as more (resp. less) favorable to bacteria adhesion on NH_2-rich (resp. CH_3-rich) surfaces than static conditions, which may explain the slightly opposite trend of adhesion rate vs. NH_2 / CH_3 surface content observed under hydrodynamic flow, compared to static conditions. Surfaces with attractive, electrostatic properties for glob-

ally, negatively charged objects may be therefore more colonized by bacteria compared to CH_3 and CH_3-rich surfaces, on the contrary to what happens in static culture conditions.

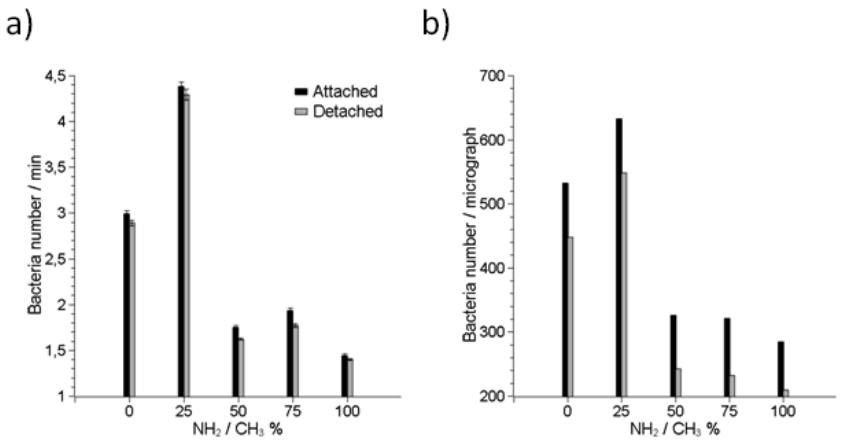

Figure 4.19: Attachment and detachment of bacteria on five surfaces of different NH_2/CH_3 % contents. Injection of bacteria in the flow experimental system is performed during the 3.8 first minutes of experiment. The experimental system is closed 20 min after starting of injection. (a) Rate of attachment and detachment from 20 to 150 min after the experiment began. (b) Total number of attached and detached bacteria throughout the experiment duration (i.e., cumulated attached and detached bacteria number after 150 min of experiment).

Conclusion

Using well-organized and well-controlled model surfaces providing various surface ratios of NH_2 in CH_3 end groups, we demonstrated that *E. coli* and *S. epidermidis* behaviors on surfaces with chemical heterogeneities at the molecular scale do not follow a straight evolution with the density of functional groups. Rather, our results show that the ability of bacteria to sense chemical heterogeneities may vary according to ranges of surface concentrations in chemical groups, depending on bacteria species. Transition zones are highlighted, that may be related to the ability of bacteria to distinguish differences in the nature and surface concentrations of functional groups through their own envelope chemical composition. An optimal concentration of the positive charges on the material surface exists, that matches with the concentration of the positively charged molecular groups on the bacterial envelope, leading to a threshold of chemical heterogeneities concentration up to which bacterial adhesion is maximal. Surfaces with concentrations in a range in which bacteria may be unable to distinguish weak differences in concentration may allow more stable adhesion, leading to "plateaus" in the relationship between bacterial adhesion and NH_2 /CH_3 surface content. Nevertheless, in dynamic culture conditions too, the abrupt variations of bacterial behavior observed for slight variations of the chemical composition of the surface also demonstrates that chemical surfaces heterogeneities at the molecular scale can strongly affect adhesion and proliferation rates of bacteria on surfaces.

Acknowledgments Work in the authors' lab is supported by the Centre National de la Recherche Scientifique. The present project was especially financially supported by Region Alsace and the University Haute-Alsace.

Bibliographic references

An, Y. H. and R. J. Friedman (1998). "Concise review of mechanisms of bacterial adhesion to biomaterial surfaces." Journal of biomedical materials research **43**(3): 338-348.

Anselme, K., P. Davidson, et al. (2010). "The interaction of cells and bacteria with surfaces structured at the nanometre scale." Acta Biomaterialia **6**(10): 3824-3846.

Aswal, D. K., S. Lenfant, et al. (2006). "Self assembled monolayers on silicon for molecular electronics." Analytica Chimica Acta **568**(1-2): 84-108.

Bakker, D. P., H. J. Busscher, et al. (2004). "Multiple linear regression analysis of bacterial deposition to polyurethane coatings after conditioning film formation in the marine environment." Microbiology **150**: 1779-1784.

Balachander, N. and C. N. Sukenik (1990). "Monolayer transformation by nucleophilic substitution: Applications to the creation of new monolayer assemblies." Langmuir **6**(11): 1621-1627.

Barth, K. A., G. Coullerez, et al. (2008). "An engineered mannoside presenting platform: Escherichia coli adhesion under static and dynamic conditions." Advanced Functional Materials **18**: 1459-1469.

Basu, S., K. Nandakumar, et al. (1997). "A model for detachment of a partially wetting drop from a solid surface by shear flow." Journal of Colloid and Interface Science **190**: 253-257

Böhmler, J., L. Ploux, et al. (2011). "The necessity of a thorough characterization of functionalized silicon wafers before biointerface studies." Journal of Physical Chemistry C **115**(22): 11102-11111

Böhmler, J., A. Ponche, et al. "Well controlled platforms allow to demonstrate the importance of functional groups accessibility for bacterial adhesion." In preparation.

Briandet, R., T. Meylheuc, et al. (1999). "Listeria monocytogenes Scott A: Cell Surface Charge, Hydrophobicity, and Electron Donor and Acceptor Characteristics under Different Environmental Growth Conditions." Applied and Environmental Microbiology **65**(12): 5328-5333.

Brzoska, J. B., I. Ben Azouz, et al. (1994). "Silanization of solid substrates: a step toward reproducibility." Langmuir **10**(11): 4367-4373.

Burton, E. A., K. A. Simon, et al. (2009). "Molecular Gradients of Bioinertness Reveal a Mechanistic Difference between Mammalian Cell Adhesion and Bacterial Biofilm Formation." Langmuir **25**(3): 1547-1553.

Casadevall, A. and L.-a. Pirofski (2000). "Host-Pathogen Interactions: Basic Concepts of Microbial Commensalism, Colonization, Infection, and Disease." Infection and Immunity **68**(12): 6511-6518.

Coico, R., T. Kowalik, et al., Eds. (2005). Current Protocols in Microbiology. Hoboken, NJ, USA, Eds.John Wiley & Sons, Inc., .

Cottenye, N. (December 2010). Antimicrobial surfaces based on self-assembled nanoreactors: from block copolymer synthesis to bacterial adhesion study, University of Basel / University of Haute-Alsace. **PhD thesis**.

Cottenye, N., K. Anselme, et al. (2012). "Vesicular structures self-assembled from oligonucleotide-polymer hybrids: mechanical prevention of bacterial colonization upon their surface tethering through hybridization " Advanced Functional Materials **in print**.

Dague, E., J. Duval, et al. (2006). "Probing Surface Structures of Shewanella spp. by Microelectrophoresis." Biophysical Journal **90**: 2612-2621.

Deeg, J. A., I. Louban, et al. (2011). "Impact of Local versus Global Ligand Density on Cellular Adhesion." Nano Letters **11**(4): 1469-1476.
Disney, M. D., J. Zheng, et al. (2004). "Detection of Bacteria with Carbohydrate-Functionalized Fluorescent Polymers." Journal of the American Chemical Society **126**(41): 13343-13346.
Harkes, G., J. Feijen, et al. (1991). "Adhesion of Escherichia coli on to a series of poly(methacrylates) differing in charge and hydrophobicity." Biomaterials **12**(853-860).
Harkes, G., H. C. Van der Mei, et al. (1992). "Physicochemical characterization of Escherichia coli. A comparison with gram-positive bacteria." Cell Biophysics **20**: 17-32.
Heise, A., H. Menzel, et al. (1997). "Grafting of polypeptides on solid substrates by initiation of N-carboxyanhydride polymerization by amino-terminated self-assembled monolayers." Langmuir **13**: 723-728.
Hermansson, M. (1999). "The DLVO theory in microbial adhesion." Colloids and Surfaces B: Biointerfaces **14**: 105-119.
Hori, K. and S. Matsumoto (2010). "Bacterial adhesion: from mechanism to control." Biochemical Engineering Journal **48**: 424-434.
Katsikogianni, M. and Y. Missirlis (2010). "Bacterial adhesion onto materials with specific surface chemistries under flow conditions." Journal of Materials Science: Materials in Medicine **21**(3): 963-968.
Katsikogianni, M. and Y. F. Missirlis (2004). "Concise review of mechanisms of bacterial adhesion to biomaterials and of techniques used in estimating bacteria-material interactions." European Cells and Materials **8**: 37-57.
Katsikogianni, M. G. and Y. F. Missirlis (2010). "Interactions of bacteria with specific biomaterial surface chemistries under flow conditions." Acta Biomaterialia **6**(3): 1107-1118.
Krsko, P., J. B. Kaplan, et al. (2009). "Spatially controlled bacterial adhesion using surface-patterned poly(ethylene glycol) hydrogels." Acta Biomaterialia **5**(2): 589-596.
Liu, Y. and J.-H. Tay (2001). "Metabolic response of biofilm to shear stress in fixed-film culture." Journal of Applied Microbiology **90**: 337-342.
Miao, H., S. Ratnasingam, et al. (2009). "Dual fluorescence system for flow cytometric analysis of Escherichia coli transcriptional response in multi-species context." Journal of Microbiological Methods **76**(2): 109-119.
Mougin, K., H. Haidara, et al. (2001). "Shear-Induced Detachment of Micrometer-Scale Soft Droplets Embedded onto a Rigid Substrate. Relation to Biological Systems." Langmuir **17**(19): 5952-5957.
Navarre, W. W. and O. Schneewind (1999). "Surface proteins of gram-positive bacteria and mechanisms of their targeting to the cell wall envelope." Microbiology and Molecular Biology Reviews **63**(1): 174-229.
Ploux, L., S. Beckendorff, et al. (2007). "Quantitative and morphological analysis of biofilm formation on self-assembled monolayers." Colloids and Surfaces B: Biointerfaces **57**: 174-181.
Ploux, L., A. Ponche, et al. (2010). "Bacteria/Material interfaces: role of the material and cell wall properties." Journal of Adhesion Science and Technology **24**: 2165-2201.
Poortinga, A. T., R. Bos, et al. (2002). "Electric double layer interactions in bacterial adhesion to surfaces." Surface Science Reports **47**(1): 1-32.
Qian, X., S. J. Metallo, et al. (2002). "Arrays of Self-Assembled Monolayers for Studying Inhibition of Bacterial Adhesion." Analytical Chemistry **74**(8): 1805 LP - 1810.
Rasband, W., U. S. National Institutes of Health, Bethesda, Maryland, USA (1997). ImageJ.
Roberts, J. A. (2004). "Inhibition and enhancement of microbial surface colonization: the role of silicate composition." Chemical Geology **212**: 313-327.

Roy, H., K. Dare, et al. (2009). "Adaptation of the bacterial membrane to changing environments using aminoacylated phospholipids" Molecular Microbiology **71**(3): 547-550.
Sbalzarini, I. F. and P. Koumoutsakos (2005). "Feature point tracking and trajectory analysis for video imaging in cell biology." Journal of Structural Biology **151**: 182-195.
Selinummi, J., J. Seppälä, et al. (2005). "Software for quantification of labeled bacteria from digital microscope images by automated image analysis." Biotech. **39**: 859-863.
Terada, A., A. Yuasa, et al. (2005). "Elucidation of dominant effect on initial bacterial adhesion onto polymer surfaces prepared by radiation-induced graft polymerization." Colloids and Surfaces B: Biointerfaces **43**(2): 99-107.
Vidal, O., R. Longin, et al. (1998). "Isolation of an Escherichia coli K-12 Mutant Strain Able To Form Biofilms on Inert Surfaces: Involvement of a New ompR Allele That Increases Curli Expression." Journal of Bacteriology **180**(9): 2442-2449.
Walter, N., C. Selhuber, et al. (2006). "Cellular Unbinding Forces of Initial Adhesion Processes on Nanopatterned Surfaces Probed with Magnetic Tweezers." Nano Letters **6**(3): 398-402.
Whitehead, K. A., J. Colligon, et al. (2005). "Retention of microbial cells in substratum surface features of micrometer and sub-micrometer dimensions." Colloids and Surfaces B: Biointerfaces **41**(2-3): 129-138.
Whitehead, K. A. and J. Verran (2006). "The Effect of Surface Topography on the Retention of Microorganisms." Trans IChemE, Part C, Food and Bioproducts Processing **84**(4): 253-259.
Wiencek, K. M. and M. Fletcher (1995). "Bacterial adhesion to hydroxyl- and methyl-terminated alkanethiol self-assembled monolayers." Journal of Bacteriology **177**(8): 1959-1966.
Wiencek, K. M. and M. Fletcher (1997). "Effects of substratum wettability and molecular topography on the initial adhesion of bacteria to chemically defined substrata." Biofouling **11**(4): 293-311.

Supporting Information

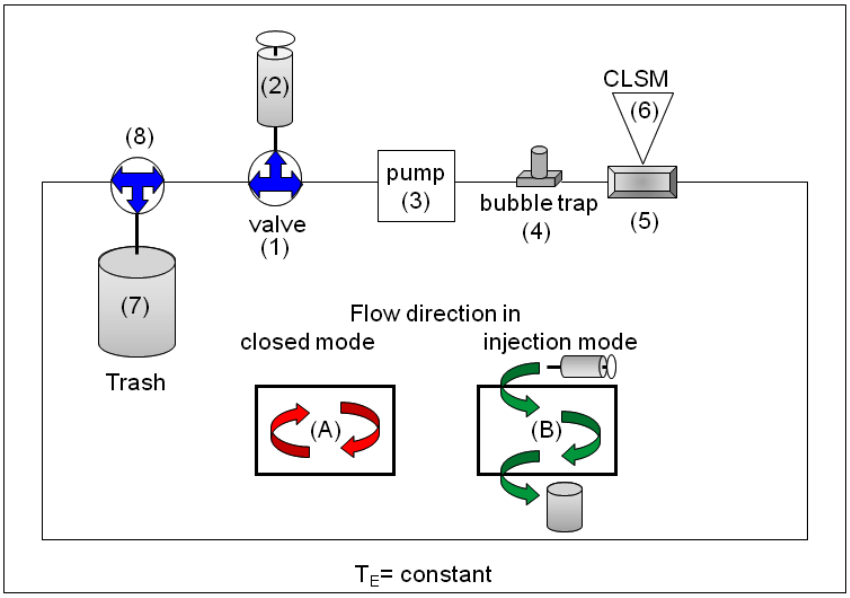

Figure 4.20: Scheme of the flow set-up used for bacterial adhesion and proliferation experiments under hydrodynamic conditions, in closed mode (A). The three way connector (1) allows to inject bacteria or rinsing medium (2) and to close the system. Solutions are pumped (3) with a constant flow rate (depending on pump speed and tubing diameters). To remove bubbles from the system, a bubble trap (4) is inserted between pump and flow cell (5). The flow chamber is placed under the confocal microscope equipped with a long working distance objective (6). Just before connector "1", another three way connector (7) allows to open the flow system in injection mode (B). To keep the volume constant during the rinsing steps for example, this connector allows to eliminate liquid into a trash container (8).

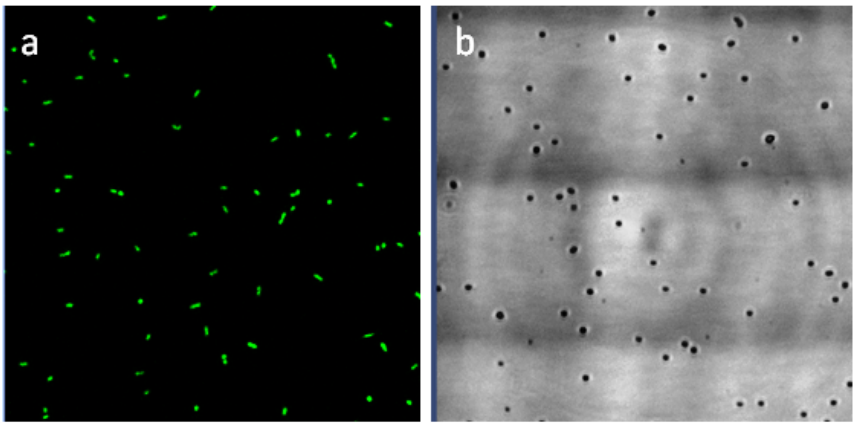

Figure 4.21: Example of micrographs taken during real-time experiments in fluorescence mode (a) and reflection mode (b) to observe *E. coli* and *S. epidermidis*, respectively.

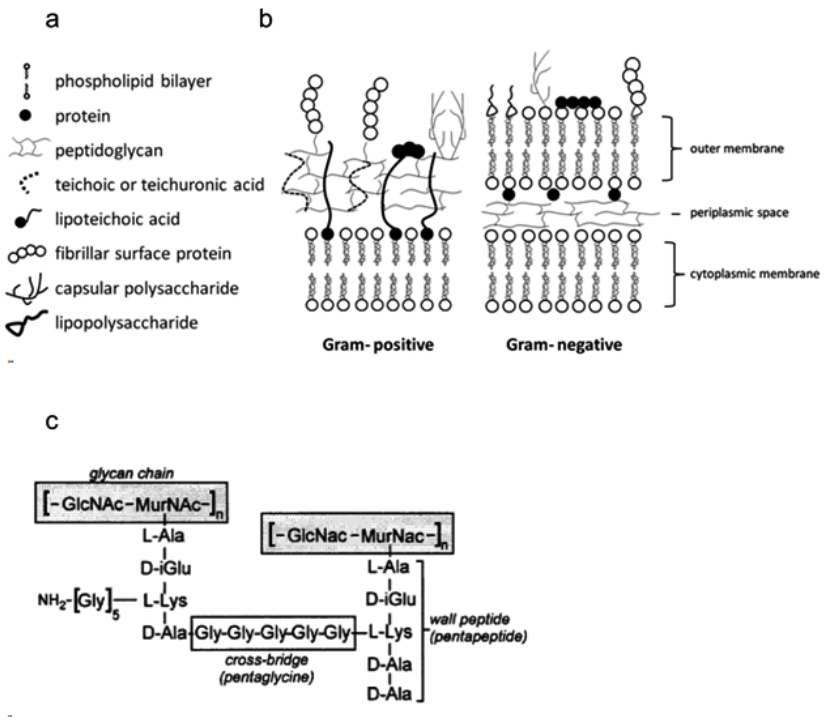

Figure 4.22: Bacterial membrane of gram-negative (like *E.coli*) and gram-positive (like *S.epidermidis*) bacteria. (a) Schematic representation of a gram-positive bacteria membrane adapted from (Poortinga 2002). (b) Schematic representation of a gram-negative bacteria membrane adapted from (Poortinga 2002). (c) Example of peptidoglycan structure (*Staphylococcus aureus*) in which glycan chains are composed of a repeating disaccharide, GlcNAc and MurNAc, that are linked to short peptides (adapted from (Navarre 1999).

4.6 Supplementary Information: Part 1

4.6.1 Flow cell

For the real-time experiment a flow cell (dimensions: 4.0 x 2.2 x 0.5 cm) was designed in IS2M [250], with the purpose to examine experiments *in situ* on a large variety of substrates and in a large variety of experimental conditions. The Technical University of Denmark (Lyngby, Denmark) fabricated the flow cell according to the final design depicted in figure 4.23 from polycarbonate. The flow cell is autoclavable at 150 °C for 30 min. Various substrates with thicknesses up to 3 mm can be placed inside the flow cell. For the experiment, the lid is glued onto the upper part and autoclaved. Afterwards the substrate is posed into the flow cell, and a sterile glass cover lid is glued over the cut-out in the cover lid and sterile tubes are connecting pump, flow cell bubble trap and trash. Finally, the entire system was placed in a thermostatic box (Okolab, Germany) under the confocal laser scanning microscope (CLSM, Zeiss LSM700).

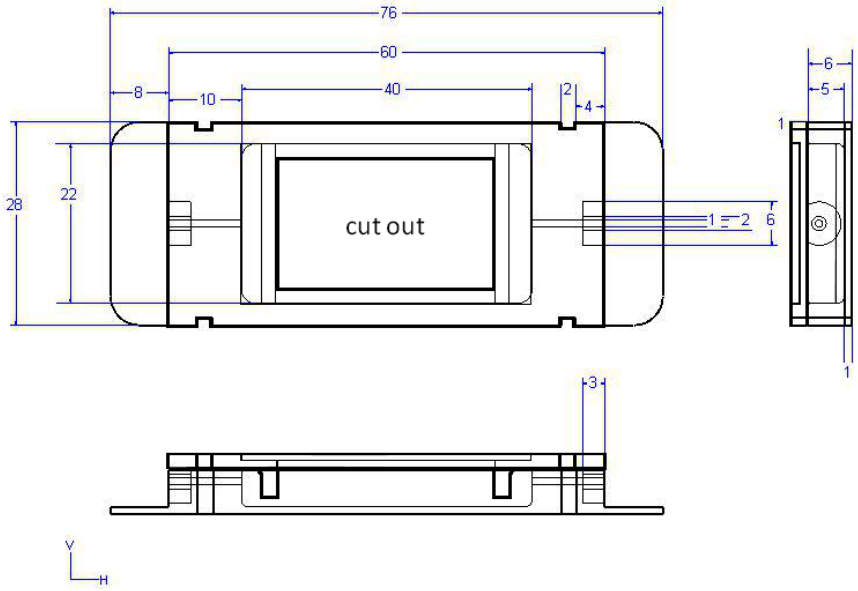

Figure 4.23: Design of the flow cell with the dimension 4.0 x 2.2 x 0.5 cm. The total volume (4.78 cm^3) is suitable for substrates of various sizes. The cut-out in the lid allows for the examination of the experiment in situ, when installed under microscope.

Velocity profiles of flow chambers used for bacterial adhesion studies can be easily compared by their Reynolds number (Re) and possible shear shear rates [255]. The Re number is given in the following equation 4.1:

$$Re = \frac{\rho \cdot Q_{pp}}{(w_0 + h_0)\eta}, \tag{4.1}$$

whereρ is the fluid density, Q_{pp} is the volumetric flow rate, η is the absolute viscosity, w_0 and h_0 are the width and the height (distance between the parallel plates) [255]. The absolute η for diluted bacteria suspension is thereby assumed to be $1 \cdot 10^{-3}$ $m^{-1}s^{-1}$ at room temperature.
The shear rate of laminar flow is given in equation 4.2:

$$\sigma = \frac{3 \cdot Q_{pp}}{2(\frac{h_0}{/2})^2 \cdot w_0} \tag{4.2}$$

The used shear rate and *Re* used in the real-time studies of this work are compared to one example from literature (see table 4.9). The dimensions of the flow cell used in the first part of this

Table 4.9: Comparison of *Re* and shear rate.

	Wieneck *et al.* [10,49]	part1 this work	part2 this work, on page 195
Flow rate (mL/min)	2.0	2.6	0.5 5.0
Shear rate (s^{-1}	57	0.47	27 270
Re	2.3	1.6	3.25 32.5

chapter, allow a laminar flow for real-time bacterial adhesion experiments, at the used flow rate of 2.6 mL/min. The laminar flow was expected through calculation of the Reynold's number (Re = 1.6) that should be inferior to 1400 [255]. It was further confirmed by experiments performed with polystyrene particles (ø 2-3 μm), installed under a phase contrast microscope. Figure 4.24 shows particles moving forward in one direction and at a certain height. Additional flow cell experiments were performed to confirm the laminar flow at a shear rate of 0.47 s^{-1} with *E. coli* and installed under CLSM. Thereby, z-stacks were taken at the beginning, the middle, the sides and the end of the substrate. Bacteria were well distributed in the flow cell and the substrate (thickness of 380 μm) did not cause turbulences in the flow cell.
Nevertheless, to avoid possible border effects, images are captured in an area of about 1 cm^2 located in the middle of the flow chamber.

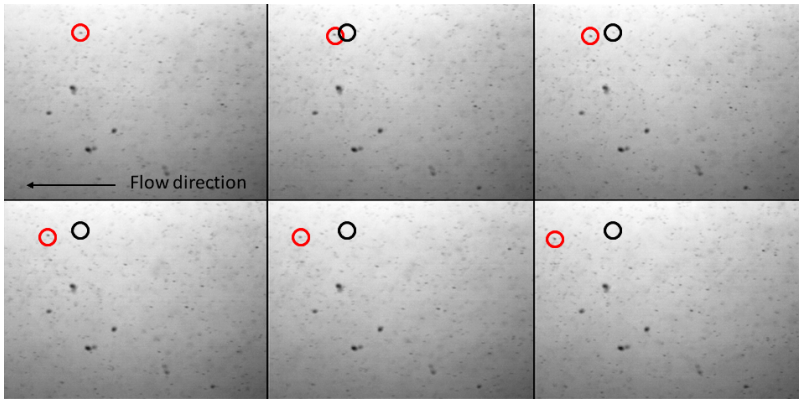

Figure 4.24: The laminar flow was investigated with polystyrene particles observed by light microscopy. The particles moved in flow direction staying at the same height. The laminar flow is demonstrated by following a well-visible particle (red circle), while its starting point is marked by a black circle.

4.6.2 Starvation of bacteria during the real-time experiments

Preliminary bacterial adhesion experiments of *E. coli* SCC1 were performed during 6-18 h at 30 °C in 0.09 % NaCl solution and a shear rate of 0.47 s^{-1}. The examination of the data obtained in reflexion mode after 6 h indicate that more bacteria were attached to the surface than encounter on images taken with fluorescence mode. This demonstrates a weak production of GFP by the bacteria in NaCl solution, probably due to the lack of nutrition. Moreover, there was a fairly small amount of bacteria attached on the surfaces, after 18 h of experiment compared to experiment conducted in M63g-B1, probably also due to the leaking nutrition that did not allow bacteria to grow on the surface. However, figure 4.25 shows that less than 1 % of the attached bacteria, stained with live/dead®, were detected as "dead" after 18 h.

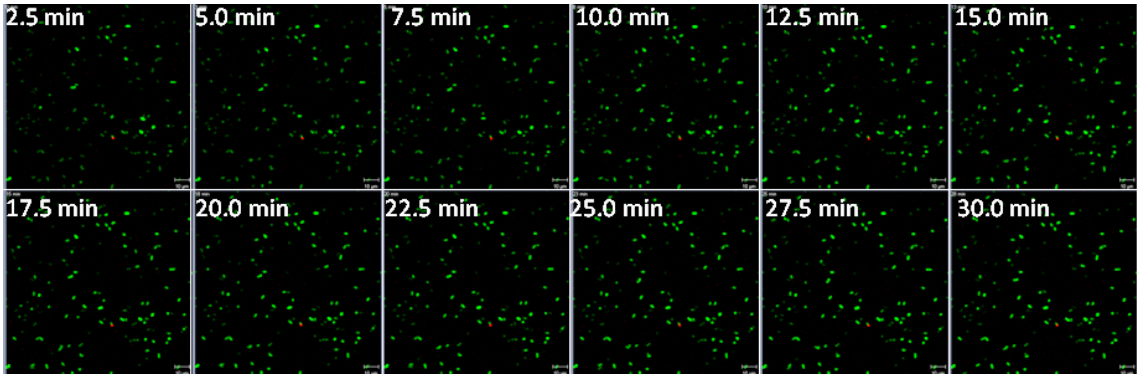

Figure 4.25: After an 18 h of real-time experiment in saline solution, the bacteria in the flow cell were stained with the same flow rate and 3 μL of live/dead staining over 30 min. Pictures were captured, every 2.5 min and the staining seems to be complete after 30 min.

The differences in the actually attached bacteria after 6 h can be explained by the fact that saline solution is not a nutritive medium, therefore no proliferation is expected. In the minimal media, bacteria are still able to reproduce themselves. Consequently, by experiments conducted in saline solution, the bacteria change their metabolism, as confirmed by the decrease in GFP production, and do not proliferate, as confirmed by the number of attached bacteria after 6 h. The fluorescent bacteria were enumerated with CellC and plotted versus time (see figure 4.26a), the fluorescent signal of bacteria being confirmed by CLSM reflexion mode examination of the surface. At the beginning of the experiment, the behavior of the bacterial adhesion was similar. Nevertheless, the number of attached bacteria decreased with time (see figure 4.26b). Analysis of the captured images show that bacteria adhere but did not fluoresce. Thus less GFP was produced and less bacteria were counted (see figure 4.26c). The GFP production started to be affected by the used medium after about 2 h.

To avoid heavy starving effects resulting in potential unexpected changes in bacteria behavior, the following bacterial adhesion experiments were performed for 2 h in either saline solution or in minimal medium.

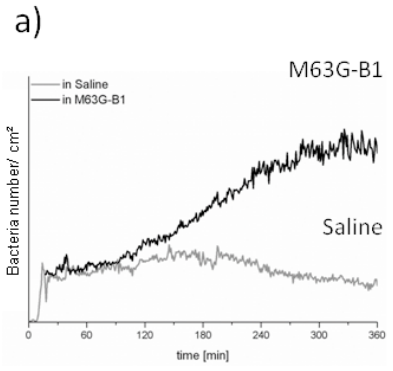

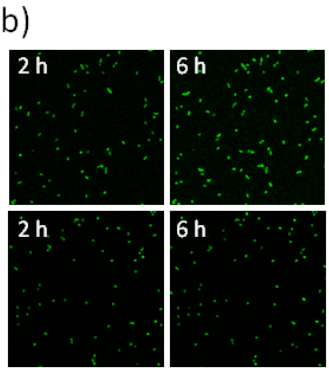

c)

Nr of bacteria after	20 min	360 min
M63G-B1	39	186
Saline	37	32
Syto9		78

Figure 4.26: The intensity of the fluorescent signals of attached bacteria starts to significantly differ after 2 h. This difference is due to the absent nutrition, the lack of proliferation and the decrease in GFP production of bacteria in saline solution. (a) shows the number of bacteria plotted versus the time, (b) shows adherent bacteria captured after 2 and 6 h, and (c) shows the number of bacteria after 20 min and at the end of the experiment.

4.6.3 Analysis of real-time experiments

For the analysis of real-time bacterial adhesion experiments, the number of bacteria was plotted versus the time. In all cases, a similar shape is obtained for the bacterial adhesion curve. Two linear slopes were used to compare the different experiments (see figure 4.27). The first linear slope is obtained during the bacteria injection and the rinsing procedure and it is hence considered as the bacterial adhesion rate. The second linear part is considered as the proliferation rate of the adherent bacteria population on the surface. Proliferation of the population can be the result of both bacterial growing and positive balance of attachment/detachment events, since the real-time experimental set-up is used in the closed mode as described in paragraph 4.3.3.

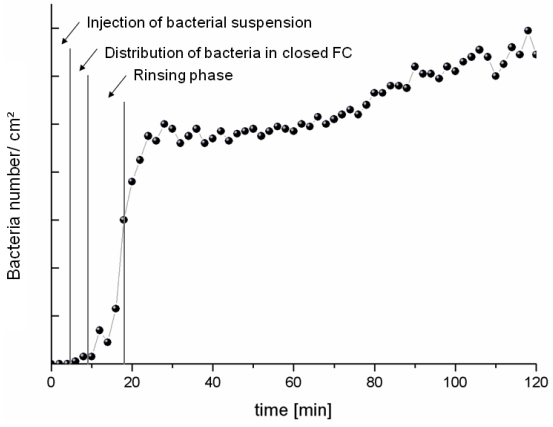

Figure 4.27: The number of bacteria attached on the surface plotted versus the time. The figure shows an experimentally obtained bacterial adhesion curve and the schematic description. Two typical linear slopes, which represent the bacterial adhesion rate and the proliferation rate, were used to compare the bacterial behavior on different substrates.

4.6.4 Proliferation rate in real-time experiments

The proliferation rates of *E. coli* SCC1 and *S. epidermidis* ATCC35984, for different surfaces are depicted in figure 4.28. In contrast to the bacterial adhesion rate (see article 3, on page 169), the proliferation rate is almost similar between the two bacteria strains and onto the different surfaces. Further, the proliferation rate is significantly lower than the adhesion rate. The low proliferation rate and its similarity between used bacteria species may be due to the saline medium. As already evoked above, saline does not provide nutrition and hence low proliferation is therefore expected. However, the experiment is performed for 2 h and as shown above the starving effect seems to be negligible within the first 2 h. Aside from the actual proliferation, the proliferation rate also considers detached and newly attached bacteria. Although, the quantity of planktonic bacteria freely moving in the experimental system is expected to be low, they probably, significantly contribute to the measured low proliferation rate.
In summary, the global proliferation rate of bacteria is (i) similar on surfaces with different amount of NH_2 and (ii) similar between the two strains. The impact of different surface and thus the different density of NH_2 on bacterial behavior seems to be more important in the first step (the bacterial adhesion rate) than in the second step (the proliferation rate).
However, as shown in the article (see paragraph 4.5) some differences exist for *E. coli*, when data are thoroughly analyzed. The obtained values that represent the proliferation rate are not actually related to proliferation of bacteria, but rather to attachment/detachment events. Thereby, number of bacteria which attach on and detach from the surface, were highest on the two surfaces with highest concentration of CH_3 (0 $\%NH_2$, 25 $\%NH_2$). Hence, those surfaces seems to attract bacteria in the first time but most of bacteria detach, further demonstrating that bacteria are not irreversibly attached to those surfaces. In contrast, on surfaces with a high concentration of NH_2, the attachment/detachement behavior of the bacteria was comparable but significant lower that on the two other surfaces. Most bacterial attachment and detachment "activity" was obtained on the surfaces with about 25 $\%NH_2$.

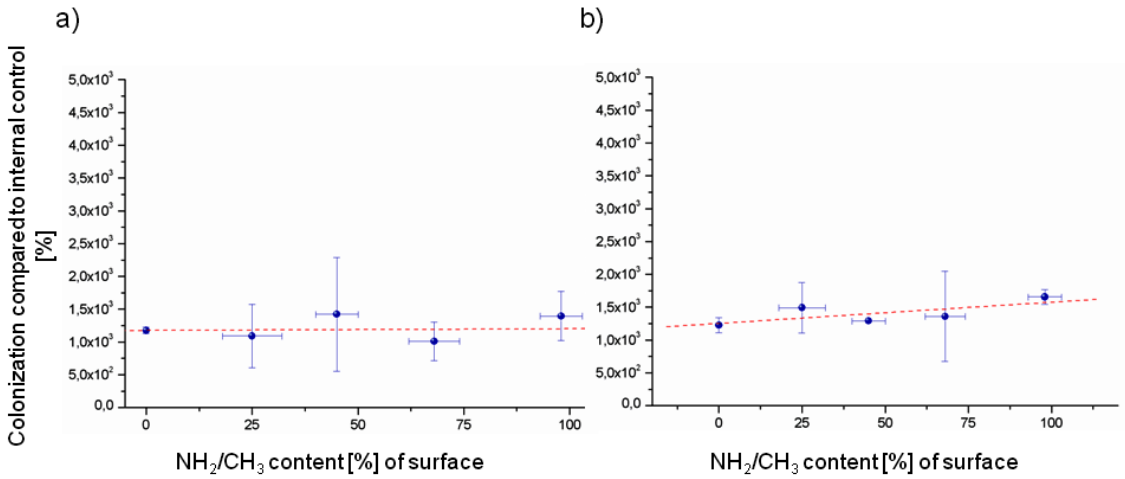

Figure 4.28: The number of attached bacteria plotted for different surfaces. (a) shows the proliferation rate of *S. epidermidis* and (b) shows the proliferation rate of *E. coli*. The proliferation rates are similar for the two bacteria strains and for the different surfaces.

4.7 Results and Discussion: Part 2

4.7.1 The impact of surface chemistry on adhesion of *S. epidermidis* ATCC35984

4.7.1.1 Influence of the bacteria concentration on the PIA production

S. epidermidis ATCC35984 strain is known to produce polysaccharide intercellular adhesin (PIA). However, in the batch and real-time experiments which were performed in the first part of this chapter, no exopolysaccharide was detected. The concentration of bacteria that were inoculated was suspected to potentially control the time at which adherent bacteria start to produce PIA. Therefore, the production of exopolysaccharide substances, mainly PIA was investigated by performing real-time experiments over 2 h with different concentrations of bacteria. Except the concentration of bacteria, the same conditions were used for the real-time experiments. After 2 h in the flow cell system bacteria/biofilms adhered on the reference silicon wafer substrate were stained with a EPS marker TexasRed®. The results are depicted in figure 4.29. Low concentration of adherent bacteria was shown to lead to the absence of PIA (see figure 4.29 a). With the increase of the bacteria concentration, the bacteria form little aggregates on the surface, and a significant production of PIA (see figure 4.29b). As expected PIA is located in aggregates of bacteria.

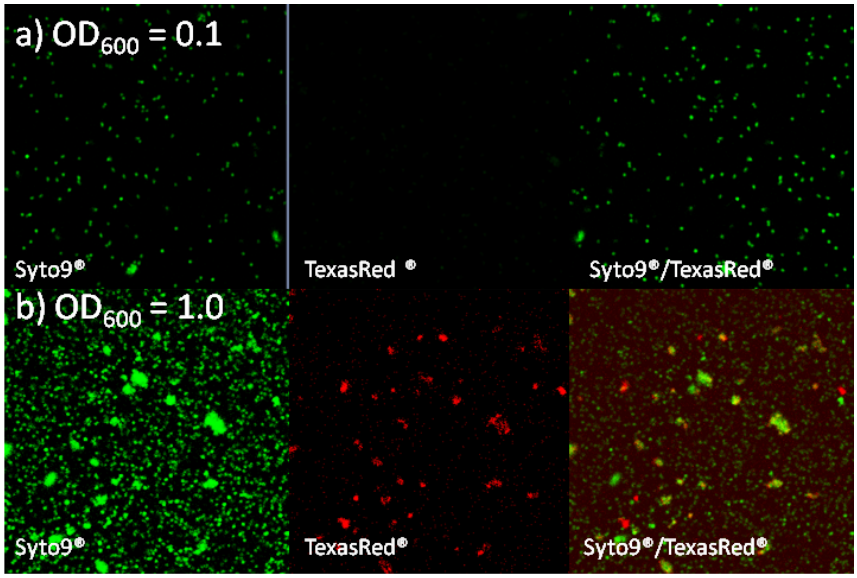

Figure 4.29: The production of PIA in bacteria cultivated in the same conditions (real-time conditions, saline solution, 37 °C) depends on the concentration of inoculated bacteria. (a) shows adherent *S. epidermidis* after 2 h stained with an injection concentration of $Abs_{600} = 0.1$, stained with Syto9® and TexasRed®. There are single bacteria adherent on the surfaces and no PIA (red color) could be detected (b) shows the same experiment with an injection concentration of $Abs_{600} = 1.0$. *S. epidermidis* formed aggregates on the surface and in these aggregates, the bacteria started to produce PIA.

This preliminary experiment leads to the assumption that a critical concentration of bacteria (C_{BC}) is necessary for bacteria to produce the exopolysaccharide substances (EPS), which, to our knowledge, has never been proposed in literature. This may be governed by quorum sensing signal. Therefore, at a low bacterial concentration, EPS does not play a crucial role in bacterial adhesion, contrary to at high concentration of bacteria. In this process, one can imagine that surface chemistry or other stresses such as shear stress, media and nutrition etc., may shift the C_{BC} to smaller concentration to provide to bacteria the protection offered by biofilms. Supplementary experiments and comprehensive study should be done to further investigate this aspect. However, this result already allow to expect different behavior of bacteria regarding PIA production, between experiments realized in the first and second part of this chapter.

4.7.1.2 Observation with inverse confocal laser scanning microscopy

Observations of bacteria adherent on surfaces with different densities of NH_2, after 2 h of real-time experiments, show single, adherent bacteria and bacteria aggregates on all surfaces, independently on the shear stresses of 27 s^{-1} and 270 s^{-1}. Figure 4.30 shows images of the different surfaces captured by inverse confocal microscopy in both, high shear rate of 270 s^{-1} (figure 4.30 a) and a low shear rate of 27 s^{-1} (figure 4.30 b) conditions. The bacterial adhesion (green) and the production of PIA (red) seem to be independent of the surface chemistry, when experiments are performed with a high flow rate. The attached bacteria are mostly gathered in defined aggregates and a high amount of PIA is observed in and around this aggregates. In contrast, bacterial adhesion and production of PIA on surfaces under low shear rate are influenced by the surface chemistry on surfaces with high amount of CH_3 groups. Attached bacteria are mostly single bacteria and almost no PIA was detected. With the increase of the NH_2 groups the behavior of attached bacteria resembles the surfaces obtained under high shear rates. Finally, the aggregates seem denser under a high shear rate than under a low shear rate.

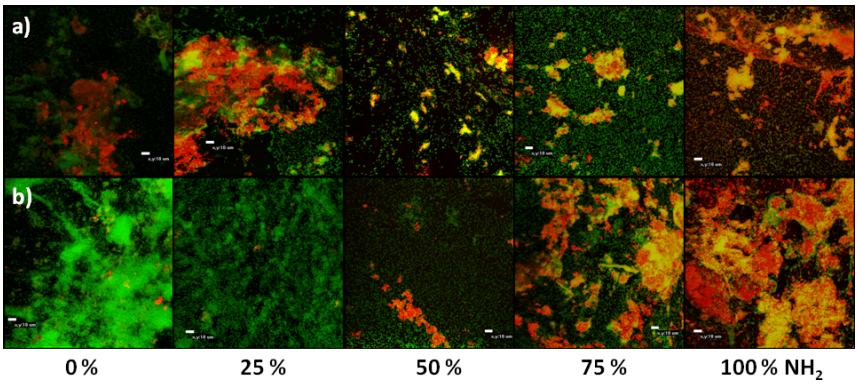

Figure 4.30: *S. epidermidis* (green) and PIA (red) on the surfaces with different densities of NH_2 were stained and analyzed by CLSM. The experiments were performed under high flow conditions (a) and low flow conditions (b).

4.7.1.3 RT-PCR

Aside from the analysis by confocal microscopy, the over-expression of *icaA* and *icaD*, which are involved in the PIA production, were investigated via RT-PCR of the attached and planktonic bacteria cells cultured as in paragraph 4.7.1.2.

4.7.1.3.1 Isolation of mRNA

The production of PIA was investigated after experiments in a parallel plate flow chamber (PPFC) as previously described in paragraph 4.4.1.1. In these experiments, the concentration was increased up to $Abs_{550} = 1.7$ to reach the quantity of cells sufficient for RT-PCR detection. Bacteria cells were detached from the surface and used for RT-PCR experiments. In the first step the mRNA was isolated. The purity of the isolated mRNA solution was first tested for residual DNA by a PCR for the housekeeping gene *lin*. An agarose-gel was charged with the PCR products and stained with EtBr. Figure 4.31 shows an example of the obtained agarose-gel. The samples are free of DNA, when the PCR is negative, hence no *lin* replicate is visible in the agarose-gel. Most samples show a bulk of mRNA, but no signal of the PCR product, of the *lin* gene. Consequently, these samples contain only RNA. Samples, for which the PCR product of the *lin* gene was obtained, were treated for 1 h with DNase at 37 °C. After this additional treatment with DNase, no more PCR product was detected.

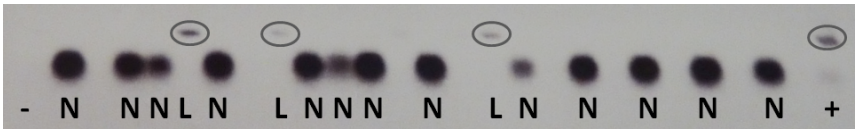

Figure 4.31: The isolation of mRNA and the destruction of DNA were tested by a PCR with primers for the housekeeping gene of *S. epidermidis*. Extraction samples without residual DNA were called "N", while samples, in which *lin* was detected were called "L". "L" samples were retreated with DNase to destroy residual DNA. The - and the + on the agarose-gel indicates the negative and the positive control.

4.7.1.3.2 Synthesis of cDNA

The absorbance of the DNA-free mRNA were measured at two different wavelengths, 260 nm and 280 nm. The ratio of both absorbances gives information about proteins impurity. A ratio of $\frac{A_{260}}{A_{280}} >$ 1.7 indicates a good purity of RNA. The concentration of the mRNA samples were calculated based on the absorbance values at 260 nm. For the following cDNA synthesis, a mRNA concentration of 0.5 ng/10μL is necessary. The successful synthesis of cDNA was confirmed by another PCR test for the housekeeping gene *lin* (see figure 4.32).

4.7.1.3.3 qPCR of *icaAD* of attached and planktonic bacteria cells

The synthesized cDNA was used for the quantitative PCR. The values obtained for *icaA* and *icaD* were normalized with the values obtained for the housekeeping gene *lin*.
The analysis of the planktonic bacteria showed that they over-express *icaA* and *icaD*. As expected, this expression was not dependent on the surface chemistry (see figure 4.33). This is not surprising,

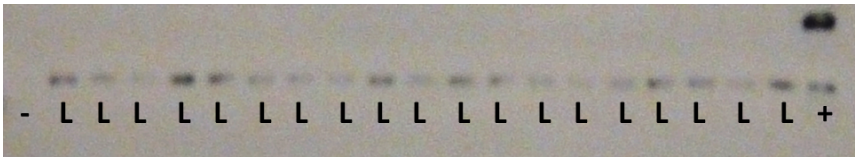

Figure 4.32: The isolated mRNA was used as template for the cDNA synthesis. After the synthesis, all extracted samples showed the PCR product (*lin*: "L"), + shows the positive control and - shows the negative control.

since bacteria were cultivated before experiments until high concentration was reached. Between the cultivation and cell harvesting, and the real-time experiment, bacteria aggregates probably remain, and were not destroyed by a sonication step. In these aggregates, PIA is present, which provides intercellular adhesion and stabilizes bacteria aggregates (see paragraph 4.2.1.4).

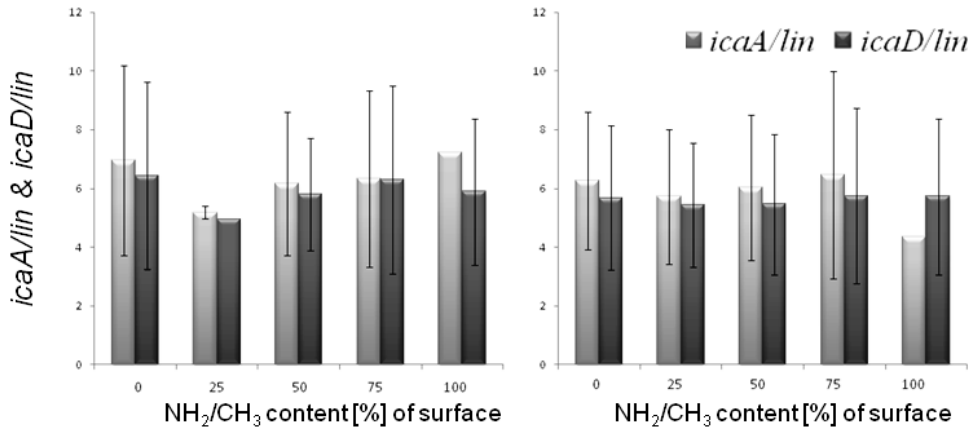

Figure 4.33: Beside the analysis of the expression of *icaA* and *icaD* in adherent bacteria, the expression of *icaA* and *icaD* in planktonic bacteria was examined. (a) shows the over-expression of *icaA* and *icaD* after experiment with a shear stress of 272 s^{-1} and (b) with a shear stress of 27 s^{-1}. Both genes are expressed in the planktonic cells, and the expression seems to be not influenced by the surface chemistry or the shear stress.

Figure 4.34 shows the normalized values for *icaA* and *icaD*, of adherent bacteria under high flow rates (figure 4.34 a) and low flow rates (figure 4.34 b).

On the contrary, the adherent bacteria seem to sense the surface chemistry in experiments performed under a shear stress of 27 s^{-1} (low flow rate). Indeed, bacteria present different expression of *icaA* and *icaD* compared to the planktonic cells, on some of the model surfaces. The bacteria attached on surfaces with a high amount of CH_3, produce significantly less PIA than on surfaces with 50 % NH_2/CH_3 ratio or more.

In general, attached and planktonic bacteria with an elevated expression of *icaA* and *icaD* show a high standard deviation. This indicates that there are several different states of bacteria together: bacteria that do and that do not over-express *icaA* and *icaD*. However, on surfaces with high amounts of CH_3 groups, the adherent bacterial population seems to be composed of bacteria in

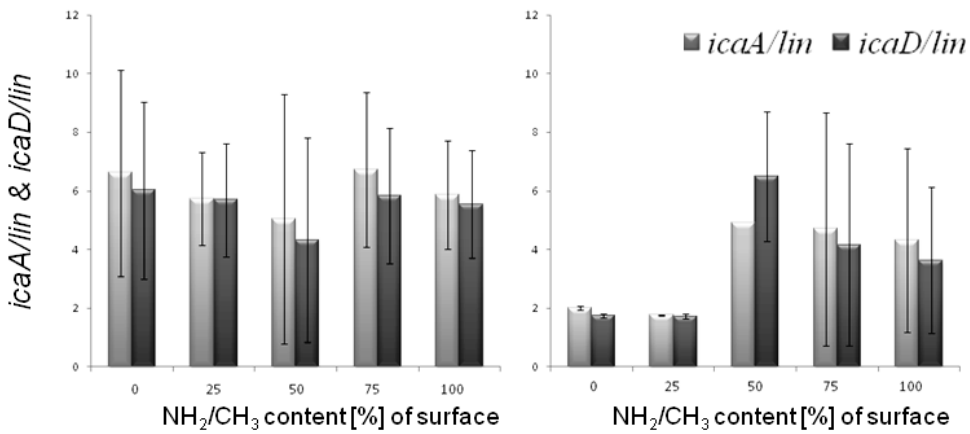

Figure 4.34: The over-expression of the *icaA* and *icaD* genes, involved in the PIA production, were examined by RT-PCR and normalized with the expression of the housekeeping gene *lin*. The figure shows the ratios of normalized over-expression of *icaA/lin* and *icaD/lin* obtained after real-time experiments (a) under a shear stress of 272 s^{-1} and (b) under a shear stress of 27 s^{-1}. The over-expression of *icaA* and *icaD* under the higher flow rate shows no significant differences according to surface chemistry. Adherent bacteria on surfaces with a high amount of CH_3 and under a lower shear stress express less *icaA* and *icaD* compared to bacteria adhered on surfaces with a high amount of NH_2.

similar states. Moreover, on these surfaces, bacteria produce PIA in small quantity, suggesting that bacteria are single rather than in aggregates. This is confirmed by confocal micrographs that show that CH_3 rich surfaces are colonized by a large proportion of single bacteria, while NH_2-rich ones are covered by rare single bacteria but frequent bacteria aggregates, rich in PIA (see figure 4.30). Our hypothesis is that the hydrophilic character of the PIA polysaccharide is more favorable to the adhesion on CH_3-rich surfaces of aggregates. They probably immediately detach from the surfaces. In contrast, surfaces with a higher amount of NH_2 does not seem to be selective for single PIA-free bacteria or aggregates of bacteria embedded in PIA (see figure 4.35). Finally, we believe that these results do not reflect the response of bacteria to properties of the surface. Rather, they may indicate a selection of certain states of bacteria (single PIA free bacteria or aggregates) due to the physico-chemical properties of the surface.

Beside the impact of the surface properties, the bacterial adhesion is also influenced by the state of bacteria, whether there are single bacteria or bacteria aggregates. Therefore, for the investigation of the surface impact on single bacterial adhesion and to avoid strong influences of "neighboring" bacteria cells, a lower concentration of bacteria cells is required for the experiment. However, such reduction of the bacteria concentration may lead to problems with the detection limit of the first steps of the RT-PCR process.

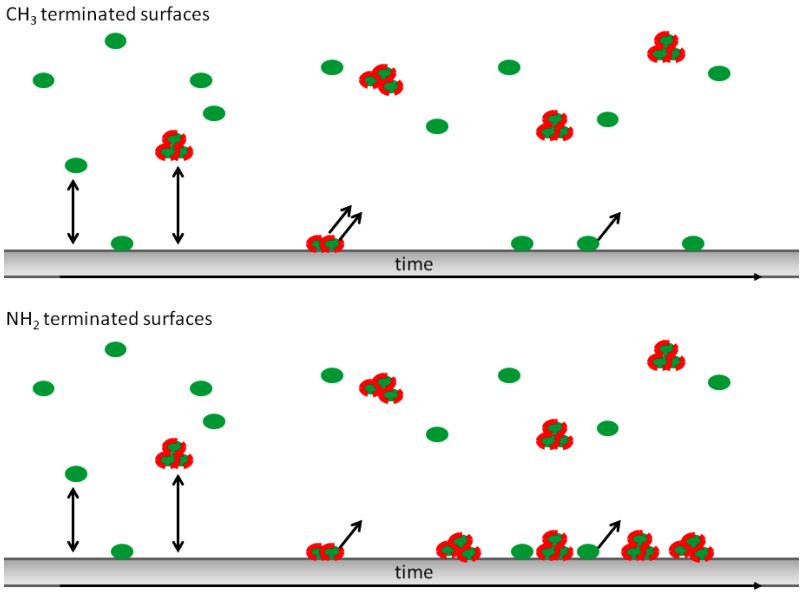

Figure 4.35: Single planktonic bacteria and planktonic bacteria aggregates approach the surface and interact with it. It seems that the neutral and hydrophobic surfaces with a high amount of CH_3 are unfavorable for the aggregates or PIA. Therefore, these surfaces are selective for bacteria producing less PIA, while surfaces with a high amount of NH_2 do not show any selectivity.

4.7.2 The impact of the surface chemistry on membrane proteins of adherent bacteria

The first experiments done with the objective to analyze membrane proteins of adherent bacteria showed that an Abs_{600} of 0.1 is necessary to obtain enough strong signals of the SDS-gel and to be able to compare two gels with each other. In figure 4.36 two SDS gels charged with samples of bacteria detached from 0 % NH_2 (figure 4.36 a) and 100 % NH_2 (figure 4.36 b) surfaces are shown. The two samples may present different proteins caused by the surface chemistry. Nevertheless, comparison cannot be done. Indeed, the same concentration of Abs_{600}=0.1 of detached bacteria cells is needed for all the model surfaces to compare different samples.
However, difficulty to harvest bacteria on CH_3-rich surfaces occurred. Indeed, attached bacteria were detached from the surfaces after an inoculation time of 2 h. In this process, the substrate with the attached bacteria was transferred into a new petri dish for further detachment treatment. However, surfaces with a high amount of CH_3 have a highly hydrophobic character. Hence, when substrates are transferred into the new petri dish, the surfaces was immediately dewatered and consequently, the quantity of attached bacteria was significantly reduced. Therefore, different alternatives of the protocol were envisaged. The most promising consists in the following: The transferring step of the substrate into a new petri dish, will be removed to avoid dewatering of bacteria adhered on hydrophobic substrates. However, a certain quantity of bacteria, which are attached onto the petri dish will be also gathered with the attached bacteria from the surface. These additional bacteria will influence the results, but this background will be present in all samples and may be negligible. Tests will be therefore necessary to study this aspect.

.

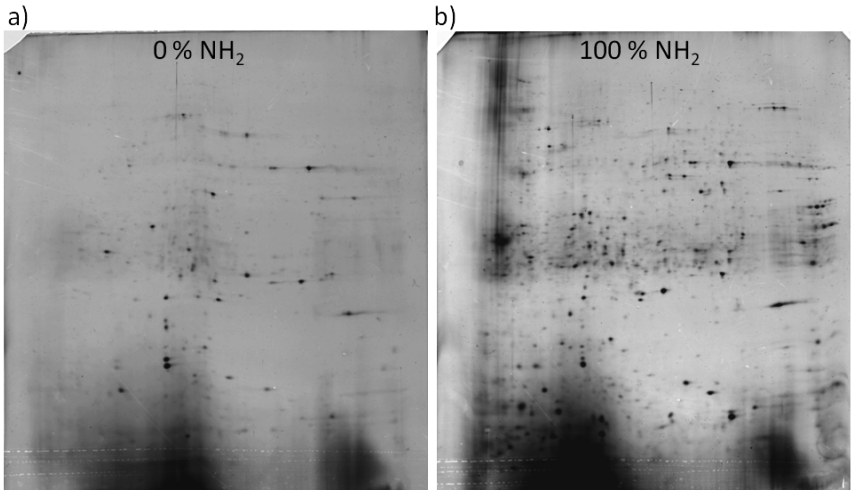

Figure 4.36: The proteins of detached bacteria were extracted and a 2D electrophoresis was performed. (a) represents the gel with separated proteins of bacteria detached from 0 % NH_2 surfaces and (b) of bacteria detached from 100 % NH_2 surfaces. The two gels may indicate some differences. Nevertheless the detached and gathered quantity of bacteria attached on 0 % NH_2 was fairly low. Hence, for a firm interpretation of the gels, a minimal concentration of Abs_{600}=0.1 is required.

4.8 Conclusion

The fourth chapter was separated in two parts: The first part dealt with bacterial adhesion studies on MML substrates, which were developed in the frame of the work and described before. The second part dealt with possible changes of the metabolism, thus differences in gene expression and protein production, of bacteria interacting with surfaces. Both parts required for a part the development of methodologies.

Bacterial adhesion studies were performed under static and dynamic conditions. There are already well-established protocol to study bacteria adhesion under static conditions. However, for the direct study of bacteria adhesion, a dynamic system had to be established. The experimental system is now operational and can be used for other projects (co-cultures for example). For the analysis of the metabolism of attached bacteria, bacteria were first detached and subsequently their metabolism was investigated. Since the used techniques (PCR and proteomic analysis) requires an adequate number of attached bacteria, the protocols used for the bacterial adhesion experiments and for harvesting the sessile bacteria had to be adapted. Due to the adoption, quantities of gathered bacteria cells, and hence the obtained proteins or nucleic acids, higher than the detection limit were reached.

For the investigation of the interaction between bacteria (*E. coli* and *S. epidermidis*) and well-defined surfaces, static bacterial adhesion experiments were performed in saline and for *E. coli* additionally in a minimal media with a similar ionic strength but different valency of ions. Surprising bacterial adhesion results were obtained. The behavior of both bacteria strains, could be described by acid-base like titration curves, for experiments performed in saline solution. There is no linear correlation, but in function of the amount of NH_2 on the surface, there are plateaus and sharp transitions zones. The number of adherent bacteria is stable in a certain range of % NH_2 until the number of bacteria changed drastically. We propose therefore, that certain features of the bacterial membrane may play a crucial role for the interaction of bacteria and the surfaces with different densities of NH_2.
These features may be the positively charged structures like membrane proteins and, especially for gram-positive bacteria, peptides linked to glycan chains of peptidoglycan. Their distribution on the membrane may govern the range of NH_2 % of MMLs leading to the transition zones. Furthermore, experiments with *E. coli* in two media reveal a conversely bacterial adhesion behavior on the same surfaces. The crucial parameter that influences bacterial adhesion may be the double ion layer on the bacteria and the substrate surfaces, which might have an impact on bacteria adhesion by hinderancing surface chemistry effects. Despite similar absence of linear correlation between bacterial adhesion and NH_2/CH_3 surface content and the presence of sharp transition zones, trends in dynamic conditions were significantly different compared to static conditions. However, the analysis of the attachment and detachment rates of bacteria revealed NH_2/CH_3 ranges leading to more stability of sessile bacteria than others, similarly to the static conditions.

Aside from the obvious interaction between bacteria and surfaces that results in bacterial adhesion, the question arise whether bacteria sense the surface, as indicated in some articles [54,237]. Hence, the impact of surfaces with different densities of NH_2 were used to study a possible impact of the surface on the production of the intercellular adhesin PIA of *S. epidermidis*, in collaboration with the laboratories of Prof. Spiliopoulous and Prof. Missirlis in Greece. Within this investigation, we could confirm that PIA is present in cell aggregates of *S. epidermidis*. However, bacterial behavior was probably influenced by the high concentration of bacteria in solution, which is required for RT-

PCR analysis. It could be shown that there is a difference in the colonization of surfaces according to NH_2/CH_3-content range: more single bacteria and rare PIA containing aggregates were observed on NH_2-rich surfaces, while only aggregates colonized CH_3-rich surfaces. Nevertheless, this was attributed to the physical-chemical properties of the PIA and no direct surface-sensing by bacteria could be highlighted. This points out that the difficulty to distinguish bacterial, own response from the global behavior of bacteria resulting from specific properties of the surface.

Since compositions of bacterial membrane proteins might vary due to the different surfaces on which bacteria adhered, change of the protein composition could be indicating if bacteria are able to sense subtle surface properties. Therefore, a protocol was established to harvest the necessary quantity of sessile bacteria, and a concentration limit of detached bacteria was determined within this work and in collaboration with the laboratory of Thierry Jouenne. This will allow to further investigate “surface sensing“ of bacteria in the future.

Chapter 5

Conclusion and Perspectives

The main objective of the thesis was to develop adequate (amine) terminated surfaces for studying the effect of heterogeneities of the material surfaces on bacterial adhesion and biofilm formation.

Characterization methodology for a comprehensive description of SAMs
For that purpose, a characterization methodology was established, dedicated to model substrates based on SAMs on silicon wafer. APTES and AHAPS amine terminated surfaces were chosen for proving the efficiency of this methodology. The combination of various techniques (XPS, static and dynamic contact angle measurements and ellipsometry measurements in air and in liquid, AFM imaging and zeta potential measurements) has revealed that APTES and AHAPS SAM structure was not controlled enough. It allowed to confirm the non-ideal structure of APTES, as already mentioned in literature and a description of a non-ideal organization of AHAPS molecules on the substrate. Thereby, we could highlight the problem of the grafting control during assembly of amine terminated silanes on silicon wafer.

Through the use of this combination of techniques, the SAMs and the MMLs model surfaces, which were used for the rest of this work, could be sufficiently described in terms of surface structure and organization. Nevertheless, several techniques might still improve the description by confirming the results. This is the case of zeta potential measurements on solid surfaces. Such measurements were performed in this work but the results suggest that the detection sensitivity is too low for the well-controlled SAMs. Potential improvements of the detection sensitivity should be first envisaged.
Furthermore, particular surfaces features of MMLs might be efficiently investigated with AFM by using functionalized AFM tips, which are able to sense and locate the different functional groups [256] For example, electrostatic interactions involving NH_2 groups on the surface could be studied.
In addition, such chemical surface features of SAMs could be investigated by X-photoemission electron microscopy (XPEEM) to confirm the organization and the control of the molecular layer. XPEEM provides micron-scale elemental and chemical information with core-level electrons, while complementary information in the 5-40 nm scale is available using secondary electrons. This technique complements surface imaging techniques and electron microscopy [257].

Well-controlled mixed monolayers
In a second part, well-controlled model surfaces were achieved, mainly by the adequate choice of the type of silane. The terminal group (Br) of the chosen silane does not interact with the substrate and its length leads to an increase in Van der Waals interactions, compared to the shorter amine terminated APTES and AHAPS layers. Therefore, the organization of the monolayer could be improved. Furthermore, control of the assembling process was improved by changing the reaction

conditions like temperature or solvent. Good control of composition, structure and organization of the bromine terminated silanes was demonstrated by using the previously established characterization methodology. To obtain amine terminated monolayers, the bromine terminal groups were converted into amine via azide functional groups. This conversion was shown not to degrade the control of the layer properties. The importance of controlling the organization of grafted monolayer for bacterial adhesion studies was highlighted in a bacterial adhesion experiment on the following amine-terminated SAMs: APTES, AHAPS and Br based NH2 terminated SAMs. The reproducibility of the experiment increased significantly with the increase of the organization of the grafted layer.

By dilution of one silane, i.e. the bromine terminated silane, a surface with a fairly low concentration of active groups could be obtained and thus are ideal substrates to graft single (bio)molecules. Studies of single molecules are an important and attractive tool to investigate specific acceptor-receptor interactions without bulk effects [258].

Furthermore, MMLs could provide a large variety of substrates for biointerface studies, if different chemical reagents are used in the conversion reaction, thus various functional groups backfilled with CH_3 surfaces could be achieved.

To further study the impact of chemical heterogeneity of surfaces on bacterial adhesion, MMLs were needed. They were realized on the basis of the well-controlled bromine terminated SAMs. Another silane that is methyl terminated was combined with the bromine terminated silane. Thus, different concentrations of Br functionalities in CH_3 were achieved. After the conversion of bromine into amine, MMLs of NH_2 backfilled with CH_3 surfaces were obtained. These MMLs provide ideal, well-controlled and well-characterized model surfaces, which were demonstrated by previously established characterization methodology. Furthermore, they hold a huge potential as a platform for diverse chemical derivatization processes for various applications.

Such MMLs could serve as substrates to graft biomolecules in different densities. Hence, preliminary experiments were conducted to graft an amino acid on homogeneous fully covered amine surfaces, indirectly via homobifunctional linker molecules and directly via activation of the amino acid. The potential of monitoring and calculating the reaction yield of the grafting process by XPS could be highlighted. However, the grafting yield via homobifunctional linker molecules remained beyond 50 %, and the reaction via activation of the amino acid resulted in uncontrolled side reactions between reagents and the surface.

The amino acid grafting protocol should be optimized to reach a maximal loading capacity and to be able to graft different densities of biomolecules on the surfaces. Another strategy than those already tested is to immobilize biomolecules via "click chemistry" on azide functionalized surfaces to obtain immobilized biomolecules in different densities on a solid support. Finally, short peptides could be achieved by using a bottom-up strategy of successively grafting several amino acids, as already reported on APTES surfaces [259].

Immobilized short sequences of amino acids or biomolecules in different densities could be further used as model surfaces to investigate the accessibility of functional groups on bacterial adhesion on more complex substrates. The density of grafted biomolecules could be an important feature of the organization of biomolecules. Especially, low densities of biomolecules may be more flexible or may more collapse on the surface. Hence different functionalities of the biomolecules would be exposed to bacteria.

Impact of chemical heterogeneities on bacterial adhesion and biofilm formation
Finally, NH_2 backfilled with CH_3 MMLs presented well-controlled and well-characterized model surfaces with chemical heterogeneities for biointerface studies. In a first approach, the effect of these chemical heterogeneities, or amine concentration on adhesion of *E. coli* and *S. epidermidis* bacteria was investigated.
The bacterial adhesion behavior could be described in acid-base like titration curves when experiments were performed in saline solution. Certain concentrations of NH_2 seem to represent a threshold that separates a plateau (stable zone) from a sharp transition zone. Such plateaus are zones including surfaces with a certain range of NH_2 concentration, on which the number of adherent bacteria is quasi-constant. In contrast, in the sharp transition zones, a small variation in the concentration of NH_2 leads to a significant change in the number of adherent bacteria, thus in bacterial adhesion. We assumed that repulsive interactions between a small amount of positive charges, distributed on the bacterial membrane, and positive charges on the surfaces play a crucial role in the bacterial adhesion process and hence result in the typical acid-base titration curve behavior.

The hypothesis of the importance of repulsive interactions between bacterial membrane and surface was supported by further bacterial adhesion experiments of *E. coli* in another culture medium, M63G-B1. The bacteria adhesion tendency in M63G-B1 was inverse to the tendency in saline solution. This is attributed to larger ions with higher valencies contained in M63G-B1 culture medium compared to saline solution. The change of the medium, from saline solution to M63G-B1, increases the ion double layer on the bacterial and substrate surfaces and might lead to a concealment of the chemical surface effects and to an increase of the distance between the bacterium and the surface. This may result in the converse tendency of bacterial adhesion behavior and in less differentiation in the attachment of bacteria on surfaces with different densities of NH_2.

Dynamic bacterial adhesion experiments performed in saline solution showed significant differences between the bacterial adhesion rate and the number of adherent bacteria obtained under static culture conditions. However, the thorough analysis of the attachment and detachment rates of *E. coli* reveals different zones in which sessile bacteria are more of less stable depending on the NH_2 concentration, similarly to that as observed in static conditions.

Finally, bacterial adhesion experiments under static and dynamic culture conditions clearly highlighted that bacteria are affected by subtle modifications of the chemical heterogeneities on surfaces.

In a second approach, the impact of surfaces with such chemical heterogeneities on the metabolism of bacteria was investigated. Therefore, the production of the polysaccharide intracellular adhesion (PIA) in sessile and planktonic *S. epidermidis* was investigated after bacterial adhesion experiments under dynamic conditions. CLSM observations highlighted that bacteria with less PIA adhered on surfaces with high concentration of CH_3, when experiments were performed under moderate flow rate. On surfaces with high concentration of NH_2 under moderate flow rate and on all surfaces under high flow rate, bacteria produced PIA similarly to bacteria in planktonic state showing furthermore no differences between surfaces with different densities of NH_2. RT-PCR confirmed that under moderate shear rate the over-expression of *icaA* and *icaD* were notably lower in sessile bacteria on surfaces with high concentration of CH_3 than in sessile bacteria on surfaces with a high concentration of NH_2, in sessile bacteria of high shear rates and in general than in planktonic bacteria. The chemical heterogeneities on the surface influenced finally the attachment behavior of single and bacteria aggregates under moderate shear rate, probably due to the hydrophilic char-

acter of PIA.
Another possibility to investigate changes in the bacterial metabolism influenced by the surface chemistry is the analysis of proteins, in particular the membrane proteins of sessile bacteria. In this frame, a detachment protocol of sessile bacteria was established to reach bacteria concentration within the detection limit of the used 2D gel-electrophoresis. However, further specific investigations have now to be done to study with this approach the possible influence of the chemical surface heterogeneity on the bacteria metabolism.

In the future, we propose to confirm our hypothesis regarding the acid-base titration curve like behavior of the bacterial adhesion, schematizing the bacterial membrane with a functionalized AFM tip. Diverse functionalizations of the tips should be considered for mimicking and understanding the *in vitro* experiments: NH_2, CH_3, NH_2 backfilled with CH_3 and NH_2 backfilled with PO_43- (mimicking *E. coli* outer wall). If the hypothesis that the positive charge on the bacterial membrane is the (main) cause of the bacterial attachment behavior, acid-base titration curves like results might be obtained by using AFM and functionalized tips on surfaces of various NH_2/CH_3 densities.

Further, the possible concealing effect of the minimal nutriment culture media (M63G-B1) could be investigated by the use of phosphate buffered saline (PBS) buffer. As saline solution, PBS buffer contains neither glucose nor vitamin like M63G-B1, but the size and the valencies of the ions is similar to M63G-B1. Since the ions are similar to M63G-B1 a comparable ion double layer on the bacteria and substrate surfaces should be obtained, hence the number of adherent bacteria is expected to be also similar.

For a thorough analysis of the attachment and detachment rate of *S. epidermidis* under dynamic culture conditions, a GFP expressing strain could significantly improve the analysis and image processing of the dynamic behavior. Creation of GFP-expressing *S. epidermidis* is currently under investigation in our laboratory.

RT-PCR is a powerful technique, however, the high concentration of bacteria in culture solution and the possibility of aggregation may be a critical feature of the use of this technique. Hence, the optimization of the protocol is necessary to investigate the over-expression in one adherent bacterium instead to bacteria aggregates.
Furthermore, genes that are known to be involved in the bacterial adhesion or in the biofilm formation could be analyzed. For *E. coli* such genes are genes that are involved in the curli and pili expression and in colonic acid, a typical exopolysaccharide of the used *E. coli* bacteria. Since PCR experiments is now available in our laboratory, preliminary test about relevant primers have been conducted to allow the investigation on *E. coli* adherent on modified silicon wafers in the future.

As mentioned in literature bacteria are able to sense the surface, which results in a change of the metabolism, and thus the production of specific proteins. Aside from the proteomic approach, we propose to investigate possible changes in proteins composition by Raman spectroscopy. Bacteria should be detached from the surface after bacterial adhesion experiment on surfaces with different chemical heterogeneities before analysis by Raman spectroscopy that allow to determine changes in the conformation and composition of proteins [260, 261]. An advantage of this method is that it can be performed in solution, therefore without dehydration process of bacteria. However, experimental set-up has to be firstly adapted. Further information of changes would be obtained, but the location in the metabolism would remain unknown.

Finally, the potential of the presented thesis will serve as basement of several possible further investigations in different topics and with objects in physical/chemistry, like optimization of thin layers with low concentrations of a functional groups, the realization of various well-controlled MMLs with different functional groups (amine, azide, etc.), the grafting of biomolecules and the investigation of loading capacity of such substrates. Furthermore, the realized substrates or their possible modifications will be used to study more characteristic features of bacterial adhesion in response to molecular heterogeneities and accessibility of the surface, in different culture media and at various shear rates for example. The bacterial adhesion process on MMLs could be imitated by AFM measurements with functionalized tips representing special features of bacterial membrane.

Bibliography

[1] J. W. Costerton, Philip S. Stewart, and E. P. Greenberg. Bacterial biofilms: A common cause of persistent infections. *Science*, 284(5418):1318–1322, May 1999.

[2] P. S. Stewart and W.J. Costerton. Antibiotic resistance of bacteria in biofilms. *The Lancet*, 358(9276):135–138, July 2001.

[3] L. Ploux, A. Ponche, and K. Anselme. Bacteria/material interfaces: Role of the material and cell wall properties. *Journal of Adhesion Science and Technology*, 24(13-14):2165–2201, 2010.

[4] H.J. Busscher, M.M. Cowan, and H.C. van der Mei. On the relative importance of specific and non-specific approaches to oral microbial adhesion. *FEMS Microbiology Letters*, 88(3–4):199–209, June 1992.

[5] H. J. Busscher and A. H. Weerkamp. Specific and non-specific interactions in bacterial adhesion to solid substrata. *FEMS Microbiology Letters*, 46(2):165–173, June 1987.

[6] P. Lejeune. Contamination of abiotic surfaces: what a colonizing bacterium sees and how to blur it. *Trends in Microbiology*, 11(4):179–184, April 2003.

[7] R. Briandet, T. Meylheuc, C. Maher, and M. N. Bellon-Fontaine. *listeria monocytogenes* scott a: Cell surface charge, hydrophobicity, and electron donor and acceptor characteristics under different environmental growth conditions. *Applied and Environmental Microbiology*, 65(12):5328–5333, December 1999.

[8] M. Naïtali, F. Dubois-Brissonnet, G. Cuvelier, and M. Bellon-Fontaine. Effects of ph and oil-in-water emulsions on growth and physicochemical cell surface properties of *listeria monocytogenes*: Impact on tolerance to the bactericidal activity of disinfectants. *International Journal of Food Microbiology*, 130(2):101–107, March 2009.

[9] E. L. Kannenberg and R. W. Carlson. Lipid a and o-chain modifications cause rhizobium lipopolysaccharides to become hydrophobic during bacteroid development. *Molecular Microbiology*, 39(2):379–392, 2001.

[10] K. M. Wiencek and M. Fletcher. Bacterial adhesion to hydroxyl- and methyl-terminated alkanethiol self-assembled monolayers. *Journal of Bacteriology*, 177(8):1959–1966, April 1995.

[11] B. Gottenbos, H. C. van der Mei, and H. J. Busscher. Models for studying initial adhesion and surface growth in biofilm formation on surfaces. In Ron J. Doyle, editor, *Biofilms*, volume Volume 310, pages 523–534. Academic Press, 1999.

[12] G.M Bruinsma, H.C van der Mei, and H.J Busscher. Bacterial adhesion to surface hydrophilic and hydrophobic contact lenses. *Biomaterials*, 22(24):3217–3224, December 2001.

[13] V. A . Tegoulia and S. L. Cooper. *staphylococcus aureus* adhesion to self-assembled monolayers: effect of surface chemistry and fibrinogen presence. *Colloids and Surfaces B: Biointerfaces*, 24(4):217–228, April 2002.

[14] N. Cerca, G. B. Pier, M. Vilanova, R. Oliveira, and J. Azeredo. Quantitative analysis of adhesion and biofilm formation on hydrophilic and hydrophobic surfaces of clinical isolates of *staphylococcus epidermidis*. *Research in Microbiology*, 156(4):506–514, May 2005.

[15] R.J. Emerson, T. S. Bergstrom, Y. Liu, E. R. Soto, C. A. Brown, W. G. McGimpsey, and T. A. Camesano. Microscale correlation between surface chemistry, texture, and the adhesive strength of *staphylococcus epidermidis*. *Langmuir*, 22(26):11311–11321, November 2006.

[16] L. Ploux, S. Beckendorff, M. Nardin, and S. Neunlist. Quantitative and morphological analysis of biofilm formation on self-assembled monolayers. *Colloids and Surfaces B: Biointerfaces*, 57(2):174–181, June 2007.

[17] S. Hou, E. A. Burton, K. A. Simon, D. Blodgett, Y. Luk, and D. Ren. Inhibition of *escherichia coli* biofilm formation by self-assembled monolayers of functional alkanethiols on gold. *Applied and Environmental Microbiology*, 73(13):4300–4307, July 1, 2007.

[18] E. A. Burton, K. A. Simon, S. Hou, D. Ren, and Y. Luk. Molecular gradients of bioinertness reveal a mechanistic difference between mammalian cell adhesion and bacterial biofilm formation. *Langmuir*, 25(3):1547–1553, 2009.

[19] N. P. Boks, H. J. Kaper, W. Norde, H. C. van der Mei, and H. J. Busscher. Mobile and immobile adhesion of staphylococcal strains to hydrophilic and hydrophobic surfaces. *Journal of Colloid and Interface Science*, 331(1):60–64, March 2009.

[20] M.G. Katsikogianni and Y.F. Missirlis. Interactions of bacteria with specific biomaterial surface chemistries under flow conditions. *Acta Biomaterialia*, 6(3):1107–1118, March 2010.

[21] P. Parreira, A. Magalhaes, I. C. Gonçalves, J. Gomes, R. Vidal, C. A. Reis, D. E. Leckband, and M. C. L. Martins. Effect of surface chemistry on bacterial adhesion, viability, and morphology. *J. Biomed. Mater. Res.*, 99A(3):344–353, 2011.

[22] D.F. Williams and European Society for Biomaterials. *Definitions in biomaterials: proceedings of a consensus conference of the European Society for Biomaterials, Chester, England, March 3-5, 1986*. Elsevier, 1987.

[23] D. F. Willams. *The Williams Dictionary of Biomaterials*. Liverpool University Press, 1999.

[24] D. F. Williams. On the nature of biomaterials. *Biomaterials*, 30(30):5897–5909, October 2009.

[25] J.R. Davis. *Handbook of materials for medical devices*. ASM International, 2003.

[26] S. Ramakrishna, J. Mayer, E. Wintermantel, and K. W Leong. Biomedical applications of polymer-composite materials: a review. *Composites Science and Technology*, 61(9):1189–1224, July 2001.

[27] J.J. Ramsden, D.M. Allen, D.J. Stephenson, J.R. Alcock, G.N. Peggs, G. Fuller, and G. Goch. The design and manufacture of biomedical surfaces. *CIRP Annals - Manufacturing Technology*, 56(2):687–711, 2007.

[28] AG Gristina. Biomaterial-centered infection: microbial adhesion versus tissue integration. *Science*, 237(4822):1588–1595, September 1987.

[29] L.T. Thevenot, P. W. Hu. Surface chemistry influences implant biocomplatibility. *Curr Top Med Chem*, 8(4):270–280, 2008.

[30] L. Tang, Y. Wu, and R. B. Timmons. Fibrinogen adsorption and host tissue responses to plasma functionalized surfaces. *J. Biomed. Mater. Res.*, 42(1):156–163, 1998.

[31] M. Shen, I. Garcia, R. V. Maier, and T. A. Horbett. Effects of adsorbed proteins and surface chemistry on foreign body giant cell formation, tumor necrosis factor alpha release and procoagulant activity of monocytes. *J. Biomed. Mater. Res.*, 70A(4):533–541, 2004.

[32] J.M. Anderson, T.L. Bonfield, and N.P. Ziats. Protein adsorption and cellular adhesion and activation on biomedical polymers. *Int J Artif Organs*, 13(6):375–82–, June 1990.

[33] T. He, Z.L. Shi, N. Fang, K.G. Neoh, E.T. Kang, and V. Chan. The effect of adhesive ligands on bacterial and fibroblast adhesions to surfaces. *Biomaterials*, 30(3):317–326, January 2009.

[34] Y. Wang, J. L. Robertson, W. B. Spillman, and R. O. Claus. Effects of the chemical structure and the surface properties of polymeric biomaterials on their biocompatibility. *Pharmaceutical Research*, 21:1362–1373, 2004.

[35] J. Wang, C.J. Pan, N. Huang, H. Sun, P. Yang, Y.X. Leng, J.Y. Chen, G.J. Wan, and P.K. Chu. Surface characterization and blood compatibility of poly(ethylene terephthalate) modified by plasma surface grafting. *Surface and Coatings Technology*, 196(1-3):307–311, June 2005.

[36] S. N. Rodrigues, I. C. Gonzalves, M.C.L. Martins, M. A. Barbosa, and B. D. Ratner. Fibrinogen adsorption, platelet adhesion and activation on mixed hydroxyl-/methyl-terminated self-assembled monolayers. *Biomaterials*, 27(31):5357–5367, November 2006.

[37] J. N. Barbosa, P. Madureira, M. A. Barbosa, and A. P. Eguas. The attraction of mac-1+ phagocytes during acute inflammation by methyl-coated self-assembled monolayers. *Biomaterials*, 26(16):3021–3027, June 2005.

[38] J. N. Barbosa, P. Madureira, M. A. Barbosa, and A. P. Eguas. The influence of functional groups of self-assembled monolayers on fibrous capsule formation and cell recruitment. *J. Biomed. Mater. Res.*, 76A(4):737–743, 2006.

[39] C. Mao, Y. Qiu, H. Sang, H. Mei, A. Zhu, J. Shen, and S. Lin. Various approaches to modify biomaterial surfaces for improving hemocompatibility. *Advances in Colloid and Interface Science*, 110(1-2):5–17, June 2004.

[40] M. M. Dowsey, T. N. Peel, and P. F.M. Choong. *Recent Advances in Arthroplasty*. InTech, 2012.

[41] S. Kurtz, E. Lau, K. Ong, K. Zhao, M. Kelly, and K. Bozic. Future young patient demand for primary and revision joint replacement: National projections from 2010 to 2030. *Clinical Orthopaedics and Related Research*, 467:2606–2612, 2009.

[42] S. Franz, S. Rammelt, D. Scharnweber, and J. C. Simon. Immune responses to implants: A review of the implications for the design of immunomodulatory biomaterials. *Biomaterials*, 32(28):6692–6709, October 2011.

[43] D. R. Murdoch, S. A. Roberts, V. G. Fowler, M. A. Shah, S. L. Taylor, A. J. Morris, and G. R. Corey. Infection of orthopedic prostheses after ***staphylococcus aureus*** bacteremia. *Clinical Infectious Diseases*, 32(4):647–649, February 2001.

[44] M. T. McCann, B. F. Gilmore, and S. P. Gorman. ***staphylococcus epidermidis*** device-related infections: pathogenesis and clinical management. *Journal of Pharmacy and Pharmacology*, 60(12):1551–1571, 2008.

[45] M. E. Rupp and G. L. Archer. Coagulase-negative ***staphylococci***: Pathogens associated with medical progress. *Clinical Infectious Diseases*, 19(2):231–245, August 1994.

[46] R. Poss, T.S. Thornhill, F.C. Ewald, W.H. Thomas, N.J. Batte, and C.B. Sledge. Factors influencing the incidence and outcome of infection following total joint arthroplasty. *Clin Orthop Relat Res*, 182:117–26, 1984.

[47] B. Gottenbos, D. W. Grijpma, H. C. van der Mei, J. Feijen, and H. J. Busscher. Antimicrobial effects of positively charged surfaces on adhering gram-positive and gram-negative bacteria. *Journal of Antimicrobial Chemotherapy*, 48(1):7–13, July 2001.

[48] M. Katsikogianni and Y. Missirlis. Bacterial adhesion onto materials with specific surface chemistries under flow conditions. *Journal of Materials Science: Materials in Medicine*, 21:963–968, 2010.

[49] K. M. Wiencek and M. Fletcher. Effects of substratum wettability and molecular topography on the initial adhesion of bacteria to chemically defined substrata a b. *Biofouling*, 11(4):293–311, 1997.

[50] K. Otto and T. J. Silhavy. Surface sensing and adhesion of ***escherichia coli*** controlled by the cpx-signaling pathway. *Proceedings of the National Academy of Sciences*, 99(4):2287–2292, February 2002.

[51] K. Otto, J. Norbeck, T. Larsson, K. Karlsson, and M. Hermansson. Adhesion of type 1-fimbriated ***escherichia coli*** to abiotic surfaces leads to altered composition of outer membrane proteins. *Journal of Bacteriology*, 183(8):2445–2453, April 2001.

[52] N. Cottenye, F. Teixeira, G. Ponche, A.and Reiter, K. Anselme, W. Meier, L. Ploux, and C. Vebert-Nardin. Oligonucleotide nanostructured surfaces: Effect on ***escherichia coli*** curli expression. *Macromol. Biosci.*, 8(12):1161–1172, 2008.

[53] K. Sauer and A. K. Camper. Characterization of phenotypic changes in ***pseudomonas putida*** in response to surface-associated growth. *Journal of Bacteriology*, 183(22):6579–6589, November 2001.

[54] C. Prigent-Combaret, O. Vidal, C. Dorel, and P. Lejeune. Abiotic surface sensing and biofilm-dependent regulation of gene expression in *escherichia coli*. *Journal of Bacteriology*, 181(19):5993–6002, October 1999.

[55] S. Vilain, P. Cosette, M. Hubert, C. Lange, G. Junter, and T. Jouenne. Comparative proteomic analysis of planktonic and immobilized *pseudomonas aeruginosa* cells: a multivariate statistical approach. *Analytical Biochemistry*, 329(1):120–130, June 2004.

[56] G. H. Ryu, W. Yang, H. Roh, I. Lee, J. K. Kim, G. H. Lee, D. H. Lee, B. J. Park, M. S. Lee, and J. Park. Plasma surface modification of poly (d,l-lactic-co-glycolic acid) (65/35) film for tissue engineering. *Surface and Coatings Technology*, 193(1-3):60–64, April 2005.

[57] S. Dyshlovenko, L. Pawlowski, I. Smurov, and V. Veiko. Pulsed laser modification of plasma-sprayed coatings: Experimental processing of hydroxyapatite and numerical simulation. *Surface and Coatings Technology*, 201(6):2248–2255, December 2006.

[58] H. Yamamoto, Y. Shibata, and T. Miyazaki. Anode glow discharge plasma treatment of titanium plates facilitates adsorption of extracellular matrix proteins to the plates. *Journal of Dental Research*, 84(7):668–671, July 2005.

[59] E. Ruckenstein and Z.F. Li. Surface modification and functionalization through the self-assembled monolayer and graft polymerization. *Advances in Colloid and Interface Science*, 113(1):43–63, March 2005.

[60] Y. Arima and H. Iwata. Effect of wettability and surface functional groups on protein adsorption and cell adhesion using well-defined mixed self-assembled monolayers. *Biomaterials*, 28(20):3074–3082, July 2007.

[61] W.C. Bigelow, D.L. Pickett, and W.A. Zisman. Oleophobic monolayers: I. films adsorbed from solution in non-polar liquids. *Journal of Colloid Science*, 1(6):513–538, December 1946.

[62] P. Silberzan, L. Leger, D. Ausserre, and J. J. Benattar. Silanation of silica surfaces. a new method of constructing pure or mixed monolayers. *Langmuir*, 7(8):1647–1651, August 1991.

[63] J. Sagiv. Organized monolayers by adsorption. 1. formation and structure of oleophobic mixed monolayers on solid surfaces. *J. Am. Chem. Soc.*, 102(1):92–98, January 1980.

[64] R. G. Nuzzo and D. L. Allara. Adsorption of bifunctional organic disulfides on gold surfaces. *J. Am. Chem. Soc.*, 105(13):4481–4483, June 1983.

[65] A. Ulman. Formation and structure of self-assembled monolayers. *Chemical Reviews*, 96(4):1533–1554, 1996.

[66] M. Pomerantz, A. Segmüller, L. Netzer, and J. Sagiv. Coverage of si substrates by self-assembling monolayers and multilayers as measured by ir, wettability and x-ray diffraction. *Thin Solid Films*, 132:153–162, October 1985.

[67] R. Maoz and J. Sagiv. On the formation and structure of self-assembling monolayers. i. a comparative atr-wettability study of langmuir-blodgett and adsorbed films

on flat substrates and glass microbeads. *Journal of Colloid and Interface Science*, 100(2):465–496, August 1984.

[68] J. Gun, R. Iscovici, and J. Sagiv. On the formation and structure of self-assembling monolayers: Ii. a comparative study of langmuir-blodgett and adsorbed films using ellipsometry and ir reflection absorption spectroscopy. *Journal of Colloid and Interface Science*, 101(1):201–213, September 1984.

[69] S.H. Lee, T. Ishizaki, N. Saito, and O. Takai. Surface characterization on binary nano/micro-domain composed of alkyl- and amino-terminated self-assembled monolayer. *Applied Surface Science*, 254(22):7453–7458, September 2008.

[70] D.K. Aswal, S. Lenfant, D. Guerin, J.V. Yakhmi, and D. Vuillaume. Self assembled monolayers on silicon for molecular electronics. *Analytica Chimica Acta*, 568(1-2):84–108, May 2006.

[71] A. Heise, M. Stamm, M. Rauscher, H. Duschner, and H. Menzel. Mixed silane self assembled monolayers and their in situ modification. *Thin Solid Films*, 327-329:199–203, August 1998.

[72] D. L. Angst and G. W. Simmons. Moisture absorption characteristics of organosiloxane self-assembled monolayers. *Langmuir*, 7(10):2236–2242, October 1991.

[73] J. B. Brzoska, I. Ben Azouz, and F. Rondelez. Silanization of solid substrates: A step toward reproducibility. *Langmuir*, 10(11):4367–4373, November 1994.

[74] A. Y. Fadeev and T. J. McCarthy. Self-assembly is not the only reaction possible between alkyltrichlorosilanes and surfaces: Monomolecular and oligomeric covalently attached layers of dichloro- and trichloroalkylsilanes on silicon. *Langmuir*, 16(18):7268–7274, 2000.

[75] T. P. Sullivan and W. T. S. Huck. Reactions on monolayers: Organic synthesis in two dimensions. *European Journal of Organic Chemistry*, 2003(1):17–29, 2003.

[76] J. Böhmler, L. Ploux, V. Ball, K. Anselme, and A. Ponche. Necessity of a thorough characterization of functionalized silicon wafers before biointerface studies. *The Journal of Physical Chemistry C*, 115(22):11102–11111, 2011.

[77] X. Qian, S. J. Metallo, I. S. Choi, H. Wu, M. N. Liang, and G. M. Whitesides. Arrays of self-assembled monolayers for studying inhibition of bacterial adhesion. *Analytical Chemistry*, 74(8):1805–1810, 2002.

[78] A. Komaromy, R. I. Boysen, H. Zhang, I. McKinnon, F. Fulga, M. T.W. Hearn, and D. V. Nicolau. Micro-structures modulate bacterial cell viability and attachment. *Microelectronic Engineering*, 86(6):1431–1434, 2009.

[79] A. Razatos, Y. Ong, F. Boulay, D. L. Elbert, J. A. Hubbell, M. M. Sharma, and G. Georgiou. Force measurements between bacteria and poly(ethylene glycol)-coated surfaces. *Langmuir*, 16(24):9155–9158, 2000.

[80] M. Katsikogianni, E. Amanatides, D. Mataras, and Y.F. Missirlis. *staphylococcus epidermidis* adhesion to he, he/o2 plasma treated pet films and aged materials: Contributions of surface free energy and shear rate. *Colloids and Surfaces B: Biointerfaces*, 65(2):257–268, September 2008.

[81] A. Hequet, V. Humblot, J. Berjeaud, and C. Pradier. Optimized grafting of antimicrobial peptides on stainless steel surface and biofilm resistance tests. *Colloids and Surfaces B: Biointerfaces*, 84(2):301–309, June 2011.

[82] I. C. Fernández Saldarriaga, H. C. van der Mei, M. J. Lochhead, D. W. Grainger, and H. J. Busscher. The inhibition of the adhesion of clinically isolated bacterial strains on multi-component cross-linked poly(ethylene glycol)-based polymer coatings. *Biomaterials*, 28(28):4105–4112, October 2007.

[83] Z. Shi, K.G. Neoh, E.T. Kang, and W. Wang. Antibacterial and mechanical properties of bone cement impregnated with chitosan nanoparticles. *Biomaterials*, 27(11):2440–2449, April 2006.

[84] P. Chua, K. Neoh, E. Kang, and W. Wang. Surface functionalization of titanium with hyaluronic acid/chitosan polyelectrolyte multilayers and rgd for promoting osteoblast functions and inhibiting bacterial adhesion. *Biomaterials*, 29(10):1412–1421, April 2008.

[85] M. Minier, M. Salmain, N. Yacoubi, L. Barbes, C. Methivier, S. Zanna, and C. Pradier. Covalent immobilization of lysozyme on stainless steel. interface spectroscopic characterization and measurement of enzymatic activity. *Langmuir*, 21(13):5957–5965, 2005.

[86] C. Huang, L. Mi, and S. Jiang. Interactions of alginate-producing and -deficient ***p**seudomonas aeruginosa* with zwitterionic polymers. *Biomaterials*, 33(14):3626–3631, May 2012.

[87] B. Zdyrko, V. Klep, X. Li, Q. Kang, S. Minko, X. Wen, and I. Luzinov. Polymer brushes as active nanolayers for tunable bacteria adhesion. *Materials Science and Engineering: C*, In Press, Corrected Proof:–, 2009.

[88] Y. Liu, J. Strauss, and T. A. Camesano. Adhesion forces between ***staphylococcus** epidermidis* and surfaces bearing self-assembled monolayers in the presence of model proteins. *Biomaterials*, 29(33):4374–4382, November 2008.

[89] A. Shukla, K. E. Fleming, H. F. Chuang, T. M. Chau, C. R. Loose, G.N. Stephanopoulos, and P. T. Hammond. Controlling the release of peptide antimicrobial agents from surfaces. *Biomaterials*, 31(8):2348–2357, March 2010.

[90] K. A. Barth, G. Coullerez, L. M. Nilsson, R. Castelli, P. H. Seeberger, V. Vogel, and M. Textor. An engineered mannoside presenting platform: ***e**scherichia coli* adhesion under static and dynamic conditions. *Adv. Funct. Mater.*, 18(9):1459–1469, 2008.

[91] P. J. Majewski. Removal of organic matter in water by functionalised self-assembled monolayers on silica. *Separation and Purification Technology*, 57(2):283–288, October 2007.

[92] G. Gao, D. Lange, K. Hilpert, J. Kindrachuk, Y. Zou, J. T.J. Cheng, M. Kazemzadeh-Narbat, K. Yu, R. Wang, S. K. Straus, D. E. Brooks, B. H. Chew, R. E.W. Hancock, and J. N. Kizhakkedathu. The biocompatibility and biofilm resistance of implant coatings based on hydrophilic polymer brushes conjugated with antimicrobial peptides. *Biomaterials*, 32(16):3899–3909, June 2011.

[93] J. Kim, P. Seidler, L. S. Wan, and C. Fill. Formation, structure, and reactivity of amino-terminated organic films on silicon substrates. *Journal of Colloid and Interface Science*, 329(1):114–119, January 2009.

[94] S. Choi and B. Zhang Newby. Suppress polystyrene thin film dewetting by modifying substrate surface with aminopropyltriethoxysilane. *Surface Science*, 600(6):1391–1404, March 2006.

[95] J.-P. Cloarec, Y. Chevolot, E. Laurenceau, M. Phaner-Goutorbe, and E. Souteyrand. A multidisciplinary approach for molecular diagnostics based on biosensors and microarrays. *IRBM*, 29(2-3):105–127, 2008.

[96] F. Basarir and T. Yoon. Preparation of y-aps monolayer with complete coverage via contact printing. *Journal of Colloid and Interface Science*, 336(2):393–397, August 2009.

[97] D. Briggs and Grant J.T. *Surface analysis by Auger and X-ray photoelectron spectroscopyb*. IM Publications and Surface Spectra Ldt., Chichester, UK, 2003.

[98] S. R. Wasserman, Y. T. Tao, and G. M. Whitesides. Structure and reactivity of alkylsiloxane monolayers formed by reaction of alkyltrichlorosilanes on silicon substrates. *Langmuir*, 5(4):1074–1087, 1989.

[99] B. Rothenhausler, C. Duschl, and W. Knoll. Plasmon surface polariton fields for the characterization of thin films. *Thin Solid Films*, 159(1):323–330, May 1988.

[100] T. Nakagiri, K. Sakai, A. Iida, T. Ishikawa, and T. Matsushita. X-ray standing wave method applied to the structural study of langmuir-blodgett films. *Thin Solid Films*, 133(1):219–225, November 1985.

[101] N. Tillman, A. Ulman, J. Schildkraut, and T. Penner. Incorporation of phenoxy groups in self-assembled monolayers of trichlorosilane derivatives. effects on film thickness, wettability, and molecular orientation. *Journal of the American Chemical Society*, 110(18):6136–6144, 1988.

[102] S. Evans, E. Urankar, A. Ulman, and N. Ferris. Self-assembled monolayers of alkanethiols containing a polar aromatic group: effects of the dipole position on molecular packing, orientation, and surface wetting properties. *Journal of the American Chemical Society*, 113(11):4121–4131, May 1991.

[103] H. Liu, N. V. Venkataraman, T. E. Bauert, M. Textor, and S. Xiao. Multiple transmission reflection infrared spectroscopy for high-sensitivity measurement of molecular monolayers on silicon surfaces. *The Journal of Physical Chemistry A*, 112(48):12372–12377, December 2008.

[104] H. Liu, S. Xiao, Y. Chen, J. Chao, J. Wang, Y. Wang, Y. Pan, X. You, and Z. Gu. Grazing angle mirror-backed reflection (gmbr) for infrared analysis of monolayers on silicon. *The Journal of Physical Chemistry B*, 110(36):17702–17705, 2006.

[105] V.K. Srivastava and Ajit Ram Verma. Interferometric and x-ray diffraction study of built-up molecular films of some long chain compounds. *Solid State Communications*, 4(8):367–371, August 1966.

[106] A. Bonnerot, P.A. Chollet, H. Frisby, and M. Hoclet. Infrared and electron diffraction studies of transient stages in very thin langmuir-blodgett films. *Chemical Physics*, 97(2-3):365–377, August 1985.

[107] L. Valkova, A. Menelle, N. Borovkov, V. Erokhin, M. Pisani, F. Ciuchi, F. Carsughi, F. Spinozzi, M. Pergolini, R. Padke, S. Bernstorff, and F. Rustichelli. Small-angle x-ray scattering and neutron reflectivity studies of langmuir-blodgett films of copper tetra-tert-butyl-azaporphyrines. *J. Appl. Cryst.*, 36(3):758–762, June 2003.

[108] R Becker, M R Ashton, T S Jones, N V Richardson, and H Sotobayashi. An electron energy loss study of the vibrations of polyimide layers deposited by langmuir-blodgett techniques. *Journal of Physics: Condensed Matter*, 3(S):S29–, 1991.

[109] T. Takenaka. Effect of electrolyte on the molecular orientation in monolayers adsorbed at the liquid-liquid interface: studies by resonance raman spectra. *Chemical Physics Letters*, 55(3):515–518, May 1978.

[110] K. Bierbaum, M. Kinzler, Ch. Woell, M. Grunze, G. Haehner, S. Heid, and F. Effenberger. A near edge x-ray absorption fine structure spectroscopy and x-ray photoelectron spectroscopy study of the film properties of self-assembled monolayers of organosilanes on oxidized si(100). *Langmuir*, 11(2):512–518, February 1995.

[111] A. Fujimori, M. Ishitsuka, H. Nakahara, E. Ito, M. Hara, K. Kanai, H. Ishii, Y. Ouchi, and K. Seki. Changes in the near-edge x-ray absorption fine structure spectra of long-chain diacetylene derivatives through photopolymerization in langmuir-blodgett films. *J. Polym. Sci. B Polym. Phys.*, 42(12):2329–2336, 2004.

[112] I. Doudevski, W. A Hayes, J. T Woodward, and D. K Schwartz. Atomic force microscope imaging of molecular aggregation during self-assembled monolayer growth. *Colloids and Surfaces A: Physicochemical and Engineering Aspects*, 174(1):233–243, November 2000.

[113] D. K. Schwartz, S. Steinberg, J. Israelachvili, and J. A. N. Zasadzinski. Growth of a self-assembled monolayer by fractal aggregation. *Phys. Rev. Lett.*, 69(23):3354–3357, December 1992.

[114] E. Sabatani and I. Rubinstein. Organized self-assembling monolayers on electrodes. 2. monolayer-based ultramicroelectrodes for the study. *Physical Chemistry*, 91(12):6663–6669, 1987.

[115] V. Ganesh, Ravi R. Pandey, B.D. Malhotra, and V. Lakshminarayanan. Electrochemical characterization of self-assembled monolayers (sams) of thiophenol and aminothiophenols on polycrystalline au: Effects of potential cycling and mixed sam formation. *Journal of Electroanalytical Chemistry*, 619–620(0):87–97, July 2008.

[116] D. Kong, Z. Yu, and S. Yuan. The blocking and structural properties of a schiff base self-assembled monolayer on the surface of au(111). *Journal of Solid State Electrochemistry*, 9:174–180, 2005.

[117] P. J. Cumpson. Estimation of inelastic mean free paths for polymers and other organic materials: use of quantitative structure-property relationships. *Surface and Interface Analysis*, 31(1):23–34, 2001.

[118] P. Facci, D. Alliata, L. Andolfi, B. Schnyder, and R. Katz. Formation and characterization of protein monolayers on oxygen-exposing surfaces by multiple-step self-chemisorption. *Surface Science*, 504(0):282–292, April 2002.

[119] New Fairley Casa Software Ltd. *CasaXPS Manual 2.3.15 Introduction to XPS and AES*, 2009.

[120] D Y Kwok, T Gietzelt, K Grundke, H J Jacobasch, and A W Neumann. Contact angle measurements and contact angle interpretation. 1. contact angle measurements by axisymmetric drop shape analysis and a goniometer sessile drop technique. *Langmuir*, 13(10):2880–2894, 1997.

[121] H.A. Tompkins and E.A Irene. *Handbook of Ellipsometry*. William Andrew Publishing and Springer-Verlag GmbH & Co. KG, 2005.

[122] K. Cai, M. Frant, J. Bossert, G. Hildebrand, K. Liefeith, and K. D. Jandt. Surface functionalized titanium thin films: Zeta-potential, protein adsorption and cell proliferation. *Colloids and Surfaces B: Biointerfaces*, 50(1):1–8, June 2006.

[123] H. J; Butt, Graf K. H, and Kappl M. *Physics and chemistry of interfaces*. Wiley-VCH Verlag, Weinheim, revised and enlarged ed. edition, 2006.

[124] Veeco Metrology Group Digital Istruments. *NanoScope Command Reference Manual*. Digital Istruments, Veeco Metrology Group, 4.42 edition, 1999.

[125] Veeco Instruments Inc. *NanoScope Software 6.13 User Guide*. Veeco Instruments Inc., 2004.

[126] L. Longo, G. Vasapollo, M. Guascito, and C. Malitesta. New insights from x-ray photoelectron spectroscopy into the chemistryof covalent enzyme immobilization, with glutamate dehydrogenase (gdh) on silicon dioxide as an example. *Analytical and Bioanalytical Chemistry*, 385:146–152, 2006.

[127] S. S. Jedlicka, J. L. Rickus, and D. Y. Zemlyanov. Surface analysis by x-ray photoelectron spectroscopy of sol-gel silica modified with covalently bound peptides. *The Journal of Physical Chemistry B*, 111(40):11850–11857, 2007.

[128] J. Bicerano. Prediction of the properties of polymers from their structures. *Journal of Macromolecular Science, Part C: Polymer Reviews*, 36(1):161–196, February 1996.

[129] A. Jane, R. Dronov, A. Hodges, and N. H. Voelcker. Porous silicon biosensors on the advance. *Trends in Biotechnology*, 27(4):230–239, April 2009.

[130] J. J. Pancrazio, J. P. Whelan, D. A. Borkholder, W. Ma, and D. A. Stenger. Development and application of cell-based biosensors. *Annals of Biomedical Engineering*, 27:697–711, 1999.

[131] N. Balachander and C. N. Sukenik. Monolayer transformation by nucleophilic substitution: Applications to the creation of new monolayer assemblies. *Langmuir*, 6(11):1621–1627, November 1990.

[132] G. E. Fryxell, P. C. Rieke, L. L. Wood, M. H. Engelhard, R. E. Williford, G. L. Graff, A. A. Campbell, R. J. Wiacek, L. Lee, and A. Halverson. Nucleophilic displacements in mixed self-assembled monolayers. *Langmuir*, 12(21):5064–5075, January 1996.

[133] A. Heise, H. Menzel, H. Yim, M. D. Foster, R. H. Wieringa, A. J. Schouten, V. Erb, and M. Stamm. Grafting of polypeptides on solid substrates by initiation of n-carboxyanhydride polymerization by amino-terminated self-assembled monolayers. *Langmuir*, 13(4):723–728, 1997.

[134] C. Barbot, O. Bouloussa, W. Szymczak, M. Plaschke, G. Buckau, J.-P. Durand, J. Pieri, J.I. Kim, and F. Goudard. Self-assembled monolayers of aminosilanes chemically bonded onto silicon wafers for immobilization of purified humic acids. *Colloids and Surfaces A: Physicochemical and Engineering Aspects*, 297(1-3):221–239, April 2007.

[135] J. Shyue, M. R. De Guire, T. Nakanishi, Y. Masuda, K. Koumoto, and C. N. Sukenik. Acid-base properties and zeta potentials of self-assembled monolayers obtained via in situ transformations. *Langmuir*, 20(20):8693–8698, 2004. PMID: 15379494.

[136] A. D. McNaught and A. Wilkinson. *Compendium of Chemical Terminology, the "Gold Book"*. Blackwell Scientific Publications, Oxford, 2 edition, 1997.

[137] H. Becker, R. Mayer, W. Berger, K. Müller, G. Domschke, D. Pavel, E. Fanghänel, H. Schmidt, J. Faust, K. Schollberg, M. Fischer, F. Gentz, K. Gewald, R. Gluch, K. Schwetlick, E. Seiler, G. Zeppenfeld, R. Beckert, W. Habicher, and P. Metz. *Organikum 21. Auflage*. Wiley-VCH, 2000.

[138] S. Morgenthaler, S. Lee, S. Zürcher, and N. D. Spencer. A simple, reproducible approach to the preparation of surface-chemical gradients. *Langmuir*, 19(25):10459–10462, 2003.

[139] R. A. Singh, J. Kim, S. W. Yang, J. Oh, and E. Yoon. Tribological properties of trichlorosilane-based one- and two-component self-assembled monolayers. *Wear*, 265(2):42–48, June 2008.

[140] B. D. Beake and G. J. Leggett. Variation of frictional forces in air with the compositions of heterogeneous organic surfaces. *Langmuir*, 16(2):735–739, November 1999.

[141] G. J. Leggett, N. J. Brewer, and K. S. L. Chong. Friction force microscopy: towards quantitative analysis of molecular organisation with nanometre spatial resolution. *Phys. Chem. Chem. Phys.*, 7(6):1107–1120, 2005.

[142] V. Chechik, R. M. Crooks, and C. J. M. Stirling. Reactions and reactivity in self-assembled monolayers. *Adv. Mater.*, 12(16):1161–1171, 2000.

[143] L. Perlin, S. MacNeil, and S. Rimmer. Production and performance of biomaterials containing rgd peptides. *Soft Matter*, 4(12):–, 2008.

[144] P. Jonkheijm, D. Weinrich, H. Schröder, C. M. Niemeyer, and H. Waldmann. Chemical strategies for generating protein biochips. *Angewandte Chemie International Edition*, 47(50):9618–9647, 2008.

[145] J. J. Gooding and S. Ciampi. The molecular level modification of surfaces: from self-assembled monolayers to complex molecular assemblies. *Chem. Soc. Rev.*, 40(5):2704–2718, 2011.

[146] V. N. Wong, G. Fernando, A. R. Wagner, J. Zhang, G. R. Kinsel, S. Zauscher, and D. J. Dyer. Separation of peptides with polyionic nanosponges for maldi-ms analysis. *Langmuir*, 25(3):1459–1465, 2009.

[147] U. Hersel, C. Dahmen, and H. Kessler. Rgd modified polymers: biomaterials for stimulated cell adhesion and beyond. *Biomaterials*, 24(24):4385–4415, November 2003.

[148] Z. Ma, Z. Mao, and C. Gao. Surface modification and property analysis of biomedical polymers used for tissue engineering. *Colloids and Surfaces B: Biointerfaces*, 60(2):137–157, November 2007.

[149] R. Benters, C. M. Niemeyer, and D. Wöhrle. Dendrimer-activated solid supports for nucleic acid and protein microarrays. *ChemBioChem*, 2(9):686–694, 2001.

[150] J. Razumovitch, W. Meier, and C. Vebert. A microcontact printing approach to the immobilization of oligonucleotide brushes. *Biophysical Chemistry*, 139(1):70–74, January 2009.

[151] F. Fenaille, P. A Guy, and J. Tabet. Study of protein modification by 4-hydroxy-2-nonenal and other short chain aldehydes analyzed by electrospray ionization tandem mass spectrometry. *Journal of the American Society for Mass Spectrometry*, 14(3):215–226, March 2003.

[152] K. Glinel, P. Thebault, V. Humblot, C.M. Pradier, and T. Jouenne. Antibacterial surfaces developed from bio-inspired approaches. *Acta Biomaterialia*, 1(0):–, 2012.

[153] S. North, E. Lock, C. Taitt, and S. Walton. Critical aspects of biointerface design and their impact on biosensor development. *Analytical and Bioanalytical Chemistry*, 397:925–933, 2010.

[154] F. R. Blattner, G. Plunkett, C. A. Bloch, N. T. Perna, V. Burland, M. Riley, J. Collado-Vides, J. D. Glasner, C. K. Rode, G. F. Mayhew, J. Gregor, N. W. Davis, H. A. Kirkpatrick, M. A. Goeden, D. J. Rose, B. Mau, and Y. Shao. The complete genome sequence of *escherichia coli* k-12. *Science*, 277(5331):1453–1462, September 1997.

[155] H. Miao, S. Ratnasingam, C.S. Pu, M. M. Desai, and C. C. Sze. Dual fluorescence system for flow cytometric analysis of *escherichia coli* transcriptional response in multi-species context. *Journal of Microbiological Methods*, 76(2):109–119, February 2009.

[156] J. Choi, T. Ishida, T. Kato, and S. Fujisawa. Self-assembled monolayer on diamond-like carbon surface: formation and friction measurements. *Tribology International*, 36(4-6):285–290, April 2003.

[157] H.J. Busscher, M. Rinastiti, W. Siswomihardjo, and H.C. van der Mei. Biofilm formation on dental restorative and implant materials. *Journal of Dental Research*, 89(7):657–665, July 2010.

[158] F. M. Fowkes. Attractive forces at interfaces. *Industrial & Engineering Chemistry*, 56(12):40–52, 1964.

[159] J. Razumovitch. *Hybridization of surface-tethered oligonucleotide brushes*. PhD thesis, Basel, 2009.

[160] A. Y. Fadeev and T. J. McCarthy. Trialkylsilane monolayers covalently attached to silicon surfaces: Wettability studies indicating that molecular topography contributes to contact angle hysteresis. *Langmuir*, 15(11):3759–3766, April 1999.

[161] L. V. Dubey and I. Ya. Dubey. Side reactions of onium coupling reagents bop and hbtu in the synthesis of silica polymer supports. *Ukrainica Bioorganica Acta*, 1:13–19, 2005.

[162] C. Heilmann, O. Schweitzer, C. Gerke, N. Vanittanakom, D. Mack, and F. Götz. Molecular basis of intercellular adhesion in the biofilm-forming *staphylococcus epidermidis*. *Molecular Microbiology*, 20(5):1083–1091, 1996.

[163] Y. H. An and R. J. Friedman. Concise review of mechanisms of bacterial adhesion to biomaterial surfaces. *J. Biomed. Mater. Res.*, 43(3):338–348, 1998.

[164] T. Proft and E. Baker. Pili in gram-negative and gram-positive bacteria : structure, assembly and their role in disease. *Cellular and Molecular Life Sciences*, 66(4):613–635, 2009.

[165] C. Sabin, E.P. Mitchell, M. Pokorná, C. Gautier, J.P. Utille, M. Wimmerová, and A. Imberty. Binding of different monosaccharides by lectin pa-iil from pseudomonas aeruginosa: Thermodynamics data correlated with x-ray structures. *FEBS Letters*, 580(3):982–987, February 2006.

[166] L. A. Pratt and R. Kolter. Genetic analyses of bacterial biofilm formation. *Current Opinion in Microbiology*, 2(6):598–603, December 1999.

[167] H. C. Berg and R. A. Aanderson. Bacteria swim by rotating their flagellar filaments. *Nature*, 245(5425):380–382, October 1973.

[168] N. Verstraeten, K. Braeken, B. Debkumari, M. Fauvart, J. Fransaer, J. Vermant, and J. Michiels. Living on a surface: swarming and biofilm formation. *Trends in Microbiology*, 16(10):496–506, October 2008.

[169] T. J. Wiles, R. R. Kulesus, and M. A. Mulvey. Origins and virulence mechanisms of uropathogenic *escherichia coli*. *Experimental and Molecular Pathology*, 85(1):11–19, August 2008.

[170] K. Otto and M. Hermansson. Inactivation of ompx causes increased interactions of type 1 fimbriated *escherichia coli* with abiotic surfaces. *Journal of Bacteriology*, 186(1):226–234, January 2004.

[171] R. Van Houdt and C. W. Michiels. Role of bacterial cell surface structures in *escherichia coli* biofilm formation. *Research in Microbiology*, 156(5-6):626–633, 2005.

[172] G. A. Burks, S. B. Velegol, E. Paramonova, B. E. Lindenmuth, J. D. Feick, and B. E. Logan. Macroscopic and nanoscale measurements of the adhesion of bacteria with varying outer layer surface composition. *Langmuir*, 19(6):2366–2371, January 2003.

[173] S. L. Walker, J. A. Redman, and M. Elimelech. Role of cell surface lipopolysaccharides in *escherichia coli* k12 adhesion and transport. *Langmuir*, 20(18):7736–7746, August 2004.

[174] S. Stoitsova, R. Ivanova, and I. Dimova. Lectin-binding epitopes at the surface of *escherichia coli* k-12: examination by electron microscopy, with special reference to the presence of a colanic acid-like polymer. *J. Basic Microbiol.*, 44(4):296–304, 2004.

[175] W. G. Characklis. Bioengineering report: Fouling biofilm development: A process analysis. *Biotechnol. Bioeng.*, 23(9):1923–1960, 1981.

[176] K. A. Whitehead and J. Verran. The effect of surface properties and application method on the retention of *pseudomonas aeruginosa* on uncoated and titanium-coated stainless steel. *International Biodeterioration & Biodegradation*, 60(2):74–80, 2007.

[177] S.H. Flint, J.D. Brooks, and P.J. Bremer. Properties of the stainless steel substrate, influencing the adhesion of thermo-resistant *streptococci*. *Journal of Food Engineering*, 43(4):235–242, March 2000.

[178] K. J Edwards and A. D Rutenberg. Microbial response to surface microtopography: the role of metabolism in localized mineral dissolution. *Chemical Geology*, 180(1–4):19–32, October 2001.

[179] D.P. Bakker, H. J. Busscher, J. van Zanten, J. de Vries, J. W. Klijnstra, and H. C. van der Mei. Multiple linear regression analysis of bacterial deposition to polyurethane coatings after conditioning film formation in the marine environment. *Microbiology*, 150(6):1779–1784, June 2004.

[180] M C van Loosdrecht, J Lyklema, W Norde, G Schraa, and A J Zehnder. Electrophoretic mobility and hydrophobicity as a measured to predict the initial steps of bacterial adhesion. *Applied and Environmental Microbiology*, 53(8):1898–1901, August 1987.

[181] A. Terada, A. Yuasa, T. Kushimoto, S. Tsuneda, A. Katakai, and M. Tamada. Bacterial adhesion to and viability on positively charged polymer surfaces. *Microbiology*, 152(12):3575–3583, December 2006.

[182] G. Speranza, G. Gottardi, C. Pederzolli, L. Lunelli, R. Canteri, L. Pasquardini, E. Carli, A. Lui, D. Maniglio, M. Brugnara, and M. Anderle. Role of chemical interactions in bacterial adhesion to polymer surfaces. *Biomaterials*, 25(11):2029–2037, May 2004.

[183] J. Genzer and K. Efimenko. Recent developments in superhydrophobic surfaces and their relevance to marine fouling: a review. *Biofouling*, 22(5):339–360, January 2006.

[184] J. Tsibouklis, M. Stone, A. A. Thorpe, P. Graham, V. Peters, R. Heerlien, J. R. Smith, K. L. Green, and T. G. Nevell. Preventing bacterial adhesion onto surfaces: the low-surface-energy approach. *Biomaterials*, 20(13):1229–1235, July 1999.

[185] W. M. Dunne. Bacterial adhesion: Seen any good biofilms lately? *Clinical Microbiology Reviews*, 15(2):155–166, April 2002.

[186] G. A. O'Toole and R. Kolter. Flagellar and twitching motility are necessary for *pseudomonas aeruginosa* biofilm development. *Molecular Microbiology*, 30(2):295–304, 1998.

[187] D G Davies and G G Geesey. Regulation of the alginate biosynthesis gene *algC* in *pseudomonas aeruginosa* during biofilm development in continuous culture. *Applied and Environmental Microbiology*, 61(3):860–867, March 1995.

[188] R. M. Donlan. Role of biofilms in antimicrobial resistance. *ASAIO Journal*, 46(6):–, 2000.

[189] BD Hoyle and JW Costerton. Bacterial resistance to antibiotics: the role of biofilms. *Prog Drug Res*, 37:91–105–, 1991.

[190] J W Costerton, K J Cheng, G G Geesey, T I Ladd, J C Nickel, M Dasgupta, and T J Marrie. Bacterial biofilms in nature and disease. *Annu. Rev. Microbiol.*, 41(1):435–464, October 1987.

[191] H.C. van der Mei, J. de Vries, and H.J. Busscher. X-ray photoelectron spectroscopy for the study of microbial cell surfaces. *Surface Science Reports*, 39(1):1–24, July 2000.

[192] A.T. Poortinga, R. Bos, W. Norde, and H. J. Busscher. Electric double layer interactions in bacterial adhesion to surfaces. *Surface Science Reports*, 47(1):1–32, June 2002.

[193] H Nikaido and M Vaara. Molecular basis of bacterial outer membrane permeability. *Microbiological Reviews*, 49(1):1–32, March 1985.

[194] H. Nikaido. Molecular basis of bacterial outer membrane permeability revisited. *Microbiology and Molecular Biology Reviews*, 67(4):593–656, December 2003.

[195] C. Galanos and O. Lüderitz. Electrodialysis of lipopolysaccharides and their conversion to uniform salt forms. *European Journal of Biochemistry*, 54(2):603–610, 1975.

[196] R. T. Coughlin, S. Tonsager, and E. J. McGroarty. Quantitation of metal cations bound to membranes and extracted lipopolysaccharide of *escherichia coli*. *Biochemistry*, 22(8):2002–2007, April 1983.

[197] F. Gaboriaud, S. Bailet, E. Dague, and F. Jorand. Surface structure and nanomechanical properties of *shewanella putrefaciens* bacteria at two ph values (4 and 10) determined by atomic force microscopy. *Journal of Bacteriology*, 187(11):3864–3868, June 2005.

[198] F. Gaboriaud, E. Dague, S. Bailet, F. Jorand, J. Duval, and F. Thomas. Multiscale dynamics of the cell envelope of *shewanella putrefaciens* as a response to ph change. *Colloids and Surfaces B: Biointerfaces*, 52(2):108–116, October 2006.

[199] J. F.L. Duval and F. Gaboriaud. Progress in electrohydrodynamics of soft microbial particle interphases. *Current Opinion in Colloid & Interface Science*, 15(3):184–195, June 2010.

[200] R. Van Houdt and C. W. Michiels. Role of bacterial cell surface structures in *escherichia coli* biofilm formation. *Research in Microbiology*, 156:626–633, June 2005.

[201] G. W. Jones and R. E. Isaacson. Proteinaceous bacterial adhesins and their receptors. *Critical Reviews in Microbiology*, 10(3):229–260, January 1982.

[202] M. Lindahl, A. Faris, T. Wadstrom, and S. Hjerten. A new test based on "salting out" to measure relative hydrophobicity of bacterial cells. *Biochimica et Biophysica Acta (BBA) - General Subjects*, 677:471–476, November 1981.

[203] A. Olsen, A. Jonsson, and S. Normark. Fibronectin binding mediated by a novel class of surface organelles on *escherichia coli*. *Nature*, 338(6217):652–655, April 1989.

[204] O. Vidal, R. Longin, C. Prigent-Combaret, C. Dorel, M. Hooreman, and P. Lejeune. Isolation of an *escherichia coli* k-12 mutant strain able to form biofilms on inert surfaces: Involvement of a new ompr allele that increases curli expression. *J. Bacteriol.*, 180(9):2442–2449, May 1998.

[205] K. Hori and S. Matsumoto. Bacterial adhesion: From mechanism to control. *Biochemical Engineering Journal*, 48(3):424–434, February 2010.

[206] G D Christensen, W A Simpson, A L Bisno, and E H Beachey. Adherence of slime-producing strains of *staphylococcus epidermidis* to smooth surfaces. *Infection and Immunity*, 37(1):318–326, July 1982.

[207] D Mack, W Fischer, A Krokotsch, K Leopold, R Hartmann, H Egge, and R Laufs. The intercellular adhesin involved in biofilm accumulation of *staphylococcus epidermidis* is a linear beta-1,6-linked glucosaminoglycan: purification and structural analysis. *Journal of Bacteriology*, 178(1):175–183, January 1996.

[208] C. Vuong, S. Kocianova, J. M. Voyich, Y. Yao, E. R. Fischer, F. R. DeLeo, and M. Otto. A crucial role for exopolysaccharide modification in bacterial biofilm formation, immune evasion, and virulence. *Journal of Biological Chemistry*, 279(52):54881–54886, December 2004.

[209] F. Götz. *staphylococcus* and biofilms. *Molecular Microbiology*, 43(6):1367–1378, 2002.

[210] Rajagopalan R. Hiemenz P. C. *Principles of colloid and surface chemistry.* Marcel Dekker, New York, 1997.

[211] K. C. Marshall, R. Stout, and R. Mitchell. Mechanism of the initial events in the sorption of marine bacteria to surfaces. *Journal of General Microbiology*, 68(3):337–348, November 1971.

[212] M. C. M. van Loosdrecht, J. Lyklema, W. Norde, and A. J. B. Zehnder. Bacterial adhesion: A physicochemical approac. *Microbial Ecology*, 17(1):1–15, 1989.

[213] R. Bos, H.C. van der Mei, and H.J. Busscher. Physico-chemistry of initial microbial adhesive interactions – its mechanisms and methods for study. *FEMS Microbiology Reviews*, 23(2):179–230, 1999.

[214] Y. Ong, A. Razatos, G. Georgiou, and M. M. Sharma. Adhesion forces between *e. coli* bacteria and biomaterial surfaces. *Langmuir*, 15(8):2719–2725, March 1999.

[215] M. Hermansson. The dlvo theory in microbial adhesion. *Colloids and Surfaces B: Biointerfaces*, 14(1–4):105–119, August 1999.

[216] C. J. van Oss. Development and applications of the interfacial tension between water and organic or biological surfaces. *Colloids and Surfaces B: Biointerfaces*, 54(1):2–9, January 2007.

[217] R. M. Donlan. Biofilms: Microbial life on surfaces. *Emerging Infectious Diseases*, 8(8):881–890, September 2002.

[218] M C van Loosdrecht, J Lyklema, W Norde, G Schraa, and A J Zehnder. The role of bacterial cell wall hydrophobicity in adhesion. *Applied and Environmental Microbiology*, 53(8):1893–1897, August 1987.

[219] M. Herrero, E. Quemener, S. Ulve, H. Reinecke, C. Mijangos, and Y. Grohens. Bacterial adhesion to poly(vinyl chloride) films: Effect of chemical modification and water induced surface reconstruction. *Journal of Adhesion Science and Technology*, 20(2-3):183–195, 2006.

[220] A. M. Gallardo-Moreno, M. L. Navarro-Pérez, V. Vadillo-Rodriguez, J. M. Bruque, and M. L. Gonzélez-Martin. Insights into bacterial contact angles: Difficulties in defining hydrophobicity and surface gibbs energy. *Colloids and Surfaces B: Biointerfaces*, 88(1):373–380, November 2011.

[221] C. Diaz, R. C. Salvarezza, M. A. Fernandez Lorenzo de Mele, and P. L. Schilardi. Organization of ***p**seudomonas fluorescens* on chemically different nano/microstructured surfaces. *ACS Applied Materials & Interfaces*, 2(9):2530–2539, 2010.

[222] E. Dague, J. Duval, F. Jorand, F. Thomas, and F. Gaboriaud. Probing surface structures of ***s**hewanella spp.* by microelectrophoresis. *Biophysical Journal*, 90(7):2612–2621, April 2006.

[223] A. J. de Kerchove, P., Weroski, and M. Elimelech. Adhesion of nonmotile ***p**seudomonas aeruginosa* on soft polyelectrolyte layer in a radial stagnation point flow system:measurements and model predictions. *Langmuir*, 23(24):12301–12308, 2007. PMID: 17941654.

[224] H.C van der Mei, P. Brokke, J. Dankert, J. Feijen, and H.J. Busscher. Influence of electrostatic interactions on the deposition efficiencies of coagulase-negative ***s**taphylococci* to collector surfaces in a parallel plate flow chamber. *Journal of Dispersion Science and Technology*, 13(4):447–458, August 1992.

[225] G. Harkes, H. van der Mei, P. Rouxhet, J. Dankert, H. Busscher, and J. Feijen. Physicochemical characterization of ***e**scherichia coli* a comparison with gram-positive bacteria. *Cell Biochemistry and Biophysics*, 20:17–32, 1992.

[226] C. Wright-Schubert. Structural comparison of the two distinct sugar binding sites in wheat germ agglutinin isolectin ii. *Journal of Molecular Biology*, 178(1):91–104, September 1984.

[227] J. Li, H. J. Busscher, H. C. van der Mei, W. Norde, B. P. Krom, and J. Sjollema. Analysis of the contribution of sedimentation to bacterial mass transport in a parallel plate flow chamber: Part ii: Use of fluorescence imaging. *Colloids and Surfaces B: Biointerfaces*, 87(2):427–432, October 2011.

[228] B. T. Bateman, N. P. Donegan, T. M. Jarry, M. Palma, and A. L. Cheung. Evaluation of a tetracycline-inducible promoter in **s***taphylococcus aureus In Vitro* and *In Vivo* and its application in demonstrating the role of sigb in microcolony formation. *Infection and Immunity*, 69(12):7851–7857, December 2001.

[229] A. Olofsson, M. Hermansson, and H. Elwing. N-acetyl-l-cysteine affects growth, extracellular polysaccharide production, and bacterial biofilm formation on solid surfaces. *Applied and Environmental Microbiology*, 69(8):4814–4822, August 2003.

[230] Y. H. An and R. J. Friedman. Laboratory methods for studies of bacterial adhesion. *Journal of Microbiological Methods*, 30(2):141–152, August 1997.

[231] W. Ziebuhr, C. Heilmann, F. Götz, P. Meyer, K. Wilms, E. Straube, and J. Hacker. Detection of the intercellular adhesion gene cluster (ica) and phase variation in ***s**taphylococcus epidermidis* blood culture strains and mucosal isolates. *Infection and Immunity*, 65(3):890–896, March 1997.

[232] J. P. Bearinger, L. Dugan, L. C.and Wu, H. Hill, A. T. Christian, and J. A. Hubbell. Chemical tethering of motile bacteria to silicon surfaces. *BioTechniques*, 46:209–216, 2009.

[233] H. C. Bos, R.and van der Mei and H.J. Busscher. A quantitative method to study co-adhesion of microorganisms in a parallel plate flow chamber. ii: Analysis of the kinetics of co-adhesion. *Journal of Microbiological Methods*, 23(2):169–182, August 1995.

[234] A. J. Barton, R. D. Sagers, and W. G. Pitt. Measurement of bacterial growth rates on polymers. *J. Biomed. Mater. Res.*, 32(2):271–278, 1996.

[235] T. R. Garrett, M. Bhakoo, and Z. Zhang. Bacterial adhesion and biofilms on surfaces. *Progress in Natural Science*, 18(9):1049–1056, September 2008.

[236] Y. Hong and D. G. Brown. Alteration of bacterial surface electrostatic potential and ph upon adhesion to a solid surface and impacts to cellular bioenergetics. *Biotechnol. Bioeng.*, 105(5):965–972, 2010.

[237] L. Rizzello, B. Sorce, S. Sabella, G. Vecchio, A. Galeone, V. Brunetti, R. Cingolani, and P. P. Pompa. Impact of nanoscale topography on genomics and proteomics of adherent bacteria. *ACS Nano*, 5(3):1865–1876, February 2011.

[238] A. Khemiri, A. Galland, D. Vaudry, P. Chan Tchi Song, H. Vaudry, T. Jouenne, and P. Cosette. Outer-membrane proteomic maps and surface-exposed proteins of *legionella pneumophila* using cellular fractionation and fluorescent labelling. *Analytical and Bioanalytical Chemistry*, 390:1861–1871, 2008.

[239] S. Vilain, P. Cosette, I. Zimmerlin, J. Dupont, G. Junter, and T. Jouenne. Biofilm proteome: Homogeneity or versatility? *J. Proteome Res.*, 3(1):132–136, October 2003.

[240] M. Ramstedt, R. Nakao, S. N. Wai, B. E. Uhlin, and J. Boily. Monitoring surface chemical changes in the bacterial cell wall. *Journal of Biological Chemistry*, 286(14):12389–12396, April 2011.

[241] P. G. Rouxhet and M. J. Genet. Xps analysis of bio-organic systems. *Surf. Interface Anal.*, 43(12):1453–1470, 2011.

[242] P.G. Rouxhet, N. Mozes, P.B. Dengis, Y.F. Dufrêne, P.A. Gerin, and M.J. Genet. Application of x-ray photoelectron spectroscopy to microorganisms. *Colloids and Surfaces B: Biointerfaces*, 2(1-3):347–369, March 1994.

[243] W. F. Patton. Detection technologies in proteome analysis. *Journal of Chromatography B: Analytical Technologies in the Biomedical and Life Sciences*, 771(1-2):3–31, May 2002.

[244] I. Miller, J. Crawford, and E. Gianazza. Protein stains for proteomic applications: Which, when, why? *Proteomics*, 6(20):5385–5408, 2006.

[245] M. P. Molloy, B. R. Herbert, M. B. Slade, T. Rabilloud, A. S. Nouwens, K. L. Williams, and A. A. Gooley. Proteomic analysis of the *escherichia coli* outer membrane. *European Journal of Biochemistry*, 267(10):2871–2881, 2000.

[246] S. Möller, C. Sternberg, J.B. Andersen, B. B. Christensen, J. L. Ramos, M. Givskov, and S. Molin. In situ gene expression in mixed-culture biofilms: Evidence of metabolic interactions between community members. *Applied and Environmental Microbiology*, 64(2):721–732, February 1998.

[247] H. Eleaume and S. Jabbouri. Comparison of two standardisation methods in real-time quantitative rt-pcr to follow *staphylococcus aureus* genes expression during in vitro growth. *Journal of Microbiological Methods*, 59(3):363–370, December 2004.

[248] V. Cafiso, T. Bertuccio, M. Santagati, F. Campanile, G. Amicosante, M. G. Perilli, L. Selan, M. Artini, G. Nicoletti, and S. Stefani. Presence of the *ica* operon in clinical isolates of *staphylococcus epidermidis* and its role in biofilm production. *Clinical Microbiology and Infection*, 10(12):1081–1088, 2004.

[249] G D Christensen, J T Parisi, A L Bisno, W A Simpson, and E H Beachey. Characterization of clinically significant strains of coagulase-negative *staphylococci*. *J. Clin. Microbiol.*, 18(2):258–269, August 1983.

[250] Cottenye N. *Antimicrobial surfaces based on self-assembled nanoreactors:from block copolymer suynthesis to bacterial adhesion study.* PhD thesis, Naturwissenschaftlichen Fakultät der Universität Basel, Université de Haute Alsace, 2010.

[251] J. Selinummi, J. Seppaelae, O. Yli-Harja, and Puhakka J. A. The cellc software was originally published as a supplement to for the article: Software for quantification of labeled bacteria from digital microscope images by automated image analysis. *BioTechniques*, 39:859–863, 2005.

[252] I.F. Sbalzarini and P. Koumoutsakos. Feature point tracking and trajectory analysis for video imaging in cell biology. *Journal of Structural Biology*, 151(2):182–195, August 2005.

[253] M. Stavridi, M. Katsikogianni, and Y.F. Missirlis. The influence of surface patterning and/or sterilization on the haemocompatibility of polycaprolactones. *Materials Science and Engineering: C*, 23(3):359–365, March 2003.

[254] W.W. Wilfinger, K. Mackey, and P. Chomczynski. Effect of ph and ionic strength on the spectrophotometric assessment of nucleic acid purity. *Biotechniques*, 22(3):–, March 1997.

[255] D. P. Bakker, A. van der Plaats, G. J. Verkerke, H. J. Busscher, and H. C. van der Mei. Comparison of velocity profiles for different flow chamber designs used in studies of microbial adhesion to surfaces. *Applied and Environmental Microbiology*, 69(10):6280–6287, October 2003.

[256] Y. Okabe, U. Akiba, and M. Fujihira. Chemical force microscopy of —ch3 and —cooh terminal groups in mixed self-assembled monolayers by pulsed-force-mode atomic force microscopy. *Applied Surface Science*, 157(4):398–404, April 2000.

[257] O. Renault, A. Garnier, J. Morin, N. Gambacorti, and F. Bertin. High-resolution xps spectromicroscopy study of micro-patterned gold–tin surfaces. *Applied Surface Science*, (0):–, 2012.

[258] W. E. Moerner and L. Kador. Optical detection and spectroscopy of single molecules in a solid. *Phys. Rev. Lett.*, 62(21):2535–2538, May 1989.

[259] W. K. J. Mosse, M. L. Koppens, T. R. Gengenbach, D. B. Scanlon, S. L. Gras, and W. A. Ducker. Peptides grafted from solids for the control of interfacial properties. *Langmuir*, 25(3):1488–1494, 2009.

[260] G. J. Thomas. Raman spectroscopy of protein and nucleic acid assemblies. *Annu. Rev. Biophys. Biomol. Struct.*, 28(1):1–27, June 1999.

[261] U. Neugebauer, P. Rösch, M. Schmitt, J. Popp, C. Julien, A. Rasmussen, C. Budich, and V. Deckert. On the way to nanometer-sized information of the bacterial surface by tip-enhanced raman spectroscopy. *Chem. Eur. J. of Chem. Phys.*, 7(7):1428–1430, 2006.

List of Figures